MARTIN MARIETTA ENERGY SYSTEMS LIBRARIES
3 4456 0364378 8

CENTRAL RESEARCH LIBRARY
DOCUMENT COLLECTION

53

ORNL-3131
UC-25 – Metals, Ceramics, and Materials
TID-4500 (20th ed., Rev.)

IN-PILE LOOP CORROSION EXPERIMENTS WITH URANYL SULFATE SOLUTIONS AT 235 AND 250°C

G. H. Jenks
J. E. Baker

CENTRAL RESEARCH LIBRARY
DOCUMENT COLLECTION
LIBRARY LOAN COPY
DO NOT TRANSFER TO ANOTHER PERSON
If you wish someone else to see this document, send in name with document and the library will arrange a loan.

OAK RIDGE NATIONAL LABORATORY
operated by
UNION CARBIDE CORPORATION
for the
U.S. ATOMIC ENERGY COMMISSION

Printed in USA. Price: $2.75 Available from the
Office of Technical Services
U. S. Department of Commerce
Washington 25, D. C.

LEGAL NOTICE

This report was prepared as an account of Government sponsored work. Neither the United States, nor the Commission, nor any person acting on behalf of the Commission:

A. Makes any warranty or representation, expressed or implied, with respect to the accuracy, completeness, or usefulness of the information contained in this report, or that the use of any information, apparatus, method, or process disclosed in this report may not infringe privately owned rights; or

B. Assumes any liabilities with respect to the use of, or for damages resulting from the use of any information, apparatus, method, or process disclosed in this report.

As used in the above, "person acting on behalf of the Commission" includes any employee or contractor of the Commission, or employee of such contractor, to the extent that such employee or contractor of the Commission, or employee of such contractor prepares, disseminates, or provides access to, any information pursuant to his employment or contract with the Commission, or his employment with such contractor.

ORNL-3131

Contract No. W-7405-eng-26

REACTOR CHEMISTRY DIVISION

IN-PILE LOOP CORROSION EXPERIMENTS WITH URANYL SULFATE SOLUTIONS AT 235 AND 250°C

G. H. Jenks J. E. Baker

Other Contributors

E. G. Bohlmann
S. E. Bolt
J. W. Brown
R. A. Lorenz
J. R. McWherter
A. R. Olsen
M. L. Picklesimer
H. C. Savage
F. J. Walter
S. H. Wheeler

DATE ISSUED

AUG 1 1963

OAK RIDGE NATIONAL LABORATORY
Oak Ridge, Tennessee
operated by
UNION CARBIDE CORPORATION
for the
U. S. ATOMIC ENERGY COMMISSION

MARTIN MARIETTA ENERGY SYSTEMS LIBRARIES

3 4456 0364378 8

CONTENTS

Abstract 1

1. Introduction 2

2. Methods and Procedures 4

3. Equipment and Materials 10
   - 3.1 Specimens to Test Corrosion and Other Factors 10
   - 3.2 Loop Specifications 10
   - 3.3 Loop Areas 10
   - 3.4 Solution Compositions 10

4. Results and Specific Evaluations 12
   - 4.1 Preparatory Operation 12
   - 4.2 In-Pile Operation, Solution Analyses 12
   - 4.3 In-Pile Operation, Oxygen Consumption 26
   - 4.4 Radiolytic-Gas Pressure 46
   - 4.5 Uranium Balance 49
   - 4.6 Results of Qualitative Examination of Loops 49
     - 4.6.1 Loop DD 49
     - 4.6.2 Loop FF 66
     - 4.6.3 Loop GG 68
     - 4.6.4 Loop EE 71
     - 4.6.5 Loop L-4-12 74
     - 4.6.6 Loop L-4-13 76
     - 4.6.7 Loop L-4-18 77
   - 4.7 Metallographic Examination of Loops 79
     - 4.7.1 Stainless Steel Corrosion Coupons 80
     - 4.7.2 Zirconium and Zirconium-Alloy Corrosion Coupons 85
     - 4.7.3 Titanium-Alloy Corrosion Coupons 88
     - 4.7.4 Stress Corrosion Specimens 88
     - 4.7.5 Loop Components 88
     - 4.7.6 X-Ray Examination of Specimens and Scales 91
   - 4.8 Results of Fission-Power Determinations 93
     - 4.8.1 Induced Activities 93
     - 4.8.2 Cesium-137 99
     - 4.8.3 Comparison of Average Fission-Power Values from Cs^{137} and from Induced Activities 100
   - 4.9 Results of Quantitative Examination of Loops 102
     - 4.9.1 Analyses of Scale from Low-Power Density Regions 102
     - 4.9.2 Analyses for Uranium on Steel Surfaces from High-Power Density Regions 105
     - 4.9.3 Results of Specimen Weight Measurements 106

5. Discussion of Results 106

5.1 Solution Analyses 106
5.1.1 Charged Solutions, Nonradioactive Samples 129
5.1.2 Uranium, Copper, and Sulfate in Loop Solutions During Irradiations 133
5.1.3 Free Acid in Solutions During Irradiation 136
5.1.4 Nickel in Irradiated Solutions 136
5.1.5 Other Constituents of Loop Solutions 139

5.2 Corrosion of Type 347 Stainless Steel During In-Pile Exposure 140
5.2.1 General 140
5.2.2 Effects of Solution Velocity on Core Specimen Corrosion 141
5.2.3 Comparison Between Total Amounts of Steel Corrosion Determined from Oxygen Consumption and from Nickel Accumulation Data 142
5.2.4 Correlations Between Solution Compositions and Rate of Oxygen Consumption by Steel 142

5.3 Corrosion of Zircaloy-2 and Crystal-Bar Zirconium 146

5.4 Corrosion of Titanium Alloys 146

IN-PILE LOOP CORROSION EXPERIMENTS WITH URANYL SULFATE SOLUTIONS AT 235 AND 250°C

G. H. Jenks J. E. Baker

ABSTRACT

In-pile loop experiments DD, EE, FF, GG, L-4-12, L-4-13, and L-4-18 were seven of a series designed to test the radiation corrosion of zirconium, titanium, and stainless steel alloys in UO_2SO_4 solutions under various conditions of radiation intensity, temperature, solution composition, and velocity of flow. Also investigated to a lesser extent were the effects of the in-pile exposure on impact and tensile properties of various structural materials, solution stability under irradiation, rate constants for recombination of radiolytic gas by copper in solution, and the general reliability of equipment operating under the test conditions.

Steel specimens exposed in the loop cores showed increases in corrosive attack over that expected out-of-radiation. The average rates of corrosion increased with power density in adjacent solution, but below certain power densities (0.3 to 4.2 w/ml in the various experiments) the average rate was not noticeably different from that occurring on in-line specimens, nor significantly different from that expected during out-of-pile exposures. These results, indicating that the effects of in-pile exposure on steel corrosion were confined to the core, were obtained from weight-change data, oxygen consumption rates, and measurements of nickel accumulation in solution, as well as from metallographic and visual examinations of specimens and components. Stainless steel corrosion rates probably changed considerably during the course of an experiment as indicated by the changes in the rate of oxygen consumption, varying by a factor of about 40 in one experiment and by a factor of 2 in another. No effect of stress or of galvanic coupling with other materials was noted in the corrosion behavior of stainless steel specimens located in the core and in-line positions. In one experiment a definite couple attack was noted between a 17-4 PH steel stress specimen and a C-130AM titanium-alloy specimen located in the loop pressurizer. In the 235°C experiment, type 430L stainless steel specimens were affected by exposure to fissioning solution to about the same extent as type 347 stainless steel. In a 250°C experiment, type 309SCb stainless steel exhibited about the same general relationship between power density and rate as type 347 stainless steel, but at a given power density the type 309 rates were greater than those for type 347.

Data obtained in these and other experiments of the series indicate both adverse and beneficial effects on steel corrosion under exposure to fissioning uranyl sulfate solutions with increasing solution velocity. The experimental conditions under which one or the other of the effects predominates are unknown, but it is speculated that the beneficial effect may result from a reduction of sorbed uranium on the steel surfaces, and the adverse effect to result following damage to the protective film during irradiation.

It was concluded that the average rate of steel corrosion in the loop cores in the 250°C experiments was dependent on the concentration of excess H_2SO_4 and of $NiSO_4$ in the loop solution, the rate decreasing with decreasing acid and with increasing $NiSO_4$. The most likely explanation for these effects is that the corrosion was influenced by the hydrogen ion concentration at the exposure temperature, and that the $NiSO_4$ in solution tended to reduce this concentration through the formation of HSO_4^-. This ion is known to be very stable at 250°C.

Analyses of solution samples withdrawn periodically from the experiments indicated, on the average, no significant loss of uranium or sulfate from solution. Loss of copper from solution ranging from 1 to 11% was indicated in most of the experiments.

Copper rate constants at 250°C, based on an activation energy of 22,000 kcal/mole for the copper activity, ranged from 2400 to 3200 liters $mole^{-1}$ hr^{-1} and are in reasonable agreement with those determined in out-of-pile tests. The constants in the experiments employing D_2O solutions were below those measured or predicted for water solutions.

Corrosion data for zirconium and titanium alloys obtained in these experiments are presented but not discussed, since they are in general agreement with other data for these materials which have been reported and extensively discussed elsewhere.

1. INTRODUCTION

Solutions of uranyl sulfate at temperatures in the neighborhood of 250 to 300°C and contained by or in contact with various structural materials such as zirconium, titanium, and stainless steel alloys have been of interest as possible fuel systems for aqueous homogeneous reactors. A series of 18 in-pile loop experiments has been carried out with the primary objective of testing the effects of reactor radiations on corrosion in these systems. Also investigated in some of the experiments were the effects of the in-pile exposure on impact and tensile properties of various structural materials, solution stability under irradiation, rate constants for recombination of radiolytic gas by copper sulfate in solution, and the general reliability of equipment operating under the test conditions.

The methods, equipment, and procedures employed in these experiments have been described in detail elsewhere.[1] Each experiment has also been discussed or summarized in HRP quarterly progress reports. Results and conclusions were included; however, detailed reports of each experiment are planned, and some have been prepared and issued for several experiments. The present paper describes six of the eight early experiments which employed exposure temperatures of 250 and 280°C in the mainstream and pressurizer, respectively, 0.17 *m* UO_2SO_4 solutions, and were exposed to reactor radiations in the LITR (HB-4 facility). (The other two experiments have been described in separate topical reports.[2,3]) This paper also includes a report of a similar experiment, L-4-18, in which the exposure temperature was 235°C (265°C in the pressurizer).

Some general information on the composition of the solutions employed and the materials tested in these experiments is set forth in Table 1. The temperature was near the maximum which could be used with the available loop design. The 0.17 *m* UO_2SO_4 solutions were selected for investigation because they had been extensively investigated out-of-pile and because the higher fission-power densities, in solution near specimens, which were achievable at this uranium concentration were considered desirable. (The fission-power densities in the 0.17 *m* UO_2SO_4 solutions were probably near the maximum achievable for the given reactor facility and loop.[4]) The $CuSO_4$ concentration of 0.03 *m* was selected to give controllably low radiolytic-gas pressures at the fission powers employed. In general, the other conditions in a

---

[1] H. C. Savage and W. D. Reel, *In-Pile Corrosion Test Loops for Aqueous Homogeneous Reactor Solutions*, ORNL-2977 (Nov. 10, 1960).

[2] J. E. Baker and G. H. Jenks, *HRP Radiation Corrosion Studies: In-Pile Loop L-4-8*, ORNL-2042 (Aug. 8, 1956).

[3] J. R. McWherter and J. E. Baker, *HRP Radiation Corrosion Studies: In-Pile Loop L-4-11*, ORNL-2152 (June 11, 1958).

[4] L. C. Noderer, *In-Pile Test Loop and HB-6 Bomb Power Density*, ORNL CF-54-9-238 (Sept. 21, 1954).

Table 1. Test Solution Compositions and Operating Time Data for Low-Temperature Loop Experiments

Experiment Number	Date Exposed in Reactor	Initial and Final Solution Composition (M at STP)[a]						Makeup Solution Composition (M at STP)[a]					Time at Temperature with UO_2SO_4 Solution (hr)		Radiation Exposure Time (3-Mwhr LITR Energy)
		UO_2SO_4	$CuSO_4$	Ni	Cr	Excess H_2SO_4	pH[b]	UO_2SO_4	$CuSO_4$	Excess H_2SO_4	Cr as CrO_3	pH	Natural	Enriched	
DD	In 10-8-54	0.165	0.030	0	0.002 (CrO_3)	0.016[c]	1.8			H_2O			85	465	280
	Out 10-26-54	0.148	0.028	0.008	0.006	0[c]	2.5								
FF	In 12-29-54	0.170	0.028	0		0.050[c]	1.3	0.170	0.028	0.050[c]		1.3	124	692	467
	Out 1-26-55	0.167	0.030	0.015		0.015[c]	1.9								
GG	In 2-20-55	0.169	0.027	0	0.006 (CrO_3)	0.056[c]	1.25	0.169	0.028	0.056[c]	0.009	1.25	105	1064	897
	Out 4-6-55	0.170	0.028	0.031	0	0.023[c]	1.7								
EE	In 5-1-55	0.164	0.028	0	0	0.020[c]	1.7	0.163	0.026	0.050[c]		1.3	127	630	537
	Out 5-29-55	0.163	0.027	0.007	0	0.012[c]	2.0								
L-4-12	In 1-19-56	0.170	0.032	0	0	0.050[c]	1.3	0.170	0.032	0.050[c]		1.3	153	719	1462
	Out 2-21-56	0.170	0.032	0.007	0.001	0.032[c]	1.55								
	In 2-24-56	0.167	0.027	0	0	0.050[c]	1.3	0.167	0.027	0.050[c]		1.3		1301	
	Out 4-16-56	0.177	0.029	0.014	0.002	0.014[c]	1.85								
L-4-13[a]	In 9-21-56	0.176	0.034	(9 ppm)	<0.0005	0.020[d]	1.40[e]	0.176	0.031	0.044[d]		1.05[e]	170	1042	787
	Out 11-6-56	0.179	0.029	0.010	0.002	0.020[d]	1.65[e]								
L-4-18[a]	In 6-19-57	0.170	0.068	0	<0.0005	0.019[d]	1.50[e]	0.170	0.063			1.40[e]	161	860	642
	Out 7-30-57	0.176	0.072	0.003	0.0005	0.013[d]	1.75[e]								

[a] H_2O was the solvent in all experiments except L-4-13 and L-4-18, where D_2O was employed.
[b] No correction to pH readings for sample dilution which occurred with all but the original (in) solutions.
[c] Estimated from pH; final (out) values corrected for sample dilution.
[d] From analytical measurements of free acid.
[e] Values for D_2O solutions obtained with pH meter calibrated with H_2O solutions (not used in estimating acidity).

given experiment such as H_2SO_4 concentrations, H_2O or D_2O solvent, specimen arrangements, etc., were selected in attempts to elucidate factors which appeared important at the time and/or to promote solution stability.

2. METHODS AND PROCEDURES

A given overall experiment included: (1) preparing the loop for operation and proving its satisfactory performance in out-of-pile mockup operation, (2) exposing and operating the loop in Hole HB-4 of the LITR, and (3) dismantling the loop and examining corrosion specimens and other portions of the loop for evidence of corrosive attack.

The preparation, testing, and in-pile operation of a loop have been described in detail elsewhere.[1] A listing of the different types of examinations, operations, and measurements for the results included in this report and the objectives of these are given below.

1. Sampling and chemical analyses of loop solutions during out-of-pile preparatory operations. Also, measurements of oxygen consumption during high-temperature operations with some of the solutions. The objective was to determine a rough value of the stainless steel corrosion rate in test solution out-of-pile and thus establish that no materials of low corrosion resistance were included in the loop. The out-of-pile thermal stability of the different solutions was not in question, and no attempt was made to sample and analyze solutions with sufficient accuracy to establish solution stability independently.

2. Sampling of loop solution at regular intervals during in-pile operation, and analyses for various constituents. (Usually the sample was taken with the reactor at power. Sample volumes were usually about 2 ml. The LITR operation and sampling schedule are shown in Figs. 1–7.) The solution analyses were carried out primarily to aid in evaluating (1) the stability of the solution during in-pile operations, (2) the corrosion behavior of stainless steel, (3) the solubilities of corrosion products, and (4) the fission power generated in solution (Cs^{137} analyses). The sampling procedure was such that a dilution of the sample by wash water took place in the sample lines. Prior to experiment GG, the amount of this dilution was uncertain. For GG and subsequent experiments, the dilution was determined by analyzing for Li_2SO_4 tracer added to the wash water.

3. Determinations of pressures of excess oxygen and of radiolytic gases in the pressurizer. Accurate measurements of temperature and pressure in a loop pressurizer were made at frequent intervals during a run, and the partial pressure of permanent gases was determined from the results. When the reactor was at power, the gases were radiolytic hydrogen and oxygen and excess oxygen. The radiolytic-gas pressures were determined from pressure changes at reactor startup and shutdown and, except for those periods, usually did not change rapidly with time. It was thereby possible to follow trends of oxygen consumption during reactor operation. Precise measurements of the oxygen pressures were made during reactor-down periods when the radiolytic-gas pressure was negligible. When the excess oxygen partial pressure was in the range of about 30 to 50 psi, the reactor was shut down and oxygen was added to bring the pressure to some higher value (75 to 125 psi).

Oxygen consumption measurements were made to follow the overall corrosion behavior during radiation exposure and to determine the total amounts of oxidation at given times. As will be shown and discussed,

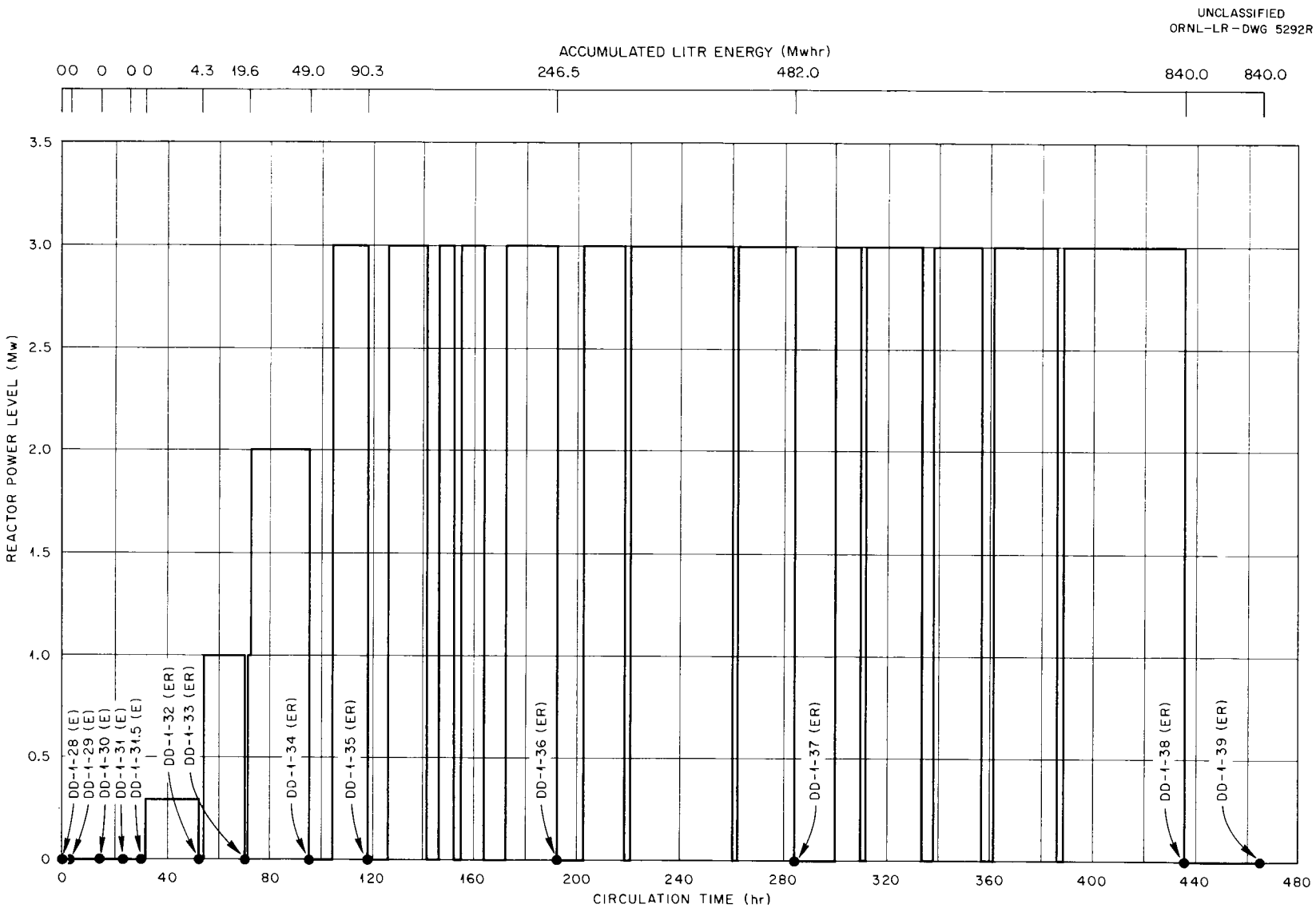

Fig. 1. LITR Operation and Loop Sampling Schedule, Loop DD.

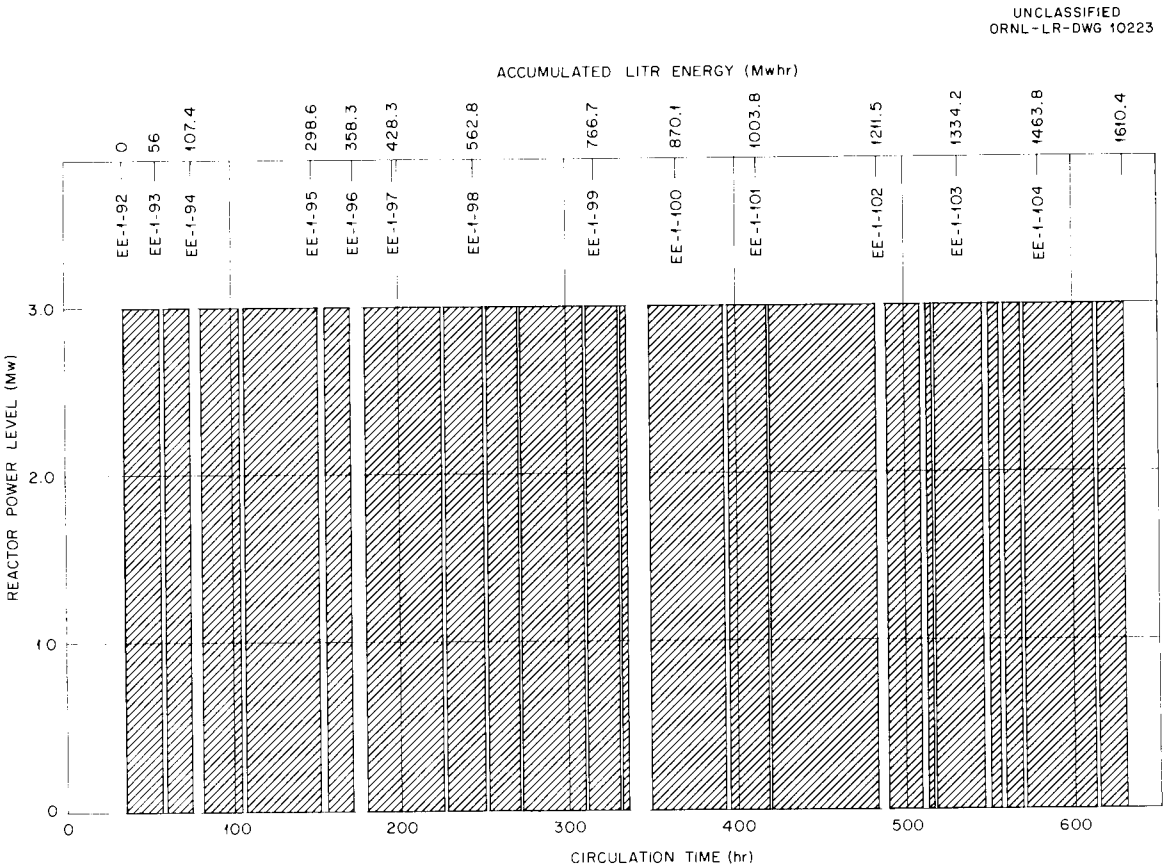

Fig. 2. LITR Operation and Loop Sampling Schedule, Loop EE.

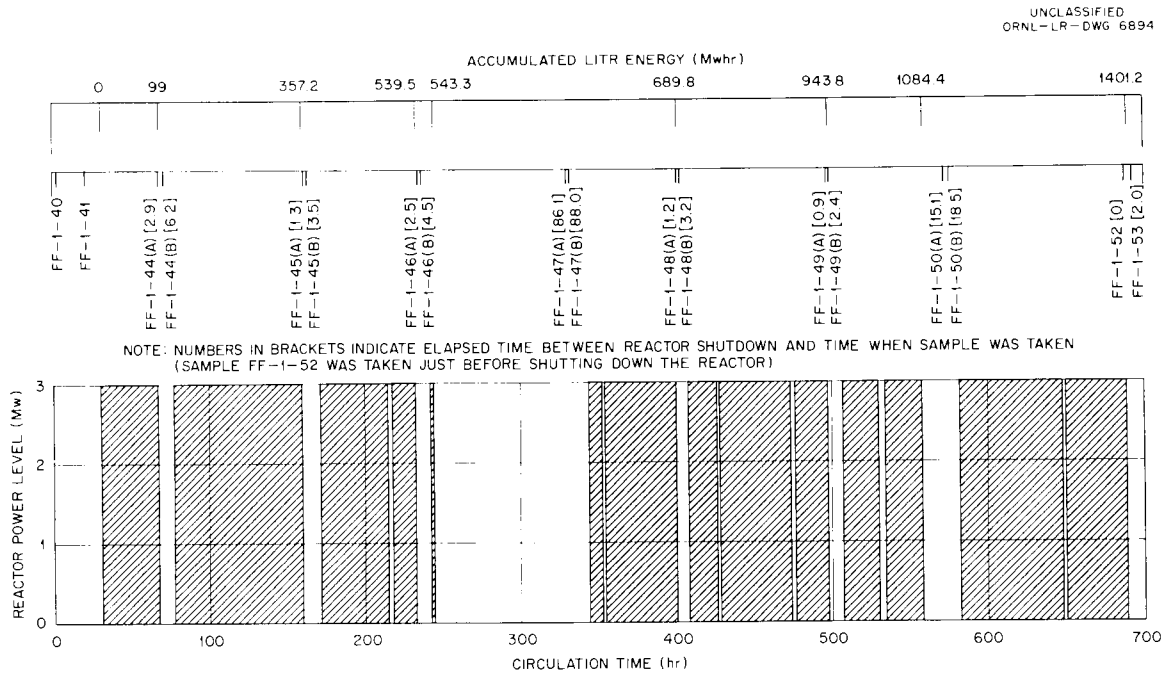

Fig. 3. LITR Operation and Loop Sampling Schedule, Loop FF.

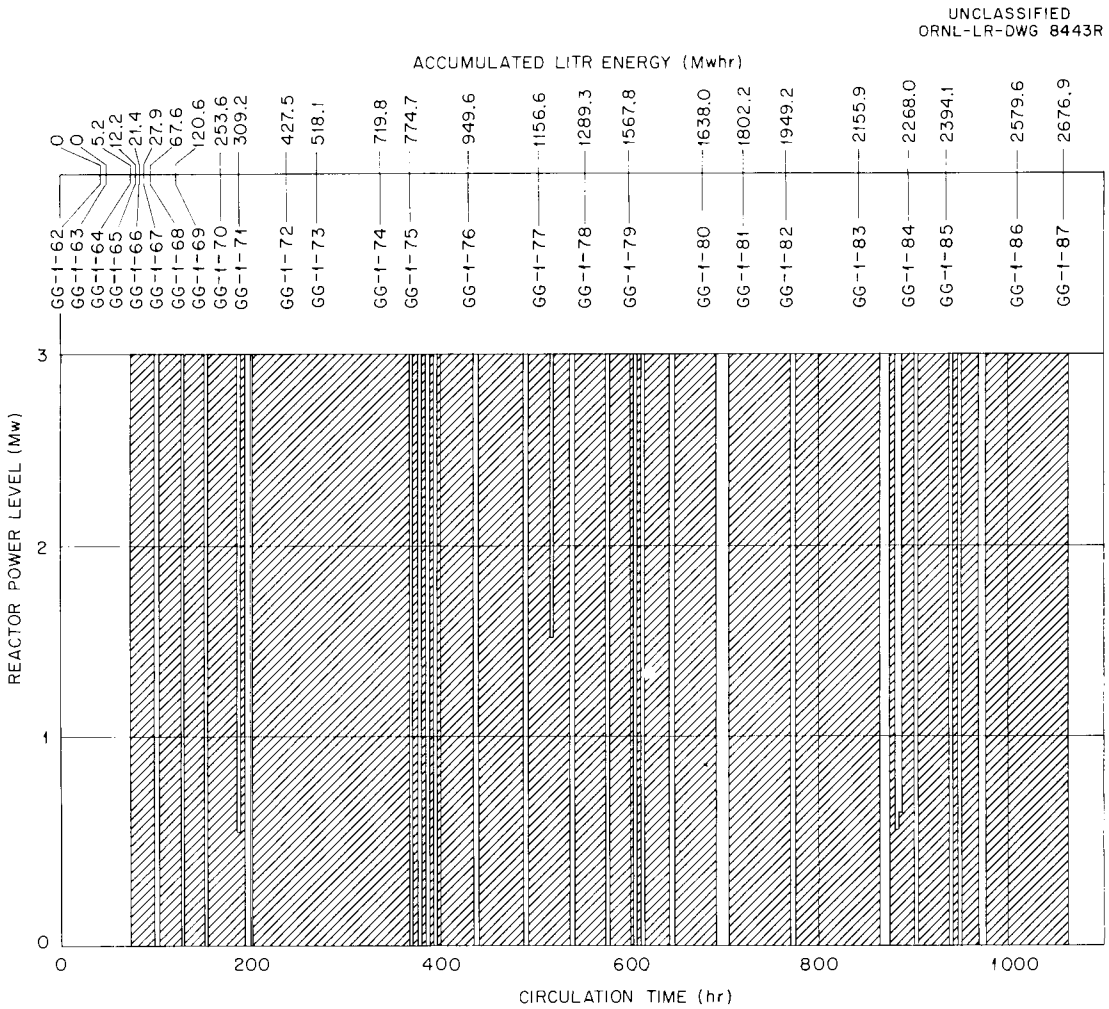

Fig. 4. LITR Operation and Loop Sampling Schedule, Loop GG.

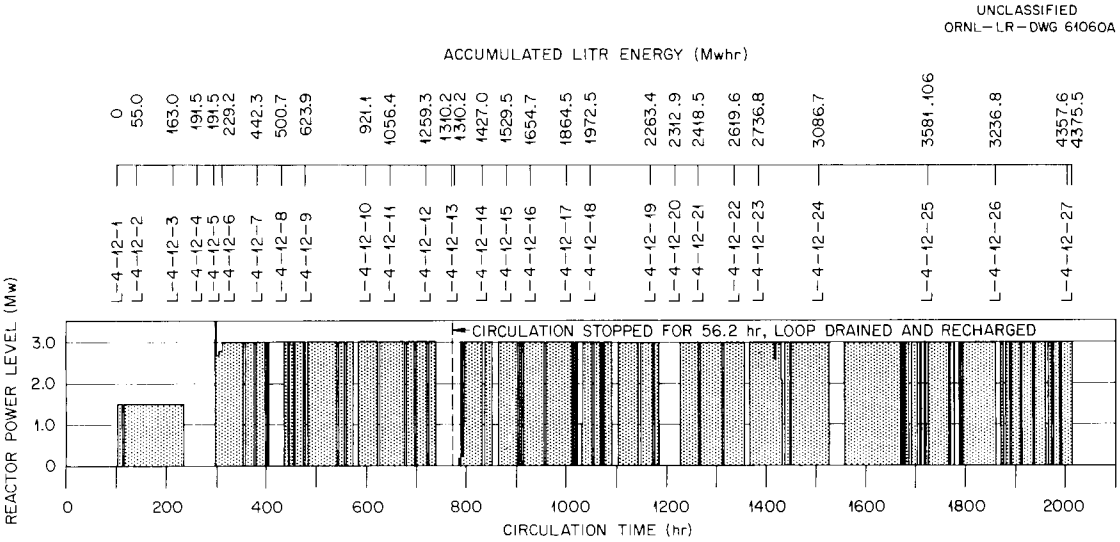

Fig. 5. LITR Operation and Loop Sampling Schedule, Loop L-4-12.

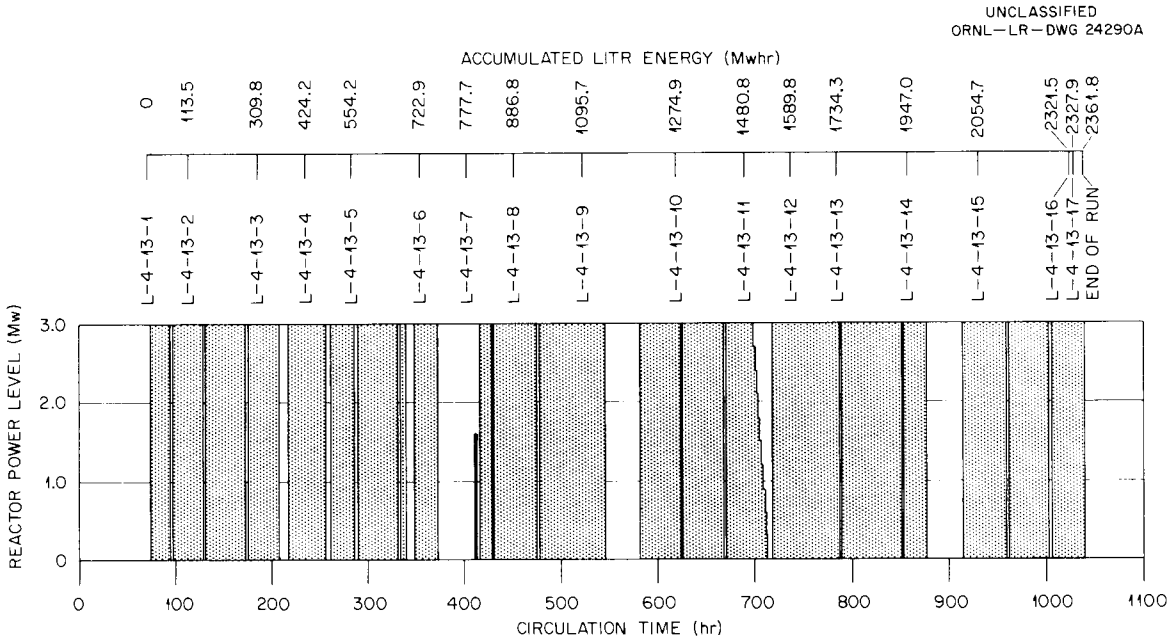

Fig. 6. LITR Operation and Loop Sampling Schedule, Loop L-4-13.

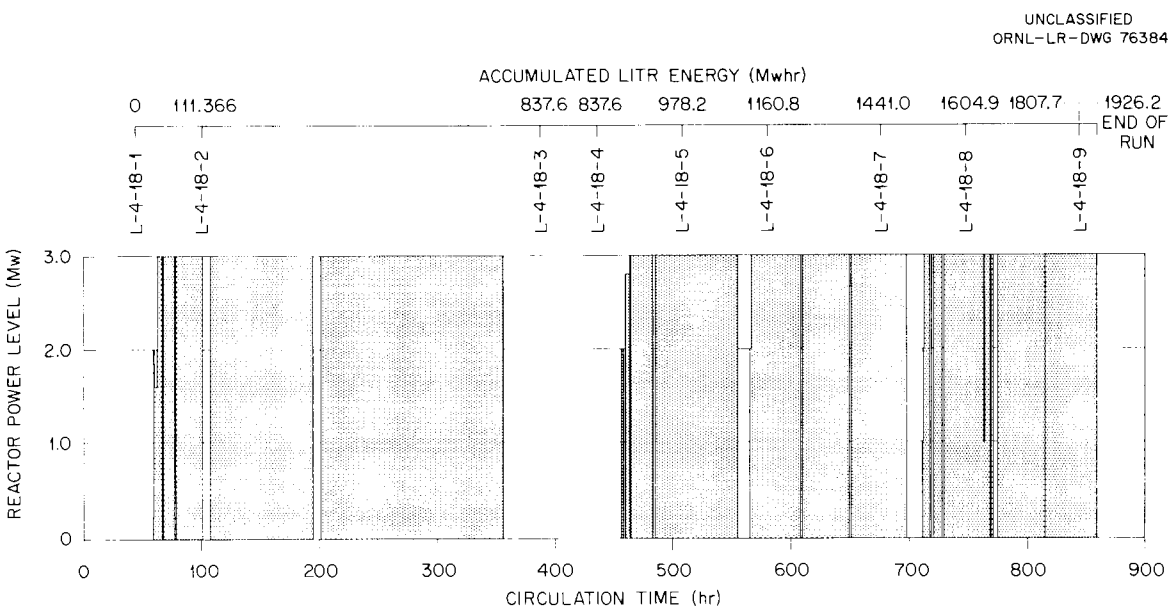

Fig. 7. LITR Operation and Loop Sampling Schedule, Loop L-4-18.

the oxygen results enabled an evaluation of the total amounts and other facets of the steel corrosion in a loop, since the amounts going to other materials, primarily zirconium alloys, could be evaluated from weight-change data, and it is believed that these other materials corroded approximately linearly with radiation time.[5] Furthermore, the consumption of oxygen by the other materials was, generally, much less than the consumption by steel.

Radiolytic pressure measurements were carried out as part of the program to define and control experimental conditions in the loop. The results of these measurements were used to calculate H_2 pressures in the mainstream and the rate constant for recombination of radiolytic gas by the copper in solution in a given experiment.

4. Sampling of solution in weigh tank (solution dump tank). After an experiment was completed, the solution and rinses were collected in the weigh tank. Several samples of solution were taken and submitted for chemical analyses. These analyses were made as part of the effort to evaluate the balance between uranium charged to and recovered from the loop.

5. Qualitative inspection of loop after radiation exposure. Following completion of the radiation exposure, the drained and rinsed loop was opened in a remote examination facility,[6] and various portions were removed and inspected visually. Corrosion specimens were examined before and after defilming. The objective was to provide information on the corrosion behavior of various components and on the types and locations of corrosion scales.

6. Determination of specimen weight losses resulting from corrosion. Specimens were usually weighed as removed from the loop, subjected to cathodic defilming to remove corrosion-product oxide, and then reweighed. The objective was to determine the average corrosion penetration of specimens from weight-change data. The defilming operation was usually effective in removing scale from steel surfaces, but was not very effective with zirconium or titanium alloys. However, the core specimens, especially those at the highest power densities, were nearly free of heavy scales, and it is assumed that the weight of oxide retained on core specimens was negligible compared with the actual loss in weight of a specimen. As will be discussed later, this assumption is probably not valid for some of the titanium specimens which exhibited only very small differences between as-installed and as-defilmed weights. Specimens from locations outside the core generally retained some film after cathodic defilming.

7. Determination of thermal-neutron fluxes adjacent to core specimens. The neutron flux adjacent to stainless steel and to zirconium-alloy specimens was determined from comparisons between the amounts of induced radioactivities in the specimens (Cr^{51} in stainless steel and Zr^{95} and Nb^{95} in zirconium alloys) and those in control specimens irradiated along with a cobalt monitor in the LITR (loops L-4-12, L-4-13, and L-4-18) or the ORNL Graphite Reactor (loops DD, FF, GG, and EE). The loop specimens were pickled before measurement to remove fission-product activity.

---

[5] G. H. Jenks, *Review and Correlation of In-Pile Zircaloy-2 Corrosion Data and a Model for the Effect of Irradiation,* ORNL-3039 (July 1961).

[6] E. G. Bohlmann, "Integrity of Metals in Homogeneous Reactor Media," p 208 in *Fluid Fuel Reactors* (ed. by J. A. Lane *et al.*), Pt. 1, Addison-Wesley, Reading, Mass., 1958.

These flux measurements were performed in order to evaluate the fission-power density in solution adjacent to core specimens. Results obtained in various loops have indicated that the flux values obtained with zirconium-alloy specimens are more reliable than those obtained with stainless steel. However, some of the early loops had more specimens of stainless steel than of zirconium alloys, and, for some of these experiments, it was assumed in the past that the stainless steel flux values were more reliable. No change will be made in the previous treatments of these data, since the conclusions drawn from these results would not be altered by use of the zirconium-alloy flux results.

8. Metallographic examination of specimens and portions of loops. Some of the parts cut from loops as well as some corrosion specimens were submitted for metallographic examination for types and amounts of corrosion attack at surfaces and for measurements of the thickness of the specimens and corrosion scales. The metallographic examinations were performed to aid in the evaluation of the corrosion behavior of various materials and the location of corrosion scales.

3. EQUIPMENT AND MATERIALS

3.1 Specimens to Test Corrosion and Other Factors

The numbers and types of corrosion and mechanical-property specimens employed in the different loops are shown in Table 2. Compositions of some of the specimen materials are given in Table 3. Nominal compositions were assumed for materials not shown.

Abbreviations used in referring to different types of specimens are the following: CC, core channel; CA, core low velocity; LC, in-line channel; LA, in-line low velocity; PV, pressurizer vapor space; and PL, pressurizer liquid space.

3.2 Loop Specifications

Specifications for each loop, including volumes and materials of construction of pump and specimen holders, are listed in Table 4.

3.3 Loop Areas

Internal surface areas of each loop are listed in Table 5. Specimen and holder areas are included in Tables 36–42.

3.4 Solution Compositions

The compositions of the uranyl sulfate test solutions charged to and recovered from the loops are listed in Table 1. The compositions of the solutions used to replace those removed in sampling are also listed. In some cases no free-acid analyses were made, and the acid concentrations were determined from pH measurements as indicated in Table 1. As discussed later (Sec 5.1.1), these acid values are considered more nearly correct than the values assumed in previous reports of these experiments.

Table 2. Corrosion Specimens Exposed in Loop Experiments

Experiment and Material	Stock[a] Item Number	Core						In-Line				Pressurizer
		Channel Coupons	Annulus Coupons	Impact Specimens	Tensile Specimens	Stress Specimens	Rod-Type Coupons	Channel Coupons	Annulus Coupons	Impact Specimens	Stress Specimens	Stress Specimens
DD												
Type 347 Stainless Steel	304 or 1149	12						12				
Zircaloy-2				8								
EE												
Type 347 Stainless Steel	1149	8				4	12	8				
Zircaloy-2	HRT plate No. 8	8				4	12	8				
Titanium-55A		8				4	12	8				
FF												
Zircaloy-2	1157	12		8				12				
GG												
Zircaloy-2	1157	12		8				12				
L-4-12												
Type 347 Stainless Steel	1146	8						8				
Type 17-4 PH Stainless Steel	376											4
Zircaloy-2	1157	8		3				8		2		
Titanium-55A	1165	8						8				
Titanium RC-A-40				3						2		
Titanium-6Al-4V	1192					4					4	6
Titanium-C-130-AM	1175											6
Titanium RC-70												
Titanium 75-A												
L-4-13												
Type 347 Stainless Steel	1149	8						8				
Type 309SCb Stainless Steel	1178	8						8				
Crystal-bar zirconium	1591-8	8						8				
Zr–20 Nb				3						3		
Zr-3a	WAPD heat 5Z-93			3	1					3		
Titanium-A40					1							
L-4-18												
Type 347 Stainless Steel	1149	8	7					8	7			
Type 430L Stainless Steel	1218	8	8					8	8			
Zircaloy-2	354 and 1157	8	4			2		8	4		2	
Zr–15 Nb	Zr 84		4						4			
Titanium-55A	1165		3						3			
Titanium-3Al	Heat 226 57		4						4			

[a]Available composition data given in Table 3.

Table 3. Alloy Compositions

Element	Analyses (%)							
	Zircaloy-2			Type 347 Stainless Steel				Crystal-Bar Zirconium
	HRT Plate No. 8	354	1157	1146	1149	304	HRT Steel[a]	1591-8
Sn	1.43	1.33	1.5					<0.05
Fe	0.12	0.108	0.5	69.6	69.2		65.5	0.5
Cr	0.075	0.052	0.2	17.9	17.8	19.11	18.5	<0.05
Ni	0.04	0.038	0.1	10.2	10.2	9.86	12.5	<0.05
C	0.05							
H_2	0.004–0.0055							
N_2	0.0060							
C				0.041	0.043	0.058		
Mn				1.40	1.43	1.15	1.8	
P						0.020		
S						0.027		
Si				0.50	0.50	0.38	0.53	
Mo				0.10	0.11			
Cu			<0.05				0.16	<0.05
Nb/Ta				0.80	0.79			
Nb							0.65	
Misc							0.42	

[a]Used in construction of loops.

4. RESULTS AND SPECIFIC EVALUATIONS

4.1 Preparatory Operation

The solutions and other experimental conditions employed in preparatory operations are listed in Tables 6–12 together with the results of analyses for corrosion products and chlorine in the various solutions. Values are also listed for the average corrosion rates of steel loop surfaces calculated from the results for nickel accumulation in solution and, where available, from oxygen consumption. In calculating the rate values it was assumed that the steel surfaces in contact with high-temperature solution corroded uniformly and that corrosion of other surfaces was negligible. In the case of the nickel data it was assumed that there was no selective oxidation of any of the components of stainless steel and that oxidized nickel was dissolved quantitatively. These assumptions were also employed in computing some values

Table 4. Loop Construction Data

	Loop						
	DD	EE	FF	GG	L-4-12	L-4-13	L-4-18
Loop volume (including pressurizer), ml	1505	1511	1560	1611	1542	1540	1551
Pressurizer volume, empty, ml	520	520	509	514	534	548	543
Pressurizer volume, loaded, ml					480		
Empty core volume, ml		375			365	372	372
Loaded core volume, ml	319	303	329	326	314	302	320
Flow rates							
Pressurizer, ml/sec	6.6	5.0	6.0	6.5	7.7	5.4	6.3
Core, gpm	5.7	5.5	5.8	6.4	5.4	5.4	5.2
Pump bearing material	*a*	*a*	*a*	*a*	Al_2O_3	Al_2O_3	Al_2O_3
Pump journal material	*b*	*c*	*d*	*d*	Al_2O_3	Al_2O_3	Al_2O_3
Loop construction material	347 SS	347 SS	347 SS	347 SS	347 SS[e]	347 SS	347 SS
Core and in-line channel coupon holders	Zircaloy-2	Zircaloy-2	Zircaloy-2	Zircaloy-2	Titanium	347 SS	347 SS
Core annulus coupon holders		347 SS, Zircaloy-2					347 SS, Ti-75A
In-line annulus coupon holders							347 SS, Ti-75A
Core impact specimen holders	Zircaloy-2[b]		Zircaloy-2	Zircaloy-2	347 SS[f]	347 SS	
In-line impact specimen holders					347 SS[f]	347 SS	
Core tensile specimen holders						347 SS	
Core annulus coupon spacers		347 SS, Zircaloy-2					
Core stress specimen holders		Zircaloy-2, 348 SS Ti-55A			347 SS, Zircaloy-2		Zircaloy-2
In-line stress specimen holders					347 SS, Zircaloy-2		347 SS
Pressurizer stress specimen holders					347 SS, Zircaloy-2, Ti-RC-70		
Design pressure, psi	1000	1000	1000	1000	1000	2000	2000

[a]Graphitar No. 14.
[b]Stellite 98 M2.
[c]Hardened 17-4 PH stainless steel.
[d]17-4 PH stainless steel.
[e]Core of loop constructed of Ti-55A.
[f]Assumed.

Table 5. Loop Areas Exposed to High-Temperature Solutions

Component	Areas Wetted by Solution (cm^2)[a]						
	DD	FF	GG	EE	L-4-12	L-4-13	L-4-18
Total main circulating lines (not including pump and core)	1553	1553	1553	1553	1553	1516	1516
Pressurizer							
Total area	(706)	(706)	(706)	(706)	(706)	(708)	(708)
Area wetted when containing 300 ml of solution	414	414	414	455[b]	445	385[c]	354[d]
Pressurizer lines	300	300	300	300	300	293	243
Core	445	445	445	445	(325)[e]	318	322
Pump							
Scroll	272	272	272	272	272	236	236
Impeller	159	159	159	159	159	215	215
Total area (347 stainless steel)	3143	3143	3143	3184	2729	2963	2886

[a]Unless otherwise specified values given are for stainless steel areas.
[b]When pressurizer contains 335 ml of solution.
[c]When pressurizer contains 374 ml of solution.
[d]When pressurizer contains 274 ml of solution.
[e]Ti-75A.

for corrosion penetrations and rates from the in-pile data presented in Figs. 15–21. The corrosion penetration or rate values presented were calculated on the basis that the nickel content in type 347 stainless steel was 12.5%.

4.2 In-Pile Operation, Solution Analyses

The results of analyses for constituents other than fission products are given in Tables 13–19. In general, the listing includes the reported concentration of a constituent in a sample, the concentration in the sample prior to dilution by wash water, which in some cases contained Li_2SO_4 tracer, and the calculated total amount of a given constituent in the loop solution. When Li_2SO_4 was added to the wash water, the correction for dilution was obtained from the amount of lithium in a sample. In a few cases the dilution factors obtained from the lithium analyses were in obvious error, and in these cases the factors were obtained from the analytical results for uranium, assuming the calculated uranium values to be correct. The calculated values for total amounts of a constituent at the time of a given sampling include corrections, where applicable, for the amounts withdrawn in prior sampling.

The reported, corrected, and calculated concentrations of uranium, sulfate, and copper in the several experiments are shown and compared graphically in Figs. 8–14. The nickel and manganese data given in the above tables are plotted against circulation time in Figs. 15–21. Values of steel corrosion which

Table 6. Analyses of Samples from Loop Inventory and Overall Corrosion Rates During Preparatory Operations,[a] Experiment DD

Remarks	Sample Number	Total Circulation Time (hr)	Solution Withdrawn for Sample (ml)	H_2O Added After Sampling (ml)	Calculated Inventory Volume Before Sampling (ml)	Uranium		Sulfate		Copper		Cobalt		Nickel		Chlorine		Chromium		Iron		Manganese		Silicon		pH, Rep	Overall Corrosion Rate of Nickel (mpy)
						Rep (mg/ml)	Cor[b] (g)	Rep (mg/ml)	Cor[b] (g)	Rep (mg/ml)	Cor[b] (g)	Rep (μg/ml)	Cor[b] (mg)	Rep (μg/ml)	Cor[b] (mg)	Rep (μg/ml)	Cor[b] (mg)	Rep (μg/ml)	Cor[b] (mg)	Rep (μg/ml)	Cor[b] (mg)	Rep (μg/ml)	Cor[b] (mg)	Rep (μg/ml)	Cor[b] (mg)		
Distilled H_2O, 100–250°C		19.0																									
3% TSP, 100°C, N_2 (85 psi)		2.9																									
5% HNO_3, original solution before charging to loop	DD-1-2	0								<1 P				ND C		<1 T		2 C		41 C							
5% HNO_3, 100°C, N_2 (85 psi)	DD-1-3	12.5								5 P		<1 C		12 C		<1 T		21 C		94 C							
	DD-1-4	12.5								9 P		10 C		15 C		<1 T		26 C		123 C							
	DD-1-5	12.5								3 P		8 C		11 C		<1 T		7 C		7 C							
Distilled H_2O, 250°C, O_2 (70 psi)	DD-1-12	12.4								ND P		ND C		ND C		<1 T		3 C		ND C							
	DD-1-13	12.4								ND P		ND C		ND C		<1 T		5 C		ND C							
Normal UO_2SO_4 solution before charging to loop	DD-1-1	0				28.5 T		15.5 IE		1.91 P		ND P		ND P		ND T		1 C		10 C						2.0	
	DD-1-1(C)	0								1.80 S				<4 S				<1 S				<1 S		2.3 S			
Charged solution to loop, 250°C, O_2 (70 psi)																											
Sample from main loop	DD-1-15	2	9	0	1109	26.6 T	29.5	15.5 IE	17.2	2.05 P	2.27	ND P		8 P	9	<1 T	1	8 C	9	17 C	19					2.0	
Sample from back of pump	DD-1-16	2	9	1.2	1100	29.5 T	32.7	15.8 IE	17.6	1.92 P	2.13	ND P		8 P	9	3 T	3	8 C	9	21 C	23					2.0	
Sample from main loop	DD-1-17	7	7	0	1092	28.3 T	31.0	16.2 IE	18.0	1.96 P	2.17	ND P		22 P	24	<1 T	1	21 C	23	34 C	38					2.0	
Sample from back of pump	DD-1-18	7	7	0	1085	30.8 T	34.1	16.7 IE	18.5	1.98 P	2.19	ND P		25 P	27	<1 T	1	16 C	18	26 C	29					2.0	
Sample from loop	DD-1-19	22	30	0	1078	28.4 T	31.5	15.5 IE	17.2	1.95 P	2.17	19 P	21	90 P	97	3.7 T	4	5.8 C	7	4.3 C	5					2.0	
Sample from loop after shutdown at Y-12	DD-I-20	24	6	0	1048	28.3 T	31.4	16.2 IE	18.4	1.76 P	1.97	ND P		77 P	84	<1 T	1	2.5 C	3	38 C	41	19 S	20	180 S	189	2.1	3.8
Loop inoperative about 20 hr between shutdown at Y-12 and startup at ORNL (inventory not removed from loop during this period)																											
Sample from main loop	DD-1-23	37.8	10	46.9	1042	27.3 T	30.4	16.6 IE	18.9	2.15 P	2.37	ND P		85 P	92	5 T	5	25 C	27	30 C	32					2.1	
Sample from main loop using loop sampling procedure	DD-1-25	64.4	47.2	0	1049	25.7 T	29.1	16.9 IE	19.5	1.90 P	2.15	163 P	172	131 P	142			34 C	37	90 C	96					2.8	
Sample from main loop after pump shutdown	DD-1-26	84.9	10	0	1032	28.2 T	32.6	15.5 IE	18.6	1.96 P	2.26	125 P	138	123 P	138	8 T	9	46 C	50	19 C	25	15 S	17	19.2 S	31	2.0	1.8
Sample from loop inventory after removal from loop	DD-1-29	84.9			1012													69 C	73			25 S	27				

[a]Where no values are given, either an analysis was not requested or the analytical results were not reliable.

ND Not detected
C Colorimetric
T Titrametric
IE Ion exchange, volumetric
P Polarographic
G Gravimetric
S Spectrographic

[b]Amount present plus accumulated amount previously withdrawn as samples.

Table 7. Analyses of Samples from Loop Inventory and Overall Corrosion Rates During Preparatory Operations,[a] Experiment EE

Treatment Conditions	Total Circulation Time for Each Solution (hr)	Inventory at Time of Sampling (ml)	Uranium		Sulfate		Copper		Cobalt		Nickel		Chlorine		Chromium		Iron		pH	Overall Corrosion Rate of Nickel (mpy)
			Conc (mg/ml)	Total (g)	Conc (mg/ml)	Total (g)	Conc (mg/ml)	Total (g)	Conc (μg/ml)	Total (mg)	Conc (μg/ml)	Total (mg)	Conc (μg/ml)	Total (mg)	Conc (μg/ml)	Total (mg)	Conc (mg/ml)	Total (g)		
3% TSP, He, 100°C	4.6	1250																		
5% HNO_3, He, 100°C	17.4	1300					0.012	0.016			272	354	<1	<1	632	822	2.25	2.92		
5% HNO_3, He, 100°C	21.0	1300					<0.001	<0.001			5	7	1	1	6	8	0.036	0.047		
3% TSP, He, 100°C	0.5	1300					<0.001	<0.001			6	8	<1	<1	4	5	0.041	0.053		
5% HNO_3, He, 100°C	19.2	1300																		
H_2O, O_2, 250°C	41.1	1100									<1	<1			1	1	<0.001	<0.001		
5% HNO_3, He, 100°C	16.7	1200					<0.001	<0.001			1	1	1	1	2	2	0.001	0.001		
H_2O, O_2, 250°C	19.1	1080																		
0.17 *m* UO_2SO_4 (normal) + 0.03 *m* $CuSO_4$ + 0.006 *m* H_2SO_4 (O_2, 250°C)	36.3	1100	38.1	42.0	18.6	20.0	2.05	2.26	1.0	1.0	5	6	3	3	18	20	0.017	0.019	2.4	0.2
0.17 *m* UO_2SO_4 (normal) + 0.03 *m* $CuSO_4$ + 0.006 *m* H_2SO_4 (O_2, 250°C)	90.6	1110	37.4	42.0	18.8	21.0	1.75	1.94	2.0	2.0	79	88			65	72	0.002	0.002	2.1	1.0

[a]Constituent concentrations and totals shown are not cumulative but represent the quantities present for operation with each solution.

Table 8. Analyses of Samples from Loop Inventory and Overall Corrosion Rates During Preparatory Operations,[a] Experiment FF

Solution	Sample Number	Total Circulation Time for Each Solution (hr)	Inventory at Time of Sampling (ml)	Uranium		Sulfate		Copper		Cobalt		Nickel		Chlorine		Chromium		Iron		pH	Overall Corrosion Rate of Nickel (mpy)
				Conc (mg/ml)	Total (g)	Conc (mg/ml)	Total (g)	Conc (mg/ml)	Total (mg)	Conc (μg/ml)	Total (mg)	Conc (μg/ml)	Total (mg)	Conc (μg/ml)	Total (mg)	Conc (μg/ml)	Total (mg)	Conc (μg/ml)	Total (mg)		
H_2O		20.8	1100																		
3% TSP	FF-1-1A	4.0	1320							1	1.3	1	1.3	13	17			1.2	1.6		
5% HNO_3	FF-1-4	18.4	1210					0.020	24.2	2.2	2.7	278	336	1	1.2	495	599	1850	2240		
5% HNO_3 (2d run)	FF-1-8	4.0	1200					0.001	1.2	1	1.2	5	6.0			3	3.6	28	34		
H_2O	FF-1-13	22.0	1054					0.001	1.1	1	1.1	1	1.1	2	2.1			1	1.1		
Enriched UO_2SO_4	FF-1-21	12.7	1092	37.0	40.4	20.8	22.7	1.80	1960			212	232	2	2.2	1	1.1	42	46	1.53	20
New pump installed																					
H_2O	FF-1-26	4.3	1190																		
Enriched UO_2SO_4	FF-1-28	4.2	975																		
H_2O		8.0	1130																		
Normal UO_2SO_4	FF-1-38	123.5	984	27.1	26.7			1.77	1740			63	62			12	11.8	1	1.0	1.92	0.6

[a]Constituent concentrations and totals shown are not cumulative but represent the quantities present for operation with each solution.

Table 9. Analyses of Samples from Loop Inventory and Overall Corrosion Rates During Preparatory Operations,[a] Experiment GG

Solution	Total Circulation Time for Each Solution (hr)	Inventory at Time of Sampling (ml)	Uranium		Sulfate		Copper		Nickel		Iron		Chromium		Chlorine		Cobalt		pH	Overall Corrosion Rate of Nickel (mpy)
			Conc (mg/ml)	Total (g)	Conc (mg/ml)	Total (g)	Conc (mg/ml)	Total (g)	Conc (μg/ml)	Total (mg)	Conc (μg/ml)	Total (mg)	Conc (μg/ml)	Total (mg)	Conc (μg/ml)	Total (mg)	Conc (μg/ml)	Total (mg)		
3% TSP, He, 100°C	4.5	1300							<1	1	3	4	<1	1						
5% HNO_3, He, 100°C	12.0	1300							17	22	65	85	7	9	<1	1	2	3		
H_2O, O_2, 250°C	33.2	1300					<0.001	0.001	<1	1	<1	1	2	3	<1	1	2	3		
Natural-uranium UO_2SO_4, O_2, 250°C	41.7	1160	37.7	43.7	21.8	25.3	1.98	2.30	103	120	18	21	7	8	4	5	<1	1	1.3	3.1
Natural-uranium UO_2SO_4, O_2, 250°C	63.3	1160	39.0	45.2			1.98	2.30	53	62	6	7	24	28	4	5	9	10	1.3	1.1

[a] Constituent concentrations and totals shown are not cumulative but represent the quantities present for operation with each solution.

Table 10. Analyses of Samples from Loop Inventory and Overall Corrosion Rates During Preparatory Operations,[a] Experiment L-4-12

Solution	Total Circulation Time for Each Solution (hr)	Inventory at Time of Sampling (ml)	Uranium		Sulfate		Copper		Nickel		Iron		Chromium		Chlorine		pH	Overall Corrosion Rate of Nickel (mpy)
			Conc (mg/ml)	Total (g)	Conc (mg/ml)	Total (g)	Conc (mg/ml)	Total (g)	Conc (μg/ml)	Total (mg)	Conc (μg/ml)	Total (mg)	Conc (μg/ml)	Total (mg)	Conc (μg/ml)	Total (mg)		
First pretreatment																		
3% TSP + He, 100°C	6.1	1340					0.003	0.004	2	3	4	5	<1	<1	<2	<2	11.6	
5% HNO_3 + He, 100°C	13.0	1300					0.006	0.008	5	7	57	7	3	4	<2	<2	0.2	
H_2O, 250–280°C	6.6	1125					0.001	0.001	<1	<1	<1	<1	<1	<1	<2	<2	4.4	
$H_2O + O_2$, 250–280°C	27.4	1130					0.001	0.001	2	2	<1	<1	1	1	<2	<2	4.1	
0.17 *m* UO_2SO_4 (natural) + 0.03 *m* $CuSO_4$ + 0.04 *m* H_2SO_4 + O_2, 250–280°C — 1st run	50.6	1112	37.9	42.1	21.8	24.2	1.82	2.02	135	150	9	10	27	30	<2	<2	1.3	3.3
0.17 *m* UO_2SO_4 (natural) + 0.03 *m* $CuSO_4$ + 0.04 *m* H_2SO_4 + O_2, 250–280°C — 2d run[b]	52.0	1112	33.2	36.9	21.9	24.4	2.05	2.28	109	121	6	7	25	28	<2	<2	1.3	2.6
Second pretreatment[c]																		
$H_2O + O_2$, 250–280°C	6.4	1125	<0.01	<0.01	<0.01	<0.01	<0.001	<0.001	<1	<1	<1	<1	6	7	<2	<2	3.9	
$H_2O + O_2$, 250–280°C	6.3	1115	<0.01	<0.01	<0.01	<0.01	<0.001	<0.001	<1	<1	<1	<1	4	4	<2	<2	4.1	
$H_2O + O_2$, 250–280°C	3.7	1125	<0.01	<0.01	<0.01	<0.01	<0.001	<0.001	1	1	<1	<1	2	2	<3	<3	3.9	
0.17 *m* UO_2SO_4 (natural) + 0.03 *m* $CuSO_4$ + 0.04 *m* H_2SO_4 + O_2, 250–280°C — 1st run	36.5	1110	37.9	42.1	21.8	24.2	1.91	2.12	61	68	2	2	19	21	<2	<2	1.3	2.1
0.17 *m* UO_2SO_4 (natural) + 0.03 *m* $CuSO_4$ + 0.04 *m* H_2SO_4 + O_2, 250–280°C — 2d run[d]	50.5	1115	38.4	42.8	22.3	24.9	1.84	2.05	21	23	14	16	19	21	<2	<2	1.3	0.5

[a] Constituent concentrations and totals shown are not cumulative but represent the quantities present for operation with each solution.

[b] The same solution was used throughout the 102.6-hr, UO_2SO_4 run.

[c] Leak developed in loop in out-of-pile operation: loop was repaired and given 2d pretreatment.

[d] Fresh solution added for 2d run.

Table 11. Analyses of Samples from Loop Inventory and Overall Corrosion Rates During Preparatory Operations,[a] Experiment L-4-13

Solution	Total Circulation Time for Each Solution (hr)	Inventory at Time of Sampling (ml)	Uranium		Sulfate		Copper		Nickel		Iron		Chromium		Chlorine		pH	Overall Corrosion Rate (mpy)	
			Conc (mg/ml)	Total (g)	Conc (mg/ml)	Total (g)	Conc (mg/ml)	Total (g)	Conc (μg/ml)	Total (mg)	Conc (μg/ml)	Total (mg)	Conc (μg/ml)	Total (mg)	Conc (μg/ml)	Total (mg)		Ni	O_2
3% TSP + He, 100°C																			
Original solution							1		<1		<1		<1		<1		11.4		
Final sample	4.7	1200					<1	1.2	1	1.2	12	14	<1	1.2	7	8	11.4		
5% HNO_3 + He, 100°C																			
Original solution							<1		<1		<1		<1		<1		0.7		
Final sample	24.5	1300					5	7	16	21	157	204	14	18	<1	<2	0.4		
H_2O, 250–280°C	9.8	1100							<1	1.1	<1	1.1	<1	1.1	<1	1.1	6.4		
$H_2O + O_2$, 250–280°C	27.2	1100					1	1.1	1	1.1	<1	1.1	1	1.1	<2	2.2	4.5		
0.17 *m* UO_2SO_4 + 0.04 *m* H_2SO_4 + 0.03 *m* $CuSO_4$ + O_2, 250–280°C[b]																			
Original solution "A"			37.0		21.4		1.94		<1		4		<1		8		1.4		
Sample 1	1.8		36.6						28		10								
Sample 2	14.3						2.04		60		26		19		4		1.3		
Sample 3	28.3		36.3		21.4		2.00		80		37		19		4		1.3		
Sample 4	38.8		37.5		22.6		1.95		83		40		22		7		1.45		
Sample 5	48.3		37.5		22.1		1.81		96		38		22		7		1.5		
Sample 6 (final)	62.9	1098	37.0	40.6	21.9	24.1	1.73	1.89	108	119	42	46	25	28	5	6	1.5	2.5	2.5[d]
H_2O rinse																			
0.17 *m* UO_2SO_4 + 0.04 *m* H_2SO_4 + 0.03 *m* $CuSO_4$ + O_2, 250–280°C[b]																			
Sample 1 (final)	23.4	1098	31.6	34.7	18.1	19.9	1.43	1.57	108	119	72	79	18	20	2	2.2	1.7		
H_2O rinse	3.3		7.2		3.8		0.33		17		8		7		<2		1.9		
0.17 *m* UO_2SO_4 + 0.04 *m* H_2SO_4 + 0.03 *m* $CuSO_4$ + O_2, 250–280°C[c]																			
Original solution "B"			38.5		22.7		1.87		4		4		<1		4		1.5		
Sample 1	3.9		37.8		21.7		1.74		10		27		4		2		1.2		
Sample 2	13.6		37.7		20.9		1.73		20		15		16		5		1.25		
Sample 3	37.6		38.1		21.9		1.73		35		45		15		2		1.30		
Sample 4	61.6		37.2		21.3		1.68		51		42		25		2		1.25		
Sample 5 (final)	86.1	1098	37.5	41.2	21.8	23.9	1.76	1.93	56	62	36	40	23	25	<2	2.2	1.3	1.0	2.5[d]

[a] Constituent concentrations and totals shown are not cumulative but represent the quantities present for operation with each solution.

[b] The 23.4-hr run was a separate run using the solution drained from the 62.9-hr run plus 60 ml of fresh solution.

[c] Fresh solution.

[d] Average rate for both runs.

Table 12. Analyses of Samples from Loop Inventory and Overall Corrosion Rates During Preparatory Operations,[a] Experiment L-4-18

Solution	Total Circulation Time for Each Solution (hr)	Inventory at Time of Sampling (ml)	Uranium		Sulfate		Copper		Nickel		Iron		Chromium		Chlorine		pH	Overall Corrosion Rate (mpy)	
			Conc (mg/ml)	Total (g)	Conc (mg/ml)	Total (g)	Conc (μg/ml)	Total (mg)	Conc (μg/ml)	Total (mg)	Conc (μg/ml)	Total (mg)	Conc (μg/ml)	Total (mg)	Conc (μg/ml)	Total (mg)		Ni	O_2
3% TSP + He, 95°C	4.5	1250							<1	1.3	8	10	<1	1	2	3	11.5		
5% HNO_3 + He, 95°C	23.8	1250							12	15.0	106	133	9	11	5	8	0.4		
H_2O, 235–275°C	12.0	1127							<1	1.1	<1	1	<1	1	<2	2	7.0		
H_2O, O_2, 235–275°C	25.1	1115							<1	1.1	<1	1	<1	1	<1	1	4.7		
H_2O, 235–275°C	5.3	1115							<1	1.1	<1	1	<1	1	8	9	6.2		
0.17 *m* UO_2SO_4 + O_2, 235–275°C; 0.10 *m* $CuSO_4$ + O_2, 235–275°C; 0.025 *m* H_2SO_4 + O_2, 235–275°C	107.2	1115	38.7	43.2	27.3	30.5	602	671.2	140	156	223	248	58	65	<2	2	1.6	1.9	3.6
0.17 *m* UO_2SO_4 + O_2, 235–275°C; 0.10 *m* $CuSO_4$ + O_2, 235–275°C; 0.025 *m* H_2SO_4 + O_2, 235–275°C	53.6	1115	39.4	43.9	26.9	30.0	614	684	16	18	98	109	32	36	2	2	1.5	0.4	0.2

[a]Constituent concentrations and totals shown are not cumulative but represent the quantities present for operation with each solution.

Table 13. Analyses of Samples From Loop Inventory During Enriched-Solution Operation,[a] Loop DD

Sample	Total Circulation Time (hr)	Accumulated LITR Energy (Mwhr)	Inventory Volume at Time of Sample, 25°C (ml)	Sample Dilution Factor[b]	Uranium		Sulfate			Copper			Chromium		Nickel		Chlorine		Iron		Cobalt		Manganese		pH	H_2SO_4[b] (*m*)
					Rep (mg/ml)	Calcd[c] (mg/ml)	Rep (mg/ml)	Cor[d] (mg/ml)	Calcd[e] (mg/ml)	Rep (mg/ml)	Cor[d] (mg/ml)	Calcd[e] (mg/ml)	Rep (mg/ml)	Calcd Total[f] (g)	Rep (mg/ml)	Calcd Total[g] (g)	Rep (mg/ml)	Calcd Total[g] (g)	Rep (mg/ml)	Calcd Total[f] (g)	Rep (mg/ml)	Calcd Total[g] (g)	Rep (mg/ml)	Calcd Total[g] (g)		
Original solution			1059		38.7		20.4			1.92			0.104		ND		<0.001		ND		ND		<0.002		1.80	
Makeup solution (H_2O only)																										
DD-1-29	2.4	0	1059	1.07	36.1	38.7	20.6	22.0	20.4	1.77	1.89	1.92	0.073	0.083	ND	0	0.001	0.001	ND	0	ND	0	0.016	0.017	2.00	0.011
DD-1-30	12.7	0	1047	1.24	31.0	38.6	17.0	21.1	20.3	1.52	1.88	1.91	0.059	0.077	ND	0	0.001	0.001	ND	0	ND	0	0.012	0.015	2.25	0.007
DD-1-31	23.2	0	1032	1.13	33.9	38.6	19.7	22.3	20.2	1.82	2.06	1.90	0.057	0.066	ND	0	0.001	0.001	ND	0	ND	0	0.012	0.014	2.25	0.006
DD-1-31.5	29.4	0	1049	1.18	31.2	37.0	18.7	22.1	19.3	1.50	1.77	1.82	0.054	0.064	ND	0	0.001	0.001	ND	0	ND	0			2.00	0.012
DD-1-32	51.7	4.3	1048	1.10	33.3	36.8	18.8	20.7	19.2	1.61	1.77	1.81	0.046	0.053	ND	0	0.001	0.001	ND	0	ND	0	0.006	0.007	2.00	0.011
DD-1-33	72.6	19.6	1047	1.11	32.7	36.3	17.8	19.8	18.9	1.61	1.79	1.78	0.040	0.046	ND	0	0.001	0.001			ND	0			2.00	0.071
DD-1-34	95.4	49.0	1045	1.21	29.7	35.8	16.5	20.0	18.6	1.42	1.72	1.75	0.018	0.023	ND	0	0.001	0.001			ND	0			2.10	0.010
DD-1-35	120.2	90.3	1044	1.30	26.9	35.1	17.0	22.1	18.2	1.43	1.86	1.72	0.003	0.004	0.079	0.107	0.001	0.001			ND	0			2.05	0.012
DD-1-36	192.9	246.5	1042	1.13	30.8	34.7	15.7	17.7	17.9	1.38	1.56	1.69	0.015	0.018	0.143	0.169	0.001	0.001	0.023	0.027	0.087	0.100			2.20	0.007
DD-1-37	289.0	482.0	1042	1.15	29.7	34.2	16.6	19.1	17.6	1.42	1.63	1.66	0.015	0.018	0.277	0.332	0.001	0.001	0.017	0.020	0.142	0.170			2.60	
DD-1-38	435.5	840.0	1039	1.23	27.3	33.6	16.2	19.9	17.3	1.41	1.73	1.64	0.017	0.022	0.368	0.472	<0.001	0.001	0.018	0.023	0.121	0.160			2.60	
DD-1-39	465.5	840.0	1037	1.03	32.1	33.2	17.9	18.4	17.0	1.55	1.60	1.62	0.042	0.045	0.410	0.439	<0.001	0.001	0.028	0.030	0.119	0.140			2.65	

[a]Where no values are given, either an analysis was not requested or the analytical results were not reliable. ND, not detected.

[b]$\frac{\text{(Calculated uranium concentration)}}{\text{(Reported uranium concentration)}}$ (Li_2SO_4 tracer not used).

[c]Determined from calculated uranium and inventory balance.

[d](Reported concentration) × (dilution factor).

[e]Determined from calculated sulfate or copper and inventory balance.

[f](Reported concentration) × (dilution factor) × (inventory volume).

[g](Reported concentration corrected for sample dilution and amounts withdrawn in previous samples) × (inventory volume).

[h]Determined from pH and sample dilution factor.

Table 14. Analyses of Samples from Loop Inventory During Enriched-Solution Operations,[a] Loop EE

Sample	Total Circulation Time (hr)	Accumulated LITR Energy (Mwhr)	Elapsed Time from LITR Shutdown to Sampling (hr)	Inventory Volume at Time of Sampling, 25°C (ml)	Sample[b] Dilution Factor	Uranium			Sulfate			Copper			Cobalt		Nickel		Chlorine		Chromium		Iron		Zirconium		Manganese		Titanium		pH	H_2SO_4[j] (m)
						Rep (mg/ml)	Cor[c] (mg/ml)	Calcd[d] (mg/ml)	Rep (mg/ml)	Cor[e] (mg/ml)	Calcd[f] (mg/ml)	Rep (mg/ml)	Cor[c] (mg/ml)	Calcd[g] (mg/ml)	Rep (mg/ml)	Calcd Total[h] (g)	Rep (mg/ml)	Calcd Total[h] (g)	Rep (mg/ml)	Calcd Total[i] (g)	Cor[c] (mg/ml)	Calcd Total[i] (g)	Cor[c] (mg/ml)	Calcd Total[i] (g)	Cor[c] (mg/ml)	Calcd Total[i] (g)	Rep (mg/ml)	Calcd Total[h] (g)	Rep (mg/ml)	Calcd Total[i] (g)		
EE-1-90[k]	0	0	0		1.00	38.6	38.6	38.6	20.9	20.9	20.9	1.76	1.76	1.76	ND[l]	0	ND	0	ND	0	ND	0	ND	0	ND	0	ND	0	ND	0	1.70	0.020
EE-1-91[m]	0	0	0		1.00	38.3	38.3	38.3	24.3	24.3	24.3	1.67	1.67	1.67	ND	0	ND	0	ND	0	ND	0	ND	0	ND	0	ND	0	ND	0	1.30	0.050
EE-1-92[n]	33.3	0	0	1057	1.20	36.4	43.7	38.5	17.5	19.6	20.8	1.47	1.75	1.75	ND	0	ND	0	ND	0	ND	0	(ND)	0	ND	0	ND	0	ND	0	1.75	0.021
Reactor started up	36.0	0																														
EE-1-93	54.8	56.0	0	1058	1.12	36.5	40.9	38.5	18.1	19.5	20.9	1.52	1.70	1.75	ND	0	0.006	0.01	ND	0	ND	0	0.011	0.01	ND	0	ND	0	ND	0	1.95	0.012
EE-1-94[n]	76.3	107.4	1.8	1059	1.14	34.6	39.4	38.5	18.4	20.1	20.9	1.43	1.63	1.75	ND	0	0.053	0.06	ND	0	ND	0	ND	0	0.040	0.05	ND	0	ND	0	2.05	0.023
EE-1-95	148.1	298.6	0	1057	1.17	34.8	40.7	38.5	18.4	20.3	21.0	1.47	1.71	1.75	ND	0	0.118	0.15	ND	0	ND	0	0.010	0.01	0.020	0.02	ND	0	ND	0	2.05	0.024
EE-1-96[n]	172.6	358.3	2.1	1056	1.10	36.2	39.8	38.5	17.9	19.1	21.0	1.59	1.75	1.75	ND	0	0.144	0.17	ND	0	0.015	0.017	0.011	0.13	0.027	0.03	ND	0	0.005	0.01	1.90	0.014
EE-1-97	196.7	428.3	0	1055	1.12	33.3	37.3	38.5	19.0	20.6	21.1	1.43	1.59	1.75	ND	0	0.179	0.22	ND	0	ND	0	0.013	0.02	0.034	0.04	ND	0	ND	0	2.00	0.011
EE-1-98	244.6	562.8	0	1055	1.24	31.3	38.8	38.5	17.1	19.5	21.2	1.33	1.65	1.75	ND	0	0.189	0.27	ND	0	0.008	0.011	0.065	0.08	0.045	0.06	0.032	0.04	0.049	0.06	2.05	0.025
EE-1-99	316.6	766.7	0	1057	1.19	34.2	40.7	38.4	18.4	20.6	21.3	1.52	1.80	1.75	ND	0	0.371	0.50	ND	0	ND	0	0.003	0.01	ND	0	0.037	0.05	ND	0	2.05	0.024
EE-1-100	364.3	870.1	0	1058	1.18	34.5	40.7	38.4	18.7	20.8	21.5	1.36	1.60	1.75	ND	0	0.307	0.44	ND	0	ND	0	0.008	0.01	0.019	0.02	0.031	0.04	0.040	0.05	2.00	0.012
EE-1-101	412.4	1003.8	0	1058	1.21	32.2	39.0	38.4	18.6	21.1	21.5	1.59	1.93	1.75	ND	0	0.333	0.49	ND	0	ND	0	0.005	0.01	0.006	0.01	0.037	0.05	ND	0	2.10	0.010
EE-1-102[n]	484.4	1211.5	1.9	1058	1.22	31.2	38.1	38.4	18.1	20.6	21.5	1.59	1.94	1.75	ND	0	0.261	0.41	ND	0	ND	0	0.011	0.01	0.055	0.07	0.045	0.06	ND	0	2.10	0.010
EE-1-103	532.2	1334.2	0	1058	1.16	33.0	38.3	38.4	18.9	20.9	21.6	1.41	1.63	1.75	ND	0	0.364	0.53	ND	0	0.002	0.002	0.016	0.02	0.054	0.07	0.043	0.06	ND	0	1.95	0.013
EE-1-104	580.5	1463.8	0	1059	1.14	30.6	34.9	38.4	19.4	21.1	21.6	4.19	4.76	1.75	ND	0	0.469	0.65	ND	0	ND	0	0.015	0.02	0.031	0.04	0.051	0.07	ND	0	2.00	0.011
Reactor down	630.2	1610.4		1057				38.4			21.6																					
Circulation pump down	630.3	1610.4		1057				38.4			21.6																					

[a]Where no values are given, either an analysis was not requested or the analytical results were not reliable.
[b]Dilution factors calculated on lithium concentration found in sample.
[c](Reported concentration) × (dilution factor).
[d]Determined from calculated uranium and inventory balance.
[e](Reported concentration) × (dilution factor, corrected for SO_4^{2-} from Li_2SO_4).
[f]Determined from calculated sulfate and inventory balance.
[g]$\frac{\text{(Original concentration)} \times \text{(calculated uranium concentration at time of sample)}}{\text{Original uranium concentration}}$
[h]Corrected for sample dilution and for amounts withdrawn in previous samples.
[i]From calculated inventory and from concentration corrected for sample dilution.
[j]Determined from pH dilution factor.
[k]Original solution.
[l]ND, not detected.
[m]Makeup solution.
[n]Taken with reactor down.

Table 15. Analyses of Samples from Loop Inventory During Enriched-Solution Operations,[a] Loop FF

Sample	Total Circulation Time (hr)	Accumulated LITR Energy (Mwhr)	Elapsed Time from LITR Shutdown to Sample (hr)	Inventory Volume (25°C) at Time of Sample (ml)	Sample[b] Dilution Factor	Uranium Rep (mg/ml)	Uranium Calcd[c] (mg/ml)	Sulfate Rep (mg/ml)	Sulfate Cor[d] (mg/ml)	Sulfate Calcd[e] (mg/ml)	Copper Rep (mg/ml)	Copper Cor[d] (mg/ml)	Copper Calcd[e] (mg/ml)	Cobalt Rep (mg/ml)	Cobalt Calcd Total[f] (g)	Nickel Rep (mg/ml)	Nickel Calcd Total[f] (g)	Chlorine Rep (mg/ml)	Chlorine Calcd Total[g] (g)	Chromium Cor[d] (mg/ml)	Chromium Calcd Total[g] (g)	Iron Cor[d] (mg/ml)	Iron Calcd Total[g] (g)	Zirconium Cor[d] (mg/ml)	Zirconium Calcd Total[g] (g)	pH	H_2SO_4[b] (m)
Original solution																											
FF-1-42, FF-1-43	0	0	0	1170	1.0	40.0 G	40.0	25.2 IE	25.2	25.2	1.79 P	1.79	1.79	ND C	0	ND C	0	<0.001 T	<0.002	0.025 C	0.03	ND C	0	ND C	0	1.3	0.050
Y-12 operation																											
FF-1-40	1.5	0	0	1186	0.99	40.0 T	39.4	25.1 IE	24.8	24.8	1.87 P	1.85	1.76	ND C	0	ND C	0	<0.001 T	<0.002	0.004 C	0.01	ND C	0	ND C	0	1.45	0.035
FF-1-41	20.8	0	0	1151	0.99	39.9 T	39.4	23.4 IE	23.2	24.8	1.84 P	1.82	1.76	ND C	0	0.016 C	0.02	0.005 T	0.006	0.019 C	0.02	0.011 C	0.01	ND C	0	1.3	0.050
Pump[i] shut down	23.1	0																									
X-10 operation[j]	30.8	0																									
FF-1-44 (a)	67.8	99.0	2.9	1142	1.00	39.4 T	39.4	23.9 IE	23.9	24.8	1.75 P	1.75	1.76	0.016 T	0.019	0.178 P	0.20	0.005 T	0.007	0.030 C	0.03	0.092 C	0.11	0.072 C	0.08	1.55	0.028
(b)	71.1	99.0	6.2	1121	1.03	38.3 T	39.4	22.6 IE	23.3	24.8	1.73 P	1.79	1.76	0.013 T	0.015	0.168 P	0.20	0.004 T	0.005	0.014 C	0.02	0.095 C	0.11	0.061 C	0.07	1.55	0.029
FF-1-45 (a)	161.2	357.2	1.3	1054	1.11	35.6 T	39.4	21.7 IE	24.1	24.8	1.76 P	1.96	1.76	0.133 T	0.157	0.520 P	0.62	0.003 T	0.004	0.017 C	0.02	0.033 C	0.04	0.139 C	0.15	1.65	0.024
(b)	163.4	357.2	3.5	1043	1.09	36.2 T	39.4	23.4 IE	25.5	24.8	1.81 P	1.97	1.76	0.021 T	0.026	0.579 P	0.68	0.005 T	0.006	0.007 C	0.01	0.058 C	0.06	0.065 C	0.07	1.65	0.024
FF-1-46 (a)	234.4	536.5	2.5	1051	1.23	32.0 T	39.3	21.5 IE	26.5	24.8	1.60 P	1.96	1.76	0.021 T	0.028	0.581 P	0.78	0.004 T	0.006	0.011 C	0.01	0.085 C	0.09	0.076 C	0.08	1.70	0.025
(b)	236.4	536.5	4.5	1038	1.21	32.6 T	39.3	24.4 IE	29.5	24.8	1.84 P	2.22	1.76	0.019 T	0.024	0.451 P	0.61	0.004 T	0.006	0.007 C	0.01	0.068 C	0.07	0.053 C	0.06	1.75	0.021
FF-1-47 (a)	330.1	543.3	86.1	1047	1.12	35.0 T	39.3	21.8 IE	24.4	24.8	1.74 P	1.95	1.76	0.022 T	0.027	0.660 P	0.82	0.014 T	0.005	0.047 C	0.05	0.041 C	0.04	0.047 C	0.05	1.50	0.035
(b)	332.0	543.3	88.0	1034	1.20	32.7 T	39.3	21.9 IE	26.3	24.8	1.64 P	1.97	1.76	0.020 T	0.029	0.648 P	0.86	0.004 T	0.006	0.070 C	0.07	0.050 C	0.05	0.058 C	0.06	1.75	0.021
FF-1-48 (a)	401.6	689.8	1.2	1054	1.17	33.5 T	39.3	22.2 IE	26.0	24.8	1.71 P	2.00	1.76	0.025 T	0.035	0.855 P	1.12	0.006 T	0.008	0.025 C	0.03	0.034 C	0.04	0.036 C	0.04	1.70	0.023
(b)	403.6	689.8	3.2	1041	1.23	31.9 T	39.3	23.5 IE	28.9	24.8	1.67 P	2.05	1.76	0.026 T	0.038	0.800 P	1.11	0.006 T	0.009	0.025 C	0.03	0.043 C	0.05	0.043 C	0.05	1.70	0.025
FF-1-49 (a)	497.3	943.8	0.9	1053	1.23	31.9 T	39.3	22.0 IE	27.0	24.8	1.55 P	1.90	1.76			0.928 P	1.30	0.006 T	0.009	0.012 C	0.01	0.032 C	0.03	0.082 C	0.09	1.88	0.016
(b)	498.8	943.8	2.4	1041	1.27	30.9 T	39.3	21.0 IE	26.6	24.8	1.61 P	2.04	1.76	0.022 T	0.035	0.078 P	1.27	0.006 T	0.009	0.023 C	0.02	0.034 C	0.04	0.041 C	0.04	1.88	0.017
FF-1-50 (a)	572.1	1084.4	15.1	1052	1.14	34.6 T	39.3	20.0 IE	22.8	24.8	1.75 P	1.99	1.76	0.034 T	0.047	0.820 P	1.11	0.006 T	0.009	0.046 C	0.05	0.050 C	0.05	0.023 C	0.02	1.80	0.018
(b)	575.5	1084.4	18.5	1039	1.16	34.0 T	39.3	24.0 IE	27.8	24.8	1.86 P	2.16	1.76	0.017 T	0.027	0.729 P	1.02	0.005 T	0.007	0.046 C	0.05	0.035 C	0.04	0.022 C	0.02	1.80	0.018
FF-1-52[k]	687.9	1401.2	0	1050	1.05	37.4 T	39.3	24.3 IE	25.5	24.8	1.80 P	1.90	1.76			0.818 P	1.05	0.006 T	0.008	0.013 C	0.01	0.028 C	0.03	0.029 C	0.03	1.90	0.013
FF-1-53	692.3	1401.2	3.5	1038	1.08	36.4 T	39.3	22.8 IE	24.7	24.8	1.72 P	1.85	1.76			0.802 P	1.06	0.005 T	0.007	0.025 C	0.03	0.029 C	0.03	0.041 C	0.04	1.90	0.014

[a] Where no values are given, either an analysis was not requested or the analytical results were not reliable.

G Gravimetric; P Polarographic; C Colorimetric; S Spectrographic; IE Ion exchange, volumetric; ND Not detected; T Titrimetric

[b] $\frac{\text{(Original uranium concentration)}}{\text{(Reported uranium concentration at time of sample)}}$

[c] Determined from calculated uranium and inventory balance.

[d] (Reported concentration) × (dilution factor).

[e] $\frac{\text{(Original concentration)} \times \text{(calculated uranium concentration at time of sample)}}{\text{(Original uranium concentration)}}$

[f] Corrected for sample dilution and for amounts withdrawn in previous samples.

[g] From calculated inventory and from concentration corrected for sample dilution.

[h] Determined from pH and sample dilution factor.

[i] Loop inoperative about 170 hr between shutdown at Y-12 and startup at X-10. (Inventory was not removed from loop during this period.)

[j] Started reactor at 3 Mw.

[k] Taken with reactor on.

Table 16. Analyses of Samples from Loop Inventory During Enriched-Solution Operation,[a] Loop GG

Sample	Total Circulation Time (hr)	Accumulated LITR Energy (Mwhr)	Inventory Volume at Time of Sample, 25°C (ml)	Lithium (mg/ml)	Sample Dilution Factor[b]	Uranium			Sulfate			Copper			Chromium		Nickel		Chlorine		Iron		Zirconium		Manganese		pH	H_2SO_4[i] (m)
						Rep (mg/ml)	Cor[d] (mg/ml)	Calcd[c] (mg/ml)	Rep (mg/ml)	Cor[d] (mg/ml)	Calcd[e] (mg/ml)	Rep (mg/ml)	Cor[f] (mg/ml)	Calcd[e] (mg/ml)	Rep (mg/ml)	Calcd Total[g] (g)	Rep (mg/ml)	Calcd Total[h] (g)	Rep (mg/ml)	Calcd Total[h] (g)	Rep (mg/ml)	Calcd Total[g] (g)	Rep (mg/ml)	Calcd Total[g] (g)	Rep (mg/ml)	Calcd Total[h] (g)		
Original charge																												
GG-1-60	0	0	1039			39.8			23.5			1.75			0.320		ND		ND		ND		ND				1.25	0.056
Makeup solution																												
GG-1-61	0	0				39.4			23.5			1.81			0.482		ND		ND		ND		ND				1.25	0.056
GG-1-62[j]	45.2	0	1039		1.14	34.9		39.8	22.7	25.8	23.5	1.74	1.99	1.75	0.182	0.216	ND	0	ND	0	ND	0	ND	0			1.30	0.057
GG-1-63[j]	47.2	0	1015		1.10	36.1		39.8	22.0	24.2	23.5	1.63	1.79	1.75	0.133	0.149	ND	0	ND	0	ND	0	ND	0			1.30	0.055
GG-1-64	77.8	5.2	1035		0.98	40.8		39.8	23.4	22.9	23.5	1.94	1.90	1.75	0.089	0.090	0.058	0.06	<0.001	<0.001	0.024	0.02	0.039	0.04			1.30	0.049
GG-1-65	80.1	12.2	1016		0.97	40.9		39.8	23.2	22.5	23.5	1.78	1.72	1.75	0.053	0.052	0.103	0.10	<0.001	<0.001	0.032	0.03	0.037	0.04			1.30	0.049
GG-1-66	83.1	21.4	1001		1.10	36.3		39.8	21.4	23.6	23.5	1.68	1.85	1.75	0.035	0.039	0.082	0.09	<0.001	<0.001	0.018	0.02	0.042	0.05			1.45	0.039
GG-1-67	85.3	27.9	986		1.11	35.7		39.8	21.4	23.7	23.5	1.57	1.75	1.75	0.038	0.042	0.091	0.10	<0.001	<0.001	0.023	0.03	0.037	0.04			1.50	0.036
GG-1-68	98.6	67.6	1033		1.22	32.7		39.8	20.9	25.5	23.5	1.72	2.10	1.75	0.032	0.040	0.188	0.24	<0.001	<0.001	0.012	0.02	0.029	0.04			1.50	0.039
GG-1-69	120.6	120.6	1032		1.19	33.3		39.8	22.9	27.2	23.5	1.55	1.84	1.74	0.028	0.034	0.263	0.33	<0.001	<0.001	0.014	0.02	0.027	0.03			1.50	0.038
GG-1-70	169.2	253.6	1034		1.14	34.9		39.7	21.8	24.8	23.5	1.62	1.85	1.74	0.012	0.014	0.470	0.57	<0.001	<0.001	0.029	0.03	0.073	0.09			1.60	0.029
GG-1-71	190.8	309.2	1036		1.17	34.2		39.7	20.0	23.4	23.5	1.79	2.09	1.74	0.011	0.013	0.440	0.56	<0.001	<0.001	0.025	0.03	0.057	0.07			1.60	0.029
GG-1-72	239.5	427.5	1032		1.27	31.1		39.7	20.6	26.1	23.5	1.46	1.86	1.74	0.001	0.001	0.746	1.01	<0.001	<0.001	0.014	0.02	0.043	0.06			1.60	0.032
GG-1-73	269.7	518.1	1032		1.12	35.5		39.7	21.6	24.2	23.5	1.41	1.58	1.74	0.001	0.001	0.520	0.66	<0.001	<0.001	0.027	0.03	0.037	0.04			1.65	0.025
GG-1-74	337.3	719.8	1032		1.16	34.1		39.7	22.0	25.5	23.5	1.51	1.75	1.74	0.026	0.031	0.854	1.09	<0.001	<0.001	0.005	0.01	0.033	0.04			1.70	0.023
GG-1-75[j]	365.3	774.7	1034		1.20	33.1		39.6	22.9	27.5	23.4	1.79	2.15	1.74	0.025	0.031	0.684	0.93	<0.001	<0.001	0.005	0.01	0.032	0.04			1.70	0.024
GG-1-76	433.1	949.6	1037		1.24	31.9		39.6	20.9	25.9	23.4	1.39	1.72	1.73	0.005	0.006	0.698	1.00	<0.001	<0.001	0.007	0.01	0.017	0.02			1.70	0.025
GG-1-77	504.9	1156.6	1038		1.19	33.4		39.5	21.8	25.9	23.4	1.35	1.60	1.73	0.006	0.007	0.791	1.10	<0.001	<0.001	0.017	0.02	0.031	0.04			1.70	0.024
GG-1-78[b]	553.0	1289.3	1040		1.28	30.8		39.5	20.4	26.1	23.4	1.52	1.94	1.73	0.001	0.001	0.984	1.45	<0.001	<0.001	0.015	0.02	0.040	0.05			1.70	0.026
GG-1-79[k]	603.5	1567.8	1037	0.79	1.09	34.9	38.0	39.5	28.6	25.2	23.4	1.44	1.57	1.73	0.010	0.011	0.905	1.18	<0.001	<0.001	0.020	0.02	0.028	0.03			1.70	0.022
GG-1-80[k]	678.4	1638.0	1034	1.24	1.15	33.6	38.6	39.5	30.9	25.7	23.4	1.41	1.62	1.73	0.005	0.006	0.833	1.17	<0.001	<0.001	0.017	0.02	0.020	0.02			1.75	0.020
GG-1-81[k]	721.0	1802.2	1034	1.84	1.24	30.6	37.9	39.5	35.0	27.6	23.4	1.34	1.66	1.73	0.001	0.001	0.939	1.40	<0.001	<0.001	0.021	0.03	0.050	0.06			1.85	0.017
GG-1-82[k]	769.0	1949.2	1033	1.78	1.23	33.8	41.6	39.5	33.4	25.9	23.4	1.32	1.62	1.73	0.001	0.001	1.046	1.55	<0.001	<0.001	0.021	0.03	0.030	0.04			1.88	0.016
GG-1-83[k]	842.5	2155.9	1034	1.36	1.17	33.3	39.0	39.5	30.2	24.3	23.4	1.39	1.62	1.73	0.005	0.001	0.749	1.15	<0.001	<0.001	0.021	0.03	0.034	0.04	0.151	0.18	2.15	0.008
GG-1-84[k]	894.2	2268.0	1035	1.86	1.24	30.4	37.7	39.5	34.5	26.7	23.4	1.34	1.66	1.73	0.001	0.001	0.923	1.45	<0.001	<0.001	0.018	0.02	0.033	0.04	0.182	0.24	1.95	0.014
GG-1-85[l]	936.6	2394.1	1034	0.28	1.42	29.6	42.0	39.5	23.8	31.1	23.4	1.35	1.91	1.73	0.001	0.001	0.929	1.65	<0.001	<0.001	0.049	0.07	0.032	0.05	0.140	0.21	2.00	0.014
GG-1-86[l]	1009.5	2579.6	1036	0.15	1.19	38.9	46.3	39.5	22.9	26.0	23.4	1.41	1.68	1.73	0.001	0.001	0.954	1.49	<0.001	<0.001	0.014	0.02	0.020	0.03	0.133	0.18	1.90	0.015
GG-1-87[l]	1057.8	2676.4	1035	0.13	1.16	34.4	39.9	39.5	22.7	25.3	23.4	1.51	1.76	1.73	0.001	0.001	1.572	1.64	<0.001	<0.001	0.015	0.02	0.031	0.04	0.168	0.22	1.70	0.023
End of run	1063.7	2692.3	1035																									

[a]Where no values are given, either an analysis was not requested or the analytical results were not reliable. ND, not detected

[b]Dilution factors calculated through sample GG-1-78 on uranium basis; balance calculated on lithium concentration found in sample.

[c]Determined from calculated uranium and inventory balance.

[d](Reported concentration) × (dilution factor); samples GG-1-79 to GG-1-87 corrected for SO_4 from Li_2SO_4.

[e](Original concentration) × (calculated uranium concentration)/(original uranium concentration).

[f](Reported concentration) × (dilution factor).

[g](Reported concentration) × (dilution factor) × (inventory volume).

[h](Reported concentration corrected for sample dilution and amounts withdrawn in previous samples) × (inventory volume).

[i]Determined from pH and dilution factor.

[j]Sample taken with reactor down.

[k]Wash water contained Li_2SO_4 at 0.688 *M*.

[l]Wash water contained Li_2SO_4 at 0.068 *M*.

Table 17. Analyses of Samples from Loop Inventory During Enriched-Solution Operation,[a] Loop L-4-12

Sample	Total Circulation Time (hr)	Accumulated LITR Energy (Mwhr)	Inventory Volume at Time of Sample, 25°C (ml)	Lithium[b] (mg/ml)	Sample Dilution Factor[c]	Uranium			Sulfate			Copper			Chromium		Nickel		Chlorine		Iron		Zirconium		Manganese		pH	H_2SO_4[i] (m)
						Rep (mg/ml)	Cor[d] (mg/ml)	Calcd[e] (mg/ml)	Rep (mg/ml)	Cor[d] (mg/ml)	Calcd[f] (mg/ml)	Rep (mg/ml)	Cor[d] (mg/ml)	Calcd[f] (mg/ml)	Cor[d] (mg/ml)	Calcd Total[g] (g)	Cor[d] (mg/ml)	Calcd Total[b] (g)	Cor[d] (mg/ml)	Calcd Total[b] (g)	Cor[d] (mg/ml)	Calcd Total[g] (g)	Cor[d] (mg/ml)	Calcd Total[g] (g)	Cor[d] (mg/ml)	Calcd Total[b] (g)		
Original and makeup solutions																												
L-4-12	0	0		0	1.0	39.9	39.9	39.9	24.6	24.6	24.6	2.02	2.02	2.02	0.003	0.003	0.008	0.01	ND	0	0.006	0.01	ND	0	ND	0	1.30	0.050
L-4-12-1[j]	84.9	0	1092	0	1.00	37.5	37.5	39.9	21.7	21.7	24.6	1.77	1.77	2.02	0.030	0.033	0.062	0.07	ND	0	0.002	0.002	ND	0	ND	0	1.55	0.029
L-4-12-2	143.0	55.0	1092	0.161	1.21	33.8	40.9	39.9	22.7	26.1	24.6	1.57	1.90	2.02	0.039	0.042	0.090	0.10	ND	0	0.051	0.06	0.054	0.06	ND	0	1.65	0.025
L-4-12-3	215.0	163.0	1092	0.157	1.20	33.5	40.3	39.9	21.7	24.8	24.6	1.75	2.10	2.02	0.004	0.004	0.158	0.17	ND	0	0.046	0.05	0.023	0.03	ND	0	1.60	0.030
L-4-12-4[j]	262.1	191.5	1093	0.157	1.20	32.8	39.5	39.8	21.8	26.1	24.5	1.48	1.78	2.01	0.066	0.072	0.202	0.23	ND	0	0.036	0.04	0.025	0.03	ND	0	1.60	0.030
L-4-12-5[j]	295.3	191.5	1092	0.133	1.17	34.6	40.3	39.8	21.4	23.9	24.5	1.88	2.20	2.01	0.090	0.098	0.231	0.26	ND	0	0.034	0.04	0.008	0.01	ND	0	1.55	0.033
L-4-12-6	311.0	229.2	1092	0.140	1.14	34.7	39.6	39.8	21.8	23.7	24.5	1.95	2.22	2.01	0.072	0.079	0.207	0.23	ND	0	0.043	0.05	0.024	0.03	0.023	0.03	1.50	0.036
L-4-12-7	383.3	442.3	1092	0.150	1.19	32.2	38.4	39.8	20.9	23.7	24.5	2.18	2.60	2.01	0.090	0.098	0.192	0.22	ND	0	0.024	0.03	0.021	0.02	0.031	0.03	1.60	0.030
L-4-12-8[j]	430.9	500.7	1092	0.164	1.21	33.5	40.7	39.8	23.6	27.2	24.5	1.99	2.42	2.01	0.124	0.135	0.304	0.34	ND	0	0.029	0.03	0.049	0.05	0.034	0.04	1.70	0.024
L-4-12-9[j,k]	479.9	623.9	1091	0.527	2.31	20.7		39.8			24.5	0.73		2.01														
L-4-12-10	598.6	921.1	1093	0.157	1.20	34.1	41.0	39.8	23.8	27.3	24.5	2.13	2.56	2.01	0.045	0.049	0.248	0.29	ND	0	0.028	0.03	0.052	0.06	0.024	0.03	1.60	0.030
L-4-12-11	648.2	1056.4	1092	0.160	1.21	34.8	42.1	39.8	23.1	26.6	24.5	1.96	2.36	2.01	0.053	0.058	0.350	0.40	ND	0	0.079	0.09	0.060	0.07	0.043	0.05	1.70	0.024
L-4-12-12	718.7	1259.3	1092	0.121	1.15	34.6	39.8	39.8	22.8	25.3	24.5	1.77	2.04	2.01	0.068	0.074	0.413	0.47	ND	0	0.046	0.05	0.046	0.05	0.044	0.05	1.55	0.032
2d Original and makeup solutions																												
L-4-12	0	0		0	1.0	39.2	39.2	39.2	24.6	24.6	24.6	1.73	1.73	1.73	ND	ND	0.001	0.001	ND	0	0.010	0.01	0.006	0.01	ND	0	1.60	0.025
L-4-12-13[j]	774.7	1310.2	1106	0.128	1.16	36.2	42.0	39.2	24.3	26.8	24.6	2.41	2.79	1.73	0.042	0.046	ND	0	ND	0	0.041	0.05	0.018	0.02	0.041	0.05	1.35	0.051
L-4-12-14[j]	831.0	1427.0	1093	0.124	1.15	37.6	43.4	39.2	24.1	26.4	24.6	2.86	3.30	1.73	0.042	0.046	0.358	0.39	ND	0	0.049	0.05	0.054	0.06	0.012	0.01	1.55	0.032
L-4-12-15	878.4	1519.5	1093	0.184	1.25	33.4	41.6	39.2	22.2	26.1	24.6	1.54	1.92	1.73	0.041	0.045	0.590	0.65	ND	0	0.057	0.06	0.030	0.03	ND	0	1.30	0.063
L-4-12-16	926.3	1654.7	1093	0.091	1.11	35.6	39.5	39.2	23.1	25.0	24.6	2.10	2.32	1.73	0.031	0.034	0.312	0.35	ND	0	0.059	0.07	0.027	0.03	ND	0	1.50	0.034
L-4-12-17	998.5	1864.5	1093	0.144	1.18	37.3	44.1	39.2	24.9	27.3	24.6	2.32	2.14	1.73	0.105	0.115	0.507	0.57	ND	0	0.071	0.08	0.043	0.05	ND	0	1.50	0.037
L-4-12-18	1046.0	1972.5	1093	0.125	1.16	37.2	43.0	39.2	23.6	26.3	24.6	1.84	2.13	1.73	0.004	0.004	0.509	0.57	ND	0	0.052	0.06	ND	0	0.043	0.05	1.65	0.026
L-4-12-19	1166.0	2263.4	1093	0.153	1.20	32.9	39.4	39.2	21.4	24.4	24.6	1.78	2.13	1.73	0.054	0.059	0.633	0.72	ND	0	0.046	0.05	0.126	0.14	0.049	0.05	1.70	0.024
L-4-12-20[j]	1214.3	2312.9	1093	0.122	1.15	38.3	44.1	39.2	24.3	27.1	24.6	1.73	1.99	1.73	0.085	0.093	0.525	0.61	ND	0	0.050	0.05	0.044	0.05	0.062	0.07	1.50	0.036
L-4-12-21	1262.0	2418.5	1093	0.131	1.16	36.2	42.2	39.2	23.8	26.7	24.6	1.71	1.99	1.73	0.022	0.024	0.371	0.44	ND	0	0.034	0.04	0.009	0.01	0.050	0.06	1.80	0.018
L-4-12-22	1334.0	2619.6	1093	0.128	1.16	34.3	39.8	39.2	22.3	24.9	24.6	1.54	1.79	1.73	0.010	0.011	0.593	0.69	ND	0	0.032	0.04	0.032	0.04	0.046	0.05	1.45	0.042
L-4-12-23	1382.3	2736.8	1093	0.160	1.21	34.9	42.2	39.2	22.5	26.2	24.6	1.76	2.12	1.73	0.039	0.043	0.556	0.65	ND	0	0.031	0.03	0.072	0.08	0.072	0.08	1.40	0.048
L-4-12-24	1503.0	3086.7	1093	0.014	1.02	39.5	40.0	39.2	24.8	25.7	24.6	1.88	1.90	1.73	0.066	0.072	0.653	0.77	ND	0	0.083	0.09	0.497	0.54	0.063	0.08	1.80	0.016
L-4-12-25	1720.4	3591.1	1094	0.030	1.03	39.6	41.0	39.1	25.1	25.8	24.5	2.13	2.20	1.73	0.047	0.051	0.814	0.95	ND	0	0.103	0.11	0.055	0.06	0.085	0.10	1.75	0.018
L-4-12-26	1838.7	3936.8	1093	0.017	1.02	40.8	41.5	39.1	23.9	24.2	24.5	1.91	1.94	1.73	0.111	0.121	0.759	0.90	ND	0	0.079	0.09	0.070	0.08	0.077	0.09	1.70	0.020
L-4-12-27	2006.7	4357.6	1093	0.016	1.02	40.6	41.5	39.1	24.3	24.7	24.5	1.80	1.83	1.73	0.071	0.078	0.794	0.94	ND	0	0.104	0.11	0.024	0.26	0.957	0.11	1.85	0.014
Reactor down	2012.7	4375.5																										
Pump stopped	2019.6	4375.5																										

[a]Where no values are given, either an analysis was not requested or the analytical results were not reliable. ND, not detected.
[b]Wash water contained Li_2SO_4 at 0.068 *M*
[c]Dilution factors calculated on lithium concentration found in sample.
[d](Reported concentration) × (dilution factor).
[e]Determined from calculated uranium and inventory balance.
[f](Original concentration) × (calculated uranium concentration)/(original uranium concentration).
[g](Reported concentration) × (dilution factor) × (inventory volume).
[h](Reported concentration corrected for sample dilution and amounts withdrawn in previous samples) × (inventory volume). Note: Calculated separately for both solutions.
[i]Determined from pH and dilution factor.
[j]Sample taken with reactor down.
[k]Reported values not corrected for dilution because of abnormally high lithium concentration.

Table 18. Analyses of Samples from Loop Inventory During Enriched-Solution Operation,[a] Loop L-4-13

Sample	Total Circulation Time (hr)	Accumulated LITR Energy (Mwhr)	Inventory Volume at Time of Sample, 25°C (ml)	Lithium[b] (mg/ml)	Sample Dilution Factor[b]	Uranium			Sulfate			Copper			Chromium		Nickel		Chlorine		Iron		Zirconium		Manganese		pH[j]	Fluorine Reported (mg/ml)	D_2SO_4 (M)		
						Rep (mg/ml)	Cor[c] (mg/ml)	Calcd[d] (mg/ml)	Rep (mg/ml)	Cor[e] (mg/ml)	Calcd[f] (mg/ml)	Rep (mg/ml)	Cor[c] (mg/ml)	Calcd[g] (mg/ml)	Rep (mg/ml)	Calcd Total[h] (g)	Rep (mg/ml)	Calcd Total[i] (g)	Rep (mg/ml)	Calcd Total[i] (g)	Rep (mg/ml)	Calcd Total[h] (g)	Rep (mg/ml)	Calcd Total[h] (g)	Rep (mg/ml)	Calcd Total[i] (g)			Rep	Cor[c]	Calcd[k]
Original charge	0	0	1097	ND		41.3			22.0			2.15			0.012		0.008		<0.001		0.030						1.40		0.020		
Makeup solution	0	0		ND		41.3			24.0			1.95			0.010		0.010		<0.001		0.024						1.05	0.003	0.044		
L-4-13-1[l]	71.5	0	1098	0.13	1.17	39.4	46.0	41.2	21.5	24.0	22.0	2.14	2.50	2.15			0.041	0.05			0.028	0.04					1.35				0.019
L-4-13-2	114.3	113.5	1099	0.08	1.09	36.3	39.5	41.2	20.0	21.2	22.0	1.70	1.85	2.15	0.072	0.086	0.101	0.12			0.155	0.19	0.125	0.15			1.70				0.018
L-4-13-3	185.7	309.8	1101	0.10	1.12			41.2			22.0	1.76	1.98	2.15			0.199	0.25											0.020	0.023	0.016
L-4-13-4	233.7	424.2	1096	0.12	1.14	38.1	43.5	41.2	20.0	22.0	22.0	1.85	2.11	2.15	0.168	0.211	0.302	0.38			0.134	0.17	0.053	0.07	0.038	0.05	1.65				0.014
L-4-13-5	282.4	554.2	1097	0.11	1.14	36.1	41.1	41.1	19.8	21.7	22.1	1.70	1.93	2.15	0.070	0.087	0.333	0.42			0.033	0.04	0.124	0.16	0.023	0.03	1.70				0.014
L-4-13-6	353.9	722.9	1091	0.13	1.16			41.1			22.1			2.15			0.423	0.56											0.019	0.022	0.012
L-4-13-7[l]	401.8	777.7	1097	0.14	1.17	35.3	41.5	41.1	20.6	23.1	22.2	1.79	2.10	2.15	0.276	0.355	0.512	0.69			0.042	0.05	0.121	0.16	0.039	0.05	1.75				0.011
L-4-13-8	450.0	886.8	1097	0.14	1.17	36.2	42.4	41.1	22.3	25.0	22.2	1.81	2.12	2.15	0.146	0.188	0.388	0.55			0.036	0.05	0.092	0.12	0.037	0.05	1.60				0.014
L-4-13-9	521.8	1095.7	1097	0.12	1.15			41.1			22.3			2.15			0.416	0.58											0.019	0.022	0.014
L-4-13-10	617.9	1274.9	1101	0.11	1.14	36.1	41.1	41.0	21.2	23.2	22.2	1.59	1.81	2.14	0.091	0.114	0.475	0.67			0.039	0.05	0.078	0.10	0.037	0.05	1.65	0.011			0.014
L-4-13-11	690.3	1480.7	1098	0.13	1.16			41.0			22.3			2.14				0.81											0.021	0.024	0.013
L-4-13-12	737.7	1589.8	1097	0.13	1.17	39.3	45.8	41.0	22.1	24.7	22.3	1.77	2.07	2.14	0.074	0.095	0.661	0.95			0.060	0.08	0.076	0.10	0.032	0.05	1.60				0.013
L-4-13-13	785.9	1734.3	1098	0.12	1.15	38.6	44.4	41.0	20.9	23.1	22.4	1.62	1.86	2.14	0.117	0.148	0.581	0.87					0.120	0.15	0.032	0.05	1.65				0.014
L-4-13-14	857.9	1947.0	1097	0.12	1.15	35.3	40.6	41.1	20.9	23.1	22.4	1.58	1.82	2.14			0.547	0.81											0.021	0.024	0.015
L-4-13-15	931.2	2054.7	1109	0.12	1.15	36.5	42.0	40.6	21.0	23.2	22.2	1.53	1.77	2.12	0.089	0.114	0.543	0.86			0.143	0.18	0.014	0.18	0.057	0.08					0.015
L-4-13-16	1025.7	2321.5	1098	0.12	1.15	36.5	42.1	40.6	20.5	22.6	22.3	1.57	1.81	2.12	0.098	0.124	0.514	0.84			0.082	0.10	ND	0	ND	0					0.017
L-4-13-17	1027.9	2327.9	1078	0.22	1.30			40.6			22.3			2.12													1.65		0.016	0.021	

[a]Where no values are given, either an analysis was not requested or the analytical results were not reliable. ND, not detected.
[b]Wash water contained Li_2SO_4 at 0.068 *M*; dilution factors calculated on lithium concentration found in sample.
[c](Reported concentration) × (dilution factor).
[d]Determined from calculated uranium and inventory balance.
[e](Reported concentration) × (dilution factor); corrected for SO_4 from Li_2SO_4.
[f]Determined from calculated sulfate and inventory balance. Corrected for amount introduced by Li_2SO_4.
[g]Determined from calculated copper and inventory balance.
[h](Reported concentration) × (dilution factor) × (inventory volume).
[i](Reported concentration corrected for sample dilution and amounts withdrawn in previous samples) × (inventory volume).
[j]Obtained with pH meter calibrated with H_2O solutions.
[k]Acid remaining after stoichiometric neutralization by nickel and manganese.
[l]Sample taken with reactor down.

Table 19. Analyses of Samples from Loop Inventory During Enriched-Solution Operation,[a] Loop L-4-18

Sample	Total Circulation Time (hr)	Accumulated LITR Energy (Mwhr)	Inventory Volume at Time of Sample, 25°C (ml)	Lithium[b] (mg/ml)	Sample Dilution Factor[c]	Uranium Rep (mg/ml)	Uranium Cor[d] (mg/ml)	Uranium Calcd[e] (mg/ml)	Sulfate Rep (mg/ml)	Sulfate Cor[f] (mg/ml)	Sulfate Calcd[g] (mg/ml)	Copper Rep (mg/ml)	Copper Cor[d] (mg/ml)	Copper Calcd[h] (mg/ml)	Chromium Rep (mg/ml)	Chromium Calcd Total[i] (g)	Nickel Rep (mg/ml)	Nickel Calcd Total[j] (g)	Chlorine Rep (mg/ml)	Chlorine Calcd Total[j] (g)	Iron Rep (mg/ml)	Iron Calcd Total[j] (g)	Zirconium Rep (mg/ml)	Zirconium Calcd Total[j] (g)	Manganese Rep (mg/ml)	Manganese Calcd Total[j] (g)	pH[k]	D_2SO_4 (M) Rep	D_2SO_4 (M) Cor	D_2SO_4 (M) Calcd[l]	Fluorine Rep (γ/ml)	Fluorine Calcd Total (g)	NO_3 Rep (γ/ml)	NO_3 Calcd Total (g)	NH_3 Rep (γ/ml)	NH_3 Calcd Total (g)
Original charge	0	0	1105	ND		39.9			24.9			4.38			ND		ND		<0.001		ND		ND		ND		1.50	0.019			ND		13		ND	
Makeup solution	0	0		ND		39.8			26.8			4.00			ND		ND		<0.001		ND		ND		ND		1.40				6		16		ND	
L-4-18-1[m]	43.8	0	1108	0.10	1.12	36.7	41.1	39.8	23.8	25.9	24.8	3.98	4.46	4.37			0.018	0.02			0.060	0.07					1.80	0.011	0.012	0.020						
L-4-18-2	100.3	111.4	1105	0.14	1.18	34.9	41.3	39.8	24.0	27.2	24.8	3.68	4.36	4.36			ND	0			0.061	0.08	0.044	0.06			1.80	0.011	0.013	0.020						
L-4-18-3[m]	388.1	837.6	1103	0.13	1.16	35.5	41.3	39.8	23.7	26.6	24.9	3.70	4.31	4.36	0.098	0.126	ND	0			0.077	0.10	0.031	0.04	ND	0	1.75	0.011	0.013	0.020						
L-4-18-4[m]	436.6	837.6	1106	0.16	1.21	35.3	42.5	39.8	24.2	27.8	24.9	3.97	4.78	4.36	0.062	0.083	0.075	0.10			0.035	0.05	0.023	0.03	ND	0	1.80	0.013	0.015	0.019						
L-4-18-5	508.1	978.2	1106	0.14	1.17	36.5	42.7	39.8	24.4	27.5	24.9	3.99	4.67	4.35	0.081	0.105	0.100	0.13			0.031	0.04	0.020	0.03	ND	0	1.75	0.014	0.016	0.019						
L-4-18-6	580.1	1160.8	1105	0.16	1.21	38.7	46.6	39.8	25.0	28.9	24.9	3.54	4.26	4.35	0.068	0.091	0.099	0.14			0.054	0.07	0.008	0.01	ND	0	1.70	0.015	0.018	0.019						
L-4-18-7	676.0	1441.0	1105	0.13	1.17	35.9	41.8	39.8	23.6	26.4	24.9	3.05	3.56	4.34	0.050	0.064	0.142	0.19			0.085	0.11	0.023	0.03	ND	0	1.80	0.010	0.012	0.018			102	0.113		
L-4-18-8	748.3	1605.0	1108	0.14	1.18	35.7	41.9	39.8	23.6	26.7	25.0	3.79	4.45	4.33	0.118	0.015	0.148	0.20			0.050	0.07	0.031	0.04	ND	0	1.80	0.013	0.015	0.018						
L-4-18-9	844.1	1807.7	1106	0.16	1.20	34.5	41.5	39.8	23.1	26.5	25.0	3.78	4.55	4.32	0.032	0.042	0.161	0.22			0.064	0.09	0.021	0.03	ND	0	1.80	0.011	0.013	0.018						

[a]Where no values are given, either an analysis was not requested or the analytical results were not reliable. ND, not detected.
[b]Wash water contained Li_2SO_4 at 0.068 M.
[c]Dilution factors calculated on lithium concentration found in sample.
[d](Reported concentration) × (dilution factor).
[e]Determined from calculated uranium and inventory balance.
[f](Reported concentration) × (dilution factor); corrected for SO_4 from Li_2SO_4.
[g]Calculated on the basis of inventory volume and resulting SO_4 concentration changes.
[h]Calculated on the basis of inventory volume and resulting Cu concentration changes.
[i](Reported concentration) × (dilution factor) × (inventory volume).
[j](Reported concentration corrected for sample dilution and amounts withdrawn in previous samples) × (inventory volume).
[k]Obtained with pH meter calibrated with H_2O solutions.
[l]Acid remaining after stoichiometric neutralization by nickel and manganese.
[m]Sample taken with reactor down.

correspond to given amounts of nickel or manganese in solution (calculated as described in Sec 4.1) are also shown.

As will be brought out in the discussion, the amount of excess H_2SO_4 in solution was an important factor in determining the steel corrosion during exposure to fissioning uranyl sulfate solutions. The results of measurements and of estimates of free H_2SO_4 in the different experiments are shown graphically in Fig. 84. The data illustrated for experiments L-4-13 and L-4-18 were obtained from analytical determinations of free acid. For the other experiments in which direct free-acid analyses were not made, the free-acid values were estimated from the results of pH measurements. For these estimates, the relationship between pH and excess H_2SO_4 in solutions containing 0.17 *m* UO_2SO_4 and 0.03 *m* $CuSO_4$ was determined in control experiments (Fig. 22). Additional control experiments showed that dilution of the control solution with water or dilute Li_2SO_4 solution to about the extent encountered in sampling resulted in pH changes which were in accord with those expected from the dilution of the excess acid. Therefore the appropriate dilution factors and the relationship shown in Fig. 22 were employed to convert pH readings into free-acid concentrations.

4.3 In-Pile Operation, Oxygen Consumption

The results of oxygen consumption measurements during radiation exposure are shown in Figs. 23–29 in plots of calculated rates of consumption on steel vs megawatt-hours of LITR energy accumulated during exposure. Each datum was obtained during periods in which the reactor operated at the 3-Mw power level (the usual level) and in which the rates of pressure loss were essentially constant for about 20 hr or more. The plotted times are midpoints of such periods. The consumption rates are in units of volume of oxygen per 3 Mwhr. Also shown in each figure are values for the average consumption rates on the zirconium and titanium alloys determined from weight data. The steel rates were obtained by reducing the observed consumption rates by these listed amounts. Values are also shown in each figure for the relationships between oxygen consumption rates and steel corrosion rates in mils per year when it is assumed in one case that all steel surfaces in contact with high-temperature solution corroded uniformly, and in another case that only the steel surfaces in the core consumed oxygen. The actual distribution of the corrosion in a loop will be considered in the discussion section.

Data for the total amounts of oxygen consumed during the in-pile exposures are listed in Tables 20–26. The corresponding steel penetration values (calculated as described in Sec 4.1) are also listed. These oxygen consumption results are shown graphically and compared with the nickel and manganese results in Figs. 15–21 as functions of total times at operating temperature. The final oxygen value in each of these plots was also corrected for the amount of oxygen consumed by zirconium and titanium alloys by the factors listed in Figs. 23–29, and the points, representing the corrected overall corrosion penetration of stainless steel determined from oxygen data, are shown for comparison. Similarly corrected, total amounts of oxygen consumed by steel surfaces are shown vs megawatt-hours of LITR energy in Fig. 30. Data from a previously reported experiment, L-4-11,[3] are also illustrated in Fig. 30. These data will be employed in the later discussions of the steel corrosion results of these experiments.

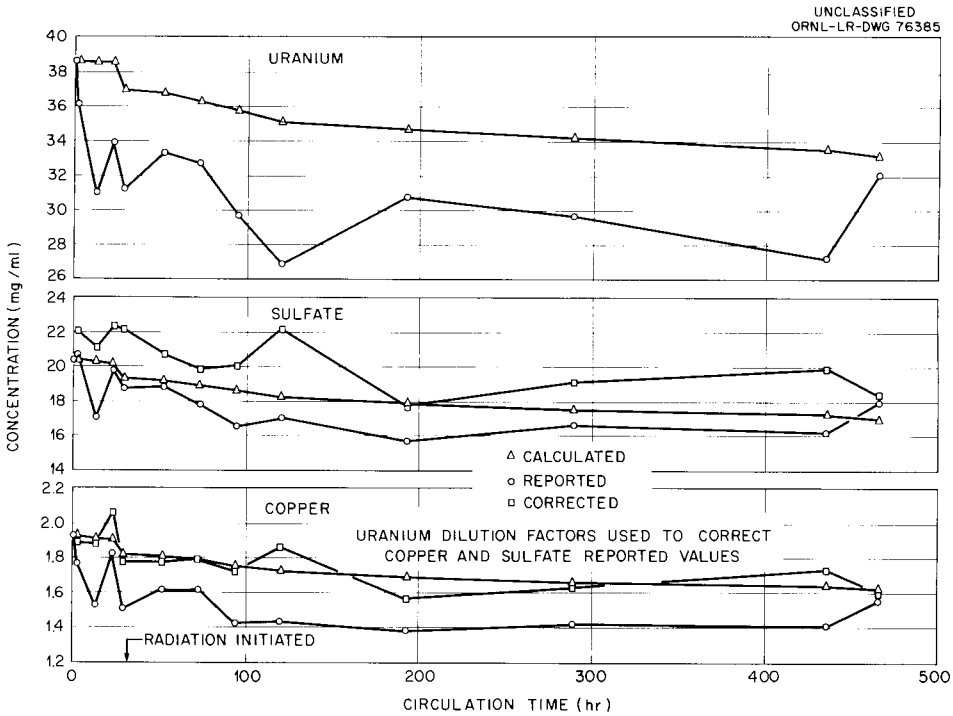

Fig. 8. Concentration of Uranium, Sulfate, and Copper in Solution Samples, Loop DD.

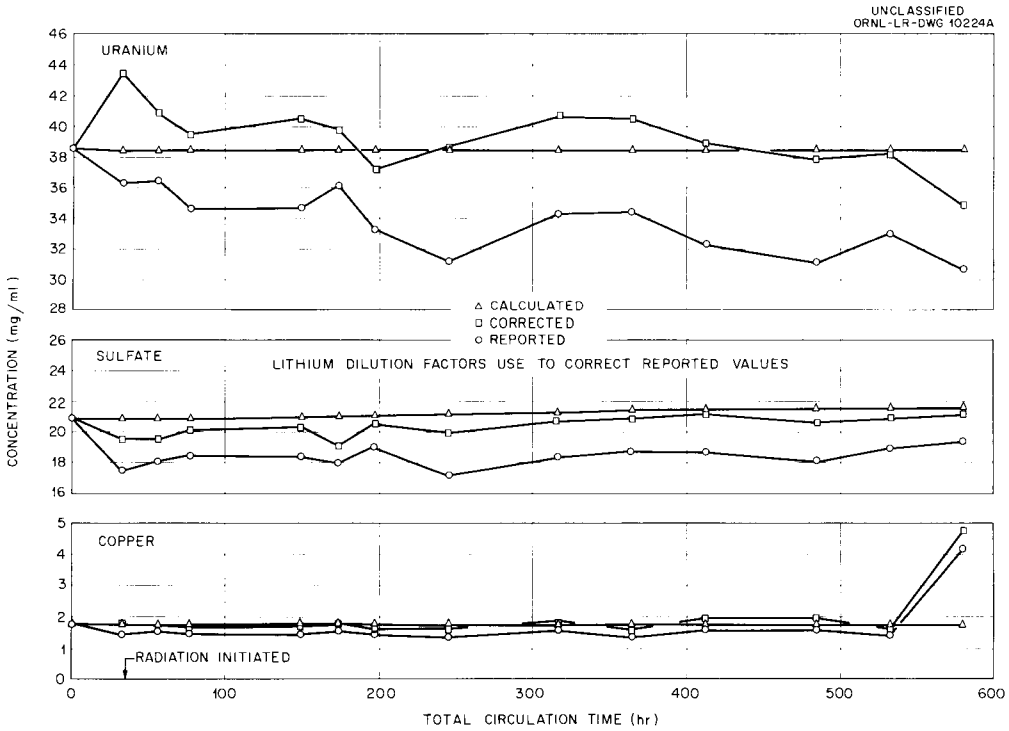

Fig. 9. Concentration of Uranium, Sulfate, and Copper in Solution Samples, Loop EE.

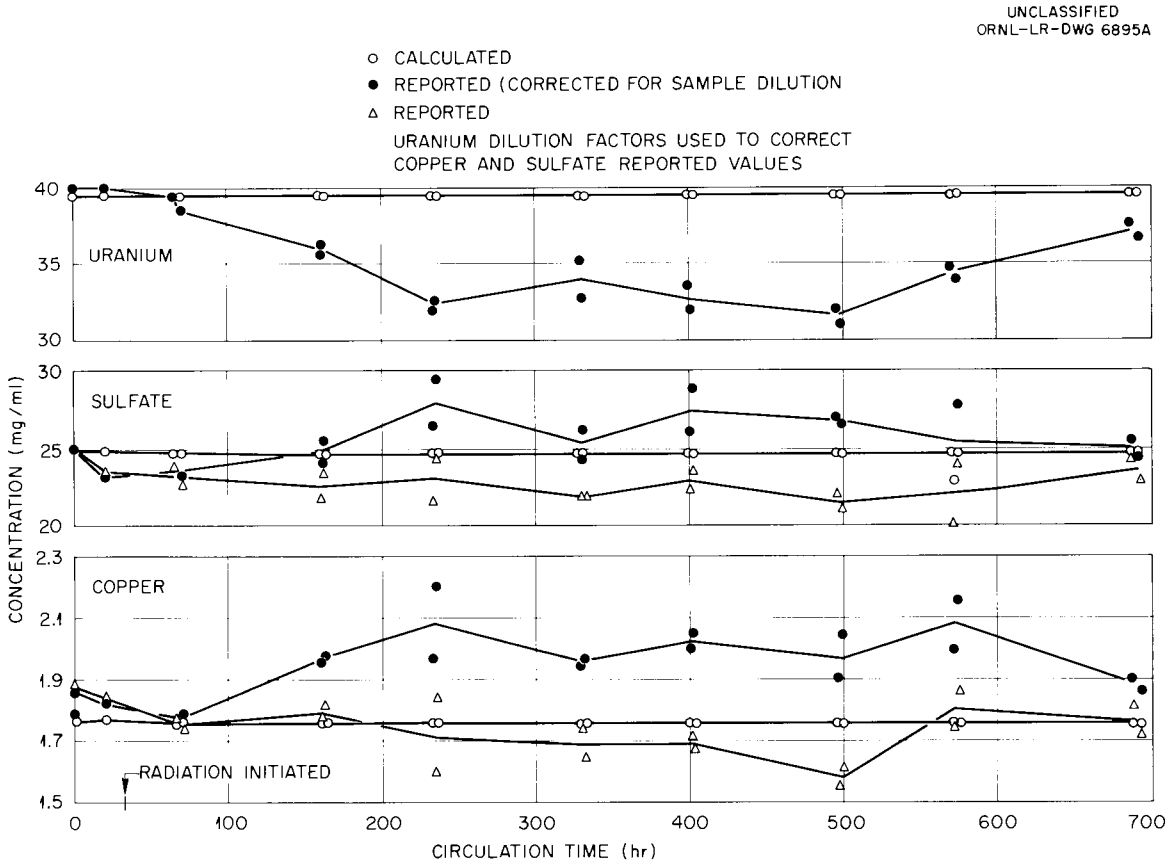

Fig. 10. Concentration of Uranium, Sulfate, and Copper in Solution Samples, Loop FF.

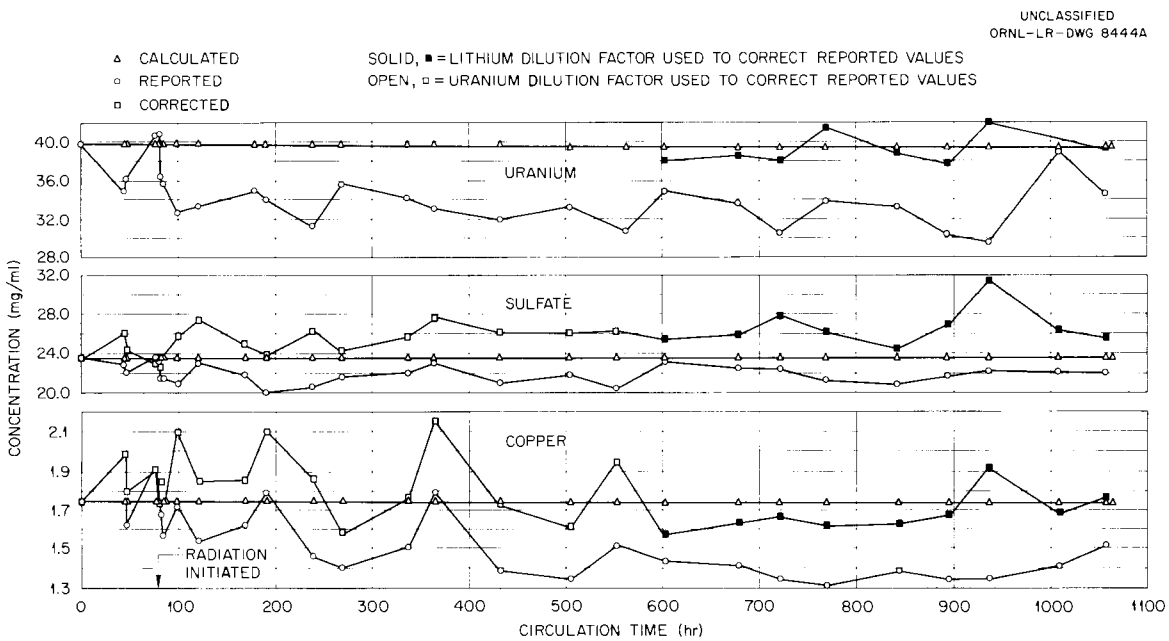

Fig. 11. Concentration of Uranium, Sulfate, and Copper in Solution Samples, Loop GG.

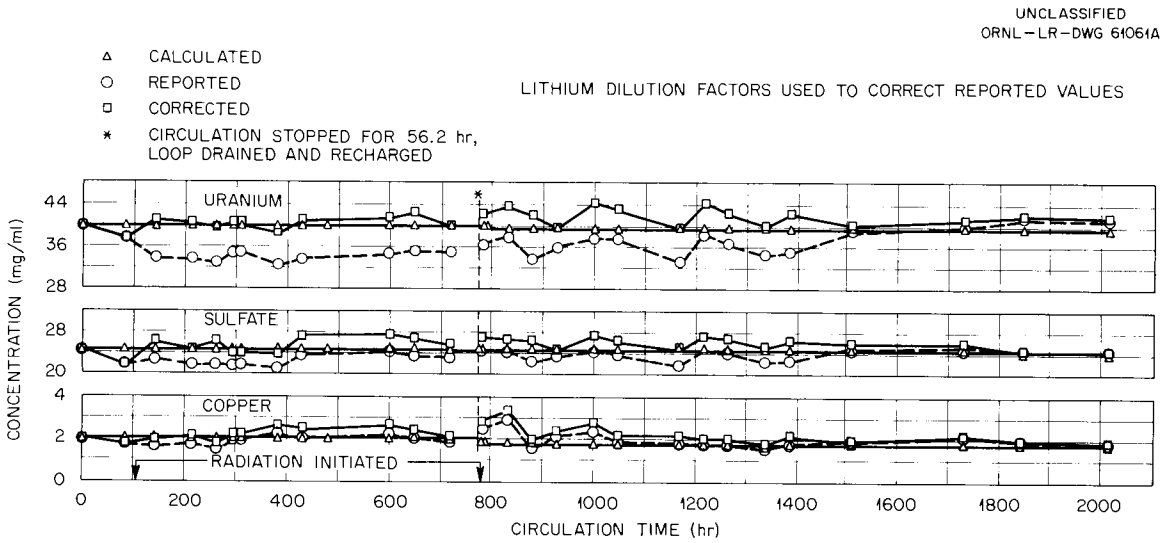

Fig. 12. Concentration of Uranium, Sulfate, and Copper in Solution Samples, Loop L-4-12.

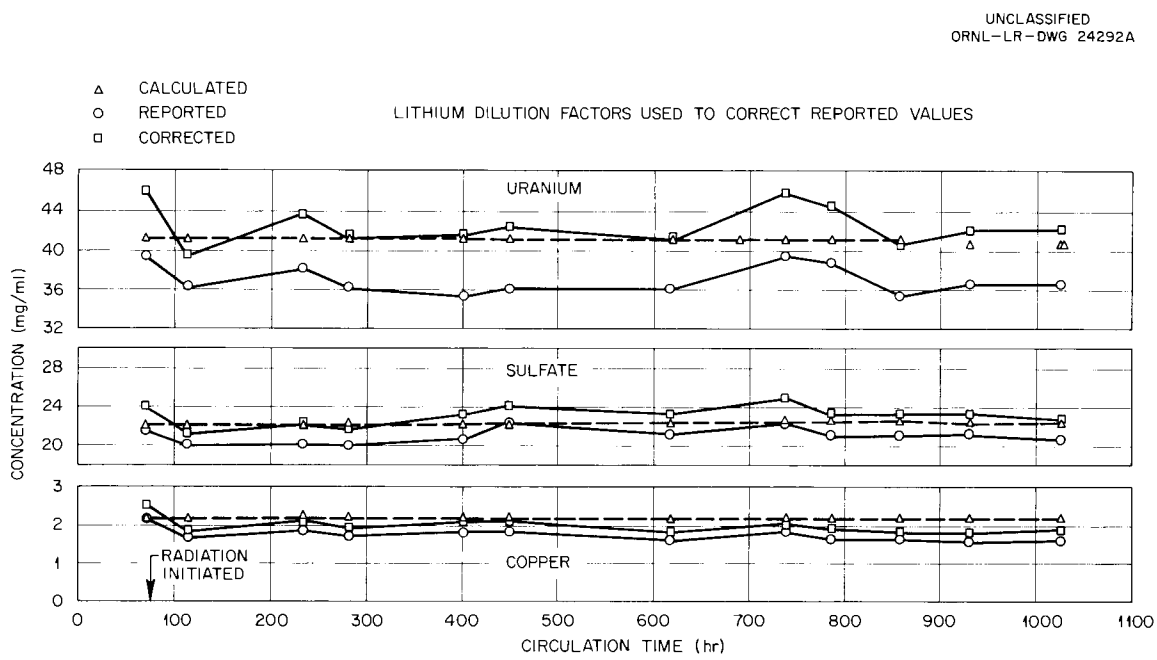

Fig. 13. Concentration of Uranium, Sulfate, and Copper in Solution Samples, Loop L-4-13.

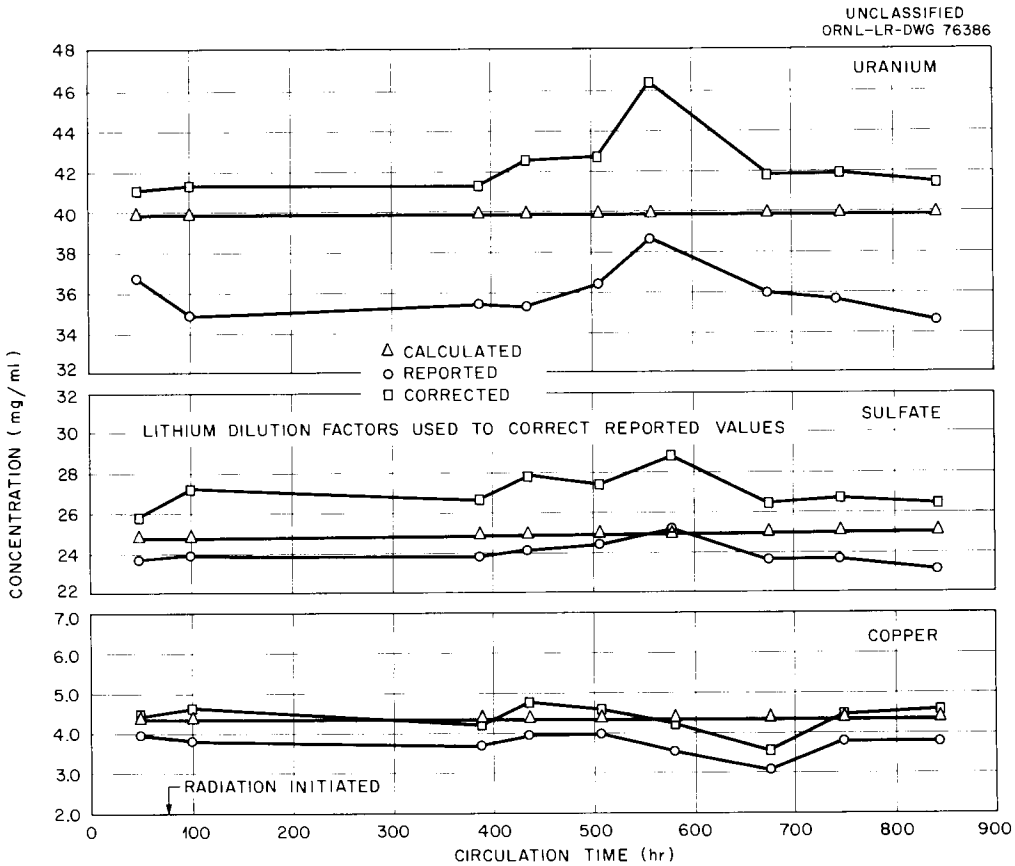

Fig. 14. Concentration of Uranium, Sulfate, and Copper in Solution Samples, Loop L-4-18.

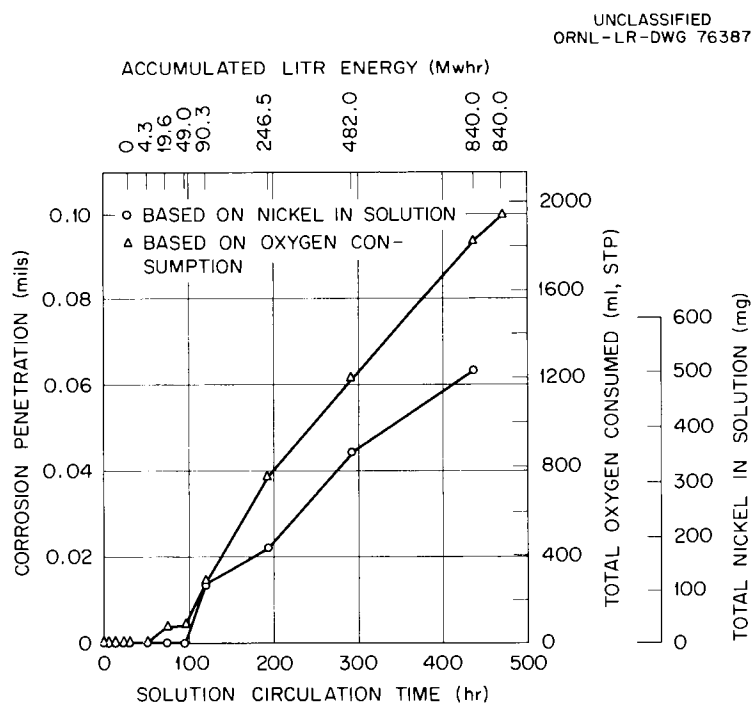

Fig. 15. Overall Corrosion Penetration of Type 347 Stainless Steel, Loop DD.

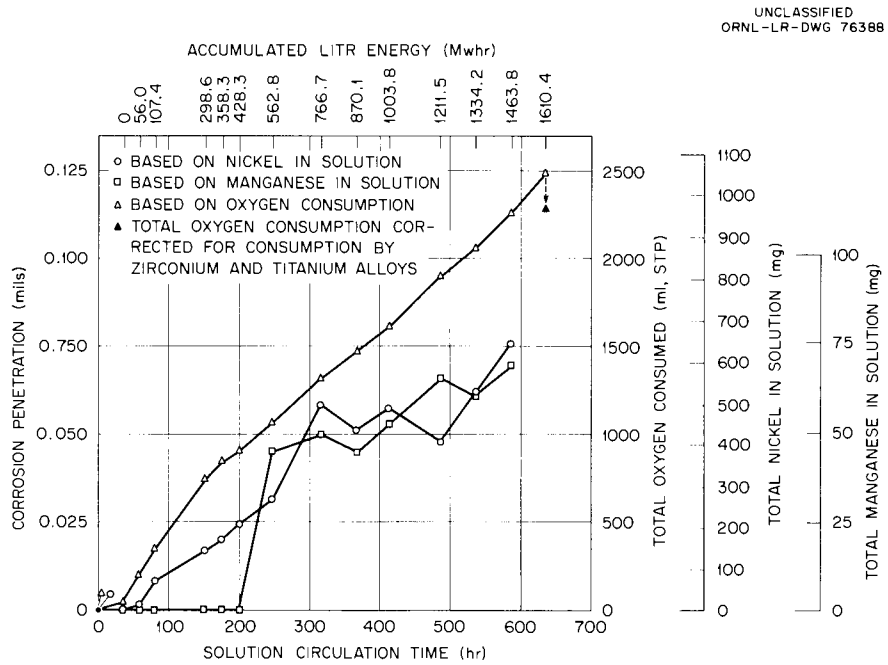

Fig. 16. Overall Corrosion Penetration of Type 347 Stainless Steel, Loop EE.

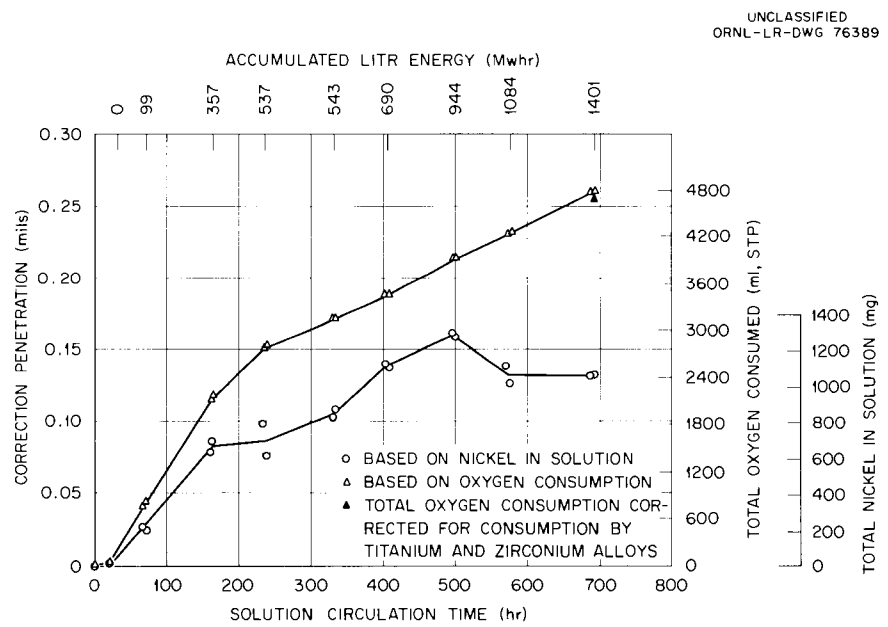

Fig. 17. Overall Corrosian Penetration of Type 347 Stainless Steel, Loop FF.

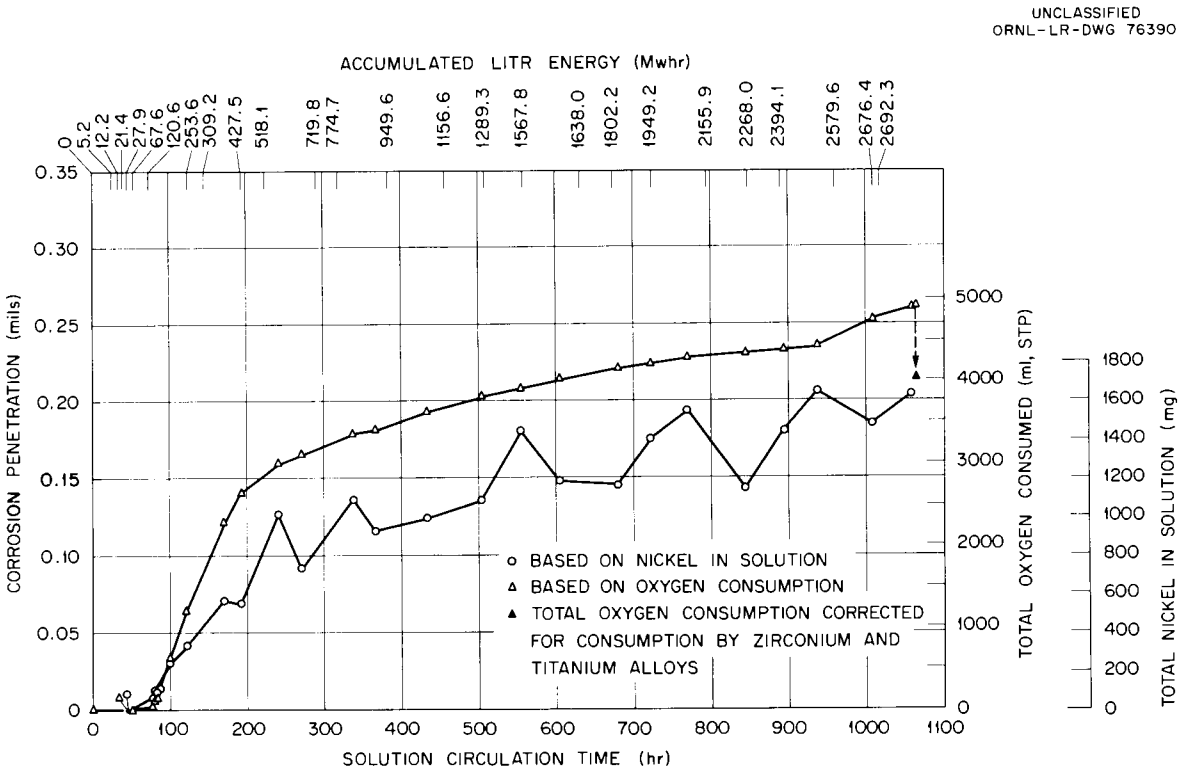

Fig. 18. Overall Corrosion Penetration of Type 347 Stainless Steel, Loop GG.

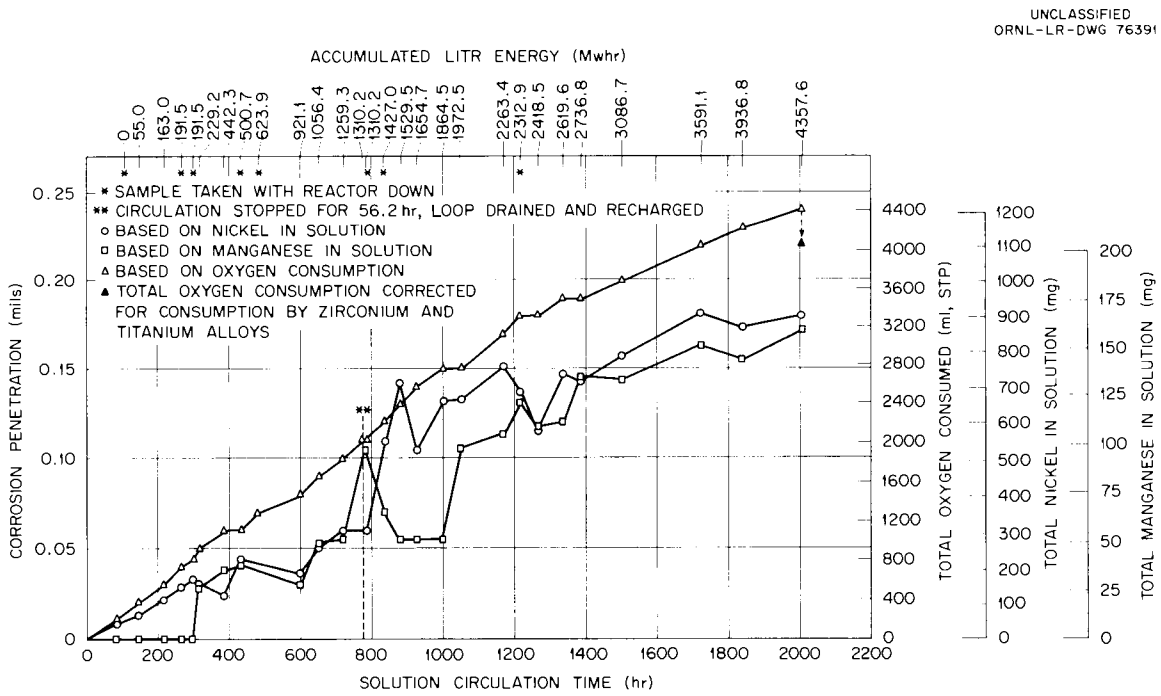

Fig. 19. Overall Corrosion Penetration of Type 347 Stainless Steel, Loop L-4-12.

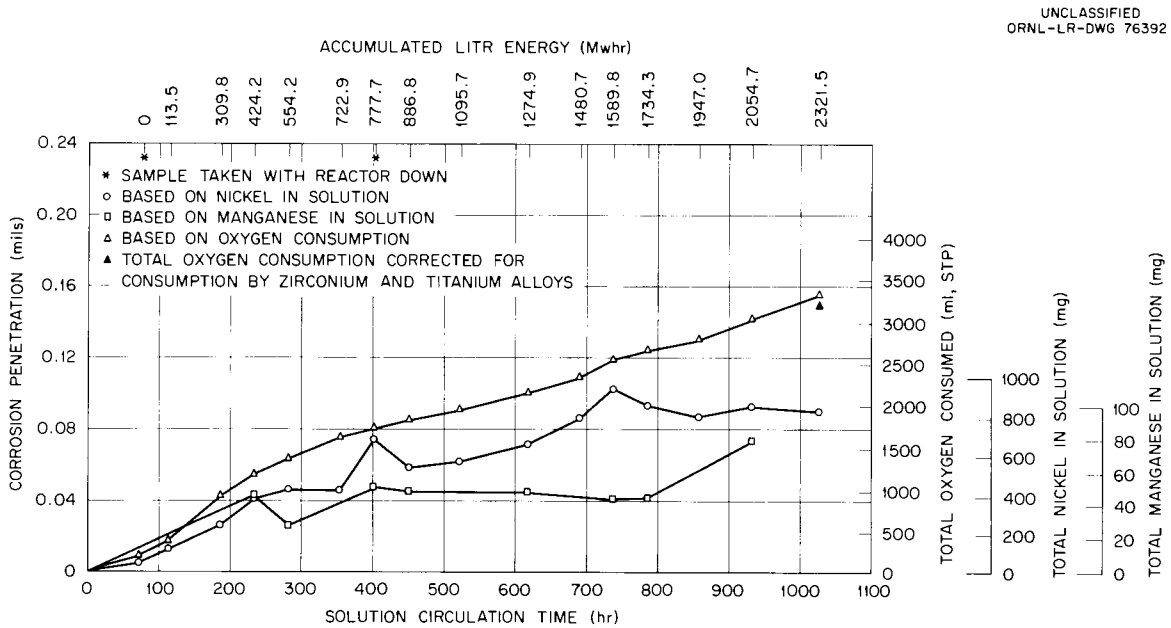

Fig. 20. Overall Corrosion Penetration of Type 347 Stainless Steel, Loop L-4-13.

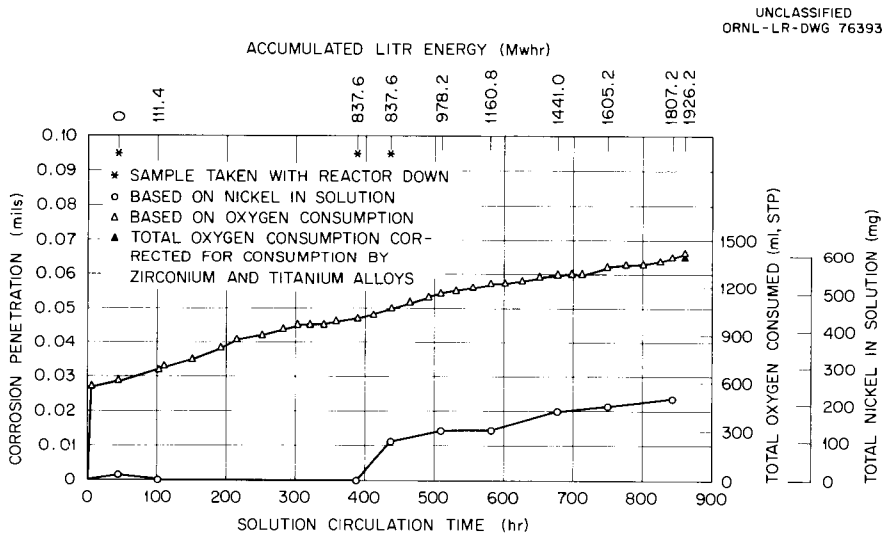

Fig. 21. Overall Corrosion Penetration of Type 347 Stainless Steel, Loop L-4-18.

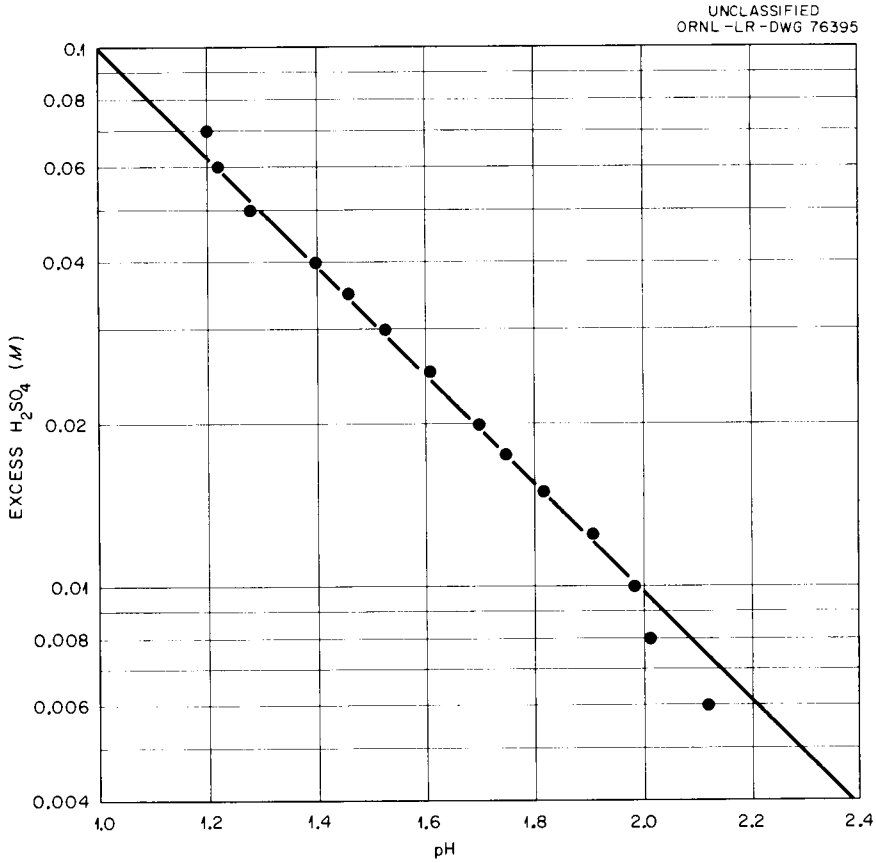

Fig. 22. Free-Acid Concentration vs pH in H_2O Solutions Containing 0.17 *m* UO_2SO_4 and 0.03 *m* $CuSO_4$.

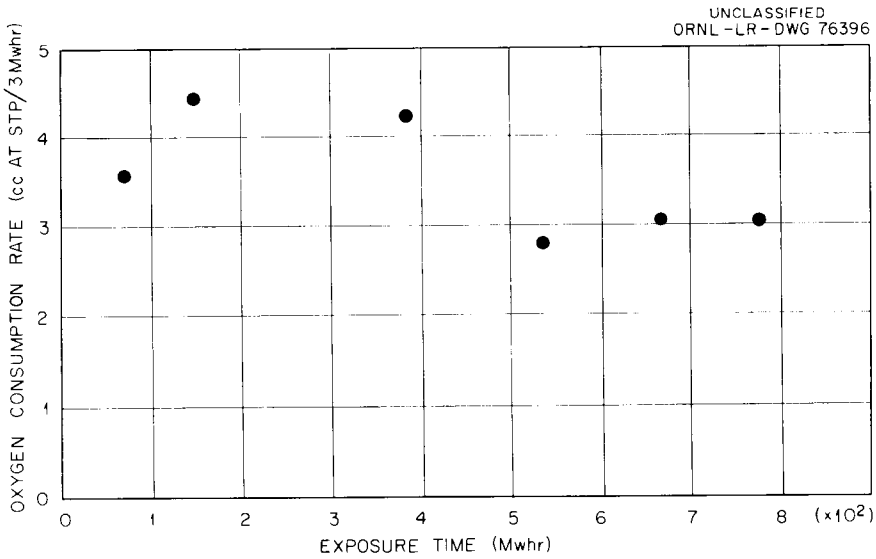

Fig. 23. Oxygen Consumption Rates on Stainless Steel, Loop DD.

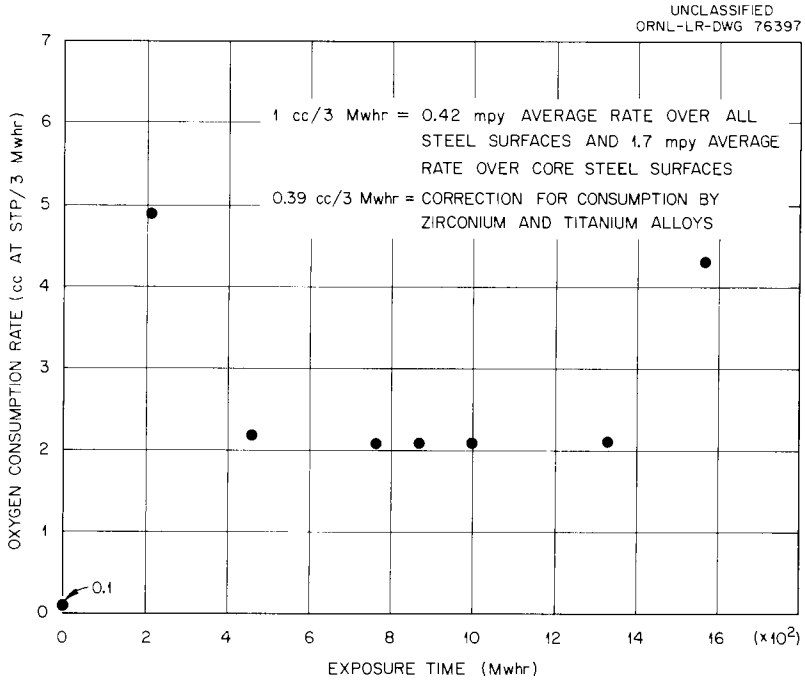

Fig. 24. Oxygen Consumption Rates on Stainless Steel, Loop EE.

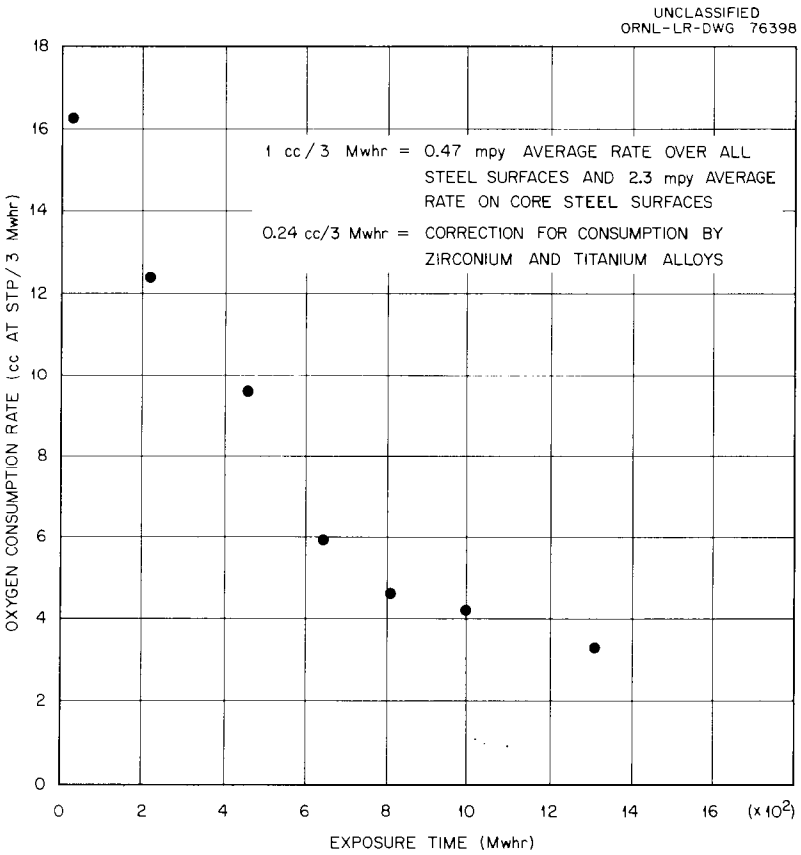

Fig. 25. Oxygen Consumption Rates on Stainless Steel, Loop FF.

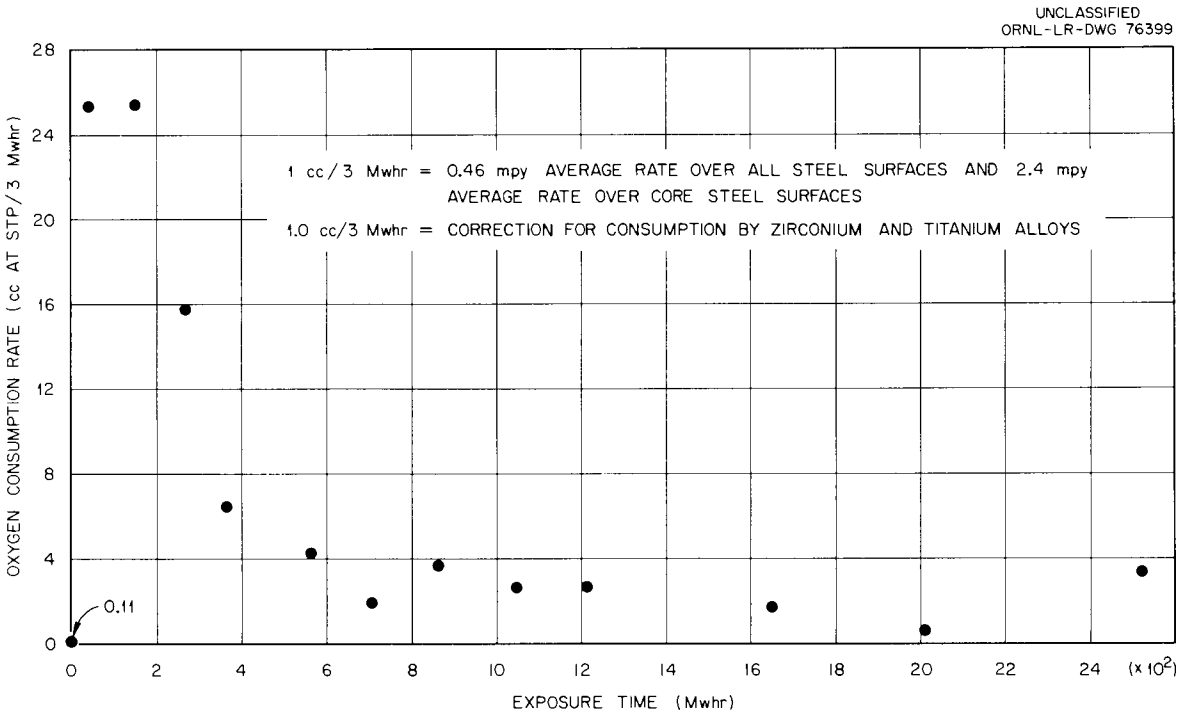

Fig. 26. Oxygen Consumption Rates on Stainless Steel, Loop GG.

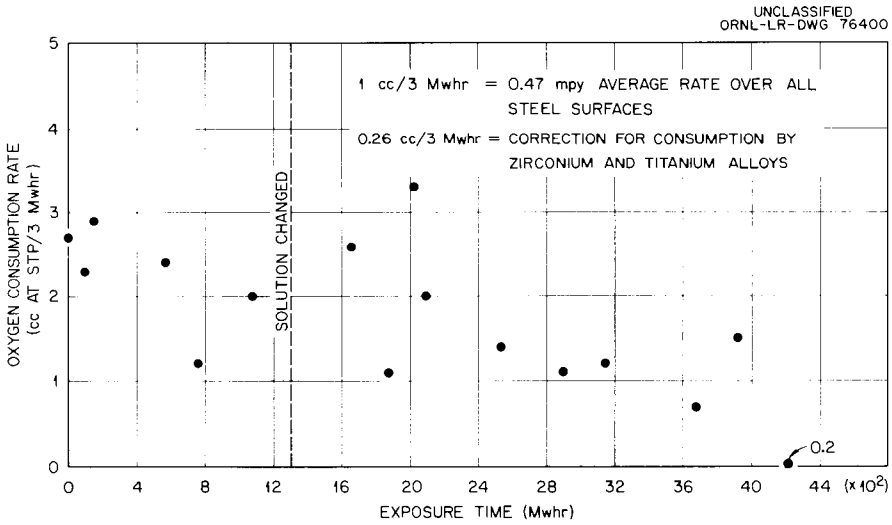

Fig. 27. Oxygen Consumption Rates on Stainless Steel, Loop L-4-12.

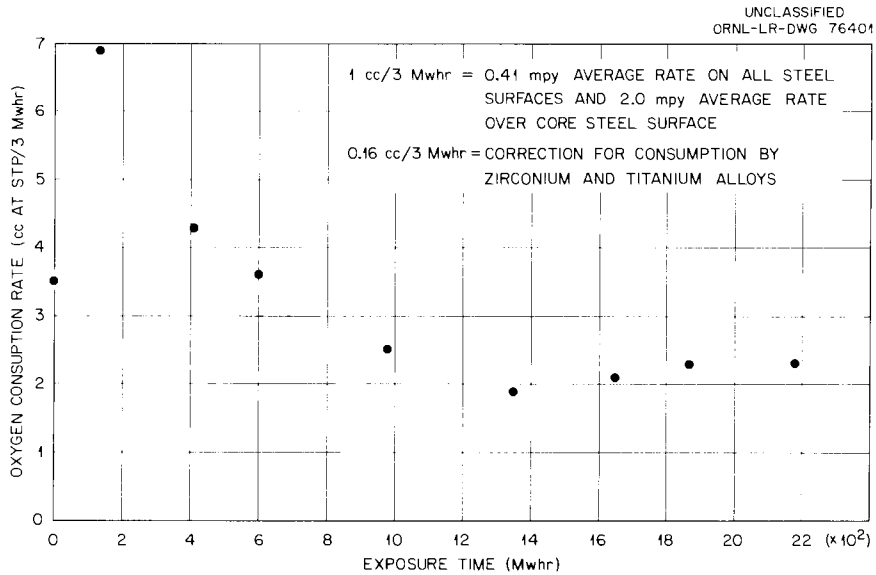

Fig. 28. Oxygen Consumption Rates on Stainless Steel, Loop L-4-13.

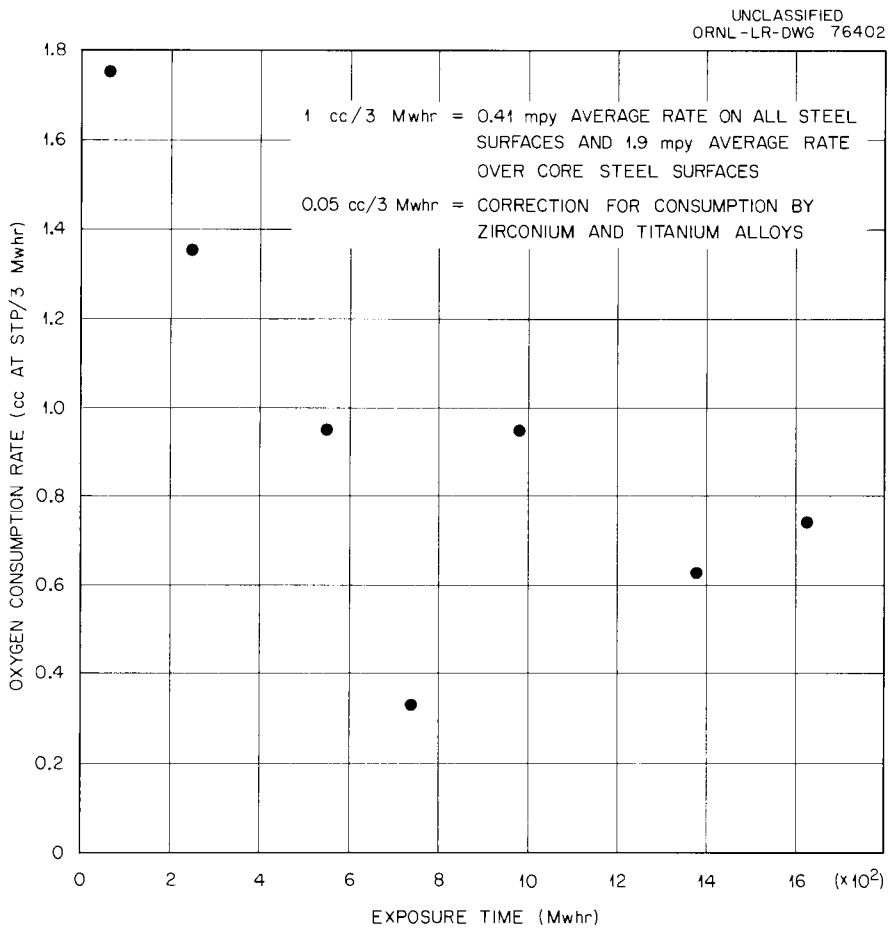

Fig. 29. Oxygen Consumption Rates on Stainless Steel, Loop L-4-18.

Table 20. Oxygen Consumption in Loop DD

Remarks	LITR Energy (Mwhr)	Sample Number	Total Fuel Circulation Time (hr)	Δ Time (hr)	O_2 Volume at Time of Previous Sample (cc at STP)	O_2 Volume at Time of Sample (cc at STP)	O_2 Additions (cc at STP)	O_2 Consumed Since Last Sample (cc at STP)	Cumulative[a] Amount of O_2 Consumed (cc at STP)	Calculated Corrosion Penetration of Type 347 Stainless Steel (mils)
Enriched solution, no radiation	0	DD-1-28(E)	0	0	912	912		0	0	
	0	DD-1-29(E)	2.4	2.4	912	912		0	0	
	0	DD-1-30(E)	12.7	10.3	912	912		0	0	
	0	DD-1-31(E)	23.3	10.6	912	912		0	0	
	0	DD-1-31.5(E)	29.4	6.1	912	912		0	0	
Radiation, Mw										
0.3	4.3	DD-1-32(ER)	51.7	22.3	912	912		0	0	0
1.0	19.6	DD-1-33(ER)	72.3	20.6	912	906		7	7	<0.01
2.0	49.0	DD-1-34(ER)	95.3	23.0	906	838		67	74	<0.01
3.0	90.3	DD-1-35(ER)	120.0	24.7	838	642		197	271	0.02
3.0	246.5	DD-1-36(ER)	192.9	72.9	642	944	745	443	714	0.04
3.0	482.0	DD-1-37(ER)	292.4	99.5	944	528		416	1130	0.06
3.0	840.0	DD-1-38(ER)	434.8	142.4	528	713	788	603	1733	0.09
0	840.0	DD-1-39(ER)	465.5	30.7	713	607		106	1839	0.10

[a] 13.2 cc at STP/psi.

Table 21. Oxygen Consumption in Loop EE

Remarks	Sample Number	Accumulated LITR Energy (Mwhr)	Total Solution Circulation Time (hr)	O_2 Additions to Loop (cc at STP)	O_2 Withdrawn from Loop[a] (cc at STP)	Total O_2 Charged to Loop Less O_2 Withdrawn in Sampling (cc at STP)	O_2 Volume at Time of Sampling (cc at STP)	O_2 Consumed Since Last Sampling (cc at STP)	Cumulative[b] Amount of O_2 Consumed (cc at STP)	Calculated Corrosion Penetration of Type 347 Stainless Steel (mils)
Original filling		0.0	0.0	795	0	795	795	0	0	0
O_2 addition (EE-2)		0.0	21.5	839	0	1634	1601		33	
	EE-1-92	0.0	33.3	0	0	1634	1583	51	51	0.003
Reactor started		0.0	36.2	0	6	1628	1572		56	
	EE-1-93	56.0	54.8	0	0	1622	1432	139	190	0.01
	EE-1-94	107.4	76.3	0	7	1616	1272	154	344	0.02
	EE-1-95	298.6	148.1	0	6	1610	868	418	762	0.04
	EE-1-96	358.3	172.6	0	4	1606	786	58	820	0.04
	EE-1-97	428.3	196.7	0	6	1600	698	82	902	0.05
	EE-1-98	562.8	244.6	0	10	1590	529	159	1061	0.05
O_2 addition (EE-3)			251.3	986	8	2567	1490		1077	
	EE-1-99	766.7	316.6	0	0	2567	1253	253	1314	0.07
	EE-1-100	870.1	364.3	0	15	2553	1093	146	1460	0.07
	EE-1-101	1003.8	412.4	0	5	2548	933	155	1615	0.08
	EE-1-102	1211.5	484.4	0	4	2544	657	272	1887	0.09
	EE-1-104	1334.2	532.2	0	3	2542	484	171	2058	0.10
O_2 addition (EE-4)			557.5	917	2	3457	1310		2147	
	EE-1-104	1463.8	580.5	0	0	3457	1205	194	2252	0.11
End of run		1610.4	630.3	0	5	3451	977	222	2474	0.12

[a]Calculated amount removed as O_2 dissolved in sample.
[b]12.0 cc at STP/psi.

Table 22. Oxygen Consumption in Loop FF

Remarks	Sample Number	LITR Energy (Mwhr)	Total Solution Circulation Time (hr)	O_2 Additions to Loop (cc at STP)	O_2 Withdrawn from Loop[a] (cc at STP)	Total O_2 Charged to Loop Less O_2 Withdrawn in Sampling (cc at STP)	O_2 Volume at Time of Sample (cc at STP)	O_2 Consumed Since Last Sample (cc at STP)	Cumulative[b] Amount of O_2 Consumed (cc of STP)	Calculated Corrosion Penetration of Type 347 Stainless Steel (mils)
Mockup operation										
Original O_2 fill		0	0	1124	0	1124		0	0	
	FF-1-40	0	1.5		24	1100				
	FF-1-41	0	20.8		7	1093				0.002
Circulating pump shut down		0	23.1		0	1093	1052		41	
LITR operation										
Reactor started up		0	30.9	0	0	1093	1052		41	0.002
	FF-1-44 (a)	99.0	67.8	0	13	1093	342	713	751	0.04
	(b)	99.0	71.1	0		1093	291	51	802	0.04
O_2 addition FF-1			71.8	1361	0	2441	1641			
	FF-1-45 (a)	357.2	161.2	0	3	2441	290	1349	2151	0.12
	(b)	357.2	163.4	0		2441	252	38	2189	0.12
O_2 addition FF-2			165.0	1092	0	3530	1344			
	FF-1-46 (a)	536.5	234.4	0	10	3530	714	627	2816	0.15
	(b)	536.5	236.4	0		3530	697	17	2833	0.15
O_2 addition FF-3			238.7	610	0	4130	1324			
	FF-1-47 (a)	543.3	330.1	0	10	4130	928	369	3202	0.17
	(b)	543.3	332.0	0		4130	928	0	3202	0.17
	FF-1-48 (a)	689.8	401.6	0	7	4120	617	301	3503	0.19
	(b)	689.8	403.6	0		4120	606	11	3514	0.19
O_2 addition FF-4			473.9	799	0	4912				
	FF-1-49 (a)	943.8	497.3	0	10	4912	908	490	4004	0.21
	(b)	943.8	498.8	0		4912	902	6	4010	0.22
	FF-1-50 (a)	1084.4	572.1	0	7	4902	582	310	4320	0.23
	(b)	1084.4	575.5	0		4902	568	14	4334	0.23
O_2 addition FF-5			576.0	682	0	5577	1245			
Sample taken with reactor on	FF-1-52	1401.2	687.9	0	9	5577	697	546	4880	0.26
Reactor shut down		1401.2	687.9			5577				
	FF-1-53	1401.2	692.3	0		5577	687	10	4890	0.26
Circulating pump shut down		1401.2	693.0	0		5577	683	4	4894	0.26

[a]Calculated amount removed as O_2 dissolved in sample.
[b]10.5 cc at STP/psi.

Table 23. Oxygen Consumption in Loop GG

Remarks	Sample Number	LITR Energy (Mwhr)	Total Solution Circulation Time (hr)	O_2 Additions to Loop (cc at STP)	O_2 Withdrawn from Loop[a] (cc at STP)	Total O_2 Charged to Loop Less O_2 Withdrawn in Sampling (cc at STP)	O_2 Volume at Time of Sample (cc at STP)	O_2 Consumed Since Last Sample (cc at STP)	Total O_2[b] Consumed (cc at STP)	Calculated Corrosion Penetration of Type 347 Stainless Steel (mils)
Original O_2 fill GG-1 started circulation		0	0	1165		1165		0	0	0
		0	0	0		1165		0	0	0
	GG-1-62	0	45.2	0	5	1160		0	0	0
	GG-1-63	0	47.2	0	5	1155		0	0	0
Reactor on		0	76.1	0		1155		0	0	0
	GG-1-64	5.2	77.8	0	6	1149		49	48	0.003
	GG-1-65	12.2	80.1	0	4	1145		62	111	0.006
	GG-1-66	21.4	83.1	0	4	1141		81	192	0.01
	GG-1-67	27.9	85.3	0	4	1138		59	251	0.01
	GG-1-68	67.6	98.6	0	3	1135		358	609	0.03
		68.7	100.6	0		1135	471		663	
O_2 addition GG-2		68.7	100.6	1521		2656	1993		663	
	GG-1-69	120.6	120.6	0	8	2648		576	1185	0.06
			151.7	0		2648	647		2000	
O_2 addition GG-3			151.7	985		3633	1632		2000	
	GG-1-70	253.6	169.2	0	5	3628		1089	2274	0.12
	GG-1-71	309.2	190.8	0	3	3625		352	2626	0.14
			193.3	0		3625	949		2675	
O_2 addition GG-4			193.3	740		4365	1689		2675	
	GG-1-72	427.5	239.5	0	3	4365	1400	338	2964	0.16

Table 23 (continued)

Remarks	Sample Number	LITR Energy (Mwhr)	Total Solution Circulation Time (hr)	O_2 Additions to Loop (cc at STP)	O_2 Withdrawn from Loop[a] (cc at STP)	Total O_2 Charged to Loop Less O_2 Withdrawn in Sampling (cc at STP)	O_2 Volume at Time of Sample (cc at STP)	O_2 Consumed Since Last Sample (cc at STP)	Total $_2O$[b] Consumed (cc at STP)	Calculated Corrosion Penetration of Type 347 Stainless Steel (mils)
O_2 addition GG-4	GG-1-73	518.1	269.7	0	3	4362	1269	128	3092	0.17
			310.0	0		4359	1091		3268	
	GG-1-74	719.8	337.3	0	3	4359	1039	228	3320	0.18
			360.8	0		4356	991		3364	
O_2 addition GG-5			360.8	707		5064	1699		3364	
	GG-1-75	774.7	365.3	0	4	5064	1680	63	3383	0.18
	GG-1-76	949.6	433.1	0	4	5060	1456	220	3603	0.19
	GG-1-77	1156.6	504.9	0	4	5056	1263	189	3792	0.20
	GG-1-78	1289.3	553.0	0	4	5051	1158	201	3893	0.21
	GG-1-79	1567.8	603.5	0	4	5048	1055	99	3992	0.21
	GG-1-80	1638.0	678.4	0	3	5045	906	146	4138	0.22
	GG-1-81	1802.2	721.0	0	2	5042	844	59	4197	0.22
	GG-1-82	1949.2	769.0	0	2	5040	777	165	4262	0.23
	GG-1-83	2155.9	842.5	0	1	5039	711	65	4327	0.23
	GG-1-84	2268.0	894.2	0	1	5038	661	49	4376	0.23
	GG-1-85	2394.1	936.6	0	1	5037	623	38	4414	0.24
O_2 addition GG-6			942.2	915	0	5951	1533		4417	
	GG-1-86	2579.6	1009.5	0	−3	5948	1218	315	4729	0.25
Shut down reactor	GG-1-87	2676.4	1057.8	0	0	5948	1088	130	4859	0.26
Shut down pump	End of run	2676.4	1063.7	0	0	5948	1072	16	4875	0.26

[a]Calculated amount removed as O_2 dissolved in sample.
[b]14.8 cc at STP/psi.

Table 24. Oxygen Consumption in Loop L-4-12

Remarks	Sample Number	LITR Energy (Mwhr)	Total Solution Circulation Time (hr)	O_2 Additions to Loop (cc at STP)	O_2 Withdrawn from Loop[a] (cc at STP)	Total O_2 Charged to Loop Less O_2 Withdrawn in Sampling (cc at STP)	O_2 Volume at Time of Sample (cc at STP)	O_2 Consumed Since Last Sample (cc at STP)	Total O_2[b] Consumed (cc at STP)	Calculated Corrosion Penetration of Type 347 Stainless Steel (mils)
Operation with 1st enriched solution										
O_2 addition (L-4-12-3)		0	0	1420	0	1420	1420	0	0	0
	L-4-12-1	0	84.9	0	0	1420	1191	230	230	0.01
	L-4-12-2	55.0	143.0	0	1	1419	1049	140	370	0.02
	L-4-12-3	163.0	215.0	0	8	1411	880	161	531	0.03
O_2 addition (L-4-12-4)				717	6	2122	1517			
	L-4-12-4	191.5	262.1	0	0	2122	1434	157	688	0.04
	L-4-12-5	191.5	295.3	0	11	2111	1302	121	809	0.04
	L-4-12-6	229.2	311.0	0	10	2101	1255	37	846	0.05
	L-4-12-7	442.3	383.3	0	9	2092	1057	189	1035	0.06
	L-4-12-8	500.7	430.9	0	8	2084	949	100	1135	0.06
	L-4-12-9	623.9	479.9	0	7	2077	811	131	1266	0.07
O_2 addition (L-4-12-5)				786	6	2857	1423			
	L-4-12-10	921.1	598.6	0	0	2857	1410	181	1447	0.08
	L-4-12-11	1056.4	648.2	0	11	2846	1226	173	1620	0.09
	L-4-12-12	1259.3	718.7	0	10	2836	1059	157	1777	0.10
Pump off		1310.2	772.9	0	8	2828	857	194	1971	0.11
Solution drain		1310.2	772.9	0	857	1971				
Operation with 2d enriched solution										
O_2 addition (L-4-12-7)				1403	0	3374	1403			
	L-4-12-13	1310.2	774.7	0	0	3374	1395	8	1979	0.11
	L-4-12-14	1427.0	831.0	0	4	3370	1160	231	2210	0.12
	L-4-12-15	1519.5	878.4	0	7	3363	992	161	2371	0.13
	L-4-12-16	1654.7	926.3	0	6	3357	856	130	2501	0.14
	L-4-12-17	1864.5	998.5	0	6	3351	666	184	2685	0.15
O_2 addition (L-4-12-8)				1062	4	4409	1682			
	L-4-12-18	1922.5	1046.0	0	0	4409	1615	109	2794	0.15
	L-4-12-19	2263.4	1166.0	0	11	4398	1256	348	3142	0.17
	L-4-12-20	2312.9	1214.3	0	9	4389	1130	117	3259	0.18
	L-4-12-21	2418.5	1262.0	0	8	4381	1002	120	3379	0.18
	L-4-12-22	2619.6	1334.0	0	7	4374	849	146	3525	0.19
	L-4-12-23	2736.8	1382.3	0	6	4368	758	85	3610	0.19
	L-4-12-24	3086.7	1503.0	0	5	4363	612	141	3751	0.20
O_2 addition (L-4-12-9)				948	4	5307	1529			
	L-4-12-25	3591.1	1720.4	0	0	5307	1215	331	4092	0.22
	L-4-12-26	3936.8	1838.7	0	8	5299	1072	135	4227	0.23
	L-4-12-27	4357.6	2006.7	0	7	5292	862	203	4430	0.24

[a]Calculated amount removed as O_2 dissolved in sample.
[b]12.8 cc at STP/psi.

Table 25. Oxygen Consumption in Loop L-4-13

Remarks	Sample Number	LITR Energy (Mwhr)	Total Solution Circulation Time (hr)	O_2 Additions to Loop (cc at STP)	O_2 Withdrawn from Loop[a] (cc at STP)	Total O_2 Charged to Loop Less O_2 Withdrawn in Sampling (cc at STP)	O_2 Volume at Time of Sample (cc at STP)	O_2 Consumed Since Last Sample (cc at STP)	Total O_2[b] Consumed (cc at STP)	Calculated Corrosion Penetration of Type 347 Stainless Steel (mils)
O_2 addition (L-4-13-1)		0	0	776	0	776	776	0	0	0
O_2 addition (L-4-13-2)		0	47	417	0	1193	1053	140	140	0.01
	L-4-13-1	0	72	0	5	1188	987	61	201	0.01
	L-4-13-2	114	114	0	4	1184	774	209	410	0.02
O_2 addition (L-4-13-3)			174	745	0	1929	1117	402	812	0.04
	L-4-13-3	310	186	0	5	1924	1000	112	924	0.04
	L-4-13-4	424	234	0	4	1920	745	251	1175	0.06
O_2 addition (L-4-13-4)			255	681	0	2601	1341	85	1260	0.06
	L-4-13-5	554	282	0	14	2587	1220	107	1367	0.06
	L-4-13-6	723	354	0	11	2576	952	257	1624	0.08
	L-4-13-7	778	402	0	10	2566	840	102	1726	0.08
	L-4-13-8	887	450	0	8	2558	719	113	1839	0.09
	L-4-13-9	1096	522	0	6	2552	551	162	2001	0.09
Loss from system				0	39	2513	436	76	2077	0.10
O_2 addition (L-4-13-5-B)			553	966	0	3479	1402	0	2077	0.10
	L-4-13-10	1275	618	0	10	3469	1249	143	2220	0.10
	L-4-13-11	1481	690	0	9	3460	1082	158	2378	0.11
	L-4-13-12	1590	738	0	9	3451	887	186	2564	0.12
	L-4-13-13	1734	786	0	7	3444	768	112	2676	0.13
	L-4-13-14	1947	858	0	6	3438	625	137	2813	0.13
O_2 addition (L-4-13-6)			886	1197	0	4635	1768	54	2867	0.13
	L-4-13-15	2055	931	0	16	4619	1572	180	3047	0.14
	L-4-13-16	2322	1028	0	13	4606	1268	291	3338	0.16
	L-4-13-17	2328								
Before loop drain			1042	0		4606	1234	34	3372	0.16

[a]Calculated amount removed as O_2 dissolved in sample.
[b]14.1 cc at STP/psi.

Table 26. Oxygen Consumption in Loop L-4-18

Remarks	Sample Number	LITR Energy (Mwhr)	Total Solution Circulation Time (hr)	O_2 Additions to Loop (cc at STP)	O_2 Withdrawn from Loop[a] (cc at STP)	Total O_2 Charged to Loop Less O_2 Withdrawn in Sampling (cc at STP)	O_2 Volume at Time of Sample (cc at STP)	O_2 Consumed Since Last Sample (cc at STP)	Total O_2[b] Consumed (cc at STP)	Calculated Corrosion Penetration of Type 347 Stainless Steel (mils)
Original O_2 fill		0	0	0	0	365	365	0	0	0
O_2 addition (L-4-18-1)		0	0	837	0	1202	1202	0	0	0
		0	5	0	0	1202	1159	43	43	0.001
	L-4-18-1	0	43.8	0	5	1197	579	575	618	0.03
O_2 addition (L-4-18-2)		0	45.4	726	0	1923	1302	3	621	0.03
	L-4-18-2	111.4	100.2		5	1918	1230	67	688	0.03
		115.0	108.8		0	1918	1216	14	702	0.03
		259.4	150.0		0	1918	1158	58	760	0.04
		358.8	190.0		0	1918	1102	56	816	0.04
		441.3	223.0		0	1918	1035	67	883	0.04
		521.1	250.0		0	1918	1008	27	910	0.04
		632.1	280.0		0	1918	980	28	938	0.04
		674.6	301.5		0	1918	957	23	961	0.05
		727.1	320.0		0	1918	952	5	966	0.05
		773.6	340.0		0	1918	943	9	975	0.05
		821.6	356.5		0	1918	933	10	985	0.05
	L-4-18-3	837.6	388.1		5	1913	893	35	1020	0.05
		837.6	410.0		0	1913	864	29	1049	0.05
	L-4-18-4	837.6	436.6		4	1909	828	32	1081	0.05
		837.6	456.3		0	1909	800	28	1109	0.05
		859.8	464.3		0	1909	792	8	1117	0.05
		923.9	490.0		0	1909	768	24	1141	0.05
	L-4-18-5	978.2	508.1		4	1905	751	13	1154	0.05
		1043.9	530.0		0	1905	730	21	1175	0.06
		1118.9	555.0		0	1905	708	22	1197	0.06
	L-4-18-6	1160.8	580.1		4	1901	684	20	1217	0.06
		1220.5	600.0		0	1901	665	19	1236	0.06
		1227.4	625.0		0	1901	650	15	1251	0.06
		1302.4	650.0		0	1901	634	16	1267	0.06
	L-4-18-7	1441.0	676.0		3	1898	618	13	1280	0.06
		1507.0	698.0		0	1898	605	13	1293	0.06
		1508.0	713.2		0	1898	599	6	1299	0.06
	L-4-18-8	1605.0	748.3		3	1895	572	24	1323	0.06
		1630.0	775.0		0	1895	549	23	1346	0.06
		1645.0	800.0		0	1895	529	20	1366	0.06
		1690.0	825.0		0	1895	508	21	1387	0.06
	L-4-18-9	1807.7	844.1		3	1892	493	12	1399	0.07
Pump failure		1926.2	859.6		0	1892	482	11	1410	0.07
Solution drained		1926.2	859.6		482	1410	0	0	1410	0.07

[a]Calculated amount removed as O_2 dissolved in sample.
[b]11.1 cc at STP/psi.

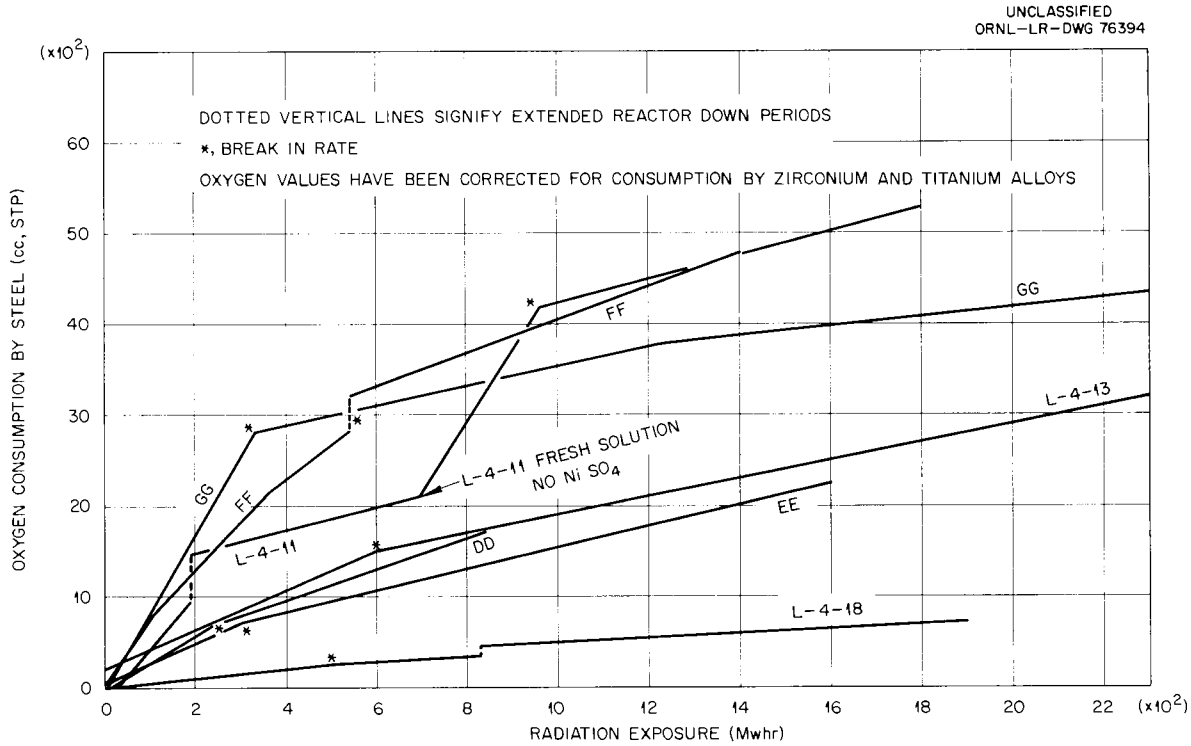

Fig. 30. Total Oxygen Consumption by Stainless Steel Corrosion vs Radiation Exposure.

4.4 Radiolytic-Gas Pressure

Average radiolytic-gas pressures in the pressurizers of the experiments at 3-Mw reactor power, calculated from pressurizer pressure-temperature measurements before and after reactor shutdowns, are listed in Table 27. These were used to calculate the copper rate constants in the different test solutions by the method previously described[7] and the equation reproduced here:

$$[H_2]^* = \frac{K_1(R^1/V_e)E}{B(K_m[Cu]/3600)^2 + (K_m[Cu]/3600)[B(R^1/V_m) + R^1/V_e] + [(R^1)^2/V_m V_e](1 - LE)} .$$

Values for the several factors employed in the calculations are also listed in Table 27. The fission-power values are those determined from Cs^{137} analyses as described in Sec 2 and were used to calculate K_1, the rate of H_2 formation in the mainstream solution, using a G_{H_2} value of 1.5. The solubility constants for O_2 (α') and H_2 or D_2(α) in the pressurizer solutions were obtained from a compilation of Battelle and ORNL solubility data by Banter.[8] The copper concentrations are those for the solutions as charged.

---

[7] G. H. Jenks and J. E. Baker, *Apparent Copper Rate Constants Determined in In-Pile Loop Experiment L-2-22*, ORNL CF-60-3-88 (Mar. 23, 1960).

[8] J. C. Banter, private communication.

Table 27. Apparent Copper Molar Rate Constants

Loop	Radiolytic-Gas Pressure in Pressurizer (psi)	P[a] Fission Power (w)	α, H_2 or D_2 Solubility at Pressurizer Temperature (psi liter^{-1} cc^{-1})	α', O_2 Solubility at Pressurizer Temperature (psi liter^{-1} cc^{-1})	R', Flow Rate Through Pressurizer (liters/sec)	V_e, Solution Volume in Pressurizer (liters)	V_m, Solution Volume in Pressurizer (liters)	L[b], Factor for Recombination of Radiolytic H_2 or D_2 and O_2 in Pressurizer Exit Line ($e^{-K_s't'}$)	E[b], Factor for Recombination of Radiolytic H_2 or D_2 and O_2 in Pressurizer Entrance Line ($e^{-K_s''t''}$)	[Cu], Copper Concentrations[c] in Solution Originally Charged to Loop (M)	$[H_2]$[a], H_2 or D_2 Concentration in Pressurizer (cc/liter)	H_2 or D_2 Concentration in Mainstream (cc/liter)	K_m[d], Apparent Copper Molar Rate Constant at Mainstream Temperatures (liters mole^{-1} hr^{-1})
DD	7.5	437	0.429	0.298	0.0051	0.241	0.644	0.956	0.854	0.030	19.0	75.6	2,500
FF	9.4	606	0.429	0.298	0.0035	0.228	0.656	0.936	0.796	0.028	23.8	112.6	2,400
GG	13	829	0.429	0.298	0.0035	0.204	0.655	0.937	0.798	0.027	32.9	157.3	2,850
EE	4.8	528	0.429	0.298	0.0034	0.252	0.621	0.934	0.788	0.028	12.1	80.3	3,180
L-4-12	10.6	730	0.429	0.298	0.0059	0.181	0.731	0.962	0.872	0.032	26.8	94.0	3,010
L-4-13	15.1	689	0.280	0.254	0.0042	0.293	0.795	0.958	0.884	0.034	39.1	165.8	1,600
L-4-18	10.8	700	0.322	0.268	0.0049	0.285	0.675	0.946	0.826	0.068	23.7	114.6	1,080

[a]Based on Cs^{137} analyses and 200 Mev/fission.

[b]K_s' and t' are, respectively, the estimated average rate constant in the pressurizer exit line (sec^{-1}) and the residence time in the line (sec), K_s'' and t'' are similarly defined factors for the entrance line.

[c]H_2O was the solvent in all experiments except L-4-13 and L-4-18, where D_2O was employed.

[d]Mainstream and pressurizer temperatures were 250 and 280°C, respectively, for all experiments except L-4-18; temperatures for L-4-18 were 235 and 265°C.

Note: All volumes and concentrations are (STP).

Another factor employed in the calculation is the ratio B of the rate constants in the pressurizer and mainstream. An activation energy of 22,000 kcal/mole for the copper activity was used to estimate these values.

The calculated values for the copper molar rate constant and the hydrogen concentration in the mainstream solutions are listed in the final columns of Table 27, and a plot of the rate-constant values is shown in Fig. 31. Also plotted is the molar rate constant (9860) determined in the 280°C experiment L-2-15[9] (0.17 m UO_2SO_4 in H_2O).

[9]G. H. Jenks and J. E. Baker, *HRP Radiation Corrosion Studies: In-Pile Loops L-2-15 and L-4-16*, ORNL-3099 (in preparation).

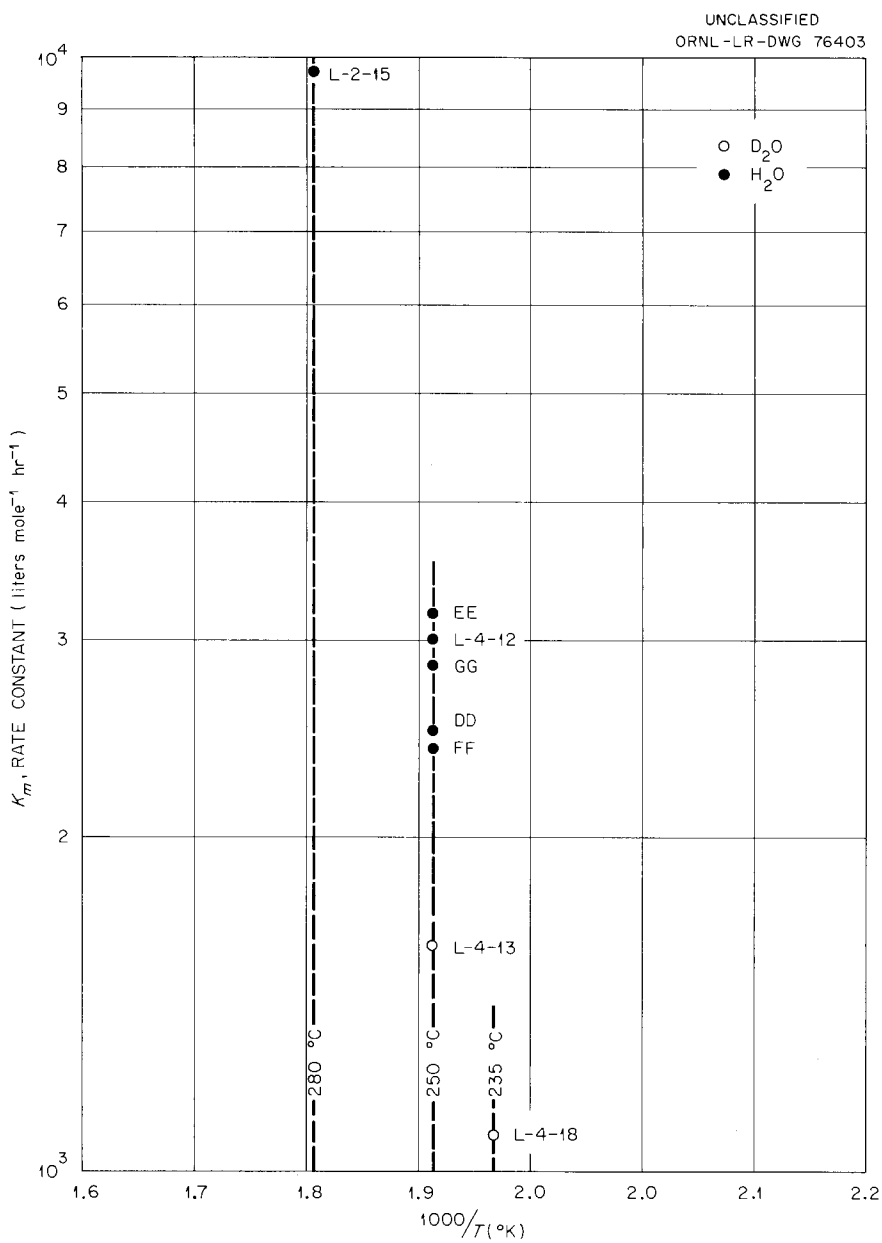

Fig. 31. Copper Molar Rate Constants vs Temperature.

The rate-constant values for H_2O solutions at 250°C are in the range 2400 to 3200 liters $mole^{-1}$ hr^{-1} and are in reasonable agreement with those determined in out-of-pile loop tests.[10] The constants in the experiments employing D_2O solutions (L-4-13 and L-4-18) were below those measured or predicted for water solutions. Similar differences between D_2O and H_2O solutions have been reported by others.[11]

4.5 Uranium Balance

The method and results of estimating the balance between the amounts of charged and recovered uranium in each of the experiments are illustrated in Table 28. Uranium balance results for the seven experiments are shown in Table 29.

In all but two of these experiments, the amount of recovered uranium, determined as shown in the table, was somewhat greater than the charged amounts. These discrepancies are believed to have resulted mainly from errors in sampling the weigh-tank contents (nonrepresentative samples) and, to a lesser extent, from uncertainties in the total volumes of solution in the weigh tank. Thus the actual uranium recovery in a given experiment is uncertain, but there is no reason to believe that recovery was significantly incomplete in any of the experiments.

4.6 Results of Qualitative Examination of Loops

Results of qualitative inspection of loop and specimens for each experiment are given in the following paragraphs. A brief description of the surface appearance of the coupons is included in Tables 36–42 and in Tables 30 and 31.

4.6.1 Loop DD

In general, the surfaces in all portions of the loop, with the exception of the forward or high-flux portion of the core, were covered with a very dark, dull scale. The nearly stagnant area on the outside of the in-line holder and the high-velocity areas of the pump impeller and housing were covered with the same dull, black film.

The films from wetted areas of the pressurizer, as well as those from vapor-phase portions, were similar to those in other portions of the loop. However, they were somewhat browner than those in the loop. The demarcation line between solution- and vapor-phase regions became less and less distinct from the inlet to the outlet of the pressurizer. The film was darker at the outlet than at the inlet.

Obvious changes in film appearance were observed in the core. At the rear or low-flux portion the film had the same dull, black appearance found in the rest of the loop. From the core rear toward areas of higher flux, the nature of the film gradually changed. It appeared to become thinner, harder, and glossier. The forward third of the core was covered with a film which had the appearance of a very glossy, baked, black enamel. The film on the core cap had this appearance and a slightly blistered appearance in addition. However, it is likely that this blistered appearance resulted from the character of the surface before

---

[10] G. H. Jenks, letter to E. G. Bohlmann, "Data from Determination of Cu^{++} in Out-of-Pile Loop Tests," Apr. 10, 1958.

[11] M. J. Kelly *et al.*, *HRP Quart. Progr. Rept. May 1–Oct. 31, 1959*, ORNL-2879, pp 93–95.

Table 28. Actual Uranium Balance in Experiment FF

Source	Solution Weight (g)	Specific Gravity	Solution Volume (ml)	Uranium Concentration by Analysis (mg/ml)	Weight of Uranium (g)
		Charged to Loop			
Original solution charged to system	1244	1,056	1178	40.0	47.0
Solution additions during operation			220	40.0	8.8
Total					55.8
		Recovered from Loop			
From weigh tank *after* sampling of contents [sample purges and flushes through sample 50 (b)]	4470[a]	1.0[b]	4470	2.4	10.7
From weigh tank *after* sampling of contents (purges from samples 52 and 53 plus loop contents and rinses)	7530[a]	1.0[b]	7530	6.2	46.5
Loop inventory samples sent to laboratory			77.3	40.0–36.4	2.9
Weigh tank samples sent to laboratory[c] Samples 51 (a) and (b) [weigh tank contents, sample purges, and flushes through sample 50 (b)]			2.1	2.4	0
Samples 54 (a) and (b), 55, 57, and 58 [weigh tank contents, sample purges, and flushes for samples following 50 (b), plus inventory drained from loop and loop rinses]			6.8	6.2	0
Total					60.1

[a]From weigh tank reading.
[b]Assumed.
[c]Weigh tank was drained of sample purges and flushes after sample 50 (b). Therefore, final contents of tank included purges and flushes from samples 52 and 53 plus loop inventory and loop rinses.

Table 29. Uranium Balance

Experiment	Uranium Charged to Experiment (g)	Uranium Recovered from Experiment (g)	Balance (%)
DD	41.5	45.0	+8.4
FF	55.8	60.1	+7.7
GG	61.7	64.1	+3.9
EE	54.0	52.9	−2.4
L-4-12	129.7	138.4	+6.7
L-4-13	81.8	78.8	−3.6
L-4-18	56.0	61.0	+9.0

Table 30. Summary of Metallographic Examination of Corrosion Coupons

Coupon Number	Average Solution Velocity Across Specimen (fps)	Solution Fission-Power Density at 3 Mw (w/ml)	Coupon Thickness (mils)	Weight Change (mg)	Remarks	Figure Number
				Loop DD		
Core-channel coupons						
Type 347 SS						
437A	12	1.5	55.2	−93.9	"Shouldered" – slight attack at grain boundaries	53
442A	45	0.8	59.0	−37.9	Many pits 2 to 3 mils in depth	
446A	13	0.3	59.3	−6.6	A few shallow pits	
In-line–channel coupons						
Type 347 SS						
449A	12		59.5	−3.5	No attack	
454A	45		59.6	−5.4	A very few shallow pits	
				Loop FF		
Core-channel coupons						
Zircaloy-2						
924A	13	3.3	59.4	−8.1	No evidence of localized or pitting type corrosive attack	
929A	46	1.6	59.8	−4.8	No evidence of localized or pitting type corrosive attack	
933A	14	0.9	59.6	−3.4	No evidence of localized or pitting type corrosive attack	
In-line–channel coupons						
Zircaloy-2						
912A	13		60.9	+0.8	No evidence of localized or pitting type corrosive attack	
917A	46		59.8	+1.3	No evidence of localized or pitting type corrosive attack	
				Loop GG		
Core-channel coupons						
Zircaloy-2						
948A	13	4.5	59.0	−16.5	Surface slightly roughened; 3-mil crack on one side	55
953A	46	2.5	59.2	−11.8	Entire surface smooth, no attack	
957A	17	1.5	60.0	−9.3	Entire surface smooth, no attack	
In-line–channel coupons						
Zircaloy-2						
941A	46		60.5	+1.6	Entire surface smooth; film not observable	
945A	17		59.3	−2.5	Entire surface smooth; no attack	
				Loop EE		
Core-channel coupons						
Type 347 SS						
743A	12	4.6		−105.5	Severely attacked – over 4 mils of surface removal	56
747A	41	2.3		−2.5	Numerous pits – approximately 1 mil in depth	
787A	10	1.0		−0.1	No evidence of corrosive attack	
Titanium-55A						
T-8	10	5.7		−0.5	No evidence of corrosive attack	
T-12	38	2.5		−1.4	No evidence of corrosive attack	
T-16	12	1.2		−0.4	No evidence of corrosive attack	
Zircaloy-2						
Z-19	10	5.3		−5.1	Numerous pits – approximately ½ mil in depth	
Z-24	35	2.7		−2.9	Slight surface roughening	
Z-37	11	1.3		−1.6	Slight surface roughening	
In-line–channel coupons						
Type 347 SS						
740A	41			+4.6[a]	A few pits – approximately ½ mil in depth	

Table 30 (continued)

Coupon Number	Average Solution Velocity Across Specimen (fps)	Solution Fission-Power Density at 3 Mw (w/ml)	Coupon Thickness (mils)	Weight Change (mg)	Remarks	Figure Number
Zircaloy-2						
Z-12	35			+6.0[a]	No evidence of corrosive attack	
Titanium-55A						
T3	38			+4.9[a]	No evidence of corrosive attack	
				Loop L-4-12		
Core-channel coupons						
Type 347 SS						
992A	40	2.1	59.8	−3.7	One side rough and uneven; one end severely attacked, 5-mil variation	
996A	10	0.9	60.0	−0.7	Smooth on both sides and ends	
Zircaloy-2						
Z-89	11	4.2	58.8	−13.8	Smooth over entire surface	
Z-92	44	1.9	59.2	−7.1	Two isolated rough spots less than 1 mil deep, otherwise smooth	
Titanium-55A						
Ti-100	9	4.8	59.4	−2.1	Smooth, no attack	
Ti-103	37	2.2	59.3	−0.9	Smooth, no attack	
Ti-107	12	1.1	58.6	−0.1	Smooth, no attack	
In-line–channel coupons						
Type 347 SS						
1121A	13		59.9	−1.2	Sides smooth; one end attacked, 3-mil variation	
1126A[b]	20			−107.5	Smooth except near one end, up to 12 mils removed at end	58
Inconel						
1125A	40			−609.4	Surface uneven, up to 40 mils general removal	
Zircaloy-2						
Z-102[c]	15		60.2		Sides smooth, all corners severely attacked	
Z-103[c]	11		61.1		Sides smooth, all corners severely attacked	59
Titanium-55A						
Ti-116[c]	17		59.9		Smooth, no attack	
Ti-118[c]	12		59.9		Smooth, no attack	
				Loop L-4-13		
Core-channel coupons						
Type 347 SS						
1022A	13	4.4	61.6–62.6	−6.8	Pits (up to 3 mils) on all surfaces	61
1027A	13	1.3	61.6–61.3	−1.2	A few 1-mil pits on all surfaces	
Type 309SCb SS						
C-53	37	2.4	58.6–60.7	−1.3	One-mil pits spread uniformly over surface	
C-57	12	1.3	59.6–60.0	−1.8	Smooth, no attack	
Crystal-bar zirconium						
Z-101	11	5.3	59.4–60.0	−7.4	Surface slightly roughened; no pits or cracks	
Z-104	44	2.0	59.1–59.9	−4.8	Surface slightly roughened; no pits or cracks	
In-line–channel coupons						
Type 347 SS						
1031A	13		58.3–61.2	−0.6	Smooth, no pits	
1037A	13		59.6–60.7	−0.8	Smooth, no pits	

Table 30 (continued)

Coupon Number	Average Solution Velocity Across Specimen (fps)	Solution Fission-Power Density at 3 Mw (w/ml)	Coupon Thickness (mils)	Weight Change (mg)	Remarks	Figure Number
Type 309SCb SS						
C-58	9		59.6–59.9	−0.7	Smooth, no attack	
C-65	12		59.6–60.7	−2.4	Corners and ends roughened	62
Crystal-bar zirconium						
Z-110	20		57.0–60.0	+2.9	Surface slightly roughened; no film visible	
Z-115	11		53.0–60.7	−3.2	Both ends attacked; ¼-mil film on some areas	63
				Loop L-4-18		
Core-channel coupons						
Type 347 SS						
SA-1563	13	4.0	58.0–58.0	−0.1	Smooth, even – no evidence of attack	
SA-1569	10	1.1	58.0–60.0	−2.3	Severely pitted on gripped edges, exposed surface smooth, even	
SL-15	10	5.2	60.0–61.0	−11.9	General surface attack at one gripped edge	
SL-16	14	3.7	60.0–60.0	−2.1	Smooth, even – no evidence of attack	
SL-22	12	1.3	60.0–62.0	−1.9	Smooth, even – no evidence of attack	
Zircaloy-2						
ZB-131	11	4.6	59.0–61.0	−3.1	Smooth, even – no evidence of attack	
ZB-143	10	1.2	60.0–61.0	−1.2	Smooth, even – no evidence of attack	
Core-annulus coupons						
Type 347 SS						
SA-1590	1.0	4.3	58.0–60.0	−4.1	General pitting on exposed faces	
Type 430L SS						
SL-31	1.0	4.5	59.0–61.0	−5.8	Possible slight surface roughening	
Zircaloy-2						
ZB-157	1.0	3.9	60.0–61.0	−2.7	Smooth, even – no evidence of attack	
Zirconium–15% Nb						
ZX-1	1.0	4.3	60.0–60.0	−1.9	Smooth, even – no evidence of attack; metallic layer on portions of exposed faces	
Titanium-55A						
T-170	1.0	4.2	60.0–60.0	−0.3	Smooth, even – no evidence of attack	
Titanium–3% Al						
TJ-11	1.0	4.1	60.0–61.0	−0.6	Smooth, irregular – no evidence of attack	
TJ-13	1.0	3.1	59.0–60.0	−0.7	Smooth, irregular – no evidence of attack	
In-line channel						
Type 347 SS						
SA-1575	19		58.0–58.0	−0.1	Smooth, even – no evidence of attack	
SA-1577	10		60.0–61.0	−2.8	Severe pitting attack on gripped edges, exposed surfaces smooth and even	
Type 430L SS						
SL-23	10		60.0–61.0	−1.6	Smooth, even – no evidence of attack	
SL-30	12		58.0–59.0	−2.3	Smooth, even – no evidence of attack	
Zircaloy-2						
ZB-147	33		60.0–62.0	+1.6	Smooth, even – no evidence of attack	
ZB-151	10		60.0–61.0	+1.4	Smooth, even – no evidence of attack	
In-line annulus						
Type 347 SS						
SA-1597	1.0		61.0–63.0	+0.4	Smooth, even – no evidence of attack	
SA-1599	1.0		57.0–59.0	−0.3	Smooth, even – no evidence of attack	

Table 30 (continued)

Coupon Number	Average Solution Velocity Across Specimen (fps)	Solution Fission-Power Density at 3 Mw (w/ml)	Coupon Thickness (mils)	Weight Change (mg)	Remarks	Figure Number
Type 430L SS						
SL-39	1.0		60.0–61.0	−2.1	Smooth, even – no evidence of attack	
SL-45	1.0		60.0–61.0	−4.6	General surface attack, one face	
Zircaloy-2						
ZB-161	1.0		60.0–61.0	+1.7	Smooth, even – no evidence of attack	
Zirconium–15% Nb						
ZN-5	1.0		60.0–60.0	+0.7	Smooth, even – no evidence of attack	
Titanium-55A						
T-173	1.0		58.0–60.0	+0.2	Smooth, even – no evidence of attack	
Titanium–3% Al						
TJ-15	1.0		61.0–61.0	+0.1	Smooth, irregular – no evidence of attack	

[a]Based on as-removed weight change.
[b]Adjacent to loose coupons.
[c]Coupons damaged – Loose in holder.

exposure, since some of the stock end caps from which this core cap was drawn have the same blistered appearance. The surfaces of the cap and core walls are shown in Figs. 32 and 33.

The Zircaloy-2 impact specimens and Zircaloy-2 sample holder also exhibited differences in appearance, depending upon their location in the core. The Zircaloy-2 surfaces in the low-flux areas were covered with a heavy black film, which gradually changed to a brown color and became thinner at the higher fluxes. The surfaces in the highest flux regions appeared to be completely free of film. The original fine machine marks were visible at the high-flux end of the Zircaloy-2 holder. The stainless steel specimens in the core were also covered with film which varied in appearance as did that on the core walls. No evidence was apparent of a velocity effect on the character of film on the specimens.

Both the in-line specimens and the core specimens were defilmed, inspected visually, and weighed. Figure 34 is a group photograph of the defilmed core and in-line coupons. Figures 35–41 are magnified photographs of the individual coupons. Only two typical in-line coupons are included, while all the coupons from the core assembly are shown. In both cases the flow pattern is from position *A* through position *L*, with the high-velocity region, approximately 50 fps, on the trailing edge of position *G* and the leading edge of position *H*. The sides of core coupons B through D, which were encased and apparently protected by the holder, stand in relief above the exposed surfaces. For coupon A, approximately 60% of the encased area was attacked to the same degree as the exposed areas. This additional attacked area has been treated as exposed area in consideration of the weight data. The calculations are listed in Table 36.

Corrosion of the core coupons appeared to start with shallow pits which apparently grew laterally until, in the case of the coupons in the highest flux, the entire surface was removed.

A further comment involves the defilming characteristics of the coupons. Since all coupons were defilmed cathodically in an inhibited sulfuric acid solution, the ease with which these films were removed

Table 31. Summary of Metallographic Examination of Stress Corrosion Specimens

Specimen Number	Solution[a] Fission-Power Density at 3-Mw (w/ml)	Weight Change (mg)	Coupled to	Remarks
		Loop EE		
Core-annulus specimens				
Type 347 SS				
SS-11	2.7	−33.7	SS-12	Slight pitting attack – less than 1 mil deep
SS-12	2.7	−35.5	SS-11	Slight pitting attack – less than 1 mil deep
SS-13	2.7	−26.1	SS-14	Slight pitting attack – less than 1 mil deep
SS-14	2.7	−30.6	SS-13	Slight pitting attack – less than 1 mil deep
Zircaloy-2				
Zr-2	2.7	−93.1	Zr-3	Very rough, uneven surface
Zr-3	2.7	−94.0	Zr-2	Very rough, uneven surface
Zr-4	2.7	−76.4	Zr-5	Very rough, uneven surface
Zr-5	2.7	−72.4	Zr-4	Very rough, uneven surface
Titanium-55A				
Ti-1	2.7	− 3.2	Ti-2	No evidence of corrosive attack
Ti-2	2.7	− 3.1	Ti-1	No evidence of corrosive attack
Ti-11	2.7	− 4.5	Ti-12	No evidence of corrosive attack
Ti-12	2.7	− 3.8	Ti-11	No evidence of corrosive attack
		Loop L-4-12		
Core-annulus specimens				
Titanium-6Al-4V				
TJ-11	2.4	−29.1	TJ-12	Small cracks in tension surface near end; otherwise smooth
TJ-12	2.4	−26.1	TJ-11	One-mil cracks at extreme end of tension surface; otherwise slightly roughened[b]
TJ-13	2.4	−29.4	TJ-14	Tension surface rough; compression surface smooth; no cracking
TJ-14	2.4	−25.2	TJ-13	One-half-mil cracks in the end of tension surface and on center of compression surface; otherwise smooth
In-line–annulus specimens				
Titanium-6Al-4V				
TJ-7		− 5.5	TJ-8	Both surfaces smooth; attack not apparent from metallographic examination
TJ-8		− 6.3	TJ-7	Tension surface smooth; compression surface slightly roughened; no cracks
TJ-9		− 4.9	TJ-10	One-half-mil cracks in tension surface at one end; other surfaces slightly roughened
TJ-10		− 2.9	TJ-9	Both surfaces slightly roughened; no cracking
Pressurizer (liquid phase)				
Type 17-4 PH SS				
SH-1		−49.1	TE-1	Tension surface slightly roughened; compression surface smooth; small cracks in both surfaces
SH-3		− 1.4	TJ-1	Both surfaces smooth

Table 31 (continued)

Specimen Number		Solution[a] Fission-Power Density at 3-Mw (w/ml)	Weight Change (mg)	Coupled to	Remarks
Titanium C-130AM					
TE-1			−27.2	SH-1	Both surfaces rough; compression 2 or 3 times as bad as tension
TE-5			− 1.0	TE-6	Both surfaces smooth; attack not apparent from metallographic examination
TE-6			− 2.9	TE-5	Both surfaces smooth; attack not apparent from metallographic examination
Titanium-6Al-4V					
TJ-1				SH-3	Both surfaces slightly roughened; maximum variation ½ mil
TJ-3			+ 0.4	TJ-4	Both surfaces slightly roughened; no cracking
TJ-4			− 6.5	TJ-3	Tension surface slightly rooughened; no cracking or pitting
Pressurizer (vapor-phase)					
Type 17-4 PH SS					
SH-2			−35.7	TE-2	Numerous pits on both surfaces, several longitudinal interior cracks near one end
SH-4			− 9.1	TJ-2	Both surfaces smooth
Titanium C-130AM					
TE-2			− 0.8	SH-2	Both surfaces smooth; attack not apparent from metallographic examination
TE-3			− 0.8	TE-4	Both surfaces smooth; attack not apparent from metallographic examination
TE-4			− 3.7	TE-3	Both surfaces smooth; attack not apparent from metallographic examination
Titanium-6Al-4V					
TJ-2				SH-4	Both surfaces slightly roughened; no cracking
TJ-5			− 4.7	TJ-6	Both surfaces smooth, attack not apparent from metallographic examination
TJ-6			− 9.6	TJ-5	Several ½-mil cracks scattered over center ⅓ of tension surface, otherwise smooth
			Loop L-4-18		
Core annulus					
Zircaloy-2					
ZB-2	2.6	2.6	−25.4	ZB-5	Smooth, even – no attack
ZB-5		2.6	−24.8	ZB-2	Smooth, even – no attack
In-line annulus					
Zircaloy-2					
ZB-6			+ 6.2	ZB-9	Smooth, even – no attack
ZB-9			+ 6.4	ZB-6	Smooth, even – no attack

[a]Average value for length of specimen

[b]Figure 60.

Note: Solution velocities across annulus specimens are ~1.0 fps; solution velocities across pressurizer specimens are negligible.

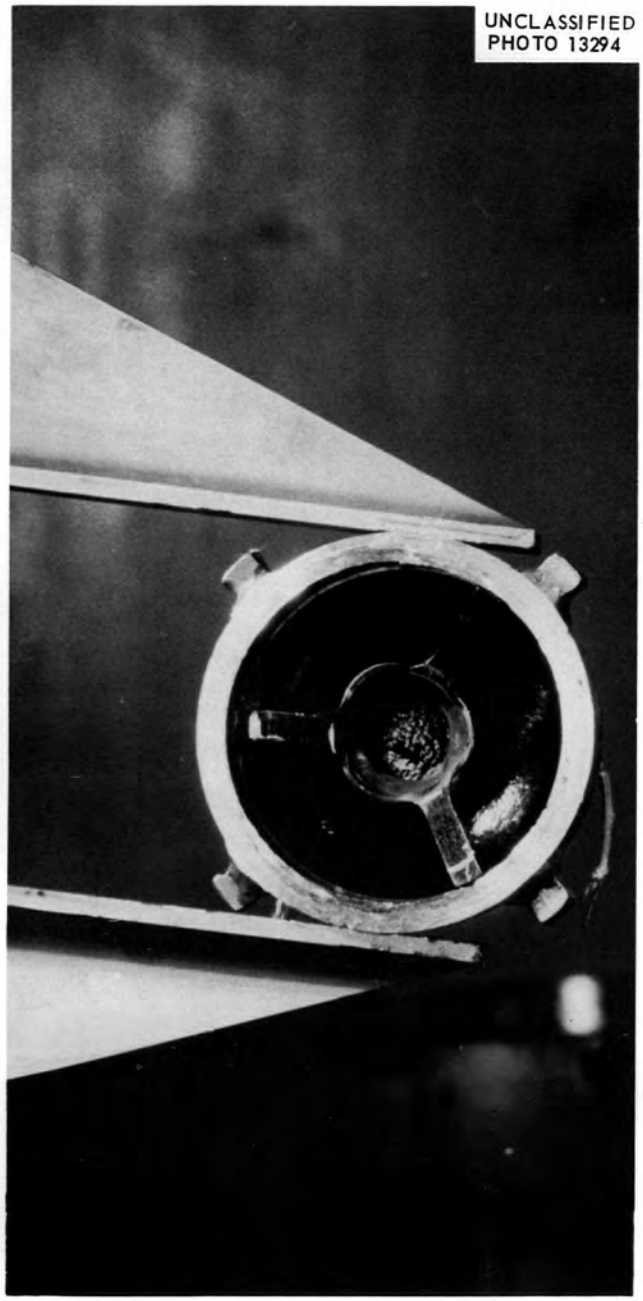

Fig. 32. Core Cap with Spider in Place, Loop DD.

Fig. 33. Core Cap Alone, Loop DD.

UNCLASSIFIED
PHOTO 13586

POSITION A

POSITION L

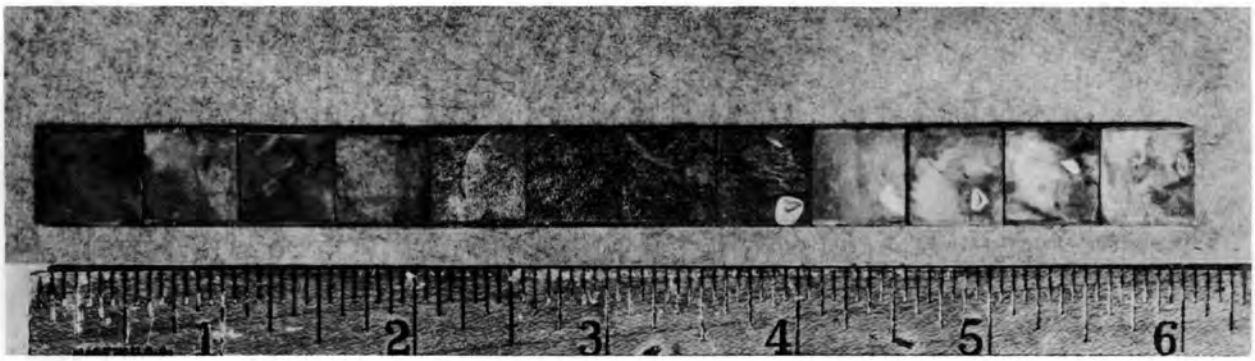

CORE ARRAY

POSITION A

POSITION L

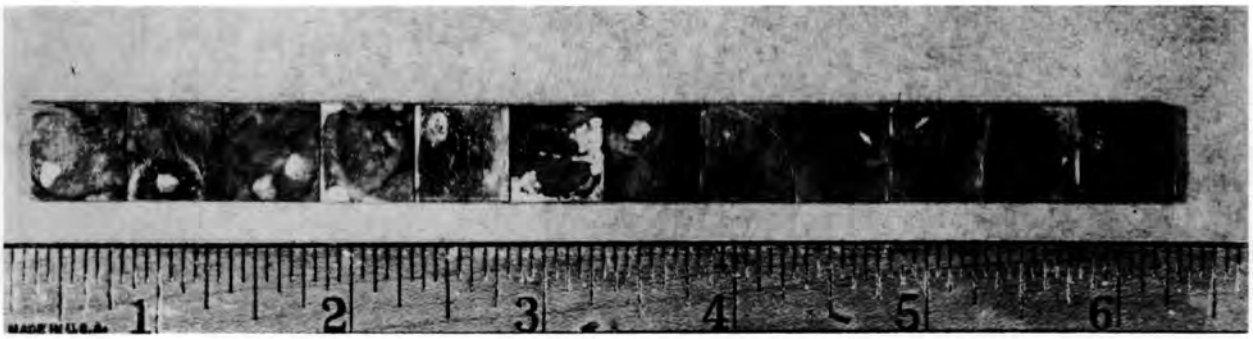

IN-LINE ARRAY

Fig. 34. HRP In-Pile Loop DD Corrosion Coupon Arrays After Defilming. 0.95 X. Reduced 2%.

UNCLASSIFIED
PHOTO 13580

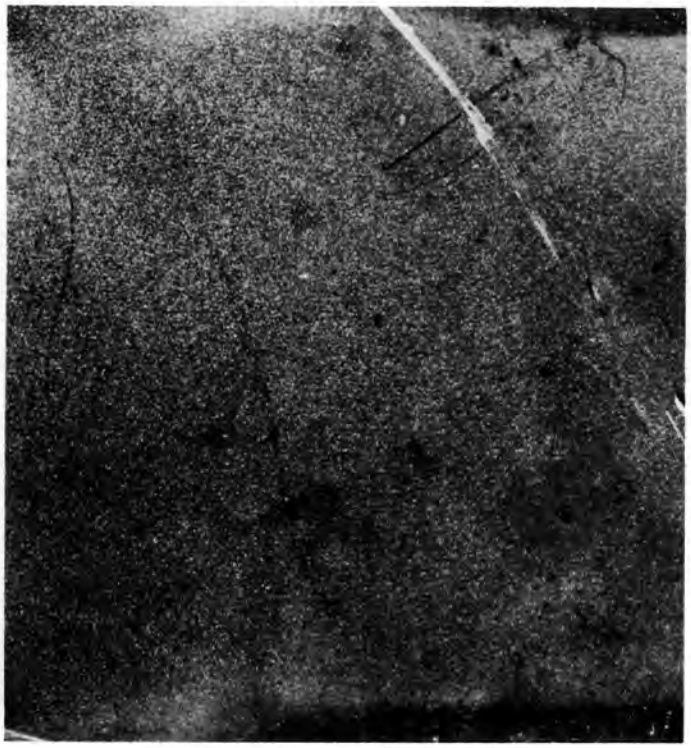

COUPON 436-A (POSITION A)

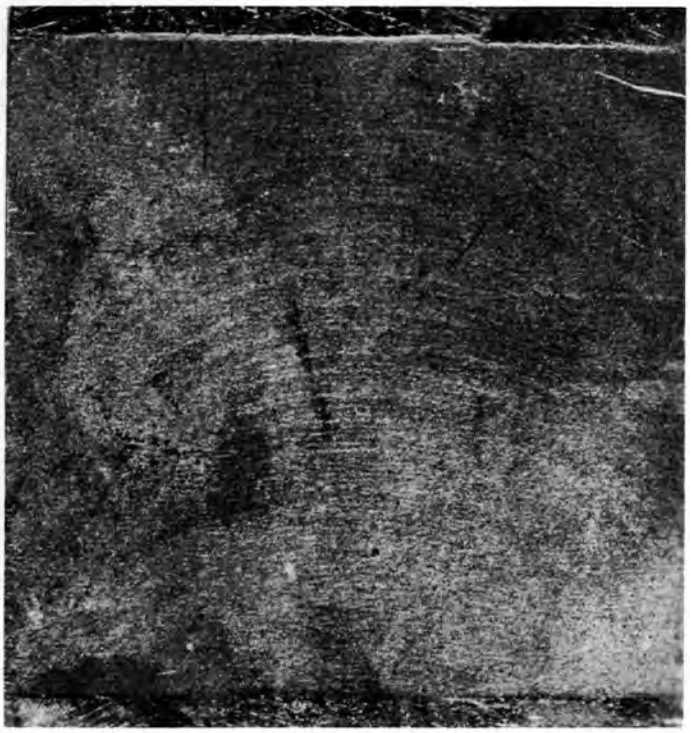

COUPON 437-A (POSITION B)

Fig. 35. Defilmed Type 347 Stainless Steel Corrosion Coupons from Core Holder of In-Pile Loop DD. 6.7 X.

UNCLASSIFIED
PHOTO 13582

COUPON 438-A (POSITION C)

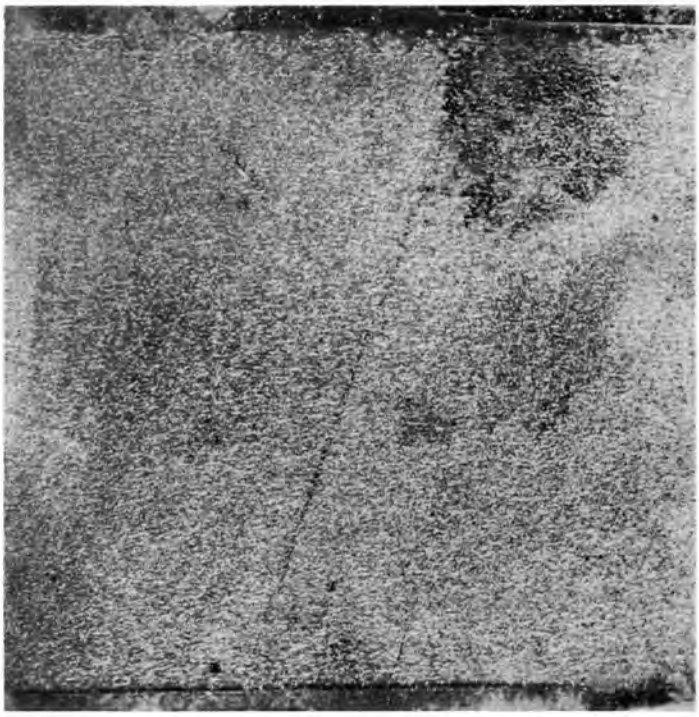

COUPON 439-A (POSITION D)

Fig. 36. Defilmed Type 347 Stainless Steel Corrosion Coupons from Core Holder of In-Pile Loop DD. 6.7 X.

UNCLASSIFIED
PHOTO 13584

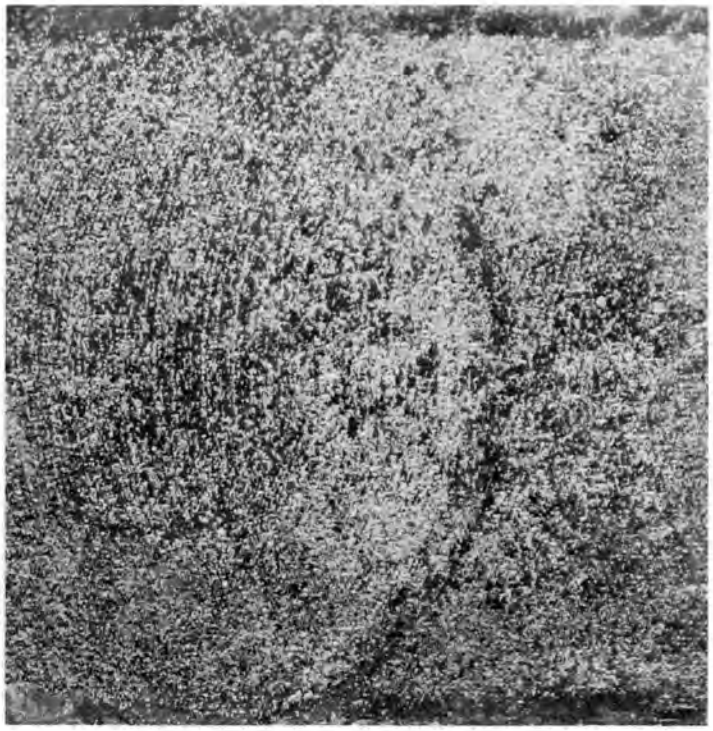

COUPON 440-A (POSITION E)

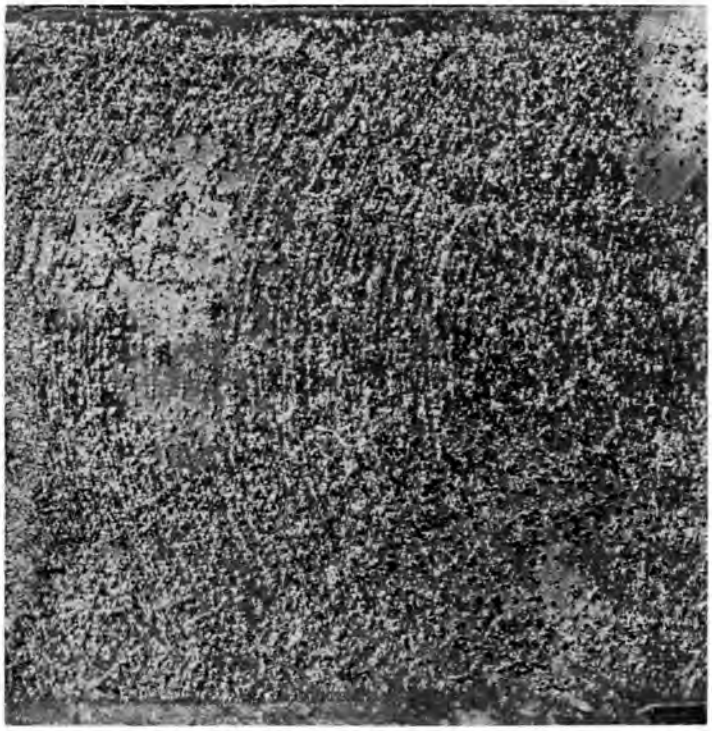

COUPON 441-A (POSITION F)

Fig. 37. Defilmed Type 347 Stainless Steel Corrosion Coupons from Core Holder of In-Pile Loop DD. 6.7 X.

UNCLASSIFIED
PHOTO 13583

COUPON 442-A (POSITION G)

COUPON 443-A (POSITION H)

Fig. 38. Defilmed Type 347 Stainless Steel Corrosion Coupons from Core Holder of In-Pile Loop DD. 6.7 X.

UNCLASSIFIED
PHOTO 13581

COUPON 444-A (POSITION I)

COUPON 445-A (POSITION J)

Fig. 39. Defilmed Type 347 Stainless Steel Corrosion Coupons from Core Holder of In-Pile Loop DD. 6.7 X.

UNCLASSIFIED
PHOTO 13587

COUPON 446-A (POSITION K)

COUPON 447-A (POSITION L)

Fig. 40. Defilmed Type 347 Stainless Steel Corrosion Coupons from Core Holder of In-Pile Loop DD. 6.7 X.

UNCLASSIFIED
PHOTO 13585

COUPON 449-A (POSITION A)

COUPON 454-A (POSITION G)

Fig. 41. Defilmed Type 347 Stainless Steel Corrosion Coupons from In-Line Holder, Loop DD. 6.7 X.

is indicative of their protective nature. Every coupon from the core holder defilmed readily in 3 min at the normal current density of 20 amp/dm^2; only the last five coupons exposed to the lowest fluxes showed any electrode effect. The electrode effect is the result of a momentary anodic reaction of the coupon caused by the voltage drop across the film. The result of this anodic reaction is a shiny area adjacent to the contact points. All the in-line coupons showed some electrode effect and each required from 10 to 15 min for defilming. Even after the application of voltage for this long period, the in-line specimens were not as completely defilmed as the core specimens.

4.6.2 Loop FF

All surfaces outside the core area were covered with a heavy rustlike scale, even in the high-velocity areas. Figure 42 is a picture of the coupons and interior surface of the in-line assembly; it shows that there was no apparent velocity effect upon the amount of deposited scale.

Figure 43 is a photograph of the core coupon and impact specimen assembly in the as-removed condition. All the stainless steel components in this region were covered with a rustlike scale. However, the deposit appeared to become thinner with increasing flux. The Zircaloy-2 holder and impact specimens were free from any scale deposit in the higher-flux regions. The only visible scale on the Zircaloy-2 holder was located around the spider at the low-flux end of the assembly. The machining marks and stamped identifications were clearly visible on both holder and coupons. There was no obvious indication of increased attack on the portions of specimens not protected by the holders, as was seen with the loop DD stainless steel core coupons.

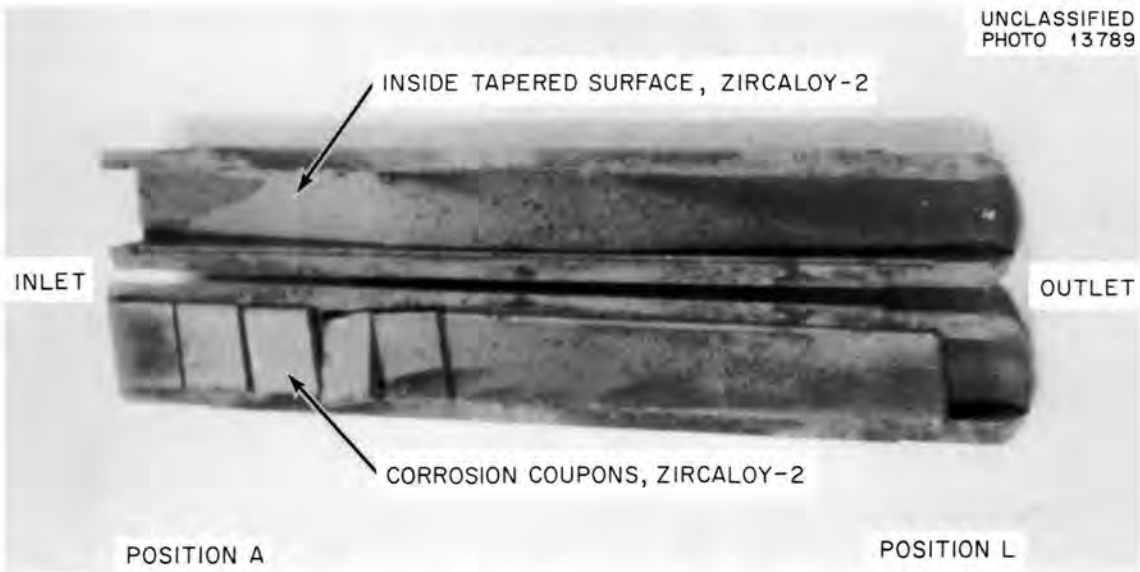

Fig. 42. In-Line Coupon Assembly Before Defilming, Loop FF.

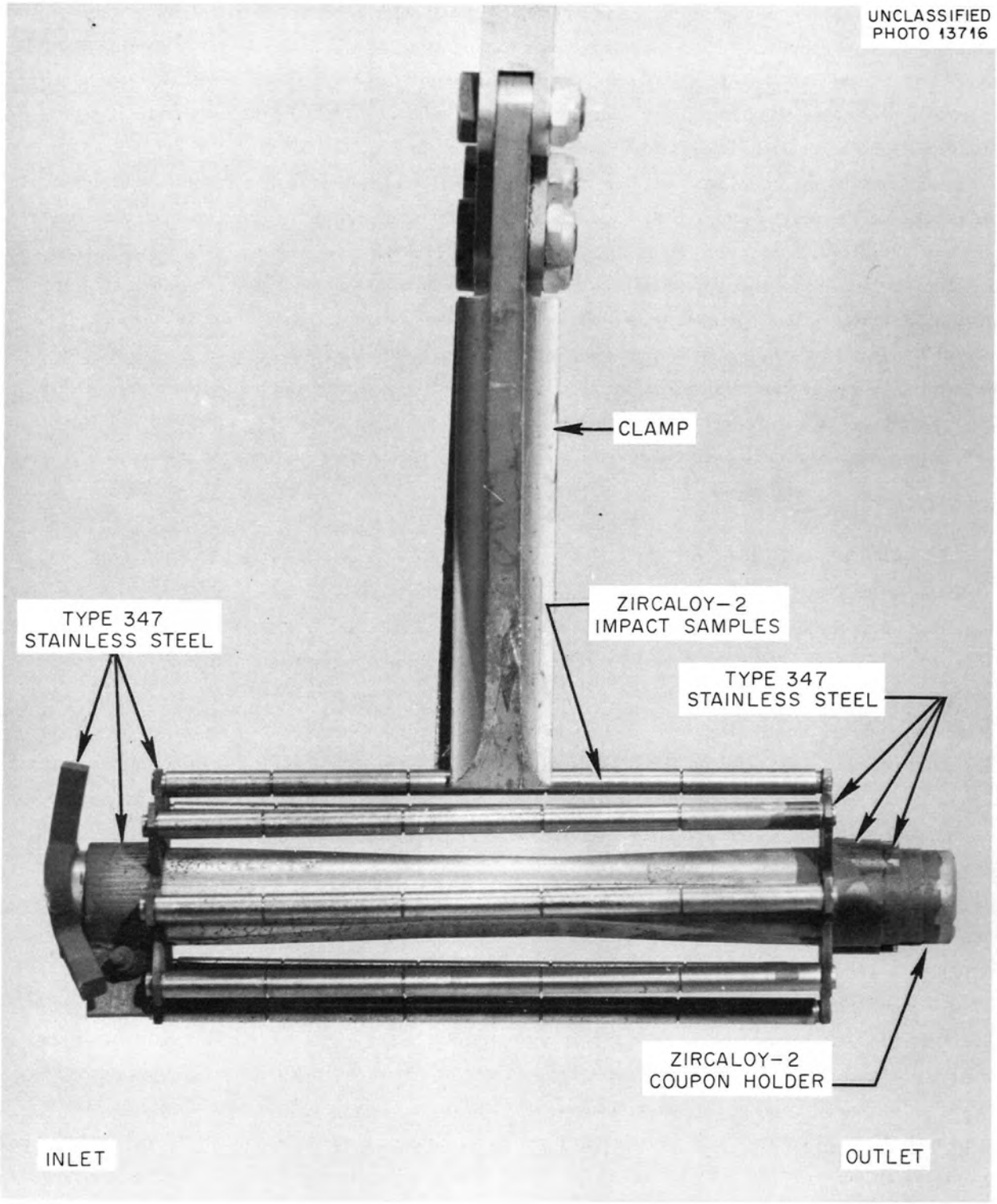

Fig. 43. Core Specimen Assembly, Loop FF.

Corrosion coupons, coupon holders, and impact specimens were all removed from the loop and weighed in the as-removed condition. Although microscopic examination of the heavy scale on the in-line coupons showed that it had flaked off in some areas, prolonged cathodic treatment and mechanical brushing failed to remove this scale. Some of the scale was pulled from the metal surface by the use of Scotch tape, but this method was not completely effective either.

Examination of the stainless steel core body and cap surfaces indicated that the relative amounts of the covering oxide scale decreased with increasing flux. However, there was little change in oxide appearance with flux. In contrast, rather distinctive changes in scale character with flux were observed in the previous loop DD. Generally, there was no evidence of localized attack. However, during the pre-irradiation testing of the loop at Y-12, a pinhole leak was detected in the reducer at the rear of the core assembly. This leak was repaired by grinding out the metal in that area and backfilling with weld metal. When the core was sectioned after irradiation, a rather large pit or cavity was found in the area of this repair. Figures 44 and 45 are general views of the core sections showing the extent of this cavity. A sample from this area was among the several samples submitted for metallographic examination.

4.6.3 Loop GG

As with the previous loops DD and FF, all surfaces outside the core area were covered with a heavy rustlike scale. There was no apparent localized attack on any component inspected. Figure 46 is a view of coupons from the in-line coupon holder and the interior tapered surface of the holder in the as-removed state. The loose, flaky nature of the bulk scale on the Zircaloy-2 coupons and holder is quite evident.

In the core region, all stainless steel surfaces appeared to be covered with a similar, but somewhat less bulky, rustlike scale. Figure 47 is a photograph of the core assembly in the as-removed condition. The stainless steel clamping bands on each end and the stainless steel "spiders" which held the impact samples were covered with a rustlike scale. As with loops DD and FF, the Zircaloy-2 impact specimens and holder surfaces appeared to be free from bulk-scale deposits in the higher flux region. Only on the extreme outlet, or low-flux, end of the core coupon holder was there any apparent buildup of scale. Closer examination under the remote microscope revealed that there was some film on all Zircaloy-2 surfaces. The thickness of the film was apparently inversely proportional to the flux at which the surface was exposed.

The core specimens were defilmed completely by cathodic treatment in 5% H_2SO_4. However, the in-line specimens, as before, could not be defilmed completely. Some of the scale was again removed by pulling it from the surface with Scotch tape, but this was only partially effective and did not remove any of the underlying film. Very extensive defilming of one in-line coupon, 939A, was attempted. Even after many repetitions of the treatment with Scotch tape and of cathodic cleaning at current densities higher than usual, the coupon still showed a 0.1-mg weight gain. Flakes of scale and a uniform coating of dark-gray film were still visible under the microscope.

A sample of the rustlike bulk scale from the in-line Zircaloy-2 holder was submitted for chemical analysis. The following composition by weight was reported: iron, 32%; uranium, 32%; zirconium, 7%; sulfate, 11%; copper, 1%; nickel, 2%; and chromium, 0.1%.

Fig. 44. Type 347 Stainless Steel Core Section, as Removed from Loop FF.

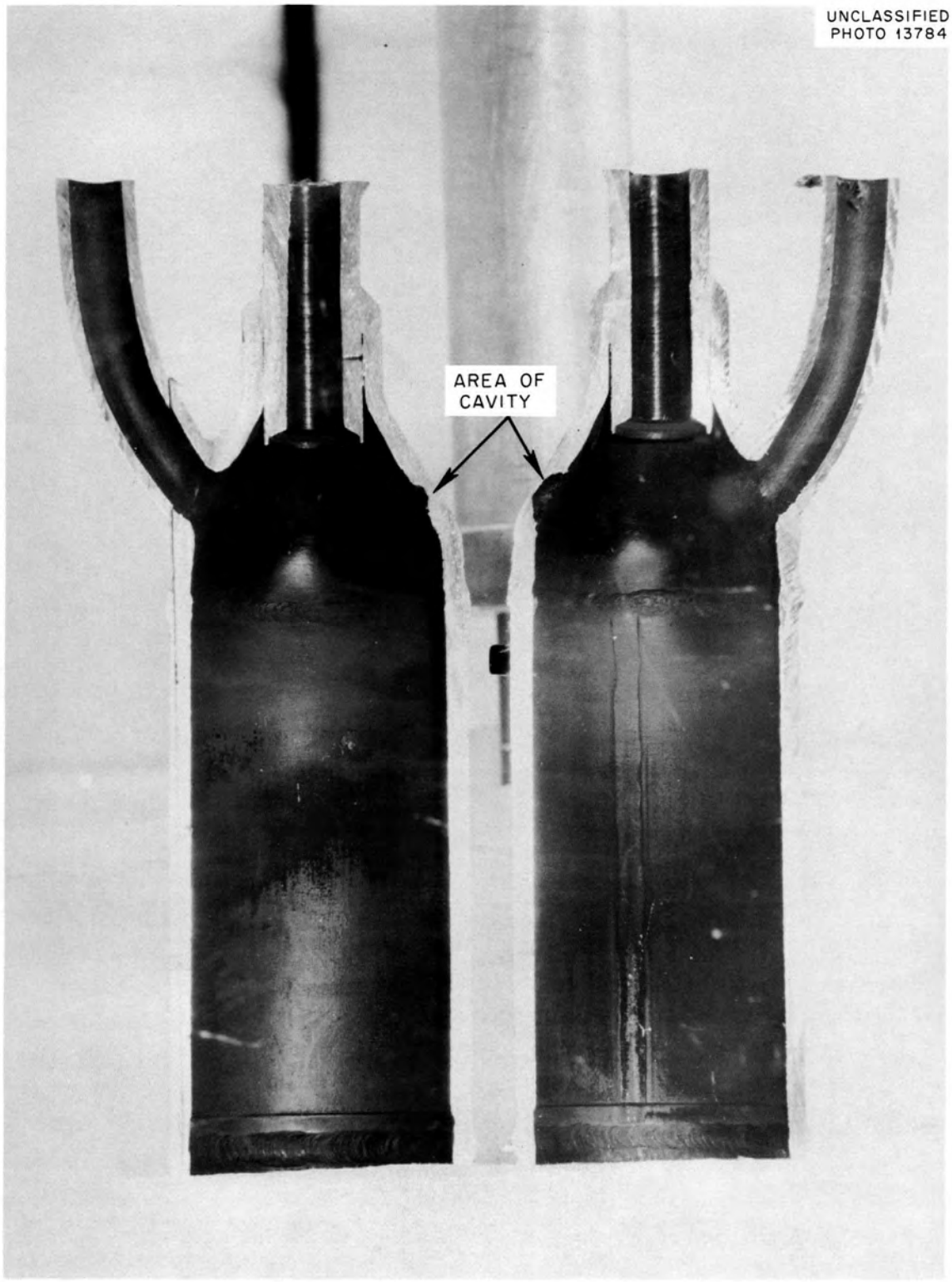

Fig. 45. Type 347 Stainless Steel Core Sections, as Removed from Loop FF.

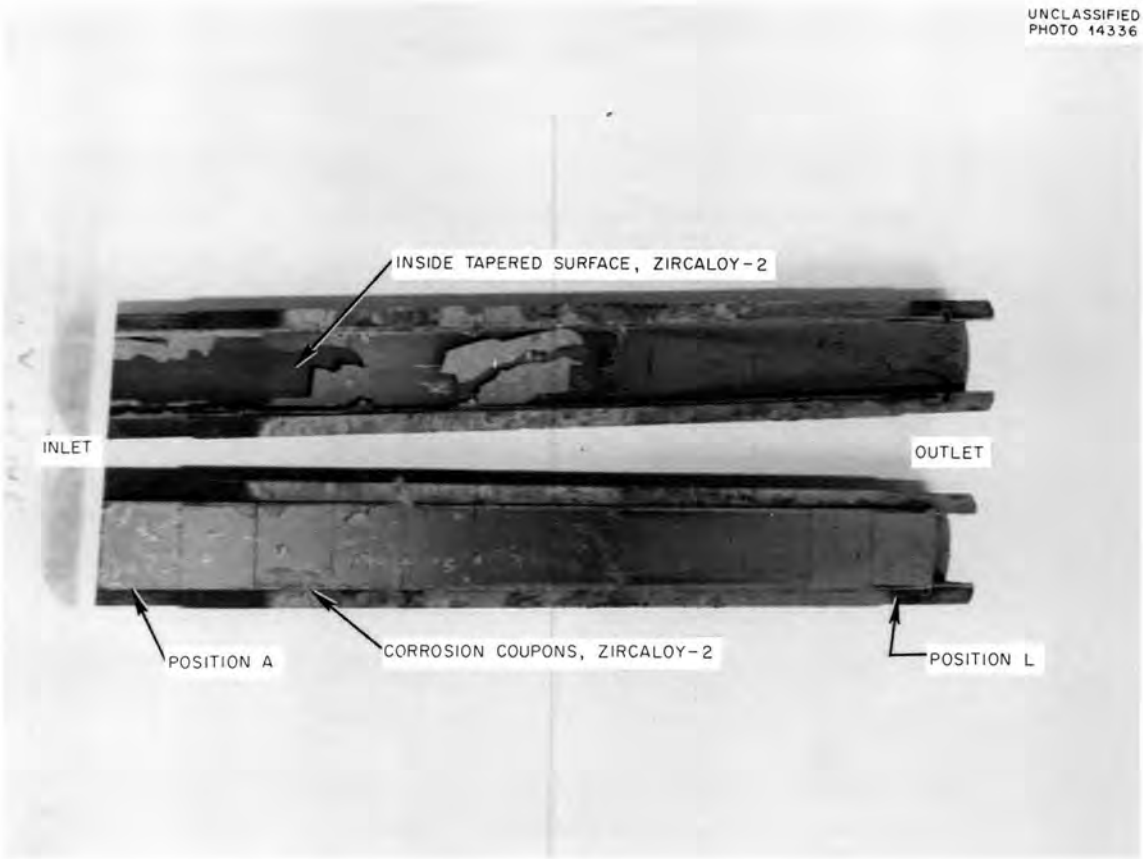

Fig. 46. In-Line Coupon Assembly, Loop GG.

4.6.4 Loop EE

As with previous loops, GG, FF, and DD, all surfaces outside the core were covered with a rustlike scale; there was no evidence of localized attack on any of the components inspected.

In the core area, all the stainless steel components were covered with a less bulky scale of similar rustlike appearance. The various titanium specimens were covered with a very thin rustlike scale, which, in general, became more bulky with decreasing flux. In contrast to previous findings for loops DD, FF, and GG, not all the Zircaloy-2 surfaces in the higher-flux regions were free from the rustlike scale. The core coupon holder and the stress specimens which were mounted in the spider around the coupon holder were free from bulk oxide deposits in the higher-flux regions. The Zircaloy-2 coupons inside the tapered holder, the coupons in the couple assemblies, and the spacers in the Zircaloy-2 couple assembly were coated with some deposited bulk scale in even the highest-flux region. The amount of this deposit, however, appeared to be inversely proportional to the flux, as usual.

A photograph of the core assembly as removed from the loop is shown in Fig. 48. The stainless steel couple assembly, a titanium stress assembly, and the Zircaloy-2 couple assembly are in the foreground.

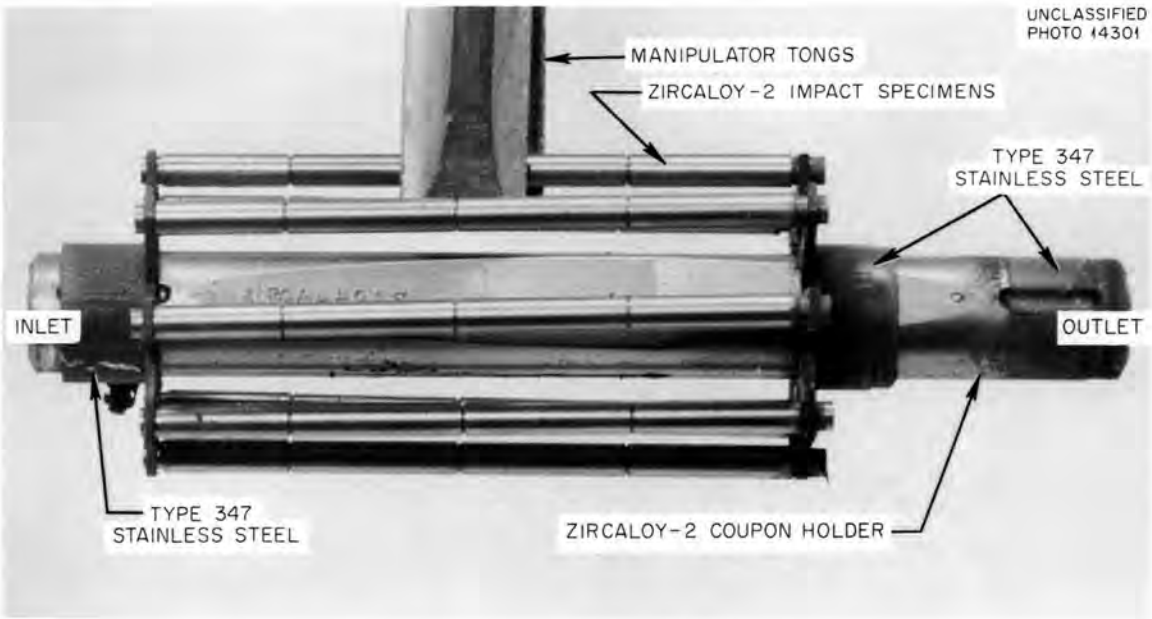

Fig. 47. Core Specimen Assembly, Loop GG.

As noted in Table 37, each titanium stress specimen exhibited a peculiar color pattern in the neighborhood of the fulcrum. This pattern can be seen in the photograph. The gradation of the quantity of scale with flux can also be seen in Fig. 48.

Microscopic examination of all the surfaces of all the stress specimens revealed no sign of stress-corrosion cracking in the type 347 stainless steel, Zircaloy-2, and titanium-55AX tested during this run.

The first three stainless steel coupons in positions 4, 5, and 7 of the core channel showed a concentration of attack in the exposed areas, with the clamped edges being protected. There was no such pattern of attack on the Zircaloy-2 or titanium coupons.

Surface examination of the various couple assemblies showed no pattern which would indicate an electrolytically enhanced corrosion rate for any of the six combinations tested. There were, however, indications of increased attack in crevice areas such as the essentially stagnant area between the spacers and rods of the couple assemblies. This was particularly true of the Zircaloy assembly, where corrosion product sealed the spacers to the rod. Disassembly of this rod required a screw-jack arrangement. Microscopic examination of the couple coupons indicated that the actual contacting spots were attacked less than were the adjacent areas in which surface roughness prevented perfect matching. This could be an indication either of protection of the contact zone or increased corrosion in the crevice. The total corrosion was too small for any difference in appearance between the crevice surfaces and the free surface of the same coupon to be determined.

The core-reducer section of this loop contained a repaired pinhole similar to the one reported for loop FF. There was no sign of a cavity or of localized attack in or around the region of the repair weld.

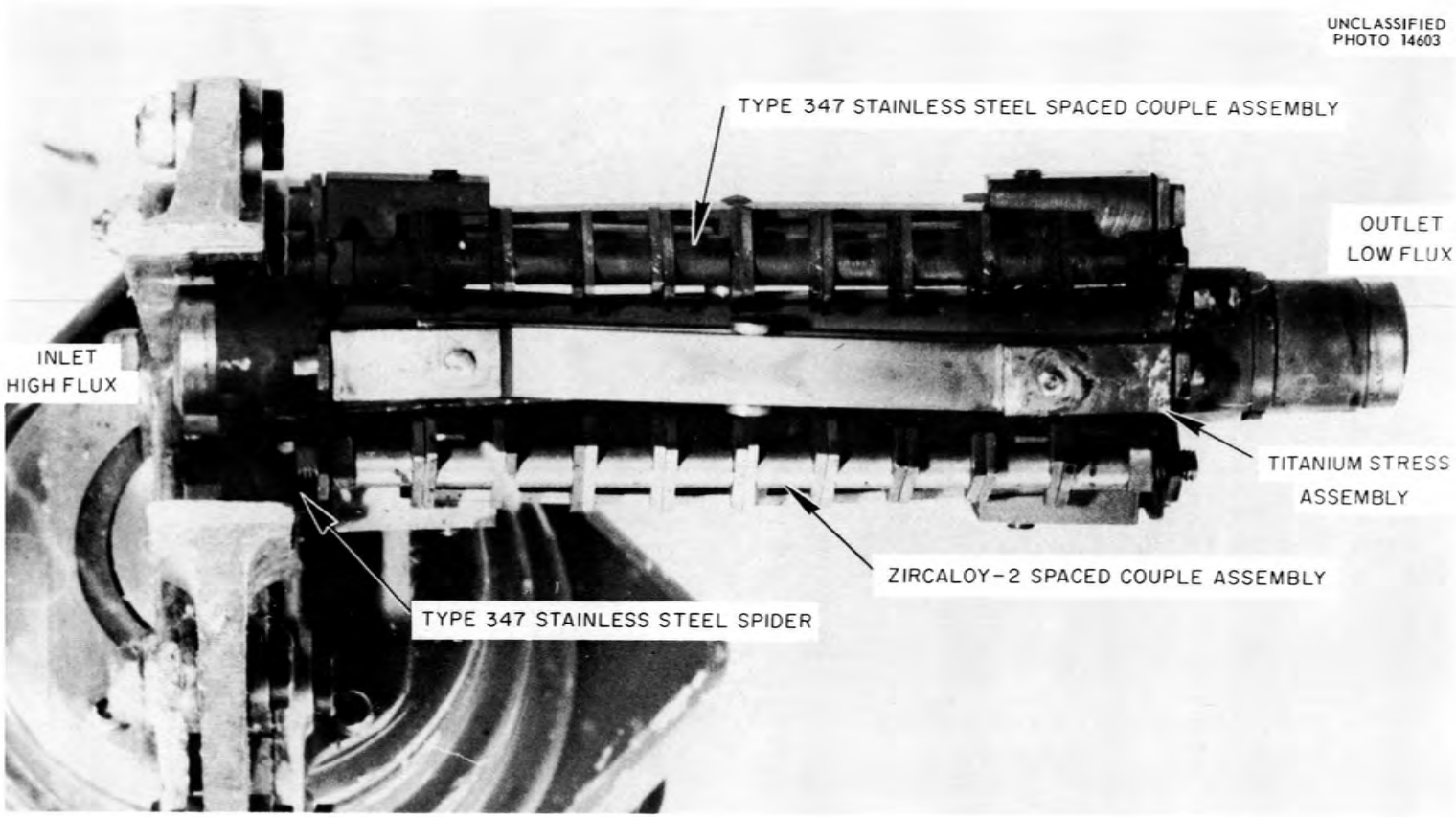

Fig. 48. Core Specimen Assembly, Loop EE.

4.6.5 Loop L-4-12

All stainless steel surfaces in the core region (titanium core) were covered with a heavy black scale. The Zircaloy-2 impact specimens and stress specimen holders were covered with a thin film that produced interference colors. All titanium surfaces were covered with a brass-colored film. Both inside and outside titanium holder surfaces and the interior titanium core surface exhibited an additional, dark, rustlike scale at the rear, low-flux portion of the core. The core specimen array as removed is shown in Fig. 49. The first three stainless steel CC coupons in the high-flux region (positions 4, 5, and 7) were found to be missing when the core holder was opened. These specimens could not be found in any of the other loop components and it was concluded that they were dissolved. Examination of the titanium holders revealed two disturbed film markings on each side of the channel, located approximately where the leading edge of two of the missing coupons should have been. These markings indicated that the coupons left the array before termination of the in-pile run.

All component surfaces outside the core were covered with a heavy rustlike scale. The scale deposit was heavier on the wall in the liquid-phase region of the pressurizer than in the vapor-phase region. Unlike the pressurizer wall, the stainless steel and titanium stress specimens located in the pressurizer vapor and liquid regions showed little difference in appearance; however, the specimens from the liquid region exhibited greater increases in the as-removed weights than did the specimens from the vapor region.

Five LC coupons located in consecutive positions near the outlet of the holder [two Zircaloy-2 (positions 20 and 23), two titanium-55A (positions 19 and 22), and one type 347 stainless steel (position 21)] showed absence of film and heavy attack on the clamped areas which destroyed the identification numbers. Examination of these coupons with a stereomicroscope revealed evidence that they had not been held firmly in place. Previous out-of-pile experience in dynamic pump loops[12] has shown that when a specimen is not held firmly the vibration during operation may prevent the accumulation of a protective film on the clamped edges and may lead to an increased attack in these areas. The mating surfaces of the two titanium holder halves in the vicinity of the five coupons, unlike the remaining holder area, were not filmed over.

Two type 347 stainless steel LC coupons, one adjacent to each end of the five-coupon group, showed heavy attack on their edges but were film-covered. The single Inconel LC coupon was also heavily attacked. The LC coupon assembly as removed is shown in Fig. 50.

Some localized attack occurred in the type 347 stainless steel pump volute. A single pit was located in the surface of the recessed shoulder at the volute inlet. The pit appearance is suggestive of the triangular-shaped pits found in stainless steel specimens located in the critical-flow velocity range in out-of-pile experiments.[13]

---

[12] J. C. Griess, *HRP Quart. Progr. Rept. July 31, 1954*, ORNL-1772, p 78.

[13] J. C. Griess and R. E. Wacker, *HRP Quart. Progr. Rept. Apr. 30, 1954*, ORNL-1753, pp 76–77.

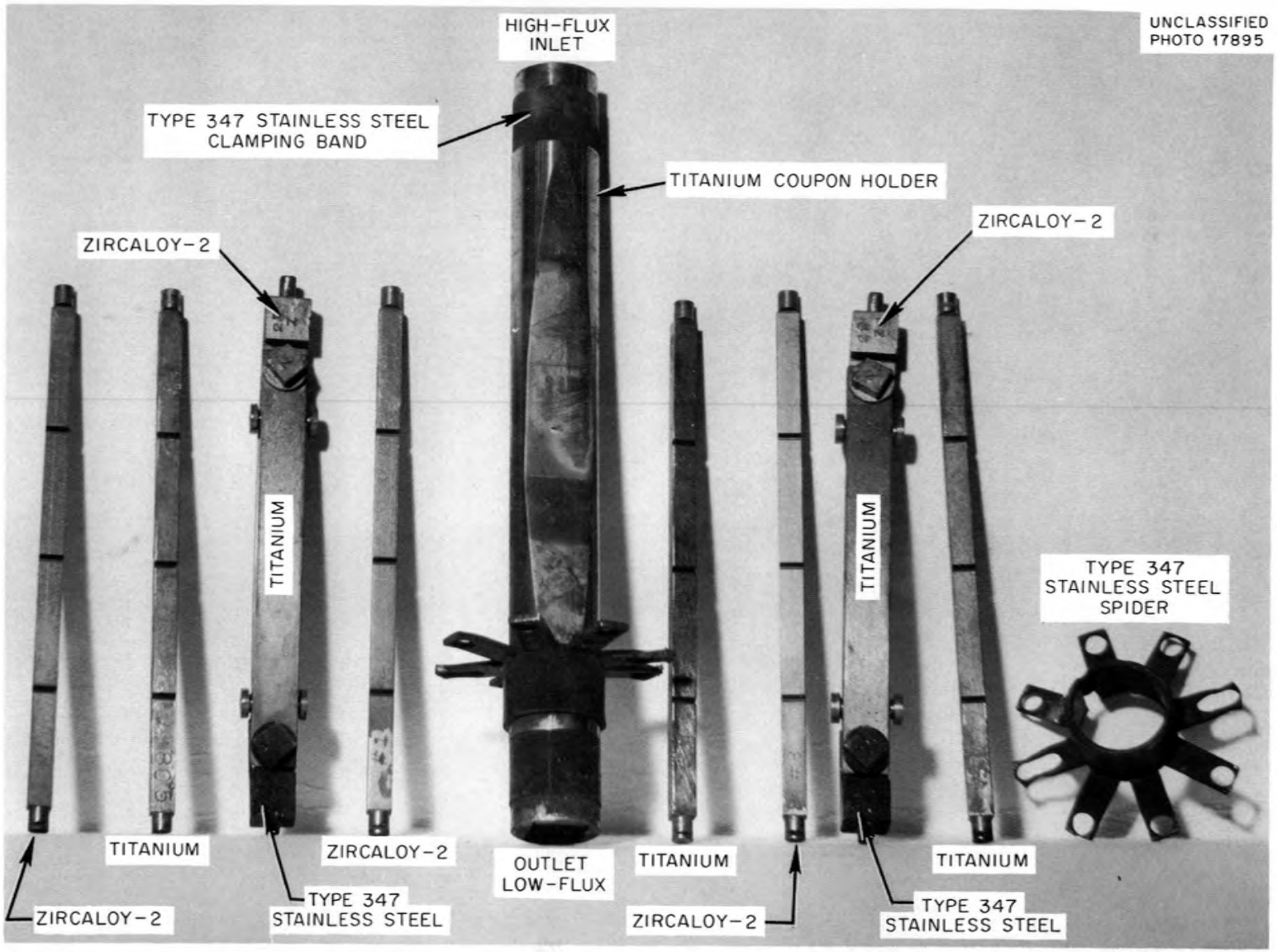

Fig. 49. Core Specimen Array as Removed, Loop L-4-12.

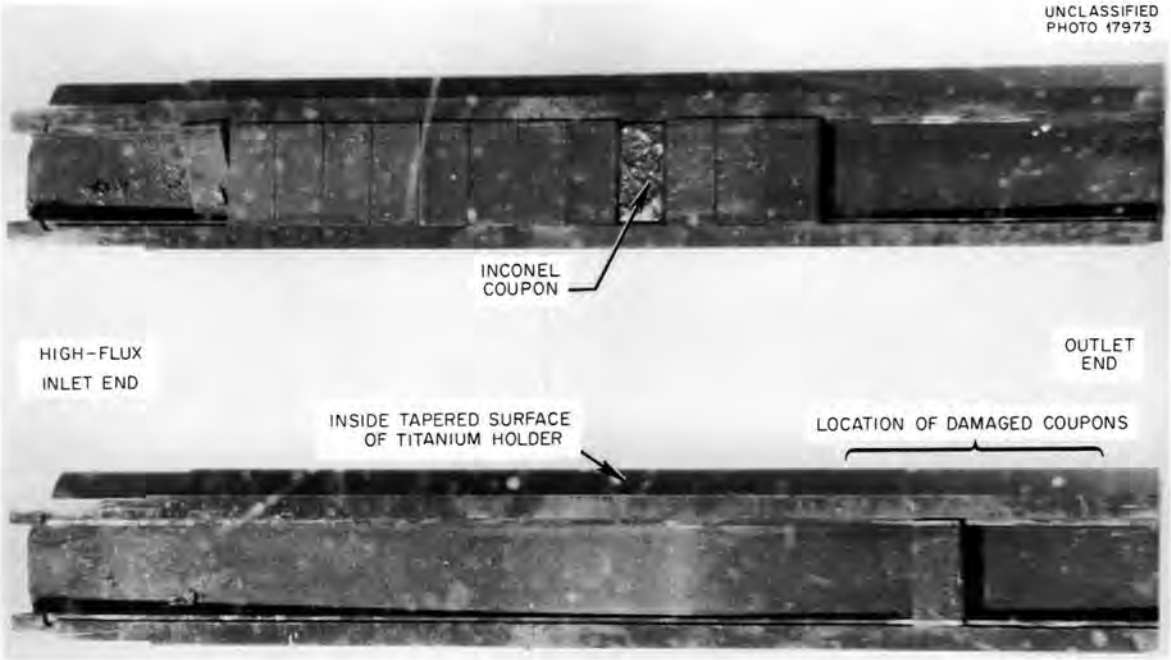

Fig. 50. In-Line Coupon Assembly, Loop L-4-12.

Separation of the titanium core from the stainless steel inlet pipe was accomplished easily by unscrewing the coupling. The titanium core–to–stainless steel outlet-pipe coupling was sectioned without dismantling. No evidence of galvanic attack was noted on either coupling, and all sealing surfaces appeared to be in excellent condition, as shown in Fig. 51.

As with all previous loops, cathodic defilming of the LC coupons was only partially effective; some film was retained by the specimens. In fact, all Zircaloy-2 LC coupons (excluding loose coupons in positions 20 and 23) showed weight increases or no weight change following the final defilming. The CA and LA impact specimens were not defilmed. A brief description of each specimen from the loop, as removed and following defilming, is given in Table 41.

4.6.6 Loop L-4-13

All loop component surfaces outside the core were covered with scale that was heavy dark-brown and rustlike in appearance except in the pressurizer. The scale in the liquid-phase portion of the pressurizer was heavy and black, while only a thin dark-gray film was found on the surfaces in the vapor-phase region.

There was no evidence of localized attack on any of the components, including the pump impeller and volute. Further examination of the pressurizer revealed that the normal oxygen addition port had been submerged in solution during operation and had become plugged with some of the heavy scale. This finding provides the explanation for oxygen addition difficulties encountered during the run. The submersion was caused by a combination of factors. The capillary entrance was not on the vertical center line, the pressurizer was tilted from the horizontal, and the liquid level in the pressurizer was higher than usual.

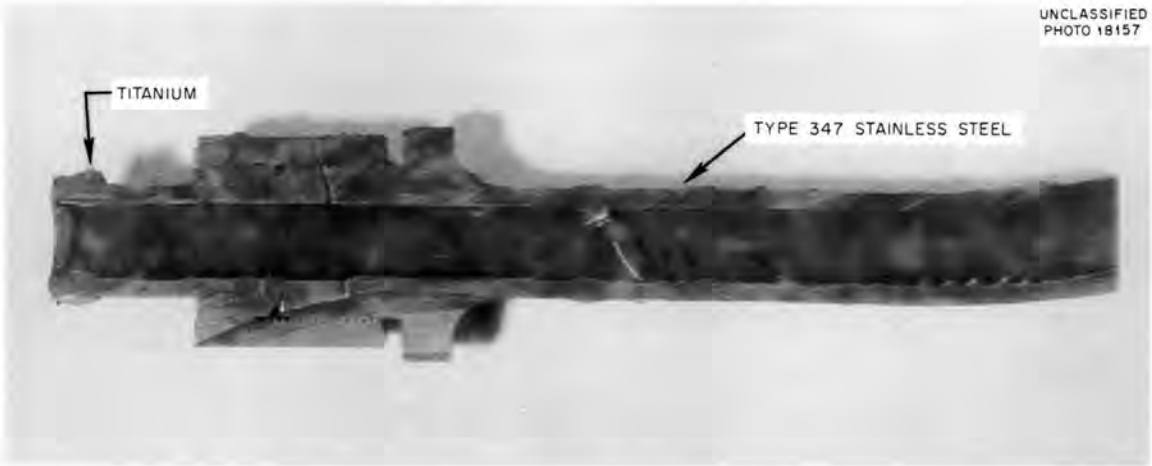

Fig. 51. Titanium–to–Stainless Steel Pipe Coupling on Core Outlet Line, Loop L-4-12.

All specimens outside the core were also uniformly coated with a heavy rustlike scale. As with all previous loops, cathodic defilming of the in-line coupons was only partially effective. All crystal-bar zirconium in-line coupons except one showed weight increases following the final defilming. The in-line impact specimens were not defilmed.

The interior of the core body and the exterior of the core channel holder, both fabricated from type 347 stainless steel, were covered with a two-colored scale. The scale at the forward, or high-flux, position was soft and sooty-black in appearance, while the low-flux end was covered with a harder, rustlike brown scale. The interior surfaces of the core channel holder and all the contained stainless steel coupons (types 309SCb and 347) were covered with a dark-gray to black scale, increasing in thickness from front to rear. All the crystal-bar zirconium CC coupons were covered with a thin iridescent film but no scale. Figure 52 is a photograph of the core holder and coupons after removal from the loop.

In disassembling the core body the impact and tensile specimens located in the annular region became loosened and fell from the holders. The single titanium tensile specimen was covered with a uniform gray film. The Zircaloy-3a tensile and impact specimens were free from scale and were covered with a thin iridescent film, while the Zr–20% Nb impact specimens were covered with a uniform, tightly adherent, thin dark scale.

4.6.7 Loop L-4-18

The loop components outside the core region were generally covered with a relatively thin dark-gray to dark-brown-black rustlike scale. The vapor region of the pressurizer was almost free of this scale, particularly at the outlet end. The liquid region of the pressurizer was uniformly covered with a heavy, black, velvet-like scale. There was no evidence of localized attack on any of the components examined.

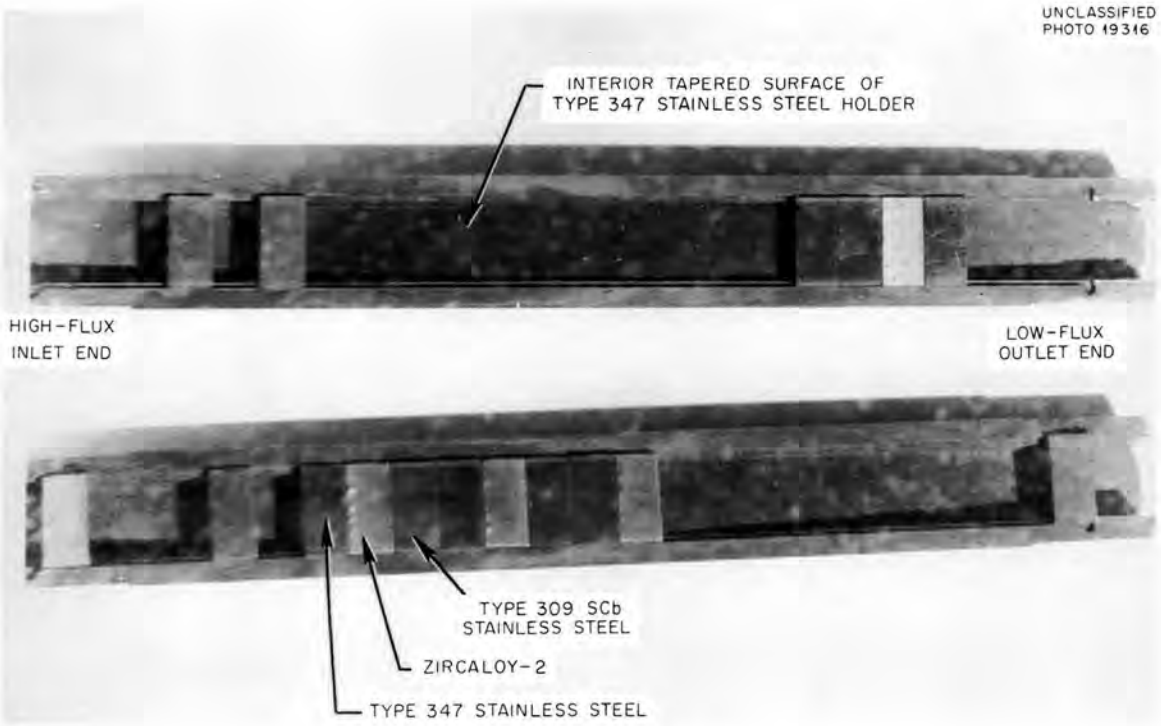

Fig. 52. Core Coupon Array, Loop L-4-13.

All the stainless steel and Zircaloy-2 coupons in the LC array were covered with the rustlike scale. The type 430L stainless steel LA coupons were covered with a light-gray scale with an overlay of dark-brown to black scale, while the type 347 stainless steel coupons contained in the same array were covered with a darker gray scale and a similar overlay. The Zircaloy-2 and Zr–15% Nb coupons contained in the second LA array were covered with dark shiny scales and some dark-brown scale, with the 15% Nb alloy scale being darker and showing some grain patterns. The Ti-55A and Ti–3% Al coupons from the same array were covered with heavy bronze-colored scale and spots of the dark-brown, transported scale.

The interior surfaces of the type 347 stainless steel core body and the type 347 stainless steel core coupon holders, spiders, and coupons were covered with a glossy rust-colored scale in the high-flux end of the core. This scale tapered gradually into a thick, dull, black scale at the low-flux end. The type 430L stainless steel coupons were similar in appearance to those in the LA coupon array. The Zircaloy-2 coupons and stress specimens were generally covered with a thin iridescent film which was predominatly gray, but with varying amounts of brown flakes of scale retained on the surfaces. The apparent film thickness and amounts of retained scale increased with decreasing flux. The Zr-Nb alloys were covered with a dark scale in a definite grain pattern, with some retained flakes of dark-brown scale. The Ti-55A coupons were covered with the typical, thin bronze-colored film. The Ti-Al alloy coupons also were covered with a shiny bronze film, but all the surfaces had a rough, etched appearance.

As with previous loops, repeated attempts to defilm the zirconium and titanium alloys by the standard cathodic defilming technique were only partially effective, and some scale was retained.

Although the pump in this experiment had failed in service, it was noted that the impeller rotated freely and that there was adequate end play before the pump was dismantled. After the pump was dismantled, examination of the rotor can and of the aluminum oxide bearings and journals showed no evidence of wear. The shaft in the region of the thermal barrier and the barrier itself were also examined. Although no evidence of localized attack was apparent, the appearance of the surface scale in different positions in this region varied markedly. The first three rings of the barrier at the high-temperature end were free from any scale accumulations, while the remainder of the barrier was covered with a dark-brown-black scale. The appearance of the scale changed along the shaft. In the low-temperature region, the shaft exhibited a light-gray, essentially film-free surface. The portion of the shaft in the scale-covered barrier region was also covered by a similar band of scale.

Samples of the bulk scale were scraped from the rear of the core, the in-line annulus holders, the pressurizer, and the pump volute and were submitted for chemical analyses. In addition, analyses were performed on solutions of the scale from one-half of the type 347 stainless steel core coupon holder. The results of these analyses are in a following section.

4.7 Metallographic Examination of Loops

Metallographic findings for the corrosion specimens and loop component specimens have been reported.[14–22] Representative corrosion coupons from core and in-line positions, stress corrosion specimens, and loop component specimens, including sections from the core body, pressurizer and pressurizer heater, pressurizer thermocouple well, pump outlet piping, sampler-line capillary tubing, coupon holder assembly, pressurizer inlet line restrictor, and various weld sections, were examined. Impact and tensile

---

[14] M. J. Feldman *et al.*, *Metallographic Examination of Coupons and Components of HRP In-Pile Loop "DD,"* ORNL CF-55-2-73 (Feb. 9, 1955).

[15] M. J. Feldman *et al.*, *Metallographic Examination of HRP In-Pile Loop "FF" Components,* ORNL CF-55-154 (May 16, 1955).

[16] A. E. Richt and J. O. Stiegler, *Metallographic Examination of Zircaloy-2 Coupons from HRP In-Pile Loop "FF,"* ORNL CF-56-8-48 (Aug. 8, 1956).

[17] A. E. Richt, *Metallographic Examination of HRP In-Pile Loop "EE" Components and Coupons,* ORNL CF-56-7-17 (July 6, 1956).

[18] A. E. Richt, *Metallographic Examination of Components and Coupons from HRP In-Pile L-4-18,* ORNL CF-58-4-30 (Apr. 3, 1958).

[19] J. O. Stiegler, *Metallographic Examination of Components and Coupons from HRP In-Pile Loop "GG,"* ORNL CF-57-3-83 (Mar. 19, 1957).

[20] J. O. Stiegler, *Metallographic Examination of Components, Coupons and Stress Corrosion Specimens from HRP In-Pile Loop L-4-12,* ORNL CF-57-2-88 (Feb. 19, 1957).

[21] J. O. Stiegler, *Supplementary Metallographic Examination of Titanium Stress Corrosion Specimens from HRP In-Pile Loop L-4-12,* ORNL CF-57-8-54 (Aug. 9, 1957).

[22] J. O. Stiegler, *Metallographic Examination of Components and Coupons from HRP In-Pile Loop L-4-13,* ORNL CF-57-3-140 (May 10, 1957).

specimens were submitted in the as-removed condition to the Metals and Ceramics Division for examination and testing.[23,24] Interior surfaces of typical sections of the loop components, all surfaces of representative cross sections of the coupons, and both the tension and compression surfaces of stress specimens were examined. In addition, coupon thicknesses were measured to determine general surface removal and the location and extent of regions of localized attack. Summaries of the examination of the corrosion coupons, stress corrosion specimens, and loop components are given in Tables 30–32.

In general, corrosion estimates from thickness measurements and metallographic observations of the corrosion coupons were in near agreement with the weight-loss data. Also, the results for specimens and loop components exposed at negligible fission-power densities show that corrosion was not appreciably different from that expected out-of-radiation. Evidence for exceptionally severe corrosion or surface cracking was found in several cases. However, these effects, in general, were not considered results of the radiation exposures but, rather, results of such factors as poor specimen material, mechanical damage in the specimen mounts, and, in the case of some of the surface cracks, fabrication techniques.

Brief summaries of the metallographic results are given in the following paragraphs. Those results indicating exceptional corrosion behavior are included.

4.7.1 Stainless Steel Corrosion Coupons

Corrosion of the stainless steel coupons exposed to fission recoils was generally of the type that commenced with the production of pits of about 1 mil in depth, which then spread laterally.

Type 347 stainless steel CC coupon 437A (loop DD) showed a "shouldering" effect where the coupon was protected by the sample holder. Near this edge, general surface removal was approximately $1\frac{1}{2}$ mils. Near the center of the coupon, thickness measurements showed approximately $2\frac{1}{2}$ mils of surface removal. There was also some evidence of corrosive penetration at the grain boundaries, especially near the center of the coupon. The appearance of the "shoulder" on this coupon is shown in Fig. 53.

Type 347 stainless steel CC coupon 743A (loop EE) exhibited significant surface removal. In this instance the attack was not of the pitting type; however, there appears reason to suspect that this coupon was improperly mounted in the sample holder in such a way as to significantly affect the corrosion rate. A photomicrograph of a section of this coupon is shown in Fig. 54.

Type 347 stainless steel LC coupon 1126A (loop L-4-12), located adjacent to the five loosened and damaged coupons, had smooth surfaces except at one corner, which had been removed. Figure 55 is a micrograph of the damaged end of this coupon.

Two type 347 stainless steel CC coupons 1022A and 1027A (loop L-4-13) were examined and showed unusually severe pitting attack up to a depth of 3 mils on all surfaces. The pits were more frequent and deeper on coupon 1022A than on coupon 1027A. Thickness measurements of both coupons showed little or no general surface removal. One of the more severely pitted areas of coupon 1022A is shown in Fig. 56.

---

[23] W. J. Fretague, *HRP Quart. Progr. Rept. Apr. 30, 1955*, ORNL-1895, p 167.

[24] W. J. Fretague, *HRP Quart. Progr. Rept. July 31, 1955*, ORNL-1943, pp 167–68.

Table 32. Summary of Metallographic Examinations of Components

Experiment	Component[a]	Metallographic Observations	Figure Number
DD	Core cap	Interior surface appeared roughened but showed no evidence of intergranular corrosive attack or cracking; the initial surface was probably rough	
	Pressurizer (liquid phase)	Indication of corrosive attack; some penetration at the grain boundaries	65
	Pressurizer (vapor phase)	Indication of corrosive attack; some penetration at the grain boundaries	
	Loop piping at pump outlet	No indication of corrosive penetration	
	Pressurizer heater	No indication of corrosive penetration	
FF	Core cap	Corrosive penetration to about ½-mil depth	
	Pressurizer (inlet end)	No evidence of corrosive attack	
	Pressurizer (outlet end)	Approximately ¼-mil corrosive penetration at grain boundaries	
	Pressurizer thermocouple well (external surface)	No evidence of corrosive attack	
	Core body weld at reducer	Large pit noted in weld metal; approximately ½-mil corrosive penetration in adjacent heat-affected zones	63
	Pressurizer heater (inlet and outlet)	No evidence of corrosive attack	
	Loop piping at pump outlet	No evidence of corrosive attack	
	Core reducer	Approximately ½-mil corrosive penetration; tendency toward intergranular type of attack	
GG	Core cap	Very rough; evidence of intertranular attack to a depth of approximately 1 mil	62
	Pressurizer heater lines (inlet and outlet)	No evidence of corrosive attack; covered with ½-mil thick film	
	Pump outlet piping	No evidence of corrosive attack; covered with ½-mil thick film	
	Pressurizer (inlet end)	No evidence of corrosive attack or film formation	
	Pressurizer outlet (liquid phase)	Slightly roughened surface; evidence of penetration at grain boundary; ¼-mil film present	
	Pressurizer outlet (vapor phase)	Slightly roughened surface; evidence of penetration at grain boundary; ¼-mil film present	
	Pressurizer thermocouple well (external surface)	Smooth; no evidence of corrosive attack	

Table 32 (continued)

Experiment	Component[a]	Metallographic Observations	Figure Number
EE	Core cap	Very rough uneven surface with some indication of corrosive attack	
	Pressurizer (liquid phase)	No evidence of corrosive attack	
	Pressurizer (vapor phase)	Evidence of slight corrosive attack at grain boundaries	
	Pressurizer heater	No evidence of corrosive attack	
	Pump outlet piping	No evidence of corrosive attack	
	Core coupon holder clamping bands	Isolated corrosive attack on band at outlet end of holder	66
L-4-12	Core cap[b]	Smooth; no evidence of corrosive attack	
	Core body to reducer weld[b]	Rough uneven surface; several 5-mil cracks emanating from inner surface	64
	Pressurizer inlet and outlet	Rough, uneven surfaces; intergranular penetration to depth of about 1 mil	
	Pressurizer thermocouple well (external surface)	Uniformly roughened; intergranular penetration to depth of about 1 mil	
	Pressurizer heater inlet and outlet	No evidence of corrosive attack	
	Pressurizer inlet line restrictor	Smooth and free from attack with $\frac{1}{4}$-mil film; a limited area exhibited slight roughening	
	Pump outlet piping	No evidence of corrosive attack	

L-4-13	Core cap	No evidence of intergranular penetration; surface irregularities of about 1-mil depth beneath $\frac{1}{4}$-mil film	
	Pressurizer inlet and outlet	Rough with about $\frac{1}{2}$-mil maximum penetration at grain boundaries; covered with $\frac{1}{4}$- to $\frac{3}{4}$-mil film	
	Pressurizer heater inlet, outlet, and U-bend	Rough appearance with $\frac{1}{4}$- to 1-mil-thick films over all surfaces	
	Pump outlet piping	No evidence of corrosive attack	
L-4-18	Core cap	Sporadic pitting attack to depth of $1\frac{1}{2}$ mils; attack probably associated with stringering of inclusions in metal	
	Pressurizer (liquid phase)	Slight attack at grain boundaries; less than $\frac{1}{4}$-mil-thick oxide scale formation all surfaces	
	Pressurizer (vapor phase)	Slight attack at grain boundaries; less than $\frac{1}{4}$-mil-thick oxide scale formation all surfaces	
	Pump outlet piping	No evidence of corrosive attack	
	Pressurizer heater inlet, outlet, and U-bend	Less than $\frac{1}{4}$-mil corrosive penetration at grain boundaries; no stress-corrosive effect observed in U-bend	
	Sample line capillary tubing	Intergranular attack to 5 mils deep in area near loop piping junction; remainder of $\frac{3}{8}$-in.-long specimens showed intergranular penetration of about 1-mil depth; all surfaces covered with 2-mil oxide scale	67

[a] All components are 347 SS except as noted.
[b] Ti-55A.

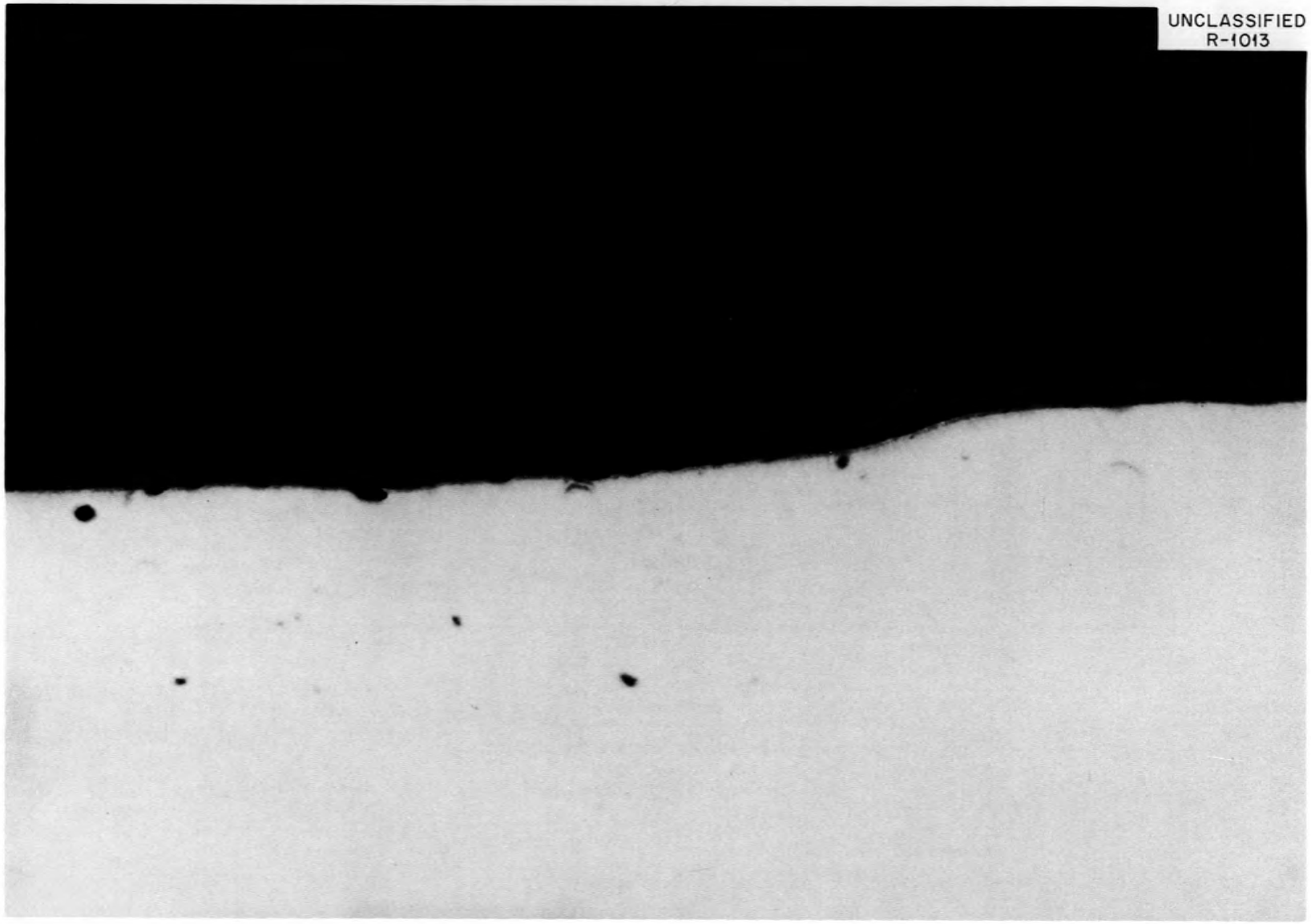

Fig. 53. Appearance of "Shoulder" Where Sample Holder Gripped Type 347 Stainless Steel, CC Coupon No. 437, Loop DD.

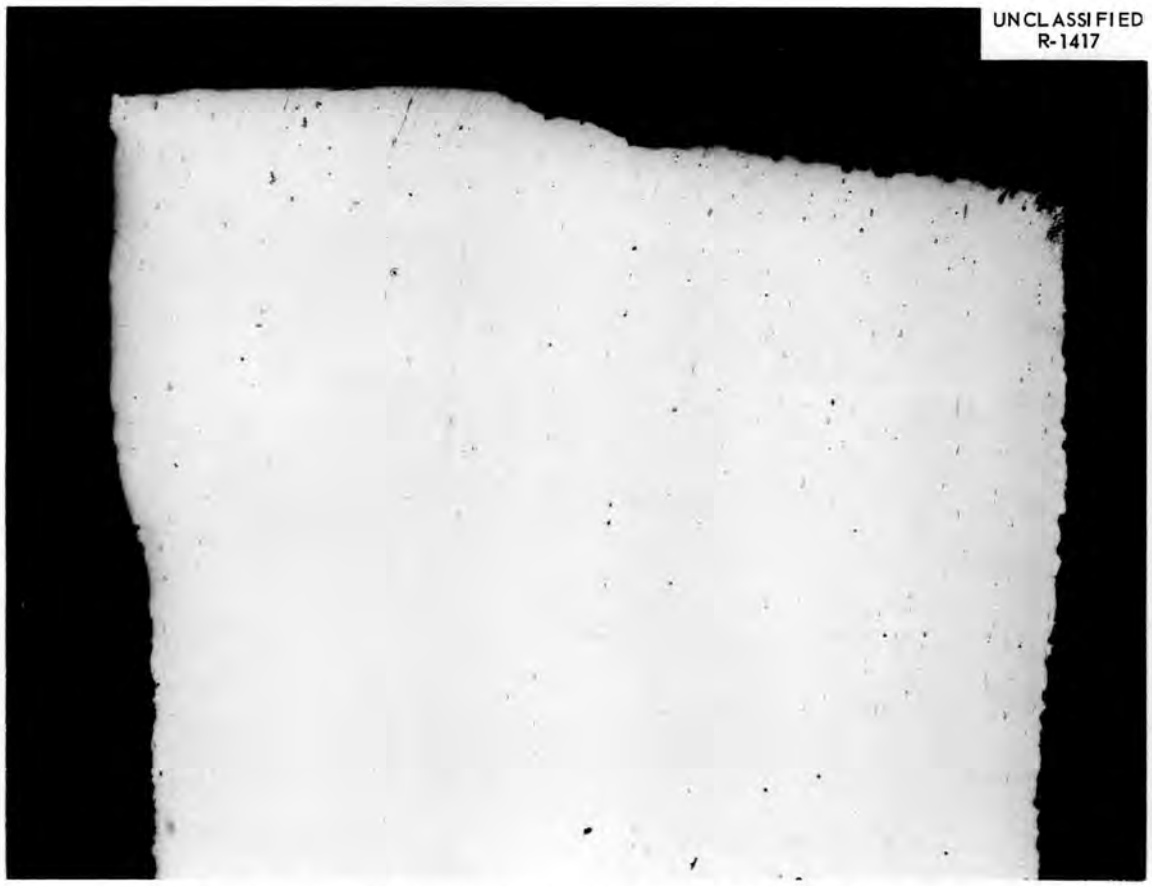

Fig. 54. Type 347 Stainless Steel – CC Coupon 743A, Loop EE. 80 X.

One of the four type 309Cb stainless steel coupons examined from loop L-4-13, LC coupon C-65, which showed the largest weight loss, was slightly roughened on all four corners and both ends, as shown in Fig. 57.

4.7.2 Zirconium and Zirconium-Alloy Corrosion Coupons

Crystal-bar zirconium, Zircaloy-2, and zirconium–15% Nb coupons appeared smooth, in general, and showed no evidence of severe corrosive attack.

Zircaloy-2 CC coupon 948A (loop GG), however, showed slight surface roughening, and a 3-mil crack of unknown origin was observed near the center of one side (Fig. 58).

Three Zircaloy-2 CC coupons from experiment EE showed slight surface roughening. In addition, numerous pits approximately ½ mil in depth were observed in the coupon exposed to the highest fission-power density. However, the frequency of such depth of attack was generally less than that shown on the stainless steel coupons. The Zircaloy-2 LC coupon from this experiment showed no evidence of corrosive attack.

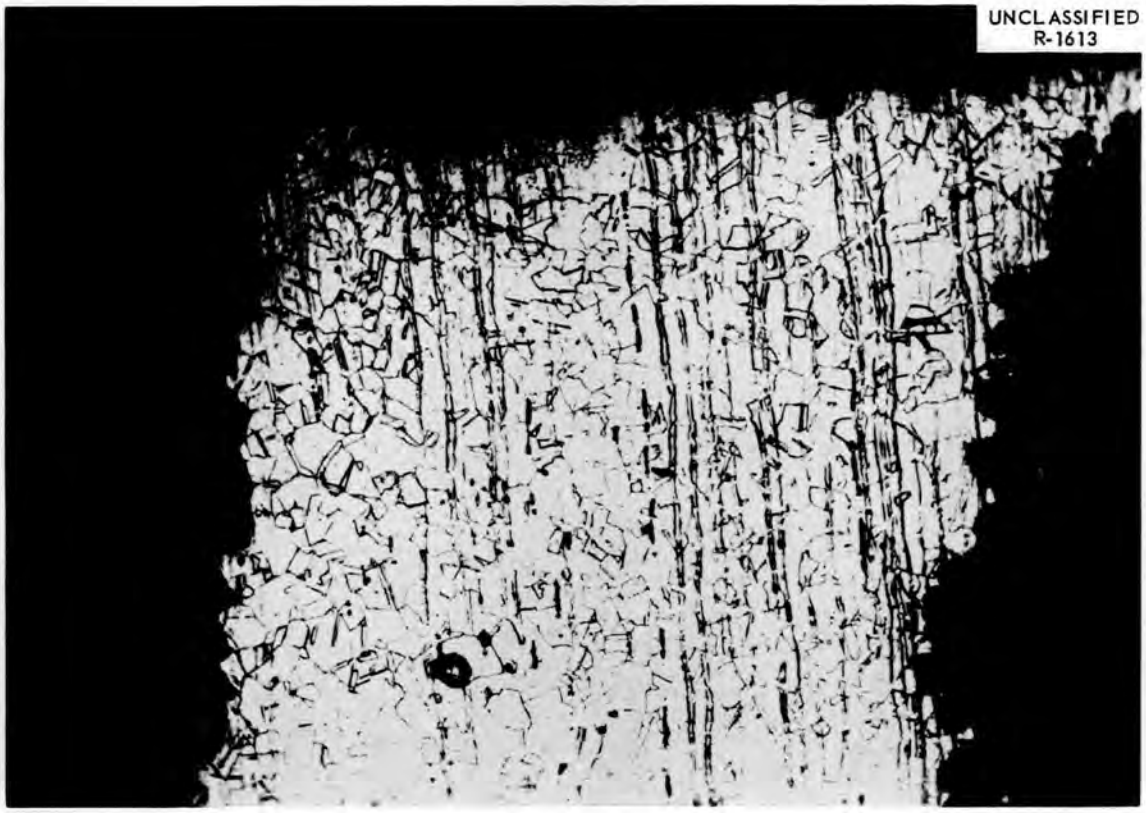

Fig. 55. End of Damaged Type 347 Stainless Steel – LC Coupon 1126A, Loop L-4-12. 250 X.

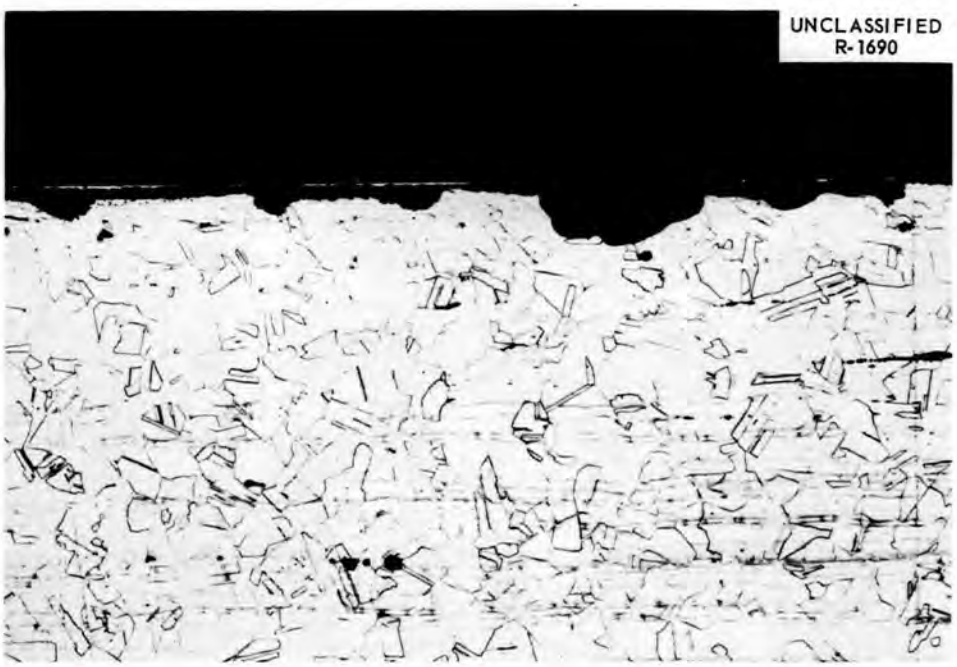

Fig. 56. Type 347 Stainless Steel – CC Coupon 1022A, Loop L-4-13. 250 X.

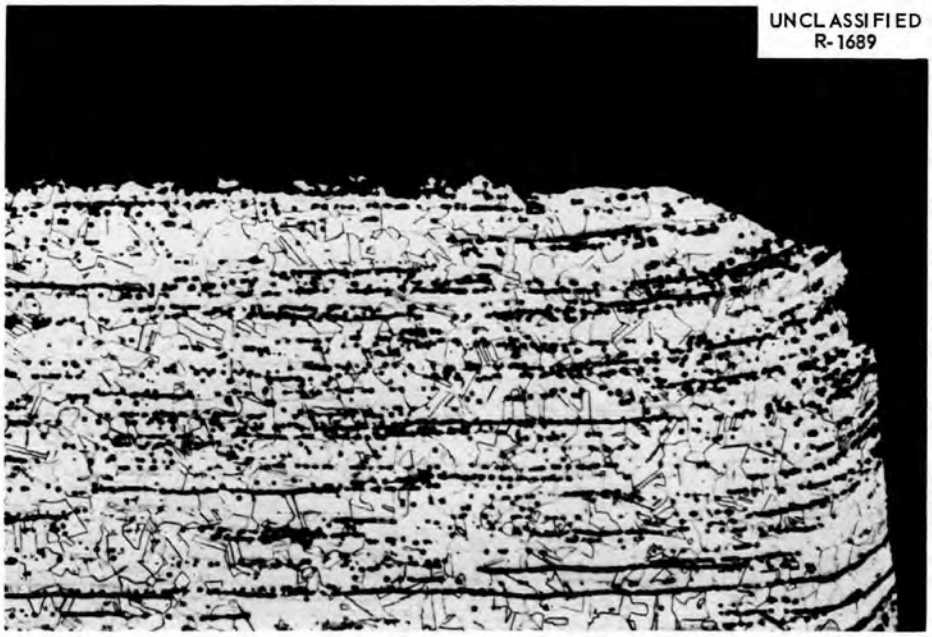

Fig. 57. Type 309SCb Stainless Steel – LC Coupon C-65, Loop L-4-13. 250 X.

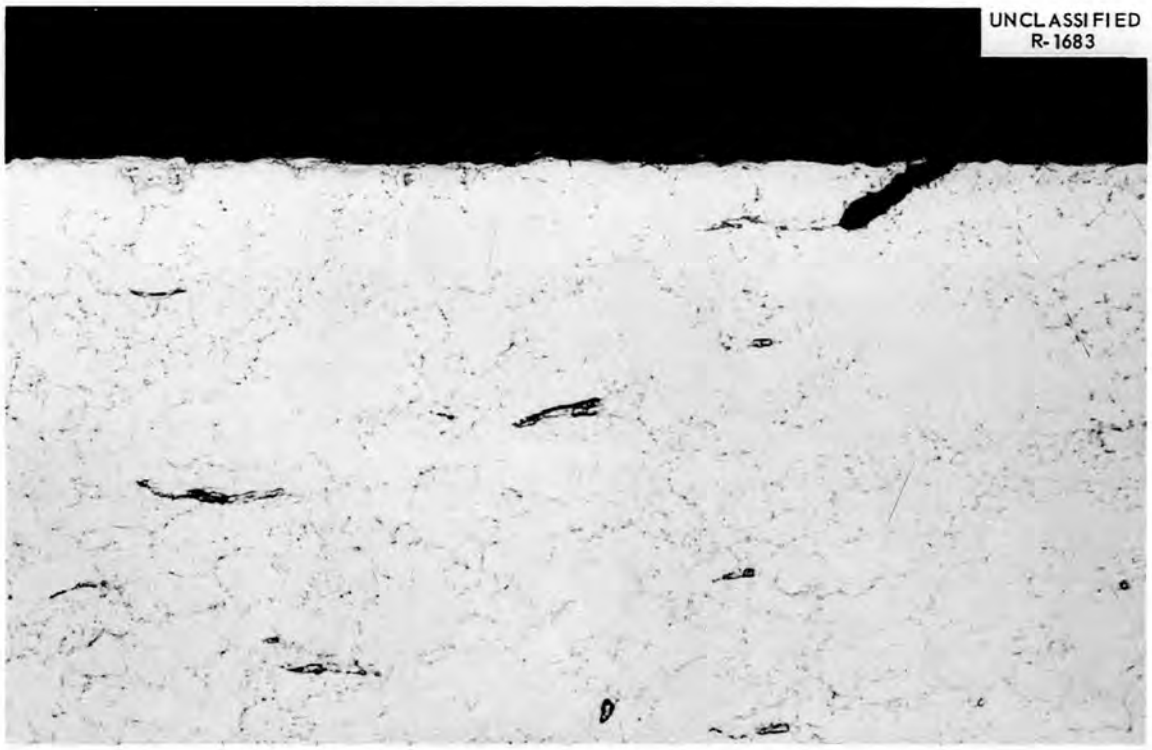

Fig. 58. Zircaloy-2 CC Coupon 948A, Loop GG. 250 X.

Attack on the two loose Zircaloy-2 LC coupons (loop L-4-12) was restricted to the normal clamping areas, while the exposed surfaces show no evidence of any surface removal. The smooth removal of clamping surface from one of these damaged coupons is shown in Fig. 59.

A crystal-bar zirconium LC coupon Z-115 (loop L-4-13) was severly attacked on both ends, and a retained surface film about $\frac{1}{4}$ mil in thickness was observed on two or three limited areas. Bright-field and polarized-light photomicrographs of a filmed region are shown in Fig. 60. Other coupons of this material showed only slight surface roughness, with no pits, cracks, or visible film.

4.7.3 Titanium-Alloy Corrosion Coupons

Titanium-55A CC corrosion coupons from experiments EE and L-4-12, Ti-55A LC coupons from experiment EE, and Ti-55A and Ti–3% Al coupons from CA and LA positions of experiment L-4-18 were examined. In addition, the two Ti-55A LC coupons which were loose in their holder upon completion of the experiment L-4-12 were examined. All coupons appeared smooth, with no evidence of corrosive attack.

4.7.4 Stress-Corrosion Specimens

Metallographic examination of the stress-corrosion specimens from loop EE revealed no tendency for localized or accelerated corrosive attack with respect to the stress or flux pattern. All stainless steel stress specimens showed light pitting attack very similar to that noted on the corrosion coupons. Stress specimens fabricated of Zircaloy-2 exhibited an extremely rough, uneven surface. However, since the roughness of the original specimen surfaces is unknown (specimens were sandblasted), it is impossible to determine what portion of this roughness is due to corrosive attack. No evidence of corrosive attack was noted in the examination of the titanium stress-corrosion specimens.

From metallographic examination of the L-4-12 stress-corrosion specimens it was apparent that there was a definite couple attack between the 17-4 PH stainless steel specimen SH-1 and the C-130 AM titanium alloy specimen TE-1. It also appears that the 6% Al–4% V–Ti alloy was somewhat more susceptible to attack in the pressurizer than the C-130 AM titanium alloy. Specimens of 6% Al–4% V–Ti exposed in the in-line and core regions of this experiment showed scattered shallow cracks. The cracking was of such a nature that stress corrosion may or may not be indicated. A typical cross section containing these cracks is shown in Fig. 61.

Core and in-line stress specimens of Zircaloy-2 contained in loop L-4-18 were smooth and even, with no evidence of pitting or cracking.

4.7.5 Loop Components

The interior surface of the type 347 stainless steel core cap from loop GG appeared very rough and uneven, with evidence of intergranular attack to a depth of approximately 1 mil (Fig. 62). The other stainless steel caps exhibited varying degrees of roughness and corrosion penetration but no intergranular attack. No evidence of corrosive attack was noted on the titanium cap employed in loop L-4-12.

UNCLASSIFIED
R-1612

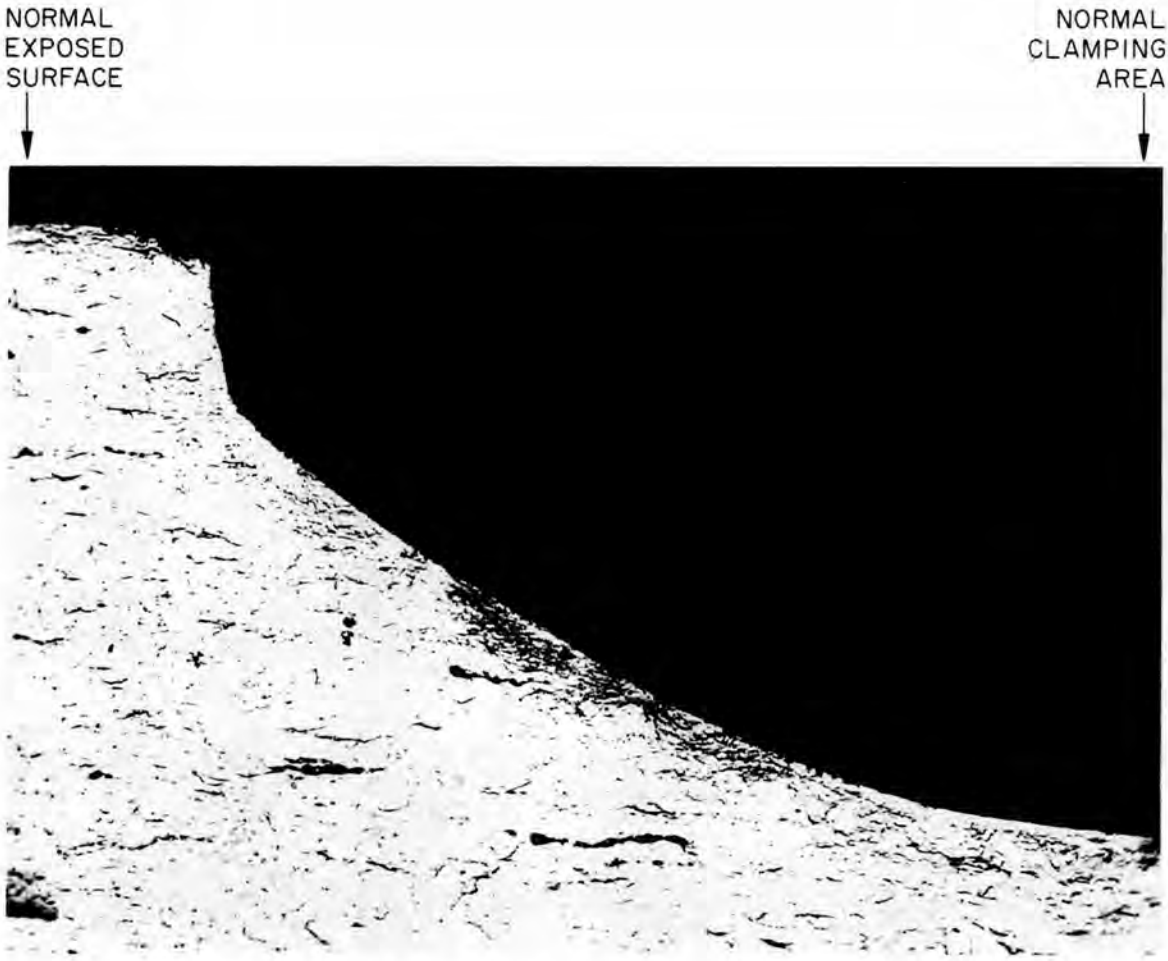

Fig. 59. End of Damaged Zircaloy-2 LC Coupon, Loop L-4-12. 250 X.

The cause of the large pit (Fig. 63) in the weld in the reducer section of the stainless steel core in loop FF is unknown but is probably the result of a bad weld.

Several cracks about 5 mils long appeared to emanate from the inner core surface at the core body–to–reducer weld in the Ti-75A core from loop L-4-12. One of these cracks is shown in Fig. 64. Subsequent examination of this area indicated that the inner surface was contaminated by oxygen.[25] This was confirmed by a microhardness traverse of the area, which showed the hardness to range from approximately 558 DPH at the inner surface to about 200 DPH at a depth of 40 mils. From this depth the hardness remained near 200 DPH through the remainder of the weld and adjacent base metal.

---

[25]M. L. Picklesimer, *Metallographic Examination of Titanium Core Weld from In-Pile Loop L-4-12,* in press.

UNCLASSIFIED
R-1693

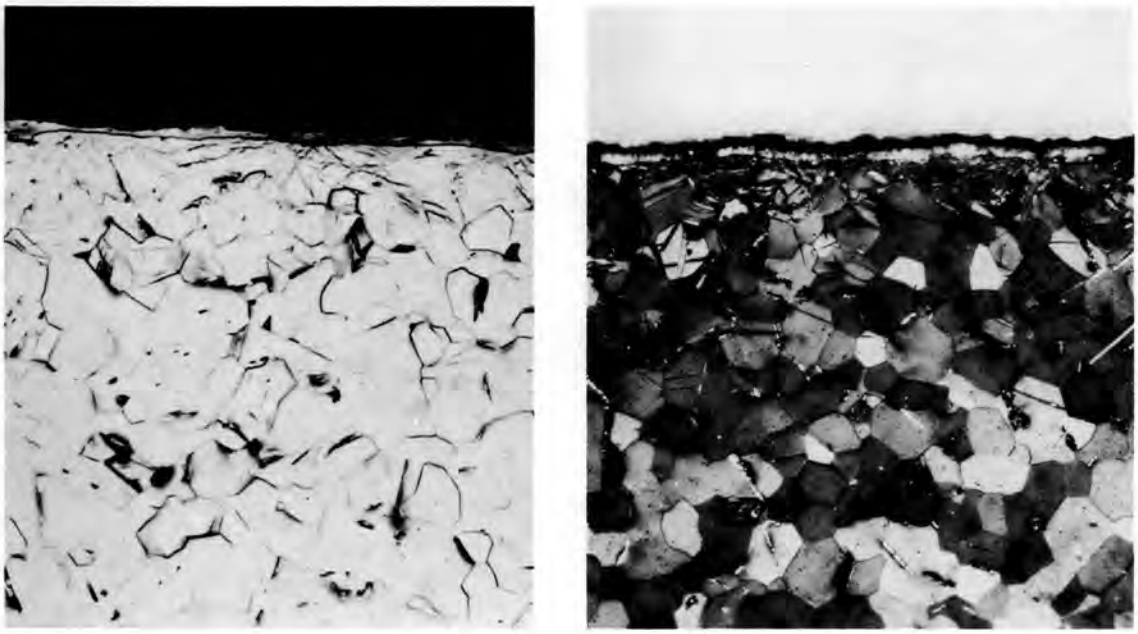

Fig. 60. Scale on Crystal-Bar Zirconium LC Coupon Z-115, Loop L-4-13. 250 X.

UNCLASSIFIED
R-1812

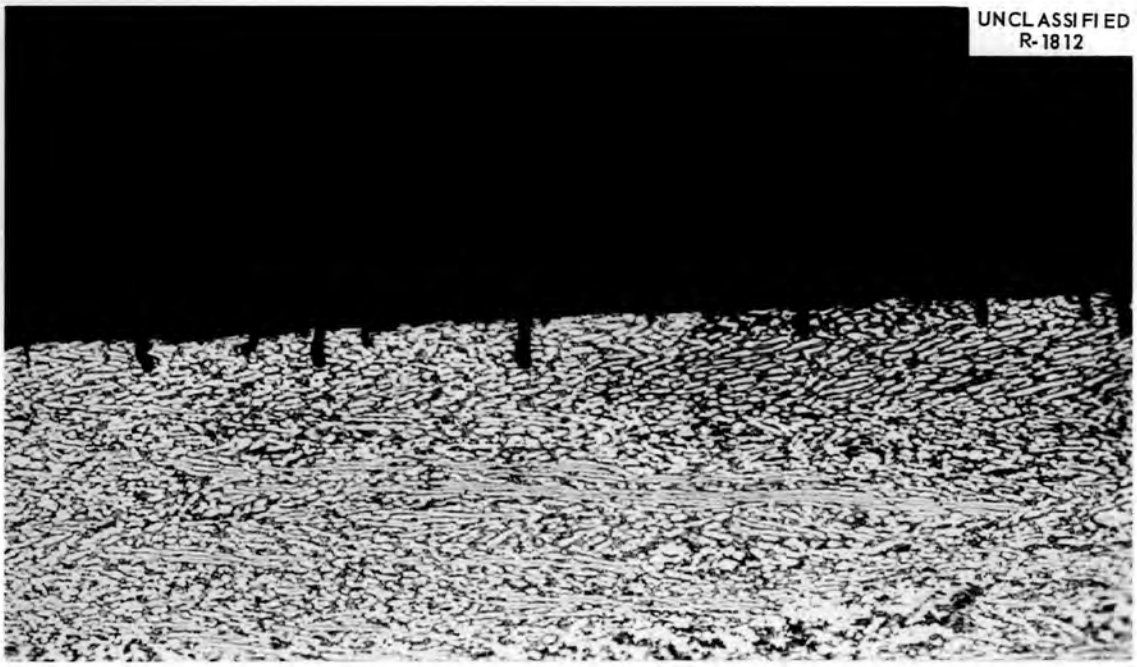

Fig. 61. Tension Surface of Titanium Specimen TJ-12 from Core, Loop L-4-12. 250 X.

Fig. 62. Type 347 Stainless Steel Core Cap, Loop GG. 250 X.

Sections from the inlet and outlet ends (exposed to liquid or vapor during operation) of the type 347 stainless steel pressurizers from all of the loops exhibited, in most cases, rough surfaces and some attack at the grain boundaries. A photomicrograph of a liquid-region section from loop DD is shown in Fig. 65.

Sections from the type 347 stainless steel pressurizer heater lines (loop L-4-18) exhibited a thin oxide film formation, with slight (less than $\frac{1}{4}$ mil) corrosive penetration at the grain boundaries. Similar sections from the other loops as well as sections of pipe from the pump outlets and pressurizer thermocouple wells showed no evidence of corrosive attack.

An unusual occurrence of corrosion was observed on one of the clamping bands of the core coupon holder from loop EE. The band, located at the core outlet end of the holder, exhibited an isolated area of attack (Fig. 66).

Intergranular attack to a depth of 5 mils was observed in a section of the sampler-line capillary tubing from loop L-4-18. A portion of the area of attack is shown in Fig. 67.

4.7.6 X-Ray Examination of Specimens and Scales

Examinations were made[26] of standard Zircaloy-2, titanium, and stainless steel coupons and in-pile loop samples, bulk oxides, loop scale, and films by using the shielded x-ray diffractometer.

---

[26] G. E. Klein, letter to A. R. Olsen, "X-Ray Examination of Zircaloy-2, Titanium, and Stainless Steel HRP In-Pile Loop Specimens and Products Therefrom," Sept. 13, 1955.

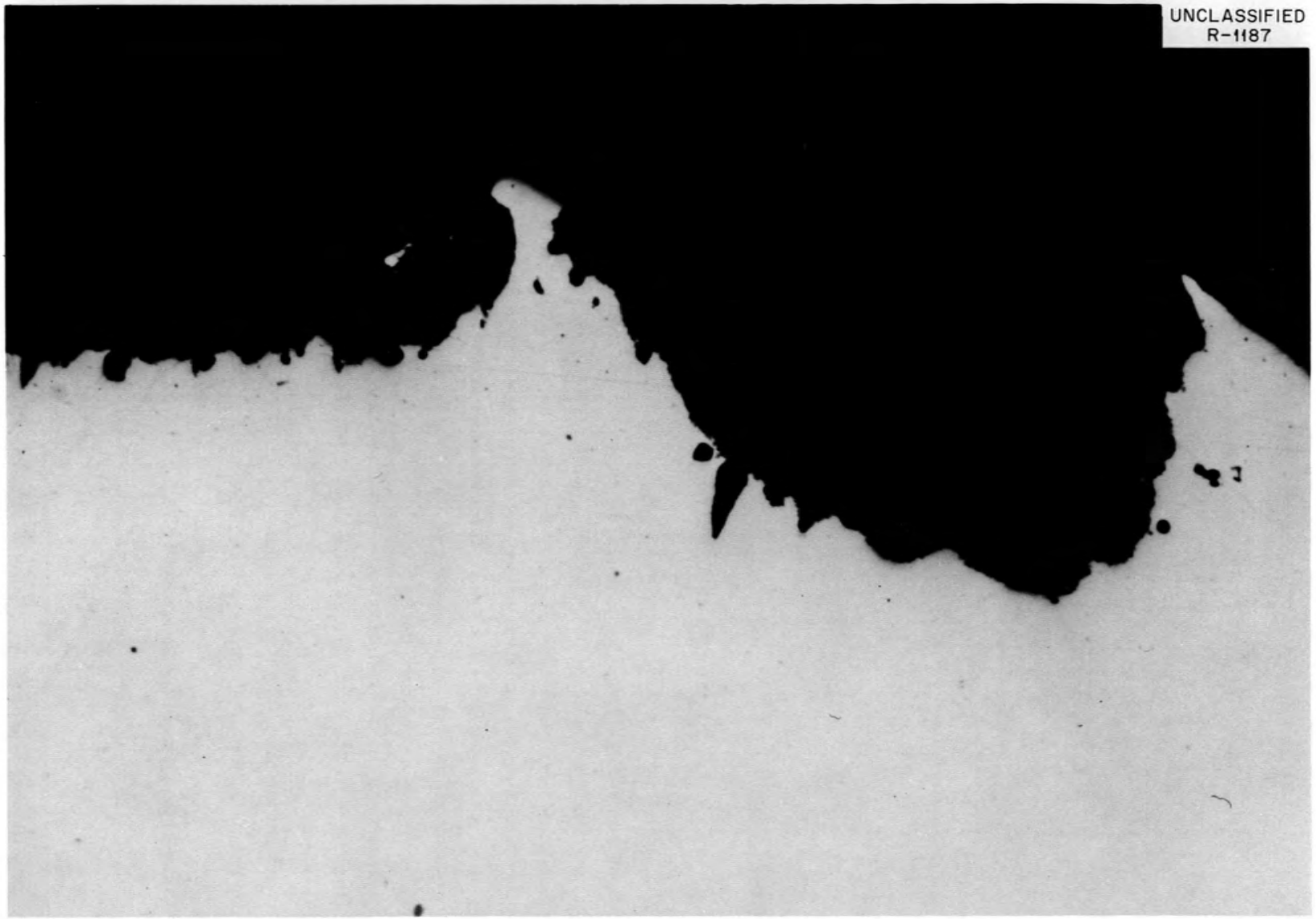

Fig. 63. Pit Area in Core Weld, Loop FF. 250 X.

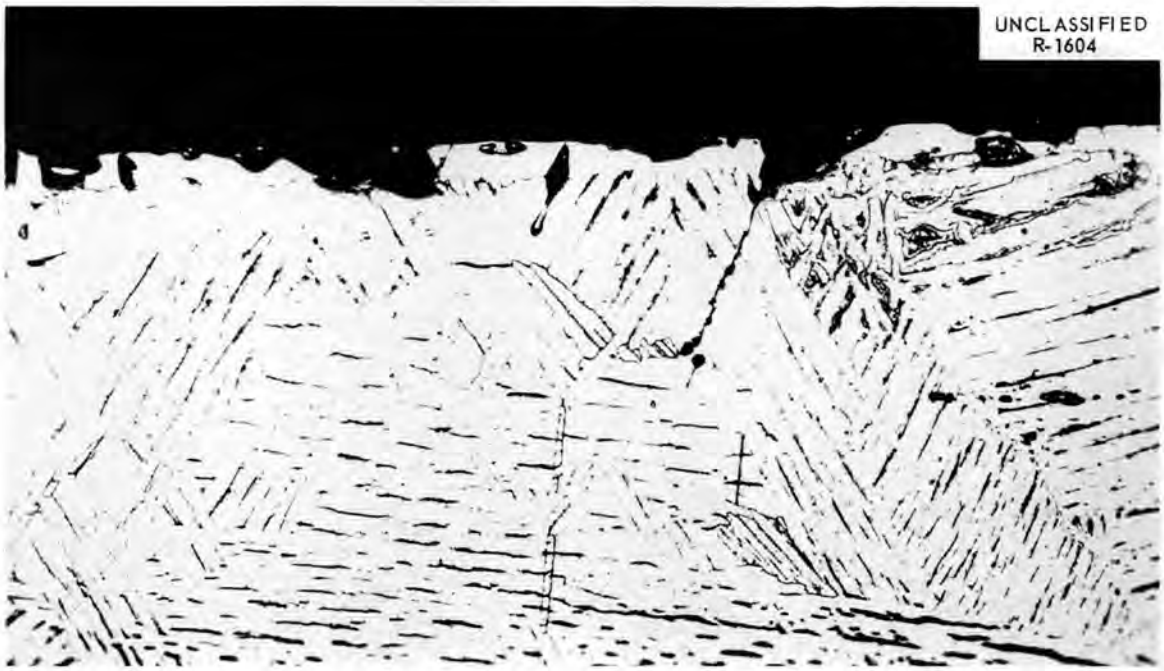

Fig. 64. Weld of Titanium-75A Core Body to Reducer, Loop L-4-12. 250 X.

All solid coupons gave an x-ray pattern of the base composition, that is, α-zirconium, titanium, or stainless steel if the covering film was stripped off. No base-metal diffraction occurred with coupons from which the scale was not removed. At the same time the scale itself showed no recorded crystallinity. Some few stripped coupons from experiment GG, namely 945A, LC position K, and 941A, LC position G, also showed the presence of the strongest lines of the monoclinic form of ZrO_2.

Both bulk oxides and stripped films revealed no x-ray structure, with the exception of the films stripped from experiment L-4-12 Zircaloy-2 CC coupon Z-92, which showed the presence of α-zirconium.

Klein concluded that the in situ scale appeared to be noncrystalline, and no reflection was obtained from the base metal. The stripped films were too thin, for the most part, to diffract properly for obtaining an x-ray pattern.

Results of these examinations are summarized in Table 33.

4.8 Results of Fission-Power Determinations

4.8.1 Induced Activities

Thermal-neutron fluxes determined from results of induced-activity measurements in each of the several experiments are illustrated in Fig. 68, where the logarithm of the flux is plotted vs the axial position in the loop core. The actual data points for four of the different experiments are plotted in Figs. 69–72. The fission-power density in solution adjacent to a specimen was computed from the flux value indicated by the plot in Fig. 68, together with values of 580 barns and 200 Mev/fission for the fission cross section

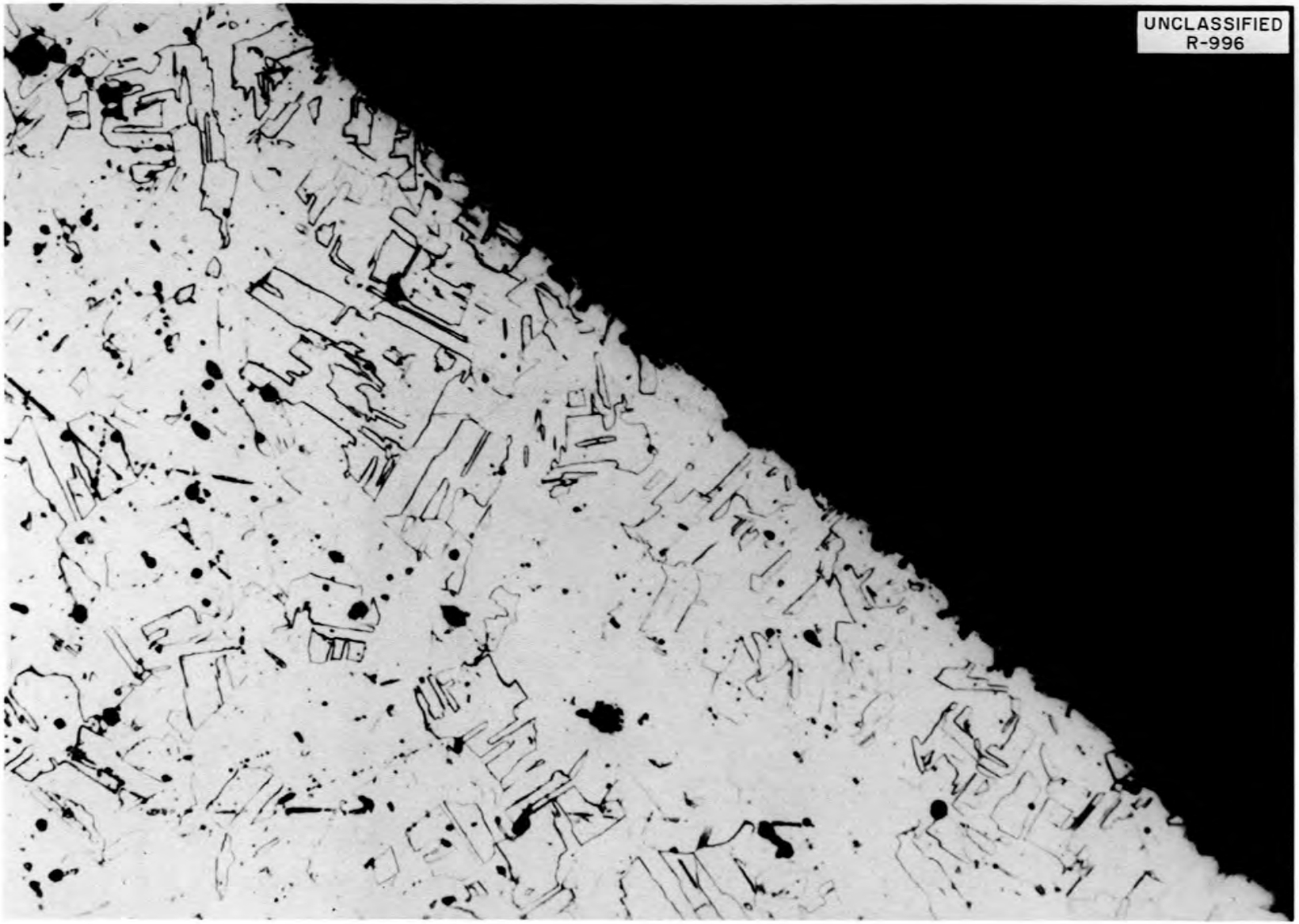

Fig. 65. Type 347 Stainless Steel Pressurizer, Loop DD. 250 X.

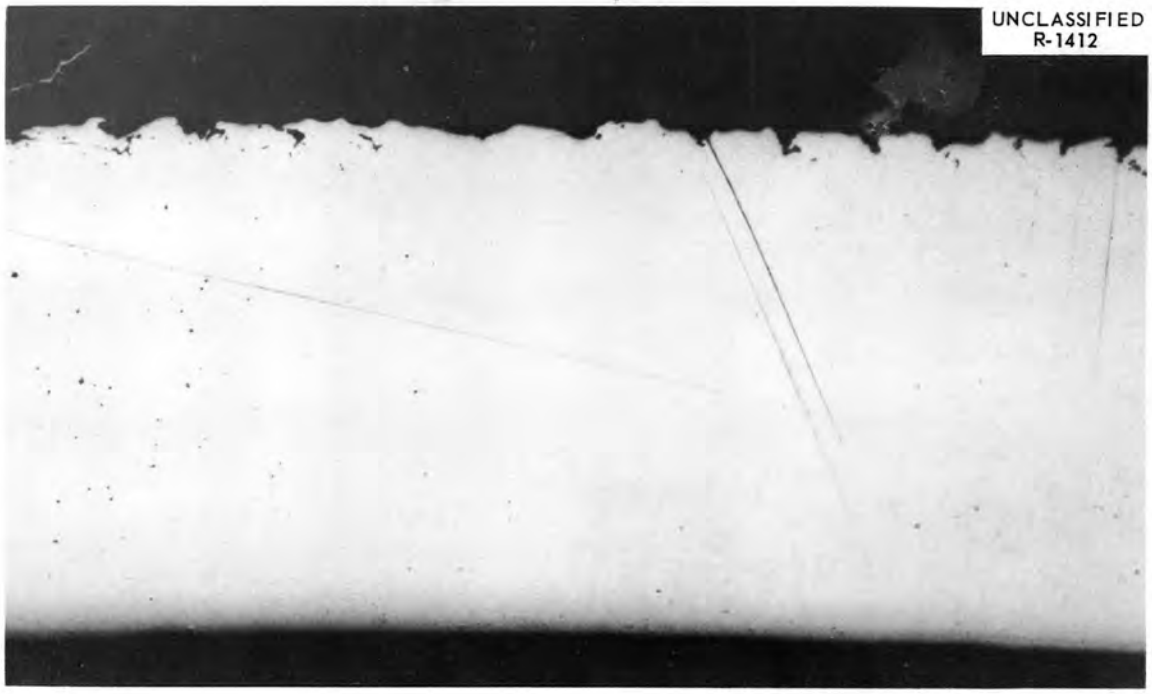

Fig. 66. Core Coupon Holder Clamping Band, Loop EE.

Fig. 67. Sampler-Line Capillary Tubing, Loop L-4-18. 250 X.

Table 33. Summary of X-Ray Examination of Specimens and Scales

Experiment	Sample Number	Material	Location	Power Density (w/ml)	Solution Velocity (fps)	Sample Condition	X-Ray Identification
None		Ti-75A				Coupon as machined	Titanium
None		Zircaloy-2				Coupon as machined	α-Zirconium
None		347 SS				Coupon as machined	Stainless Steel
GG	S-1	Scale				Scale from core holder	Unidentified pattern
	948A	Zircaloy-2	Core channel	4.5	13	Stripped coupon	α-Zirconium
	953A	Zircaloy-2	Core channel	2.5	46	Stripped coupon	α-Zirconium
	957A	Zircaloy-2	Core channel	1.5	17	Stripped coupon	α-Zirconium
	941A	Zircaloy-2	In-line channel		46	Stripped coupon	α-Zirconium + ZrO_2
	945A	Zircaloy-2	In-line channel		17	Stripped coupon	α-Zirconium + ZrO_2
EE	743A	347 SS	Core channel	4.6	12	Stripped coupon	Stainless steel
	743A	Film	Core channel	4.6	12	Stripped from coupon 743A	No pattern
	747A	347 SS	Core channel	2.3	39	Stripped coupon	No pattern
	787A	347 SS	Core channel	1.0	10	Stripped coupon	Stainless Steel
	787A	Film	Core channel	1.0	10	Stripped from coupon 787A	No pattern

	740A	347 SS	In-line channel		39	As-removed coupon	No pattern
	736A	Film	In-line channel		12	Stripped from coupon 736A	No pattern
	T-8	Ti-75A	Core channel	5.7	9	Stripped coupon	Titanium
	T-9	Ti-75A	Core channel	3.9	14	As-removed coupon	No pattern
	T-9	Film	Core channel	3.9	14	Stripped from coupon T-9	No pattern
	T-12	Ti-75A	Core channel	2.5	36	Stripped coupon	Titanium
	T-16	Ti-75A	Core channel	1.2	13	Stripped coupon	Titanium
	T-16	Ti-75A	Core channel	1.2	13	Stripped from coupon T-16	No pattern
	T-0	Film	Core channel		9	Stripped from coupon T-0	No pattern
	Z-19	Zircaloy-2	Core channel	5.3	10	Stripped coupon	α-Zirconium
	Z-20	Film	Core channel	4.5	11	Stripped coupon Z-20	No pattern
	Z-24	Zircaloy-2	Core channel	2.7	34	Stripped coupon	α-Zirconium
	Z-37	Zircaloy-2	Core channel	1.3	12	Stripped coupon	α-Zirconium
	Z-37	Film	Core channel	1.3	12	Stripped from coupon Z-37	No pattern
	Z-12	Zircaloy-2	In-line channel		34	As-removed coupon	No pattern
	Z-1	Film	In-line channel		10	Stripped from coupon Z-1	No pattern
L-4-12	Z-88	Zircaloy-2	Core channel	4.6	10	Stripped coupon	α-Zirconium
	Z-88	Film	Core channel	4.6	10	Stripped from coupon Z-88	No pattern
	Z-89	Zircaloy-2	Core channel	4.2	11	As-removed coupon	No pattern
	Z-92	Zircaloy-2	Core channel	1.9	44	Stripped coupon	α-Zirconium
	Z-92	Film	Core channel	1.9	44	Stripped from coupon Z-92	α-Zirconium
	Z-94	Zircaloy-2	Core channel	1.2	15	As-removed coupon	No pattern

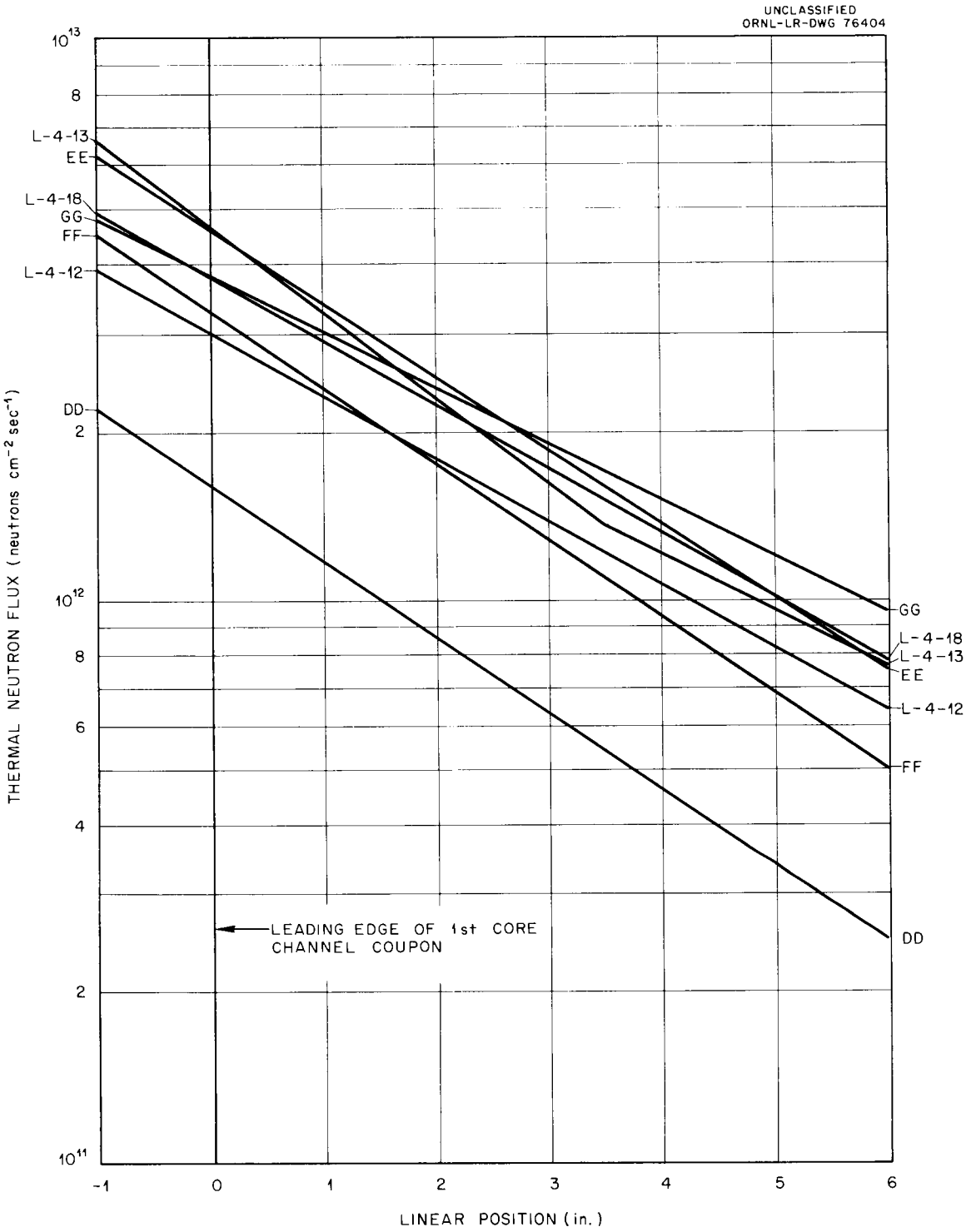

Fig. 68. Thermal Neutron Flux in Core vs Linear Position.

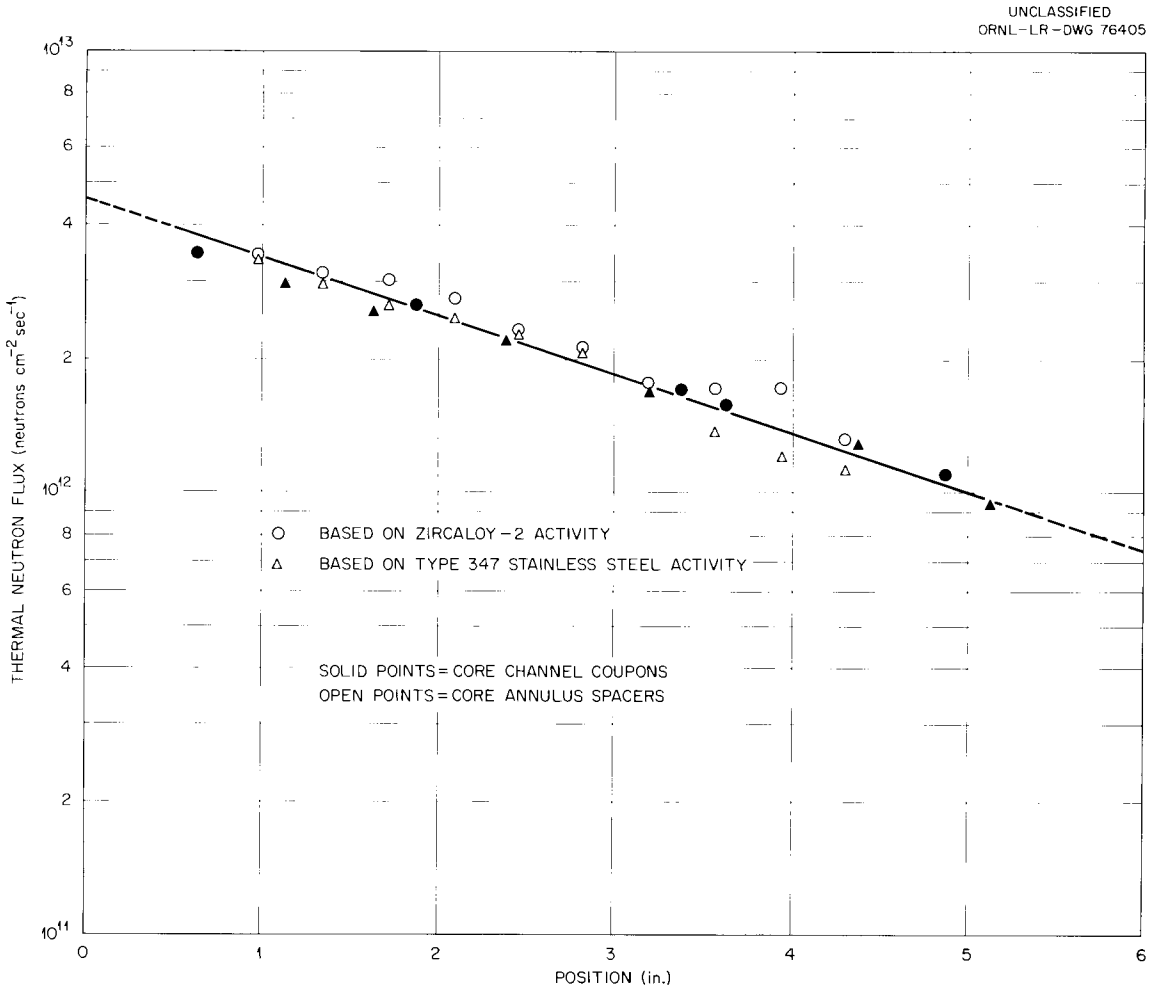

Fig. 69. Neutron Fluxes from Induced Activity Measurements, Loop EE.

and energy respectively. The calculated fission power near each specimen is set forth in the weight data, Tables 36–42.

4.8.2 Cesium - 137

The results of Cs^{137} analyses are shown in Fig. 73 in terms of the average fission powers in a loop at an LITR power of 3 Mw calculated from the analytical results and the reactor energy accumulated during the total exposure preceding the time of sampling. A further illustration of the Cs^{137} data is shown in Fig. 74, where the L-4-13 data are plotted in terms of the average fission powers in the loop during the periods between adjacent samples as indicated by the difference between the Cs^{137} content of the samples.

As may be judged from the plots, the analytical data scattered appreciably. Within the indicated uncertainty there is no evidence that the actual fission rate or uranium concentration in the loop core changed

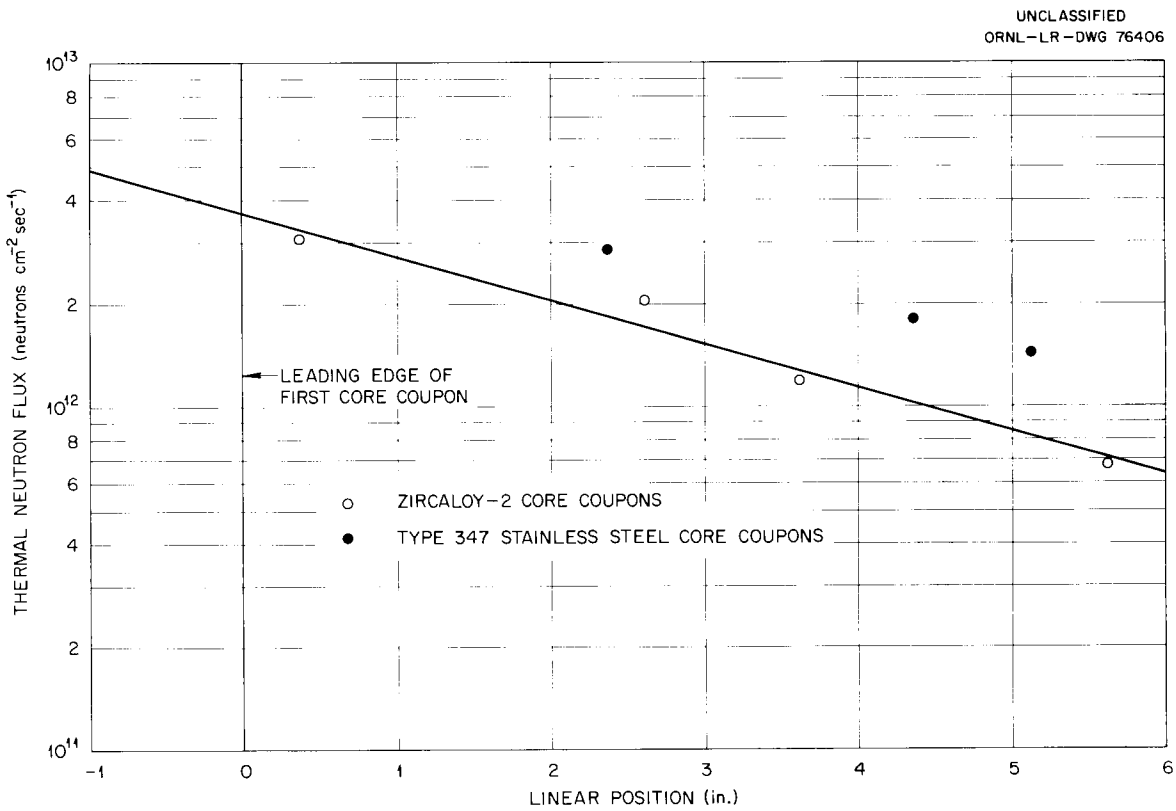

Fig. 70. Neutron Fluxes from Induced Activity Measurements, Loop L-4-12.

significantly during any of the experiments. The L-4-12 results for the second solution charge probably reflect some carry-over of Cs^{137} produced in the original solution charge.

4.8.3 Comparison of Average Fission-Power Values from Cs^{137} and from Induced Activities

Values for the cumulative average fission power in a loop experiment at 3 Mw LITR power calculated from the Cs^{137} and from induced-activity results are compared in Table 34. The average of the Cs^{137} results in each experiment is the final point shown in Fig. 73. The induced-activity calculations employed the neutron fluxes shown in Fig. 68 and the average uranium concentrations listed in Table 34. A value of 200 Mev/fission was assumed throughout.

In general, there is poor agreement between the Cs^{137} and the induced-activity values. The cesium values are the lowest values in all the experiments, except in loop DD. Other workers[27] have found that fission values determined from Cs^{137} analyses tend to be lower by about 15% than those determined from other, more standard methods. Although no completely satisfactory explanation of these differences has

[27] R. G. Hart, M. Lounsbury, and C. D. McKay, *A Comparison of Methods of Determining Burnup in Uranium Dioxide Fuel Test Specimens. Part 1. Studies on a Single Stringer Fuel Charge* (Nuclear Reactor Chemistry – First Conference, Gatlinburg, Tennessee – Oct. 12–14, 1960), TID-7610.

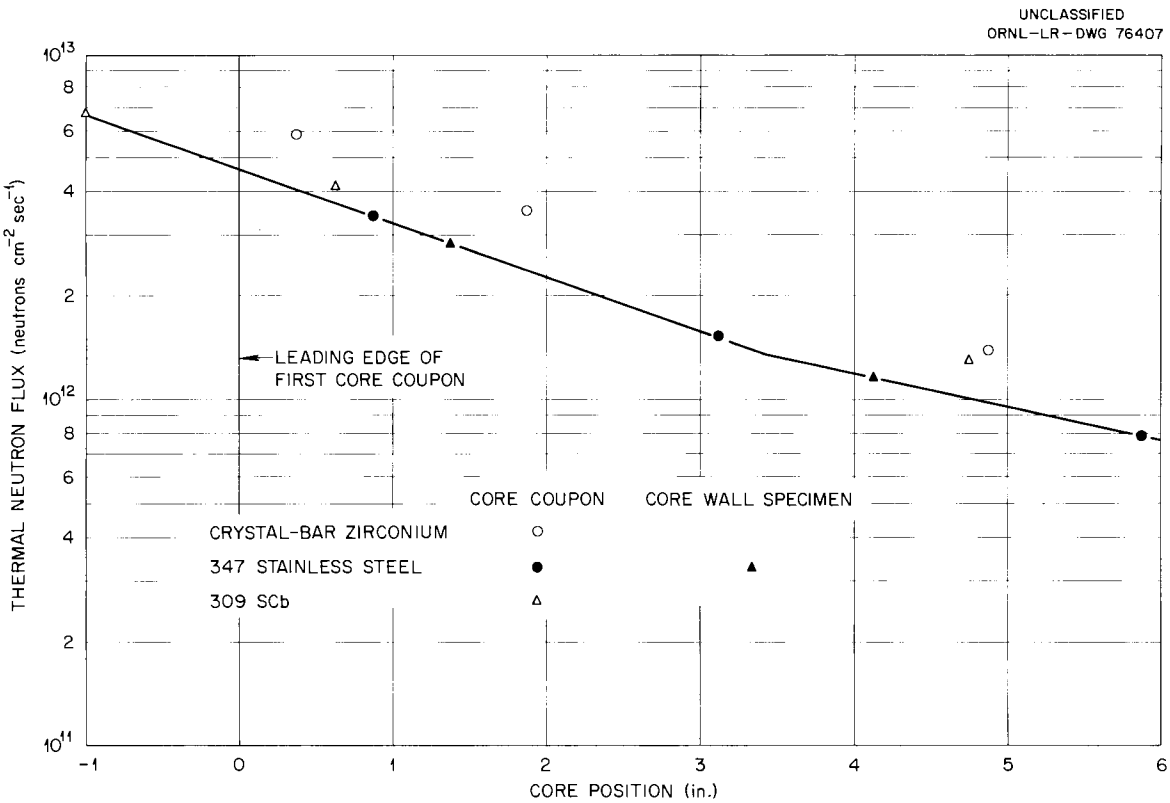

Fig. 71. Neutron Fluxes from Induced Activity Measurements, Loop L-4-13.

been evolved, the experimental Cs^{137} data for total fission power for the experiments reported here are considered more reliable than those calculated from specimen activities. In part, this belief is based on results obtained in later in-pile loop experiments which show that fission-power values determined from fission- and gamma-heat measurements were in better agreement with the power values indicated by Cs^{137} measurements than with those obtained from specimen activity data. The following factors are believed to contribute to the differences between fission powers evaluated from induced activities and cesium.

1. A value of 36.5 barns was taken for the Co^{59} cross section in preparing specimens for the induced-activity measurements.[28] The effective cross section of Co^{59} at the location of the standards may have been up to 10 to 15% greater than this, depending upon the flux of resonance-energy neutrons, so that the thermal flux at the loop specimens may have been up to 10 to 15% less than calculated.

2. No corrosion specimens were located in approximately the first inch of the core (core nose), and thermal-neutron flux values in this region were obtained from extrapolation of values from induced-activity measurements of specimens located farther to the rear in the core body. Also, the precise locations of these specimens, with respect to the core nose, were not known.

---

[28] F. J. Johnston, J. Halperin, and R. W. Stoughton, *J. Nucl. Energy, Pt. A* **11**, 95 (1960).

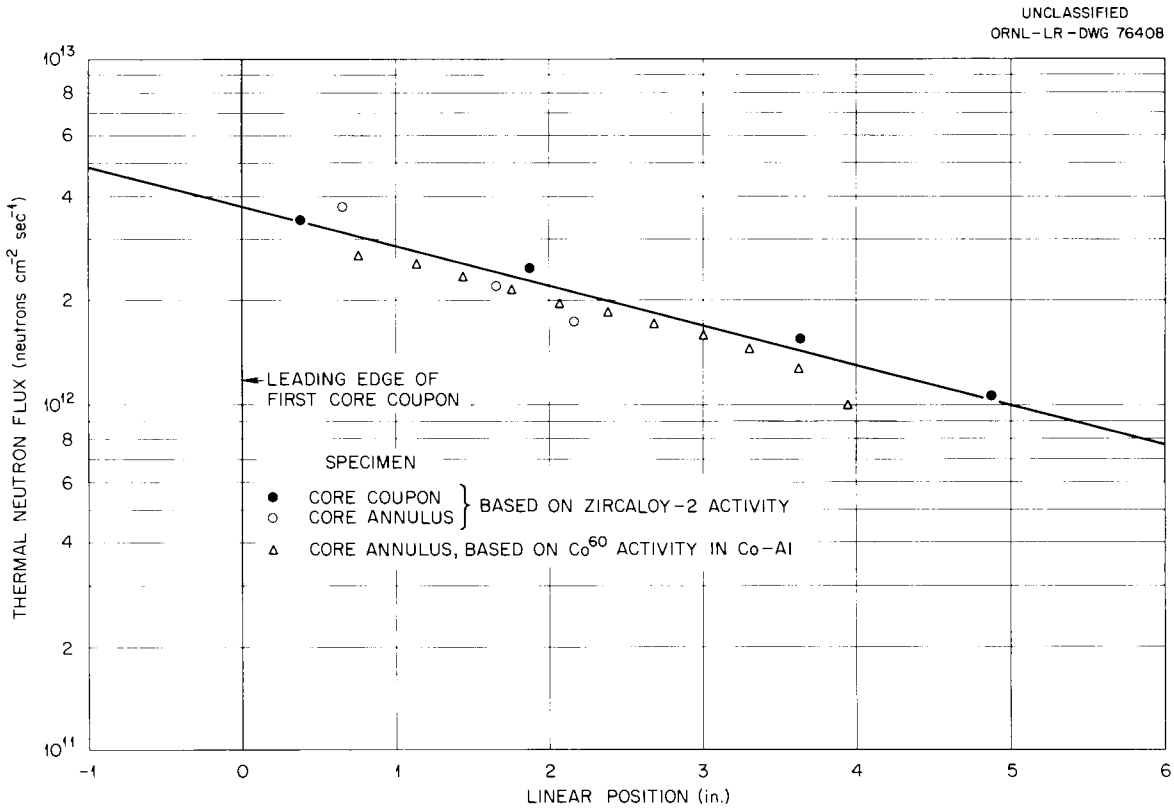

Fig. 72. Neutron Fluxes from Induced Activity Measurements, Loop L-4-18.

3. Some fission product cesium may have been sorbed on corrosion scales in the loops; however, where scales have been analyzed for Cs^{137} (Table 35, loop L-4-18 and in later experiments[29]), the results indicate negligible sorption. Hence it is considered likely that the sorption was negligible in the experiments under discussion.

4.9 Results of Quantitative Examination of Loops

4.9.1 Analyses of Scale from Low-Power-Density Regions

An attempt was made to determine the distribution of corrosion products, uranium, and Cs^{137} throughout the L-4-18 loop system by chemical analyses of samples of bulk scale removed from surfaces in various portions of the loop. The analytical results are listed in Table 35.

The results for different samples show considerable differences in composition for most of the elements, and thus the three samples cannot be considered representative of all scale in the loop. Qualitatively, the results support conclusions drawn from scale analyses in subsequent experiments at higher

[29] G. H. Jenks *et al.*, *HRP Quart. Progr. Rept. Oct. 31, 1958*, ORNL-2654, p 154.

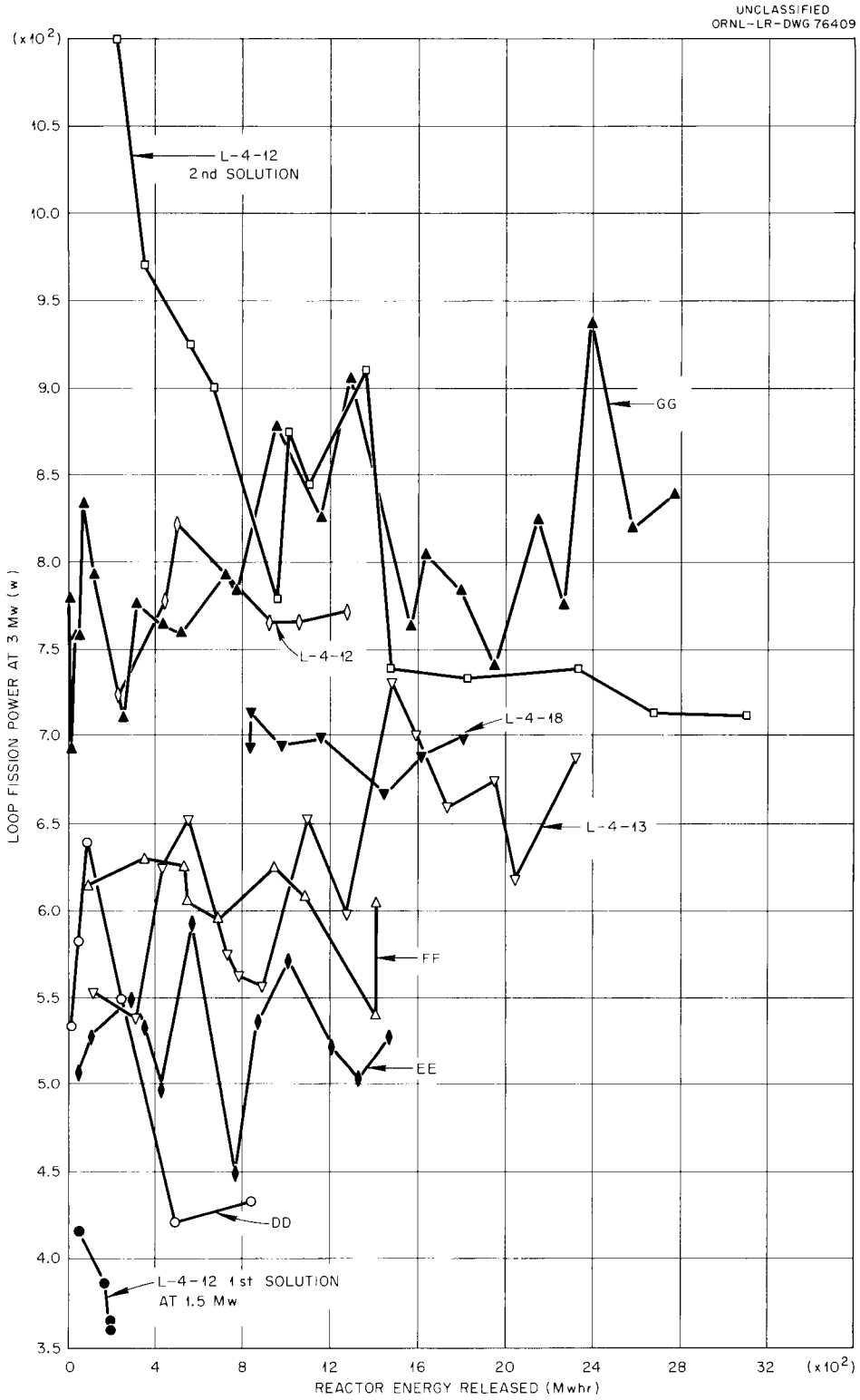

Fig. 73. Cumulative Average Fission Power at 3 Mw Based on Cs^{137} Analyses.

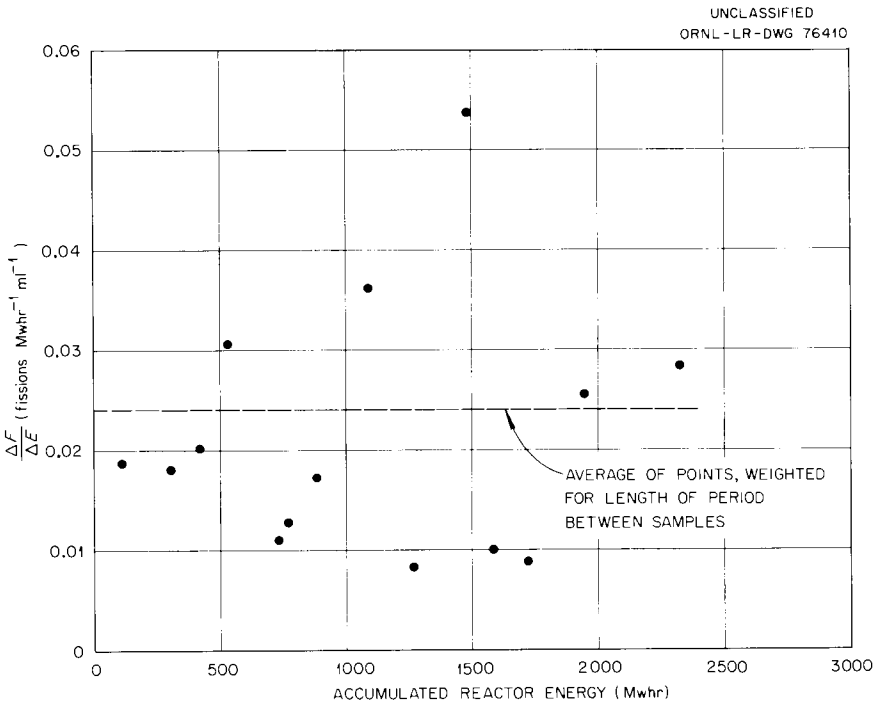

Fig. 74. $\frac{\text{Increase in Cs}^{137}\text{ During Periods Between Adjacent Samples, }\Delta F}{\text{Increase in LITR Energy Between Adjacent Samples, }\Delta E}$ **vs LITR Energy Accumulated During Exposure of Loop L-4-13.**

Table 34. Average Fission Power in Loop Experiments at 3 Mw LITR Power[a] as Determined from Cs^{137} and Specimen Activity Analyses

Loop	Cs^{137} Value (w)	Specimen Activity Value (w)	$\frac{\text{Specimen Activity}}{Cs^{137}}$	Calculated Average Concentration of Uranium (mg/ml)
DD	437	400	0.92	35.3
FF	606	843	1.39	39.3
GG	829	1073	1.29	39.6
EE	528	1053	1.99	38.5
L-4-12	730	782	1.07	39.5
L-4-13	689	801	1.16	41.1
L-4-18	700[b]	1007	1.43	39.8

[a]Based on 200 Mev/fission.
[b]Cs^{137} analyses by gamma spectrometer (all others by beta spectrometer).

Table 35. Analyses of Scale from L-4-18

Source of Scale	Scale Weight (mg)	Scale Composition (wt %)						
		U	Zr	Fe	Ni	Cu	Cs^{137}	*a*
Rear of core	19.9	0.05	4.5	48.0	7.0	0.78	0	40
In-line annulus holders	17.0	0.06	6.5	20.6	2.1	0.18	0	71
Pump volute	6.5	0.21	13.3	42.7	3.5	9.0	0	31

[a]Weight percent of scale not represented by listed constituents.

temperatures.[30,31] These indicate (1) negligible sorption of Cs^{137}, (2) transport of an appreciable fraction of the zirconium oxide found in the core to regions outside the core, and (3) the fact that scales contain large amounts of nickel and small amounts of uranium.

Recently reported[32] studies of sorption on zirconia in uranyl sulfate solutions show that some of the ions sorbed at high temperatures are removed by water-washing at room temperature or, possibly, by reversal of the sorption in uranyl sulfate solutions at low temperatures. Since all loops were rinsed with water at the completion of in-pile exposure, the possibility exists that for some elements such as uranium, cesium, and nickel, the amounts found in the scales are less than the amounts sorbed at high temperatures.

4.9.2 Analyses for Uranium on Steel Surfaces from High-Power-Density Regions

Analyses were performed on solutions containing the scale dissolved from one-half of the type 347 core channel coupon holder from experiment L-4-18. The analyses were carried out primarily to determine the amount of uranium on the steel surfaces. The as-removed holder half was sectioned into four approximately equal lengths. After being measured and weighed, these were treated separately with a 10% HCl solution, and one piece was treated with an HCl plus HNO_3 solution. Visually, the samples appeared clean after this treatment. The solution samples were analyzed for uranium, copper, and zirconium.

Five to eight micrograms of uranium per cm^2 was found on the steel surfaces, and there was little difference between amounts found at the front and the rear of the core. Copper ranged from 0 to 30 $\mu g/cm^2$ and averaged 10 $\mu g/cm^2$. No zirconium was found.

The importance of sorbed uranium in contributing to the fission recoil irradiation intensity at corroding surfaces has been discussed elsewhere.[33] The contribution from the 10 $\mu g/cm^2$ found here would not be significant, compared with that from the 0.17 *m* UO_2SO_4 solution. However, as mentioned above, the

[30]G. H. Jenks and J. E. Baker, *HRP Radiation Corrosion Studies: In-Pile Loops L-2-15 and L-4-16*, ORNL-3099 (in preparation).

[31]G. H. Jenks and J. E. Baker, *HRP Radiation Corrosion Studies: In-Pile Loop L-2-17*, ORNL-2974 (in preparation).

[32]G. H. Jenks *et al.*, *HRP Quart. Progr. Rept. Aug. 1–Nov. 30, 1960*, ORNL-3061, pp 72–73.

[33]G. H. Jenks *et al.*, *HRP Quart. Progr. Rept., Jan. 31, 1958*, ORNL-2493, p 126.

possibility is not precluded that significant amounts may have been sorbed during high-temperature exposure.

4.9.3 Results of Specimen Weight Measurements

The results of weight measurements of specimens and other components are listed in Tables 36–42, together with other data including calculated corrosion rate values, solution fission-power densities near specimens, and brief descriptions of specimens.

The zirconium-alloy corrosion rate values based on radiation time and total specimen area are plotted vs fission-power density in solution in Fig. 75. The titanium rate values determined in like manner are shown in Fig. 76.

Evidence obtained in later 280 and 300°C experiments and described elsewhere shows that covered surfaces of Zircaloy-2 are attacked at the same or at greater rates than are the exposed surfaces. It is assumed that the corrosion behavior of zirconium alloys in these lower-temperature experiments was similar and that the rates calculated with total area as a basis are more nearly correct than those based on exposed surface only. Zircaloy-2 is known to corrode linearly with radiation time. For titanium alloys, no evidence is available with respect to relative corrosion of exposed and covered surfaces. It is assumed that in this respect these alloys are similar to Zircaloy-2.

As will be discussed later, the stainless steel in the core of most of these experiments did not corrode linearly with radiation time, and the listed rates are, generally, averages of two or more rates. Also, the relative amounts of corrosion on the covered and exposed surfaces are uncertain for many of the specimens. Some of the specimens exposed to high solution velocities exhibited channeling (comparatively large rates on exposed surfaces), and, for these at least, the average rate values based on exposed surface areas are the most nearly correct.

For purposes of exhibiting and comparing steel corrosion in the various experiments, the exposed surface rates have been arbitrarily selected. Stainless steel rate values based on radiation time and exposed area are plotted in Figs. 77–81.

5. DISCUSSION OF RESULTS

5.1 Solution Analyses

The results of chemical analyses of the loop solutions during in-pile operation were subject to sampling errors resulting from dilution of the samples and to the usual uncertainties associated with remote analyses of radioactive solutions. No direct-control measurements were made of the accuracy of the overall sampling and subsequent chemical analyses, and it is necessary to estimate the significance of the results for these early experiments from considerations of (1) interconsistency of analytical values for various species in samples, (2) results of solution analyses in subsequent loop experiments, and (3) established accuracy of analytical methods.

Table 36. Corrosion Data for Stainless Steel Corrosion Specimens for Loop DD

Sample Number	Position	Exposed Coupon Area (cm^2)	Flow Velocity Leading Edge (fps)	Initial Weight (g)	As-Removed Weight (g)	Defilmed Weight (g)	Weight Loss (mg)	Corrosion Penetration (mils)	Corrosion Rate[a] (mpy) 465 hr	Corrosion Rate[a] (mpy) 280 hr	Neutron Flux at 3 Mw (neutrons cm^{-2} sec^{-1})	Power Density (w/ml)	Defilmed-Surface Appearance
											$\times 10^{12}$		
Core holder No. 11		~160									0.73	0.82	
436 A	A	3.25	9.7	1.8985	1.7827	1.7786	119.9	1.81	34.0	56.7	1.56	1.74	Exposed surface heavily attacked; clamped edges partially protected.
437 A	B	2.80	11.3	1.8852	1.7952	1.7913	93.9	1.65	31.1	51.6	1.37	1.53	Exposed surface heavily attacked; clamped edges partially protected
438 A	C	2.80	13.7	1.9166	1.8310	1.8276	89.0	1.56	29.4	48.8	1.20	1.34	Exposed surface heavily attacked; clamped edges partially protected
439 A	D	2.80	17.1	1.9072	1.8297	1.8274	79.8	1.40	26.4	43.8	1.06	1.18	Exposed surface heavily attacked; clamped edges partially protected
440 A	E	2.80	22.9	1.9104	1.8454	1.8426	67.8	1.19	22.4	37.2	0.88	0.99	~70% of the exposed surface shows shallow pits; clamped edges protected
441 A	F	2.80	35.8	1.9111	1.8555	1.8521	59.0	1.04	19.6	32.6	0.78	0.87	~50% of the exposed surface shows shallow pits; clamped edges protected
442 A	G	2.80	41.5	1.9039	1.8694	1.8660	37.9	0.66	12.4	20.7	0.68	0.76	~20% of the exposed surface shows shallow pits; clamped edges protected
443 A	H	2.80	50.5	1.8674	1.8525	1.8481	19.3	0.34	6.4	10.6	0.60	0.67	~10% of the exposed surface shows shallow pits; clamped edges protected
444 A	I	2.80	28.2	1.9138	1.9115	1.9022	11.6	0.20	3.8	6.3	0.48	0.54	Some very shallow pitting of exposed surfaces
445 A	J	2.80	19.9	1.8872	1.8947	1.8795	7.7	0.14	2.6	4.4	0.40	0.45	Machining marks quite clear; no apparent pitting
446 A	K	2.80	15.2	1.9201	1.9303	1.9135	6.6	0.12	2.2	3.8	0.29	0.32	Machining marks quite clear; no apparent pitting
447 A	L	3.00	12.1	1.8884	1.8990	1.8832	5.2	0.08	1.5	2.5	0.27	0.30	Machining marks quite clear; no apparent pitting

Table 36. (continued)

Sample Number	Position	Exposed Coupon Area (cm^2)	Flow Velocity Leading Edge (fps)	Initial Weight (g)	As-Removed Weight (g)	Defilmed Weight (g)	Weight Loss (mg)	Corrosion Penetration (mils)	Corrosion Rate[a] (mpy) 465 hr	280 hr	Neutron Flux at 3 min (neutrons cm^{-2} sec^{-1})	Power Density (w/ml)	Defilmes-Surface Appearance
In-line holder No. 10		~ 160											
448 A	A	3.00	9.4	1.9194	1.9277	1.9164	3.0	0.05	0.9	1.6			Machining marks clearly visible; some very thin, black film remaining; no pitting
449 A	B	2.80	10.9	1.8910	1.9004	1.8885	3.5	0.06	1.1	1.9			Machining marks clearly visible; some very thin, black film remaining; no pitting
450 A	C	2.80	13.2	1.9092	1.9191	1.9025	6.7	0.12	2.2	3.8			Machining marks clearly visible; some very thin, black film remaining; no pitting
451 A	D	2.80	16.5	1.9191	1.9340	1.9172	1.9	0.03	0.6	0.9			Machining marks clearly visible; some very thin, black film remaining; no pitting
452 A	E	2.80	22.1	1.8991	1.9096	1.8949	4.2	0.07	1.3	2.2			Machining marks clearly visible; some very thin, black film remaining; no pitting
453 A	F	2.80	34.6	1.8898	1.8995	1.8833	6.5	0.11	2.1	3.4			Machining marks clearly visible; some very thin, black film remaining; no pitting
454 A	G	2.80	40.1	1.8902	1.8982	1.8848	5.4	0.09	1.7	2.8			Machining marks clearly visible; some very thin, black film remaining; no pitting
455 A	H	2.80	48.8	1.9035	1.9122	1.9007	2.8	0.05	0.9	1.6			Machining marks clearly visible; some very thin, black film remaining; no pitting
456 A	I	2.80	27.2	1.8823	1.8904	1.8794	2.9	0.05	0.9	1.6			Machining marks clearly visible; some very thin, black film remaining; no pitting
457 A	J	2.80	19.2	1.9113	1.9161	1.9055	5.8	0.10	1.8	3.1			Machining marks clearly visible; some very thin, black film remaining; no pitting
458 A	K	2.80	14.7	1.9142	1.9200	1.9100	4.2	0.07	1.3	2.2			Machining marks clearly visible; some very thin, black film remaining; no pitting
459 A	L	3.00	11.7	1.9054	1.9116	1.9001	5.3	0.08	1.5	2.5			Machining marks clearly visible; some very thin, black film remaining; no pitting

[a]Two corrosion rates are presented: total operation 465 hr and radiation time with 3 Mwhr equivalent to 1 hr.

Table 37. Specimen Data for Loop EE

Sample No.	Position	Distance from Front of Core Holder to Center of Specimen (in.)	Flow Velocity at Leading Edge (fps)	Initial Weight (g)	As-Removed Weight (g)	Defilmed Weight (g)	Weight Change (mg)	Exposed Specimen Area (cm^2)	Corrosion Penetration (mils)	Corrosion Rate* (mpy) 630.3** (hr)	Corrosion Rate* (mpy) 536.8** (hr)	Total Specimen Area (cm^2)	Corrosion Penetration (mils)	Corrosion Rate* (mpy) 630.3** (hr)	Corrosion Rate* (mpy) 536.8** (hr)	Neutron Flux at 3 Mw (neutrons/ cm^2/sec $\times 10^{-12}$)	Power Density at 3 Mw (w/ml)	Surface Appearance: As Removed	Surface Appearance: After Defilming
24 Core Sample Coupons																			
Type 347 Stainless Steel Coupons																			
743 A	4	0.88	11.8	0.9512	0.8465	0.8457	−105.5	1.40	3.70	51.3	59.9	2.1	2.47	34.2	39.9	3.52	4.55	Heavy rough scale on all surfaces	Thin film, pickled appearance; clamped edges were protected
744 A	5	1.13	13.1	0.9483	0.8514	0.8503	−98.0	1.40	3.44	47.4	55.6	2.1	2.29	31.6	37.1	2.97	3.84	Heavy rough scale on all surfaces	Thin film, pickled appearance; clamped edges were protected
745 A	7	1.63	16.3	0.9474	0.8422	0.8413	−106.1	1.40	3.72	51.2	60.2	2.1	2.48	34.2	40.1	2.54	3.28	Heavy rough scale on all surfaces	Thin film on one side, heavy pickled appearance; clamped edges were protected
746 A	10	2.38	26.0	0.9630	0.9583	0.9582	−4.8	1.40	0.17	2.3	2.8	2.1	0.11	1.6	1.8	2.18	2.82	Heavy rough scale on all surfaces	Thin film, some scale; machine marks visible
747 A	13	3.13	39.2	0.9545	0.9521	0.9520	−2.5	1.40	0.09	1.2	1.5	2.1	0.06	0.8	1.0	1.79	2.31	Spotty brown scale on all surfaces	Thin film on most of the surface, pickled appearance along one edge
784 A	18	4.38	22.3	0.9583	0.9581	0.9576	−0.7	1.40	0.02	0.3	0.3	2.1	0.01	0.2	0.2	1.28	1.66	Flaky scale on all surfaces	Film on all surfaces; machine marks visible
785 A	21	5.13	14.4	0.9615	0.9621	0.9614	−0.1	1.40	0.004	0.1	0.1	2.1	0.003	0.04	0.05	0.94	1.21	Spotty brown scale on all surfaces	Thin film on all surfaces; machine marks visible
787 A	24	5.88	10.4	0.9627	0.9640	0.9626	−0.1	1.57	0.003	0.04	0.05	2.1	0.002	0.03	0.03	0.78	1.01	Heavy dark-brown scale on all surfaces	Thin film on all surfaces; machine marks visible
Zircaloy-2 Coupons																			
Z 19	2	0.38	9.9	0.7638	0.7591	0.7587	−5.1	1.40	0.22	3.1	3.6	2.1	0.15	2.0	2.4	4.10	5.30	Heavy red-brown film on all surfaces	Thin film on all surfaces, light etching; machine marks visible
Z 20	3	0.63	10.7	0.7672	0.7629	0.7623	−4.9	1.40	0.21	2.9	3.4	2.1	0.14	1.9	2.3	3.45	4.46	Heavy red-brown film on all surfaces	Thin film on all surfaces, light etching; machine marks visible
Z 21	8	1.88	18.6	0.7738	0.7695	0.7698	−4.0	1.40	0.17	2.3	2.8	2.1	0.11	1.6	1.8	2.67	3.45	Heavy brown film on all surfaces	Dark film on all surfaces; machine marks visible
Z 24	11	2.63	34.0	0.7754	0.7712	0.7725	−2.9	1.40	0.13	1.8	2.1	2.1	0.09	1.2	1.4	2.09	2.70	Mottled brown scale on all surfaces	Some scale retained in spots on all surfaces
Z 26	14	3.38	42.5	0.7728	0.7698	0.7698	−3.0	1.40	0.13	1.8	2.1	2.1	0.09	1.2	1.4	1.71	2.21	Spotted brown scale on all surfaces	Thin dark scale on all surfaces
Z 27	15	3.63	47.8	0.7671	0.7641	0.7645	−2.6	1.40	0.11	1.5	1.8	2.1	0.07	1.0	1.2	1.58	2.04	Dark-gray film on all surfaces	Thin dark film on all surfaces; some white spots visible
Z 31	20	4.88	16.1	0.7626	0.7611	0.7609	−1.7	1.40	0.07	1.0	1.1	2.1	0.05	0.6	0.8	1.10	1.43	Heavy spotty film on all surfaces	No apparent film; machine marks clearly visible
Z 37	23	5.63	11.5	0.7639	0.7624	0.7623	−1.6	1.40	0.07	1.0	1.1	2.1	0.05	0.6	0.8	0.84	1.32	Heavy gray-brown film, some white deposits on all surfaces	Thin dark film on all surfaces; machine marks visible

*Corrosion rates have been calculated both for the nominally exposed and the total specimen areas.

**Two corrosion rates are presented: one based on the total operation time of 630.3 hr and one based on the total radiation time of 536.8 hr (3 Mwhr of reactor time equivalent to 1 hr of total radiation time).

Table 37 (continued)

Sample No.	Position	Distance from Front of Core Holder to Center of Specimen (in.)	Flow Velocity at Leading Edge (fps)	Initial Weight (g)	As-Removed Weight (g)	Defilmed Weight (g)	Weight Change (mg)	Exposed Specimen Area (cm^2)	Corrosion Penetration (mils)	Corrosion Rate* (mpy) 630.3** (hr)	Corrosion Rate* (mpy) 536.8** (hr)	Total Specimen Area (cm^2)	Corrosion Penetration (mils)	Corrosion Rate* (mpy) 630.3** (hr)	Corrosion Rate* (mpy) 536.8** (hr)	Neutron Flux at 3 Mw (neutrons/cm^2/sec $\times 10^{-12}$)	Power Density at 3 Mw (w/ml)	Surface Appearance: As Removed	Surface Appearance: After Defilming
Titanium Coupons																			
T 8	1	0.13	9.2	0.5433	0.5431	0.5428	−0.5	1.57	0.03	0.4	0.5	2.1	0.02	0.3	0.4	4.40	5.66	Thin rust-red film on all surfaces	Very thin film on all surfaces; machine marks visible
T 9	6	1.38	14.4	0.5397	0.5392	0.5392	−0.5	1.40	0.03	0.4	0.5	2.1	0.02	0.3	0.3	3.04	3.93	Thin brown film on all surfaces	Thin oxide film on all surfaces; machine marks visible
T 11	9	2.13	21.7	0.5452	0.5445	0.5447	−0.5	1.40	0.03	0.4	0.5	2.1	0.02	0.3	0.3	2.41	3.12	Heavy scale on all surfaces	Film on all surfaces; machine marks visible
T 12	12	2.88	36.2	0.5390	0.5388	0.5376	−1.4	1.40	0.09	1.2	1.5	2.1	0.06	0.8	1.0	1.92	2.48	Heavy film on all surfaces	Very thin film on all surfaces; machine marks visible
T 13	16	3.88	34.1	0.5367	0.5364	0.5348	−1.9	1.40	0.12	1.7	1.9	2.1	0.08	1.1	1.3	1.42	1.84	Flaky brown scale on all surfaces	No apparent film; machine marks visible
T 14	17	4.13	26.9	0.5429	0.5425	0.5415	−1.4	1.40	0.09	1.2	1.5	2.1	0.06	0.8	1.0	1.32	1.71	Spotty film on all surfaces	Thin film on all surfaces; light etched appearance; some machine marks visible
T 15	19	4.63	18.9	0.5348	0.5354	0.5344	−0.4	1.40	0.02	0.3	0.3	2.1	0.01	0.2	0.2	1.14	1.48	Spotty scale on all surfaces	Thin rust-colored film on all surfaces
T 16	22	5.38	12.6	0.5300	0.5307	0.5296	−0.4	1.40	0.02	0.3	0.3	2.1	0.01	0.2	0.2	0.90	1.17	Heavy flaky scale, some white deposits on all surfaces	No apparent film; machine marks clearly visible
18 Coupled Specimens (Type 347 Stainless Steel Rod and Spacers)																			
Type 347 Stainless Steel Specimens																			
792 A	1	1.13		0.6936	0.6884	0.6872	−6.4	1.07	0.29	4.05	4.76	1.89	0.17	2.3	2.7	3.28	4.24	Dark-brown scale on all surfaces; disturbed in contact area	Slight etching of all free surfaces except contact areas
793 A	2	1.19		0.6794	0.6742	0.6740	−5.4	1.07	0.25	3.44	4.04	1.89	0.14	2.0	2.3	3.20	4.14	Dark-brown scale on all surfaces; disturbed in contact area	Slight etching of all free surfaces except contact areas
794 A	3	1.50		0.6852	0.6847	0.6797	−5.5	1.07	0.25	3.36	3.95	1.89	0.14	1.9	2.2	2.93	3.79	Dark-brown scale on all surfaces; disturbed in contact area	Slight etching of all free surfaces except contact areas
795 A	5	1.87		0.6807	0.6782	0.6766	−4.1	1.07	0.19	2.61	3.06	1.89	0.11	1.5	1.7	2.62	3.39	Dark-brown scale on all surfaces; disturbed in contact area	Slight etching of all surfaces; machine marks visible
808 A	13	3.35		0.6800	0.6800	0.6785	−1.5	1.07	0.07	0.96	1.13	1.89	0.04	0.5	0.6	1.66	2.15	Dark-brown scale on all surfaces; disturbed in contact area	Thin tan film on all surfaces; machine marks visible
809 A	15	3.72		0.6783	0.6775	0.6773	−1.0	1.07	0.05	0.65	0.76	1.89	0.03	0.4	0.4	1.49	1.93	Dark-brown scale on all surfaces	Thin tan film on all surfaces; machine marks visible
810 A	17	4.09		0.6826	0.6817	0.6828	+0.2	1.07				1.89				1.34	1.73	Dark-brown scale on all surfaces	Thin tan film on all surfaces; machine marks visible
811 A	18	4.15		0.6737	0.6728	0.6735	−0.2	1.07	0.01	0.13	0.15	1.89	0.006	0.1	0.1	1.31	1.69	Dark-brown scale on all surfaces	Thin tan film on all surfaces; machine marks visible
Zircaloy-2 Specimens																			
Z 48	4	1.56		0.5663	0.5626	0.5620	−4.3	1.07	0.24	3.37	3.96	1.89	0.14	1.9	2.2	2.89	3.74	Dark-gray scale on contact surfaces; dark-brown scale on free surfaces	Slight etching of contact area; machine marks on other areas
Z 49	7	2.24		0.5651	0.5625	0.5618	−3.3	1.07	0.19	2.59	3.04	1.89	0.11	1.5	1.7	2.33	3.01	Dark-gray scale on contact surfaces; dark-brown scale on free surfaces	Machine marks visible on all surfaces; some scale in contact areas
Z 50	11	2.98		0.5645	0.5620	0.5619	−2.6	1.07	0.15	2.04	2.40	1.89	0.08	1.2	1.4	1.86	2.40	Dark scale on all surfaces; cracked in contact zone	Thin dark scale on some areas; machine marks visible
Z 51	16	3.78		0.5698	0.5683	0.5680	−1.8	1.07	0.10	1.42	1.67	1.89	0.06	0.8	1.0	1.47	1.90	Dark-brown scale on all surfaces	Thin dark scale on some areas; machine marks visible

*Corrosion rates have been calculated both for the nominally exposed and the total specimen areas.

**Two corrosion rates are presented: one based on the total operation time of 630.3 hr and one based on the total radiation time of 536.8 hr (3 Mwhr of reactor time equivalent to 1 hr of total radiation time).

Table 37 (continued)

Sample No.	Position	Distance from Front of Core Holder to Center of Specimen (in.)	Flow Velocity at Leading Edge (fps)	Initial Weight (g)	As-Removed Weight (g)	Defilmed Weight (g)	Weight Change (mg)	Exposed Specimen Area (cm^2)	Corrosion Penetration (mils)	Corrosion Rate* (mpy) 630.3** (hr)	Corrosion Rate* (mpy) 536.8** (hr)	Total Specimen Area (cm^2)	Corrosion Penetration (mils)	Corrosion Rate* (mpy) 630.3** (hr)	Corrosion Rate* (mpy) 536.8** (hr)	Neutron Flux at 3 Mw (neutrons/cm^2/sec $\times 10^{-12}$)	Power Density at 3 Mw (w/ml)	Surface Appearance: As Removed	Surface Appearance: After Defilming
Titanium Specimens (55AX)																			
T 44	6	1.93		0.3938	0.3935	0.3939	+0.1	1.07				1.89				2.58	3.34	Dark-brown scale on all surfaces; disturbed in contact area	Thin dark film on all surfaces; machine marks visible
T 46	8	2.30		0.3773	0.3760	0.3773	0.0	1.07	0.00	0.00	0.00	1.89	0.00	0.00	0.00	2.29	2.96	Dark-brown scale on all surfaces; disturbed in contact area	Machine marks visible on all surfaces; some scale in contact zone
T 47	9	2.61		0.3823	0.3818	0.3817	−0.5	1.07	0.04	0.57	0.67	1.89	0.02	0.3	0.4	2.10	2.71	Dark-brown scale on all surfaces; disturbed in contact area	Thin dark film on all surfaces; machine marks visible
T 50	10	2.67		0.3869	0.3850	0.3865	−0.4	1.07	0.03	0.45	0.53	1.89	0.02	0.3	0.3	2.07	2.68	Dark-brown scale on all surfaces; disturbed in contact area	Thin dark film on all surfaces; machine marks visible
T 52	12	3.04		0.3864	0.3856	0.3862	−0.2	1.07	0.02	0.23	0.27	1.89	0.01	0.1	0.2	1.84	2.38	Dark scale on all surfaces; cracked in contact zone	Thin dark film on all surfaces; machine marks visible
T 53	14	3.41		0.3979	0.3971	0.3973	−0.6	1.07	0.05	0.67	0.79	1.89	0.03	0.4	0.5	1.64	2.12	Dark-brown scale on all surfaces; disturbed in contact area	Thin dark scale on some areas; machine marks visible
Type 347 Stainless Steel Spacers																			
S 1	1	0.97		0.5966	0.5853	0.5843	−12.3	2.23	0.27	3.73	4.38	2.42	0.25	3.4	4.0	3.32	4.29		
S 2	2	1.34		0.6123	0.6044	0.6032	−9.1	2.23	0.20	2.76	3.24	2.42	0.18	2.5	3.0	2.95	3.81		
S 3	3	1.71		0.6140	0.6083	0.6070	−7.0	2.23	0.15	2.12	2.49	2.42	0.14	2.0	2.3	2.65	3.42		
S 4	4	2.08		0.5545	0.5499	0.5486	−5.9	2.23	0.13	1.79	2.10	2.42	0.12	1.7	1.9	2.49	3.22		
S 5	5	2.45		0.5958	0.5932	0.5917	−4.1	2.23	0.09	1.24	1.46	2.42	0.08	1.1	1.4	2.27	2.93		
S 6	6	2.82		0.5524	0.5519	0.5490	−3.4	2.23	0.08	1.03	1.21	2.42	0.07	1.0	1.1	2.05	2.65		
S 7	7	3.19		0.5726	0.5715	0.5700	−2.6	2.23	0.06	0.79	0.93	2.42	0.05	0.7	0.9	1.69	2.18		
S 8	8	3.56		0.5543	0.5542	0.5525	−1.8	2.23	0.04	0.55	0.65	2.42	0.04	0.5	0.6	1.37	1.77		
S 9	9	3.93		0.5782	0.5775	0.5772	−1.0	2.23	0.02	0.30	0.35	2.42	0.02	0.3	0.3	1.21	1.57		
S 10	10	4.30		0.5483	0.5462	0.5475	−0.8	2.23	0.02	0.25	0.29	2.42	0.02	0.2	0.3	1.14	1.47		
18 Coupled Specimens (Zircaloy-2 Rod and Spacers)																			
Type 347 Stainless Steel Specimens																			
788 A	4	1.56		0.6927	0.6867	0.6853	−7.4	1.07	0.34	4.7	5.5	1.89	0.19	2.7	3.1	2.89	3.74	Dark scale on all surfaces; disturbed in contact area	Dark speckled scale on free surfaces; brown in contact zone
789 A	5	1.87		0.6896	0.6836	0.6827	−6.9	1.07	0.32	4.4	5.1	1.89	0.18	2.5	2.9	2.61	3.37	Dark scale on all surfaces; disturbed in contact area	Dark, salted scale on all surfaces
790 A	13	3.35		0.6908	0.6882	0.6867	−4.1	1.07	0.19	2.6	3.0	1.89	0.11	1.5	1.7	1.67	2.16	Dark scale on all surfaces; disturbed in contact area	Dark, salted scale on all surfaces
791 A	15	3.72		0.6905	0.6899	0.6876	−2.9	1.07	0.13	1.8	2.2	1.89	0.08	1.0	1.2	1.50	1.94	Dark scale on all surfaces; disturbed in contact area	Dark, salted scale on all surfaces

*Corrosion rates have been calculated both for the nominally exposed and the total specimen areas.

**Two corrosion rates are presented: one based on the total operation time of 630.3 hr and one based on the total radiation time of 536.8 hr (3 Mwhr of reactor time equivalent to 1 hr of total radiation time).

Table 37 (continued)

Sample No.	Position	Distance from Front of Core Holder to Center of Specimen (in.)	Flow Velocity at Leading Edge (fps)	Initial Weight (g)	As-Removed Weight (g)	Defilmed Weight (g)	Weight Change (mg)	Exposed Specimen Area (cm^2)	Corrosion Penetration (mils)	Corrosion Rate* (mpy) 630.3** (hr)	Corrosion Rate* (mpy) 536.8** (hr)	Total Specimen Area (cm^2)	Corrosion Penetration (mils)	Corrosion Rate* (mpy) 630.3** (hr)	Corrosion Rate* (mpy) 536.8** (hr)	Neutron Flux at 3 Mw (neutrons/ cm^2/sec $\times 10^{-12}$)	Power Density at 3 Mw (w/ml)	Surface Appearance: As Removed	Surface Appearance: After Defilming
Zircaloy-2 Specimens																			
Z 40	1	1.13		0.5556	0.5513	0.5503	−5.3	1.07	0.30	4.1	4.9	1.89	0.17	2.3	2.8	3.29	4.25	Dark scale on all surfaces; disturbed in contact area	Dark, salted scale on all surfaces
Z 41	2	1.19		0.5772	0.5731	0.5726	−4.6	1.07	0.26	3.6	4.2	1.89	0.15	2.0	2.4	3.21	4.15	Dark scale on all surfaces; disturbed in contact area	Dark, salted scale on all surfaces
Z 42	3	1.50		0.5686	0.5648	0.5644	−4.2	1.07	0.24	3.3	3.8	1.89	0.13	1.9	2.2	2.92	3.77	Dark scale on all surfaces; disturbed in contact area	Dark, salted scale on all surfaces
Z 43	7	2.24		0.5701	0.5675	0.5658	−4.3	1.07	0.24	3.4	4.0	1.89	0.14	1.9	2.2	2.32	3.00	Dark scale on all surfaces; disturbed in contact area	Dark, salted scale on all surfaces
Z 44	11	2.98		0.5539	0.5511	0.5502	−3.7	1.07	0.21	2.9	3.4	1.89	0.12	1.6	1.9	1.87	2.42	Dark scale on all surfaces; disturbed in contact area	Dark, salted scale on all surfaces
Z 45	16	3.78		0.5605	0.5581	0.5574	−3.1	1.07	0.18	2.4	2.8	1.89	0.10	1.4	1.6	1.47	1.90	Dark scale on all surfaces; disturbed in contact area	Dark, salted scale on all surfaces
Z 46	17	4.09		0.5628	0.5608	0.5594	−3.4	1.07	0.19	2.6	3.1	1.89	0.11	1.5	1.8	1.34	1.73	Dark scale on all surfaces; disturbed in contact area	Dark, salted scale on all surfaces
Z 47	18	4.15		0.5732	0.5712	0.5699	−3.3	1.07	0.19	2.6	3.0	1.89	0.11	1.5	1.7	1.31	1.69	Dark scale on all surfaces; disturbed in contact area	Dark, salted scale on all surfaces
Titanium Specimens (55AX)																			
T 25	6	1.93		0.3825	0.3826	0.3824	−0.1	1.07	0.01	0.1	0.1	1.89	0.01	0.1	0.1	2.54	3.28	Dark scale on all surfaces; disturbed in contact area	Dark, salted scale on all surfaces
T 26	8	2.30		0.3857	0.3866	0.3858	+0.1	1.07				1.89				2.30	2.97	Dark scale on all surfaces; disturbed in contact area	Dark brown scale on all surfaces
T 27	9	2.61		0.3864	0.3871	0.3864	0.0	1.07	0.00	0.0	0.0	1.89	0.00	0.0	0.0	2.09	2.70	Dark scale on all surfaces; disturbed in contact area	Dark brown film on free surfaces; scale on contact areas
T 29	10	2.67		0.3911	0.3913	0.3914	+0.3	1.07				1.89				2.07	2.67	Dark scale on all surfaces; disturbed in contact area	Dark brown film on free surfaces; scale on contact areas
T 38	12	3.04		0.3912	0.3916	0.3915	+0.3	1.07				1.89				1.83	2.36	Dark scale on all surfaces; disturbed in contact area	Dark brown film on free surfaces; scale on contact areas
T 42	14	3.41		0.3780	0.3782	0.3771	−0.9	1.07	0.08	1.1	1.2	1.89	0.04	0.6	0.7	1.64	2.12	Dark scale on all surfaces; disturbed in contact area	Dark brown film on free surfaces; scale on contact areas
Zircaloy-2 Spacers																			
Z 1	1	0.97		0.5210	0.5179	0.5179	−3.1	2.23	0.07	0.9	1.1	2.42	0.06	0.9	1.0	3.45	4.46		
Z 2	2	1.34		0.5207	0.5188	0.5122	−8.5	2.23	0.19	2.6	3.0	2.42	0.17	2.4	2.8	3.14	4.06		
Z 3	3	1.71		0.5190	0.5113	0.5112	−7.8	2.23	0.17	2.4	2.8	2.42	0.16	2.2	2.6	3.04	3.93		
Z 4	4	2.08		0.5245	0.5224	0.5160	−8.5	2.23	0.19	2.6	3.0	2.42	0.17	2.4	2.8	2.77	3.58		
Z 5	5	2.45		0.5183	0.5168	0.5105	−7.8	2.23	0.17	2.4	2.8	2.42	0.16	2.2	2.6	2.32	2.99		
Z 6	6	2.82		0.5317	0.5308	0.5251	−6.6	2.23	0.15	2.0	2.4	2.42	0.13	1.8	2.2	2.07	2.68		
Z 7	7	3.19		0.5199	0.5150	0.5131	−6.8	2.23	0.15	2.1	2.4	2.42	0.14	1.9	2.2	1.78	2.31		
Z 8	8	3.56		0.5244	0.5200	0.5192	−5.2	2.23	0.12	1.6	1.9	2.42	0.11	1.5	1.7	1.72	2.22		
Z 9	9	3.93		0.5228	0.5183	0.5159	−6.9	2.23	0.15	2.1	2.5	2.42	0.14	1.9	2.3	1.71	2.21		
Z 10	10	4.30		0.5163	0.5135	0.5113	−5.0	2.23	0.11	1.5	1.8	2.42	0.10	1.4	1.6	1.34	1.74		

*Corrosion rates have been calculated both for the nominally exposed and the total specimen areas.

**Two corrosion rates are presented: one based on the total operation time of 630.3 hr and one based on the total radiation time of 536.8 hr (3 Mwhr of reactor time equivalent to 1 hr of total radiation time).

Table 37 (continued)

Sample No.	Position	Distance from Front of Core Holder to Center of Specimen (in.)	Flow Velocity at Leading Edge (fps)	Initial Weight (g)	As-Removed Weight (g)	Defilmed Weight (g)	Weight Change (mg)	Exposed Specimen Area (cm^2)	Corrosion Penetration (mils)	Corrosion Rate* (mpy) 630.3** (hr)	Corrosion Rate* (mpy) 536.8** (hr)	Total Specimen Area (cm^2)	Corrosion Penetration (mils)	Corrosion Rate* (mpy) 630.3** (hr)	Corrosion Rate* (mpy) 536.8** (hr)	Neutron Flux at 3 Mw (neutrons/ cm^2/sec $\times 10^{-12}$)	Power Density at 3 Mw (w/ml)	Surface Appearance: As Removed	Surface Appearance: After Defilming
In-Line Corrosion Sample Coupons																			
Type 347 Stainless Steel Coupons																			
736 A	4		11.8	0.9547	0.9608	0.9524	−2.3	1.40	0.08	1.1	1.3	2.1	0.05	0.8	0.9			Heavy rust-colored scale on all surfaces	Clean; machine marks visible
737 A	5		13.1	0.9547	0.9606	0.9540	−0.7	1.40	0.03	0.4	0.4	2.1	0.02	0.2	0.3			Heavy rust-colored scale on all surfaces	Clean; machine marks visible
738 A	7		16.3	0.9526	0.9585	0.9506	−2.0	1.40	0.07	1.0	1.1	2.1	0.05	0.7	0.8			Heavy rust-colored scale on all surfaces	Slight staining of all surfaces; machine marks visible
739 A	10		26.0	0.9396	0.9453	0.9392	−0.4	1.40	0.01	0.2	0.2	2.1	0.01	0.1	0.2			Heavy rust-colored scale on all surfaces	Clean; machine marks visible
740 A	13		39.2	0.9509	0.9557			1.40				2.1						Heavy rust-colored scale on all surfaces	
741 A	18		22.3	0.9532	0.9570	0.9528	−0.4	1.40	0.01	0.2	0.2	2.1	0.01	0.1	0.2			Heavy rust-colored scale on all surfaces	Clean; machine marks visible
742 A	21		14.4	0.9504	0.9538	0.9499	−0.5	1.40	0.02	0.3	0.3	2.1	0.01	0.2	0.2			Heavy rust-colored scale on all surfaces	Clean; machine marks visible
786 A	24		10.4	0.9653	0.9691	0.9651	−0.2	1.57	0.01	0.1	0.1	2.1	0.004	0.1	0.1			Heavy rust-colored scale on all surfaces	Clean; machine marks visible
Zircaloy-2 Coupons																			
Z 1	2		9.9	0.7701	0.7750	0.7704	+0.3	1.40				2.1						Heavy rust-colored scale on all surfaces	Thin film on all surfaces; no machine marks visible
Z 3	3		10.7	0.7727	0.7785	0.7729	+0.2	1.40				2.1						Heavy rust-colored scale on all surfaces	Thin film on all surfaces; no machine marks visible
Z 5	8		18.6	0.7575	0.7636	0.7576	+0.1	1.40				2.1						Heavy rust-colored scale on all surfaces	Thin film on all surfaces
Z 12	11		34.0	0.7593	0.7653			1.40				2.1						Heavy rust-colored scale on all surfaces	
Z 13	14		42.5	0.7676	0.7727	0.7678	+0.2	1.40				2.1						Heavy rust-colored scale on all surfaces	Thin film on all surfaces
Z 15	15		47.8	0.7749	0.7795	0.7751	+0.2	1.40				2.1						Heavy rust-colored scale on all surfaces	Thin film on all surfaces
Z 16	20		16.1	0.7690	0.7734	0.7692	+0.2	1.40				2.1						Heavy rust-colored scale on all surfaces	Clean; machine marks visible
Z 17	23		11.5	0.7651	0.7701	0.7654	+0.3	1.40				2.1						Heavy rust-colored scale on all surfaces	

*Corrosion rates have been calculated both for the nominally exposed and the total specimen areas.

**Two corrosion rates are presented: one based on the total operation time of 630.3 hr and one based on the total radiation time of 536.8 hr (3 Mwhr of reactor time equivalent to 1 hr of total radiation time).

Table 37 (continued)

Sample No.	Position	Distance from Front of Core Holder to Center of Specimen (in.)	Flow Velocity at Leading Edge (fps)	Initial Weight (g)	As-Removed Weight (g)	Defilmed Weight (g)	Weight Change (mg)	Exposed Specimen Area (cm^2)	Corrosion Penetration (mils)	Corrosion Rate* (mpy) 630.3** (hr)	Corrosion Rate* (mpy) 536.8** (hr)	Total Specimen Area (cm^2)	Corrosion Penetration (mils)	Corrosion Rate* (mpy) 630.3** (hr)	Corrosion Rate* (mpy) 536.8** (hr)	Neutron Flux at 3 Mw (neutrons/ cm^2/sec $\times 10^{-12}$)	Power Density at 3 Mw (w/ml)	Surface Appearance: As Removed	Surface Appearance: After Defilming
Titanium (55AX) Coupons																			
T 0	1		9.2	0.5340	0.5379	0.5321	−1.9	1.57	0.11	1.5	1.7	2.1	0.08	1.1	1.3			Heavy rust-colored scale on all surfaces	Clean; slight stain on one side; no machine marks visible
T 1	6		14.4	0.5354	0.5412	0.5353	−0.1	1.40	0.006	0.1	0.1	2.1	0.004	0.1	0.1			Heavy rust-colored scale on all surfaces	Clean; machine marks visible
T 2	9		21.7	0.5384	0.5445	0.5383	−0.1	1.40	0.006	0.1	0.1	2.1	0.004	0.1	0.1			Heavy rust-colored scale on all surfaces	Slight stain on one side; machine marks visible
T 3	12		36.2	0.5379	0.5428			1.40				2.1						Heavy rust-colored scale on all surfaces	
T 4	16		34.1	0.5430	0.5472	0.5430	0.0	1.40	0.00	0.0	0.0	2.1	0.00	0.0	0.0			Heavy rust-colored scale on all surfaces	Clean
T 5	17		26.9	0.5364	0.5401	0.5363	−0.1	1.40	0.006	0.1	0.1	2.1	0.004	0.1	0.1			Heavy rust-colored scale on all surfaces	Clean
T 6	19		18.9	0.5422	0.5460	0.5422	0.0	1.40	0.00	0.0	0.0	2.1	0.00	0.0	0.0			Heavy rust-colored scale on all surfaces	Thin film on all surfaces
T 7	22		12.6	0.5348	0.5381	0.5346	−0.2	1.40	0.01	0.2	0.2	2.1	0.01	0.1	0.1			Heavy rust-colored scale on all surfaces	Thin film on all surfaces
Corrosion Sample Coupon Holders (Zircaloy-2)																			
Core Holder																			
Part A		3.00		76.0506	75.9368		−113.8	162.0	0.09	1.28	1.51	162.0	0.09	1.28	1.51	2.00	2.62		
Part B		3.00		77.0787	76.9449		−133.8									2.00	2.62		
In-Line Holder																			
Part A				96.9145	97.0823		+167.8	162.0				162.0							
Part B				94.6905	94.8652		+174.7												

*Corrosion rates have been calculated both for the nominally exposed and the total specimen areas.

**Two corrosion rates are presented: one based on the total operation time of 630.3 hr and one based on the total radiation time of 536.8 hr (3 Mwhr of reactor time equivalent to 1 hr of total radiation time).

Table 37 (continued)

Sample No.	Distance from Front of Core Holder to Center of Specimen (in.)	Initial Weight (g)	As-Removed Weight (g)	Defilmed Weight (g)	Weight Change (mg)	Exposed Specimen Area (cm^2)	Corrosion Penetration (mils)	Corrosion Rate* (mpy) 630.3** (hr)	Corrosion Rate* (mpy) 536.8** (hr)	Total Specimen Area (cm^2)	Corrosion Penetration (mils)	Corrosion Rate* (mpy) 630.3** (hr)	Corrosion Rate* (mpy) 536.8** (hr)	Strain (μin./in.)	Stress (psi)	Neutron Flux at 3 Mw (neutrons/cm^2/sec $\times 10^{-12}$)	Power Density at 3 Mw (w/ml)	Surface Appearance: As Removed	Surface Appearance: After Defilming
12 Stress-Corrosion Specimens																			
Type 347 Stainless Steel Specimens																			
SS 11	2.81	10.0773	10.0574	10.0436	−33.7	19.50	0.09	1.2	1.4	19.6	0.08	1.1	1.3	925	26,800	2.05	2.65	Thin brown scale on all surfaces; machine marks visible	Thin dark film on all surfaces
SS 12	2.81	10.1441	10.1159	10.1086	−35.5	19.50	0.09	1.2	1.4	19.6	0.09	1.2	1.4	915	26,500	2.05	2.65	Thin brown scale on all surfaces; machine marks visible	Thin dark film on all surfaces
SS 13	2.81	10.3518	10.3275	10.3257	−26.1	19.50	0.07	0.9	1.1	19.6	0.06	0.9	1.0	890	25,800	2.05	2.65	Thin brown scale on all surfaces; machine marks visible	Thin dark film on all surfaces
SS 14	2.81	10.0643	10.0416	10.0337	−30.6	19.50	0.08	1.1	1.3	19.6	0.08	1.0	1.2	945	27,400	2.05	2.65	Thin brown scale on all surfaces; machine marks visible	Thin dark film on all surfaces
Zircaloy-2 Specimens																			
Zr 2	2.81	8.6034	8.5156	8.5103	−93.1	19.50	0.29	4.0	4.7	19.6	0.28	3.9	4.5	1600	22,400	2.05	2.65	Apparently film free; scale on low flux holder and bolt only	Very thin film on all surfaces
Zr 3	2.81	8.0402	7.9518	7.9462	−94.0	19.50	0.29	4.0	4.7	19.6	0.28	3.9	4.6	1740	24,400	2.05	2.65	Apparently film free; scale on low flux holder and bolt only	Very thin film on all surfaces
Zr 4	2.81	8.4533	8.3805	8.3769	−76.4	19.50	0.24	3.3	3.8	19.6	0.23	3.2	3.7	1440	20,200	2.05	2.65	Apparently film free; scale on low flux holder and bolt only	Very thin film on all surfaces
Zr 5	2.81	7.9449	7.8722	7.8725	−72.4	19.50	0.23	3.1	3.6	19.6	0.22	3.0	3.5	1570	22,000	2.05	2.65	Apparently film free; scale on low flux holder and bolt only	Very thin film on all surfaces
Titanium Specimens (55AX)																			
Ti 1	2.81	5.8880	5.8920	5.8848	−3.2	19.50	0.01	0.2	0.2	19.6	0.01	0.2	0.2	1530	23,600	2.05	2.65	Some thin film on all surfaces; heavier at low flux end	Dark film on all surfaces; machine marks visible
Ti 2	2.81	5.8358	5.8374	5.8327	−3.1	19.50	0.01	0.2	0.2	19.6	0.01	0.2	0.2	1800	27,000	2.05	2.65	Some thin film on all surfaces; heavier at low flux end	Dark film on all surfaces; machine marks visible
Ti 11	2.81	5.8012	5.8029	5.7967	−4.5	19.50	0.02	0.3	0.3	19.6	0.02	0.3	0.3	1600	26,000	2.05	2.65	Some thin film on all surfaces; heavier at low flux end; dumbbell-shaped discoloration at fulcrum	Ski-shaped curve at low flux end; thin dark scale on all surfaces
Ti 12	2.81	5.9638	5.9647	5.9600	−3.8	19.50	0.02	0.2	0.3	19.6	0.02	0.2	0.3	1600	26,000	2.05	2.65	Some thin film on all surfaces; heavier at low flux end; dumbbell-shaped discoloration at fulcrum	Spotty thin dark scale; machine marks visible
Type 347 Stainless Steel Stress-Corrosion Specimen Holders																			
SS 1	0.75	11.2366	11.1740	11.1804	−56.2	10.00	0.28	3.8	4.5	19.6	0.28	3.8	4.5			3.50	4.52	Thin brown scale on all surfaces; machine marks visible	Some scale around bolt hole; machine marks visible
SS 2	4.75	11.1590	11.1629	11.1652	+6.2	10.00				19.6						1.10	1.42	Thin brown scale on all surfaces; machine marks visible	Some scale around bolt hole; machine marks visible
SS 3	0.75	11.1584	11.0987	11.0967	−61.7	10.00	0.30	4.2	4.9	19.6	0.30	4.2	4.9			3.50	4.52	Thin brown scale on all surfaces; machine marks visible	Some scale around bolt hole; machine marks visible
SS 4	4.75	11.2191	11.2245	11.2194	+0.3	10.00				19.6						1.10	1.42	Thin brown scale on all surfaces; machine marks visible	Some scale around bolt hole; machine marks visible

*Corrosion rates have been calculated both for the nominally exposed and the total specimen areas.

**Two corrosion rates are presented: one based on the total operation time of 630.3 hr and one based on the total radiation time of 536.8 hr (3 Mwhr of reactor time equivalent to 1 hr of total radiation time).

Table 37 (continued)

Sample No.	Distance from Front of Core Holder to Center of Specimen (in.)	Initial Weight (g)	As-Removed Weight (g)	Defilmed Weight (g)	Weight Change (mg)	Exposed Specimen Area (cm^2)	Corrosion Penetration (mils)	Corrosion Rate* (mpy) 630.3** (hr)	Corrosion Rate* (mpy) 536.8** (hr)	Total Specimen Area (cm^2)	Corrosion Penetration (mils)	Corrosion Rate* (mpy) 630.3** (hr)	Corrosion Rate* (mpy) 536.8** (hr)	Strain (μin./in.)	Stress (psi)	Neutron Flux at 3 Mw (neutrons/cm^2/sec $\times 10^{-12}$)	Power Density at 3 Mw (w/ml)	Surface Appearance: As Removed	Surface Appearance: After Defilming
Zircaloy-2 Stress-Corrosion Specimen Holders																			
Zr 1	0.75	9.4307				10.00				19.6						3.50	4.52	Apparently film free; scale on low flux holder and bolt only	Not defilmed
Zr 2	4.75	8.9833				10.00				19.6						1.10	1.42	Apparently film free; scale on low flux holder and bolt only	Not defilmed
Zr 3	0.75	9.0925	9.0716	9.0608	−31.7	10.00	0.19	2.6	3.1	19.6	0.19	2.6	3.1			3.50	4.52	Apparently film free; scale on low flux holder and bolt only	Thin film on all surfaces; machine marks visible
Zr 4	4.75	8.8223	8.8186	8.8109	−11.4	10.00	0.07	1.0	1.1	19.6	0.07	1.0	1.1			1.10	1.42	Apparently film free; scale on low flux holder and bolt only	Thin film on all surfaces; machine marks visible
Titanium Stress-Corrosion Specimen Holders (55AX)																			
Ti 1	0.75	6.5626	6.5621	6.5591	−3.5	10.00	0.03	0.4	0.5	19.6	0.03	0.4	0.5			3.50	4.52	Some thin film on all surfaces; heavier at low flux end	Beveled edges rough; flat surfaces clean
Ti 2	4.75	6.6108	6.6145	6.6103	−0.5	10.00	0.01	0.1	0.1	19.6	0.004	0.1	0.1			1.10	1.42	Some thin film on all surfaces; heavier at low flux end	Beveled edges rough; flat surfaces clean; some film around hole
Ti 3	0.75	6.4948	6.4919	6.4907	−4.1	10.00	0.04	0.5	0.6	19.6	0.04	0.5	0.6			3.50	4.52	Some thin film on all surfaces; heavier at low flux end; dumbbell-shaped discoloration at fulcrum	Beveled edges rough; flat surfaces clean; some film around hole
Ti 8	4.75	6.4321	6.4362	6.4320	−0.1	10.00	0.001	0.01	0.02	19.6	0.001	0.01	0.02			1.10	1.42	Some thin film on all surfaces; heavier at low flux end; dumbbell-shaped discoloration at fulcrum	Beveled edges rough; flat surfaces clean; some film around hole

*Corrosion rates have been calculated both for the nominally exposed and the total specimen areas.

**Two corrosion rates are presented: one based on the total operation time of 630.3 hr and one based on the total radiation time of 536.8 hr (3 Mwhr of reactor time equivalent to 1 hr of total radiation time).

Table 38. Corrosion Data for Zircaloy-2 Corrosion Specimens for Loop FF

Sample Number	Position	Exposed Coupon Area (cm^2)	Flow Velocity at Leading Edge (fps)	Initial Weight (g)	As-Removed Weight (g)	Defilmed Weight (g)	Weight Change (mg)	Corrosion Penetration (mils)	Corrosion Rate[a] (mpy) 696 hr	Corrosion Rate[a] (mpy) 467 hr	Neutron Flux at 3 Mw (neutrons cm^{-2} sec^{-1})	Power Density (w/ml)	Surface Appearance, As-Removed	Surface Appearance After Defilming
Core Coupons														
											$\times 10^{12}$			
923A	A	3.00	9.7	1.5679	1.5594	1.5590	−8.9	0.18	2.27	3.36	2.77	3.66	All surfaces have fibrous texture	All surfaces have fibrous texture; little change
924A	B	2.80	11.3	1.5759	1.5686	1.5678	−8.1	0.18	2.21	3.27	2.46	3.26	All surfaces deeply etched; one corner scratched	Fine texture or deeply etched; one corner scratched
925A	C	2.80	13.7	1.5710	1.5630	1.5628	−8.2	0.18	2.24	3.32	2.18	2.88	All surfaces deeply etched	Fine texture or deeply etched
926A	D	2.80	17.1	1.5731	1.5658	1.5656	−7.5	0.16	2.05	3.04	1.93	2.54	All surfaces deeply etched	Fine texture or deeply etched
927A	E	2.80	22.9	1.5796	1.5731	1.5729	−6.7	0.14	1.83	2.71	1.66	2.20	All surfaces deeply etched	Fine texture or deeply etched
928A	F	2.80	35.8	1.5822	1.5772	1.5769	−5.3	0.11	1.45	2.15	1.39	1.83	All surfaces stained	Fine texture or deeply etched
929A	G	2.80	41.5	1.5778	1.5730	1.5730	−4.8	0.10	1.31	1.94	1.18	1.56	Some film	Fine texture or deeply etched; machine marks visible
930A	H	2.80	50.5	1.5720	1.5678	1.5677	−4.3	0.09	1.17	1.73	1.11	1.46	Some film	Fine texture or deeply etched; machine marks visible
931A	I	2.80	28.2	1.5654	1.5619	1.5614	−4.0	0.09	1.09	1.62	0.91	1.20	All surfaces covered with film	Fine texture or deeply etched; machine marks visible
932A	J	2.80	19.9	1.5735	1.5722	1.5701	−3.4	0.07	0.93	1.38	0.83	1.09	All surfaces covered with film; some scale	Fine texture or deeply etched; some scale remaining
933A	K	2.80	15.2	1.5717	1.5686	1.5683	−3.4	0.07	0.93	1.38	0.66	0.87	All surfaces covered with scale	Fine texture or deeply etched; some scale remaining
934A	L	3.00	12.1	1.5657	1.5640	1.5631	−2.6	0.05	0.66	0.98	0.53	0.69	All surfaces covered with scale	Fine texture or deeply etched
In-Line Coupons														
911A	A	3.00	9.7	1.5625	1.5756	1.5644	+1.9						Rusty scale covered all surfaces	Thin adherent film on all surfaces; some scale along edges; machine marks visible
912A	B	2.80	11.3	1.5750	1.5906	1.5758	+0.8						Rusty scale covered all surfaces	Thin adherent film on all surfaces; some scale along edges; machine marks visible
913A	C	2.80	13.7	1.5734	1.5871	1.5782	+4.8						As above but flaked	As above; flake film spots and small arc burn
914A	D	2.80	17.1	1.5747	1.5886	1.5778	+3.1						As above but flaked	As above; flake film spots and small arc burn
915A	E	2.80	22.9	1.5741	1.5864	1.5792	+5.1						As above but flaked	Black film covered with scale flakes
916A	F	2.80	35.8	1.5774	1.5896	1.5780	+0.6						As above but flaked	Thin adherent film on all surfaces; some scale along edges; machine marks visible
917A	G	2.80	41.5	1.5604	1.5722	1.5617	+1.3						As above but flaked	Thin adherent film on all surfaces; some scale along edges; machine marks visible
918A	H	2.80	50.5	1.5730	1.5864	1.5759	+2.9						As above but flaked	Thin adherent film on all surfaces; some scale along edges; machine marks visible
919A	I	2.80	28.2	1.5748	1.5878	1.5775	+2.7						As above but flaked	Thin adherent film on all surfaces; some scale along edges; machine marks visible
920A	J	2.80	19.9	1.5673	1.5811	1.5696	+2.3						As above but flaked	Thin adherent film on all surfaces; some scale along edges; machine marks visible
921A	K	2.80	15.2	1.5634	1.5767	1.5650	+1.6						As above but flaked	Thin adherent film on all surfaces; some scale along edges; machine marks visible
922A	L	3.00	12.1	1.5857	1.6000	1.5894	+3.7						As above but flaked	Thin adherent film on all surfaces; some scale along edges; machine marks visible
Zircaloy-2 Core-Channel coupon holder														
9A		~160		80.8213	80.7517		69.6	0.055	0.7	10	1.49	1.97		
9B				82.3982	82.3216		76.6							
Zircaloy-2 In-line–channel coupon holder														
8A		~160		96.1826	96.5330		+350.4							
8B				94.6605	94.9845		+324.0							

[a]Two corrosion rates are presented: one based on the total-operation time of 696 hr and the other based on the total radiation time of 467 hr (3 Mwhr of reactor time equivalent to 1 hr of total radiation time).

Table 39. Corrosion Data for Zircaloy-2 Corrosion Specimens for Loop GG

Sample Number	Position	Exposed Coupon Area (cm^2)	Flow Velocity at Leading Edge (fps)	Initial Weight (g)	As-Removed Weight (g)	Defilmed Weight (g)	Weight Change (mg)	Corrosion Penetration (mil)	Corrosion Rate[a] (mpy) 1064 hr	Corrosion Rate[a] (mpy) 897 hr	Neutron Flux at 3 Mw (neutrons cm^{-2} sec^{-1})	Power Density (w/ml)	Surface Appearance, As-Removed	Surface Appearance, After Defilming
Core Coupons														
											$\times 10^{12}$			
947A	A	3.00	10.7	1.5730	1.5564	1.5561	−16.9	0.341	2.80	3.32	3.62	4.83	Etched surface covered with thin flaky scale	Dull etched appearance
948A	B	2.80	12.5	1.5691	1.5532	1.5526	−16.5	0.357	2.93	3.48	3.34	4.45	Etched surface covered with thin flaky scale	Dull etched appearance
949A	C	2.80	15.1	1.5723	1.5570	1.5562	−16.1	0.348	2.86	3.39	3.05	4.07	Etched surface covered with thin flaky scale	Dull etched appearance
950A	D	2.80	18.9	1.5750	1.5609	1.5600	−15.0	0.324	2.66	3.15	2.55	3.40	Etched surface covered with thin flaky scale	Dull etched appearance
951A	E	2.80	25.3	1.5735	1.5604	1.5594	−14.1	0.305	2.50	2.97	2.29	3.05	Lightly etched surface covered with thin flaky scale	Dull lightly etched appearance
952A	F	2.80	39.5	1.5724	1.5601	1.5594	−13.0	0.281	2.31	2.74	2.17	2.89	Lightly etched surface covered with thin flaky scale	Dull lightly etched appearance
953A	G	2.80	45.8	1.5576	1.5472	1.5458	−11.8	0.255	2.09	2.48	1.88	2.51	Faint machine marks in areas where scale has not been retained	Faint machine marks; lightly etched appearance; some very thin film visible
954A	H	2.80	55.7	1.5778	1.5694	1.5668	−11.0	0.238	1.95	2.32	1.60	2.13	Heavy flaky scale; machine marks visible	Faint machine marks; lightly etched appearance; some very thin film visible
955A	I	2.80	31.1	1.5582	1.5492	1.5476	−10.6	0.229	1.88	2.23	1.40	1.87	Some scale along clamping edges; machine marks visible	Faint machine marks; very lightly etched appearance
956A	J	2.80	22.0	1.5804	1.5720	1.5719	−8.5	0.184	1.51	1.79	1.25	1.67	Thin scale on all surfaces	Machine marks visible
957A	K	2.80	16.8	1.5810	1.5735	1.5717	−9.3	0.201	1.65	1.96	1.12	1.50	Scale on all surfaces	Machine marks visible
958A	L	2.80	13.4	1.5726	1.5658	1.5648	−7.8	0.157	1.29	1.53	1.00	1.33	Thin scale on all surfaces	Machine marks visible
In-Line Coupons														
935A	A	3.00	10.7	1.5733	1.6035	1.5744	+1.1						All surfaces covered with a heavy brown rustlike scale	Film on all surfaces; some scale retained particularly along edges
936A	B	2.80	12.5	1.5820	1.6080	1.5837	+1.7						All surfaces covered with a heavy brown rustlike scale	Film on all surfaces; some scale retained particularly along edges
937A	C	2.80	15.1	1.5800	1.6034	1.5814	+1.4						All surfaces covered with a heavy brown rustlike scale	Film on all surfaces; some scale retained particularly along edges
938A	D	2.80	18.9	1.5760	1.5982	1.5780	+2.0						All surfaces covered with a heavy brown rustlike scale	Film on all surfaces; some scale retained particularly along edges
939A	E	2.80	25.3	1.5817	1.6013	1.5840	+2.3						All surfaces covered with a heavy brown rustlike scale	Film on all surfaces; some scale retained particularly along edges
940A	F	2.80	39.5	1.5800	1.5996	1.5818	+1.8						All surfaces covered with a heavy brown rustlike scale	Film on all surfaces; some scale retained particularly along edges
941A	G	2.80	45.8	1.5842	1.6010	1.5858	+1.6						All surfaces covered with a heavy brown rustlike scale	Film on all surfaces; some scale retained particularly along edges
942A	H	2.80	55.7	1.5735	1.5928	1.5755	+2.0						All surfaces covered with a heavy brown rustlike scale	Film on all surfaces; some scale retained particularly along edges
943A	I	2.80	31.1	1.5737	1.5923	1.5756	+1.9						All surfaces covered with a heavy brown rustlike scale	Film on all surfaces; some scale retained particularly along edges
944A	J	2.80	22.0	1.5843	1.5985	1.5829	−1.4	0.030	0.25	0.29			All surfaces covered with a heavy brown rustlike scale	Film on all surfaces; some scale retained particularly along edges
945A	K	2.80	16.8	1.5573	1.5708	1.5548	−2.5	0.054	0.44	0.53			All surfaces covered with a heavy brown rustlike scale	Film on all surfaces; some scale retained particularly along edges
946A	L	3.00	13.4	1.5787	1.6004	1.5790	+0.3						All surfaces covered with a heavy brown rustlike scale	Film on all surfaces; some scale retained particularly along edges
Zircaloy-2 Core-channel coupon holder No. 17														
	A	160		82.5112	82.2520		−259.2	0.24	1.95	2.32	2.06	2.75		
	B			80.5849	80.2151		−369.8							
Zircaloy-2 In-line–channel coupon holder No. 16														
	A	160		93.8427	94.1495		+306.8							
	B			94.8266	95.0172		+190.6							

[a]Two corrosion rates are presented: one based on the total operation time of 1064 hr and the other based on the total radiation of 897 hr (3 Mwhr of reactor time equivalent to 1 hr of total radiation time).

Table 40. Data for Corrosion Specimens for Loop L-4-12

Sample Number	Position	Average Fluid Velocity Across Specimen (fps)	Weight Data: Initial (g)	Weight Data: As Removed (g)	Weight Data: Defilmed (g)	Weight Data: Change (mg)	Exposed Sample Area (cm^2)	Corrosion Penetration (mils)	Corrosion Rate[a] (Exposed Area) (mpy): 2020 hr	Corrosion Rate[a] (Exposed Area) (mpy): 1459 hr	Total Area (cm^2)	Corrosion Penetration (mils)	Corrosion Rate[a] (Total Area) (mpy): 2020 hr	Corrosion Rate[a] (Total Area) (mpy): 1459 hr	Distance from Front of First Core Coupon to Center of Specimen (in.)	Neutron Flux at Specimen Locations at 3 Mw (neutrons cm^{-2} sec^{-1})	Power Density at Specimen Locations at 3 Mw (w/ml)	Corrected[b] Corrosion Rate (mpy)	Strain (μ in./in.)	Stress (psi)	Remarks on Surface Appearance: As-Removed Surface	Remarks on Surface Appearance: Defilmed Surface
24 Core coupon specimens																$\times 10^{12}$						
Stainless steel, type 347																						
987-A	4	12.1	0.9450				1.40				2.1			>186	0.88	2.95	4.08					
988-A	5	13.4	0.9590				1.40				2.1			>186	1.13	2.64	3.65					
990-A	7	16.9	0.9494				1.40				2.1			>186	1.63	2.30	3.18					
991-A	10	29.4	0.9545	0.9410	0.9382	−16.3	1.40	0.57	2.5	3.4	2.1	0.38	1.7	2.3	2.38	1.83	2.53				Heavy rough dark scale over all surfaces	Central or unclamped portion of coupon roughened; some very thin film retained
992-A	13	40.1	0.9486	0.9466	0.9449	−3.7	1.40	0.13	0.6	0.8	2.1	0.09	0.4	0.5	3.13	1.49	2.06				Heavy rough dark scale over all surfaces	Machine marks visible on all surfaces; some very thin film retained
993-A	18	20.3	0.9478	0.9486	0.9471	−0.7	1.40	0.03	0.1	0.2	2.1	0.02	0.1	0.1	4.38	1.02	1.41				Heavy rough dark scale over all surfaces	Machine marks visible on all surfaces; some very thin film retained
995-A	21	13.3	0.9512	0.9522	0.9508	−0.4	1.40	0.01	0.1	0.1	2.1	0.01	0.04	0.1	5.13	0.82	1.13				Heavy rough dark scale over all surfaces	Machine marks visible on all surfaces; some stain retained
996-A	24	9.9	0.9617	0.9628	0.9610	−0.7	1.57	0.02	0.1	0.1	2.1	0.02	0.1	0.1	5.88	0.66	0.91				Heavy rough dark scale over all surfaces	Machine marks visible on all surfaces
Zircaloy-2																						
Z-88	2	10.1	0.7924	0.7782	0.7782	−14.2	1.40	0.61	2.7	3.7	2.1	0.41	1.8	2.5	0.38	3.30	4.56	3.63			Thin gray film with overlying interference colors	Lightly etched surface with faint machine marks and some very thin film retained
Z-89	3	11.0	0.7908	0.7773	0.7770	−13.8	1.40	0.60	2.6	3.6	2.1	0.40	1.7	2.4	0.63	3.05	4.22	3.52			Thin gray film with overlying interference colors	Lightly etched surface with faint machine marks and some very thin film retained
Z-90	8	19.8	0.7944	0.7843	0.7841	−10.3	1.40	0.45	1.9	2.7	2.1	0.30	1.3	1.8	1.88	2.12	2.93	2.65			Thin gray film with overlying interference colors	Lightly etched surface with faint machine marks and some very thin film retained
Z-91	11	34.5	0.7926	0.7843	0.7841	−8.5	1.40	0.37	1.6	2.2	2.1	0.25	1.1	1.5	2.63	1.71	2.36	2.18			Thin gray film with overlying interference colors	Lightly etched surface with faint machine marks and some very thin film retained
Z-92	14	44.4	0.7894	0.7827	0.7823	−7.1	1.40	0.31	1.3	1.8	2.1	0.21	0.9	1.2	3.38	1.38	1.91	1.83			Thin gray film with overlying interference colors	Slightly etched surface with machine marks and some very thin film retained
Z-93	15	40.2	0.7938	0.7874	0.7872	−5.6	1.40	0.24	1.1	1.5	2.1	0.16	0.7	1.0	3.63	1.28	1.77	1.44			Thin gray film with overlying interference colors	Slightly etched surface with faint machine marks and some very thin film retained
Z-94	20	15.0	0.7924	0.7881	0.7877	−4.7	1.40	0.20	0.9	1.2	2.1	0.14	0.6	0.8	4.88	0.88	1.22	1.22			Thin gray film with overlying thin rustlike deposit	Slightly etched surface with a thin film retained
Z-95	23	10.8	0.7749	0.7713	0.7713	−3.6	1.40	0.16	0.7	0.9	2.1	0.11	0.5	0.6	5.63	0.71	0.98	0.93			Thin gray film with overlying thin rustlike deposit	Slightly etched surface with a thin film retained
Titanium-55AX																						
Ti-100	1	9.4	0.5387	0.5372	0.5366	−2.1	1.57	0.12	0.5	0.7	2.1	0.09	0.4	0.5	0.13	3.50	4.84				Brass-colored film with visible machine marks	Thin film retained showing very light interference colors
Ti-101	6	14.9	0.5372	0.5358	0.5336	−3.6	1.40	0.22	1.0	1.3	2.1	0.15	0.6	0.9	1.38	2.47	3.42				Brass-colored film with visible machine marks	Thin film retained showing very light interference colors
Ti-102	9	23.4	0.5335	0.5327	0.5327	−0.8	1.40	0.05	0.2	0.3	2.1	0.03	0.1	0.2	2.13	1.99	2.75				Brass-colored film with visible machine marks	Thin film retained showing very light interference colors
Ti-103	12	37.0	0.5311	0.5303	0.5302	−0.9	1.40	0.06	0.2	0.3	2.1	0.04	0.2	0.2	2.88	1.60	2.21				Brass-colored film with visible machine marks	Thin film retained showing very light interference colors
Ti-104	16	30.0	0.5359	0.5351	0.5350	−0.9	1.40	0.06	0.2	0.3	2.1	0.04	0.2	0.2	3.88	1.19	1.65				Brass-colored film with visible machine marks	Thin film retained together with some brown staining
Ti-105	17	24.1	0.5297	0.5292	0.5291	−0.6	1.40	0.04	0.2	0.2	2.1	0.03	0.1	0.2	4.13	1.10	1.52				Brass-colored film with visible machine marks	Thin film retained showing very light interference colors
Ti-106	19	17.2	0.5351	0.5348	0.5345	−0.6	1.40	0.04	0.2	0.2	2.1	0.03	0.1	0.2	4.63	0.96	1.33				Brass-colored film with visible machine marks	Thin film retained together with some brown staining
Ti-107	22	11.9	0.5226	0.5226	0.5225	−0.1	1.40	0.01	0.03	0.04	2.1	0.01	0.02	0.03	5.38	0.76	1.05				Brass-colored film with visible machine marks	Thin film retained showing very light interference colors
4 Core stress specimens and holders																						
Titanium (6% Al, 4% V) specimens																						
TJ-11	C		5.4209	5.3935	5.3918	−29.1	19.5	0.13	0.6	0.8	20.0	0.13	0.5	0.8	2.69	1.75[c]	2.42		5680	90,900	Thin gray film over slightly roughened surface with overlying interference colors	Apparently clean lightly etched surfaces with visible machine marks
TJ-12	C		5.5062	5.4827	5.4801	−26.1	19.5	0.12	0.5	0.7	20.0	0.11	0.5	0.7	2.69	1.75[c]	2.42		5600	89,600	Thin gray film over slightly roughened surface with overlying interference colors	Apparently clean lightly etched surfaces with visible machine marks
TJ-13	G		5.6062	5.5786	5.5786	−29.4	19.5	0.13	0.6	0.8	20.0	0.13	0.6	0.8	2.69	1.75[c]	2.42		5740	91,800	Thin gray film over slightly roughened surface with overlying interference colors	Apparently clean lightly etched surfaces with visible machine marks
TJ-14	G		5.3879	5.3639	5.3627	−25.2	19.5	0.11	0.5	0.7	20.0	0.11	0.5	0.7	2.69	1.75[c]	2.42		5010	80,100	Thin gray film over slightly roughened surface with overlying interference colors	Apparently clean lightly etched surfaces with visible machine marks
Type 347 stainless steel holders																						
SS-27	C		10.2506	10.2456	10.2346	−16.0	10.0	0.08	0.3	0.5	10.0	0.08	0.3	0.5	3.99	1.15	1.59		5600	89,600	Dark rustlike scale over all surfaces	Some stain retained on all surfaces; machine marks visible
SS-28	G		10.2336	10.2237	10.2103	−23.3	10.0	0.11	0.5	0.9	10.0	0.11	0.5	0.7	3.99	1.15	1.59		5010	80,100	Dark rustlike scale over all surfaces	Some stain retained on all surfaces; machine marks visible
Zircaloy-2 holders																						
Z-21	C		8.5898				10.0				10.0				1.00	2.77	3.83		5680	90,900		
Z-22	G		8.7667				10.0				10.0				1.00	2.77	3.83		5740	91,800		
6 Core impact speimens																						
Zircaloy-2																						
795	A		19.0347	18.8909		−143.8	24.9	0.35	1.5	2.1	26.7	0.33	1.4	2.0	2.69	1.78[c]	2.46				Film showing interference colors over all surfaces	
796	D		18.9677	18.8433		−124.4	24.9	0.30	1.3	1.8	26.7	0.28	1.2	1.7	2.69	1.78[c]	2.46				Film showing interference colors over all surfaces	
797	F		18.8310	18.7107		−120.3	24.9	0.29	1.3	1.8	26.7	0.27	1.2	1.6	2.69	1.78[c]	2.46				Film showing interference colors over all surfaces	

Table 40 (continued)

Sample Number	Position	Average Fluid Velocity Across Specimen (fps)	Weight Data: Initial (g)	Weight Data: As Removed (g)	Weight Data: Defilmed (g)	Weight Data: Change (mg)	Exposed Sample Area (cm^2)	Corrosion Penetration (mils)	Corrosion Rate[a] (Exposed Area) (mpy): 2020 hr	Corrosion Rate[a] (Exposed Area) (mpy): 1459 hr	Total Area (cm^2)	Corrosion Penetration (mils)	Corrosion Rate[a] (Total Area) (mpy): 2020 hr	Corrosion Rate[a] (Total Area) (mpy): 1459 hr	Distance from Front of First Core Coupon to Center of Specimen (in.)	Neutron Flux at Specimen Locations at 3 Mw (neutrons cm^{-2} sec^{-1})	Power Density at Specimen Locations at 3 Mw (w/ml)	Corrected[b] Corrosion Rate (mpy)	Strain (μ in./in.)	Stress (psi)	Remarks on Surface Appearance: As-Removed Surface	Remarks on Surface Appearance: Defilmed Surface
																$\times 10^{12}$						
Titanium RC-A-40																						
805	B		13.0082	12.9959		−12.3	24.9	0.04	0.2	0.3	26.7	0.04	0.2	0.3	2.69	1.78[c]	2.46				Brass-colored film over all surfaces with a scattered dusting of scale	
806	E		13.1030	13.0916		−11.4	24.9	0.04	0.2	0.3	26.7	0.04	0.2	0.3	2.69	1.78[c]	2.46				Brass-colored film over all surfaces with a scattered dusting of scale	
807	H		13.0055	12.9930		−12.5	24.9	0.05	0.2	0.3	26.7	0.04	0.2	0.3	2.69	1.78[c]	2.46				Brass-colored film over all surfaces with a scattered dusting of scale	
24 In-line coupon specimens																						
Stainless steel, type 347																						
1117-A	4	12.1	0.9619	0.9638	0.9609	−1.0	1.40	0.04	0.2	0.2	2.1	0.02	0.1	0.1							Heavy rustlike scale over all surfaces	Machine marks visible; some stain retained
1121-A	5	13.4	0.9582	0.9600	0.9570	−1.2	1.40	0.04	0.2	0.3	2.1	0.03	0.1	0.2							Heavy rustlike scale over all surfaces	Machine marks visible; some stain retained
1122-A	7	16.9	0.9435	0.9457	0.9430	−0.5	1.40	0.02	0.1	0.1	2.1	0.01	0.1	0.1							Heavy rustlike scale over all surfaces	Machine marks visible; some stain retained
1123-A	10	29.4	0.9500	0.9521	0.9498	−0.2	1.40	0.01	0.03	0.04	2.1	0.01	0.02	0.03							Heavy rustlike scale over all surfaces	Machine marks visible; some stain retained along with few spots of scale
1125-A[d]	13	40.1	1.0188	0.4120	0.4094	−609.4	1.40	20.14	87.1	120.6	2.1	13.43	58.1	80.4							Heavy rustlike scale over heavily corroded surfaces	Tight black scale retained in all but one spot (did not attempt further defilming)
1126-A[e]	18	20.3	0.9522	0.8474	0.8447	−107.5	1.40	3.77	16.3	22.6	2.1	2.51	10.9	15.1							Heavy loose-like scale over all surfaces	Machine marks visible on exposed surfaces; some attack along edges
1127-A[f]	21	13.3	0.9578				1.40				2.1											
1128-A[e]	24	9.9	0.9681	0.9632	0.9612	−6.9	1.57	0.22	0.9	1.3	2.1	0.16	0.7	1.0							Heavy rustlike scale over all surfaces	Machine marks visible on exposed surfaces; some stain retained on clamping edges
Zircaloy-2																						
Z-96	2	10.1	0.7902	0.7924	0.7902	0.0	1.40	0.00	0.0	0.0	2.1	0.00	0.0	0.0							Heavy rustlike scale over all surfaces	Machine marks visible; scattered spots of scale retained on all surfaces
Z-97	3	11.0	0.7841	0.7868	0.7842	+0.1	1.40														Heavy rustlike scale over all surfaces	Machine marks visible; scattered spots of scale retained on all surfaces
Z-98	8	19.8	0.7848	0.7880	0.7857	+0.9	1.40														Heavy rustlike scale over all surfaces	Machine marks visible; scattered spots of scale retained on all surfaces
Z-99	11	34.5	0.7920	0.7943	0.7924	+0.4	1.40														Heavy rustlike scale over all surfaces	Machine marks visible; scattered spots of scale retained on all surfaces
Z-100	14	44.4	0.8000	0.8021	0.8006	+0.6	1.40														Heavy rustlike scale over all surfaces	Machine marks visible; scattered spots of scale retained on all surfaces
Z-101	15	40.2	0.7897	0.7920	0.7902	+0.5	1.40														Heavy rusrlike scale over all surfaces	Machine marks visible; scattered spots of scale retained on all surfaces
Z-102[f]	20	15.0	0.7965				1.40															
Z-103[f]	23	10.8	0.7956				1.40															
Titanium-55AX																						
Ti-108	1	9.4	0.5361	0.5377	0.5358	−0.3	1.57	0.02	0.1	0.1	2.1	0.02	0.1	0.1							Thin rustlike scale over all surfaces	Machine marks visible; some film retained producing interference colors
Ti-110	6	14.9	0.5346	0.5367	0.5343	−0.3	1.40	0.02	0.1	0.1	2.1	0.01	0.1	0.1							Thin rustlike scale over all surfaces	Machine marks visible; some film retained producing interference colors
Ti-111	9	23.4	0.5328	0.5351	0.5326	−0.2	1.40	0.01	0.1	0.1	2.1	0.01	0.04	0.1							Thin rustlike scale over all surfaces	Machine marks visible; some film retained producing interference colors
Ti-112	12	37.0	0.5305	0.5347	0.5301	−0.1	1.40	0.01	0.03	0.04	2.1	0.01	0.02	0.03							Thin rustlike scale over all surfaces	Machine marks visible; some film retained producing interference colors
Ti-113	16	30.0	0.5350	0.5368	0.5348	−0.2	1.40	0.01	0.1	0.1	2.1	0.01	0.04	0.1							Thin rustlike scale over all surfaces	Machine marks visible; some film retained producing interference colors
Ti-114	17	24.1	0.5410	0.5429	0.5406	−0.4	1.40	0.03	0.1	0.2	2.1	0.02	0.1	0.1							Thin rustlike scale over all surfaces	Machine marks visible; some film retained producing interference colors
Ti-116[f]	19	17.2	0.5363				1.40				2.1											
Ti-118[f]	22	11.9	0.5369				1.40				2.1											
4 In-line stress specimens and holders																						
Titanium (6% Al, 4% V) specimens																						
TJ-7	D		5.3598	5.3760	5.3543	−5.5	19.5	0.02	0.1	0.1	20.0	0.02	0.1	0.1					5065	81,100	Heavy rustlike scale over all surfaces	Machine marks visible; some film stain retained on all surfaces with some brown stain and scale
TJ-8	D		5.6125	5.6321	5.6062	−6.3	19.5	0.03	0.1	0.2	20.0	0.03	0.1	0.2					5995	95,900	Heavy rustlike scale flaked off in spots	Machine marks visible; some film stain retained on all surfaces
TJ-9	A		4.9762	4.9944	4.9713	−4.9	19.5	0.02	0.1	0.1	20.0	0.02	0.1	0.1					5560	88,900	Heavy rustlike scale over all surfaces	Machine marks visible; some film stain retained on all surfaces
TJ-10	A		5.5645	5.5822	5.5616	−2.9	19.5	0.02	0.1	0.1	20.0	0.02	0.1	0.1					5385	86,200	Heavy rustlike scale over all surfaces	Machine marks visible; some film stain retained on all surfaces with some brown stain and scale

Table 40 (continued)

Sample Number	Position	Average Fluid Velocity Across Specimen (fps)	Weight Data: Initial (g)	Weight Data: As Removed (g)	Weight Data: Defilmed (g)	Weight Data: Change (mg)	Exposed Sample Area (cm^2)	Corrosion Penetration (mils)	Corrosion Rate[a] (Exposed Area) (mpy): 2020 hr	Corrosion Rate[a] (Exposed Area) (mpy): 1459 hr	Total Area (cm^2)	Corrosion Penetration (mils)	Corrosion Rate[a] (Total Area) (mpy): 2020 hr	Corrosion Rate[a] (Total Area) (mpy): 1459 hr	Distance from Front of First Core Coupon to Center of Specimen (in.)	Neutron Flux at Specimen Locations at 3 Mw (neutrons cm^{-2} sec^{-1})	Power Density at Specimen Locations at 3 Mw (w/ml)	Corrected[b] Corrosion Rate (mpy)	Strain (μ in./in.)	Stress (psi)	Remarks on Surface Appearance: As-Removed Surface	Remarks on Surface Appearance: Defilmed Surface
Stainless steel, type 347 holders																						
SS-25	D		10.4401	10.4512	10.4418	+1.7	10.0				10.0								5995	95,900	Heavy rustlike scale over all surfaces	Clean metallic surfaces with machine marks; some scale retained in crevices
SS-26	A		10.3263	10.3393	10.3252	−1.1	10.0	0.01	0.02	0.03	10.0	0.01	0.02	0.03					5385	86,200	Heavy rustlike scale over all surfaces	Clean metallic surfaces with machine marks; some scale retained in crevices
Zircaloy-2 holders																						
Z-19	D		8.6937	8.7150	8.6921	−1.6	10.0	0.01	0.04	0.1	10.0	0.01	0.04	0.1					5065	81,100	Heavy rustlike deposit on all surfaces	Thin adherent black film over all surfaces
Z-20	A		9.0502	9.0733	9.0517	+1.5	10.0				10.0								5560	88,900	Heavy rustlike deposit on all surfaces	Thin adherent black film over all surfaces
16 Pressurizer stress specimens and holders[g]																						
Stainless steel, type 17-4 PH specimens																						
SH-1	H		10.5196	10.7911	10.4705	−49.1	19.5	0.13	0.6	0.8	20.0	0.12	0.5	0.7					2750	79,700	Thick film on one side with heavy rustlike scale on the other	Some film retained with scattered spots of scale
SH-2	G		10.4630	10.5105	10.4273	−35.7	19.5	0.09	0.4	0.5	20.0	0.09	0.4	0.5					2750	79,700	Heavy rustlike scale on all surfaces	Some film retained with scattered spots of scale
SH-3	F		10.4724	10.5954	10.4710	−1.4	19.5	0.004	0.02	0.03	20.0	0.004	0.02	0.0					2550	73,900	Heavy rustlike scale on all surfaces	Some film retained with scattered spots of scale
SH-4	E		10.4754	10.4983	10.4663	−9.1	19.5	0.02	0.1	0.1	20.0	0.02	0.1	0.1					2700	78,300	Heavy rustlike scale on all surfaces	Some film retained with scattered spots of scale
Titanium (6% Al, 4% V) specimens																						
TJ-3	B		5.3617	5.3617	5.3623	+0.4	19.5				20.0								4875	78,000	Thick film on one side with heavy rustlike scale on the other	Dark-gray film retained on all surfaces
TJ-4	B		5.5618	5.5618	5.5553	−6.5	19.5	0.03	0.1	0.2	20.0	0.03	0.1	0.2					5365	85,800	Heavy rustlike scale on all surfaces except around holes	Light-gray film retained on all surfaces
TJ-5	A		5.4780	5.4853	5.4733	−4.7	19.5	0.02	0.1	0.1	20.0	0.02	0.1	0.1					5385	86,200	Light gray film on one side; interference colors on the other	Thin film with interference colors on all surfaces; some stain retained
TJ-6	A		5.3089	5.3122	5.2993	−9.6	19.5	0.04	0.2	0.3	20.0	0.04	0.2	0.3					5420	86,700	Light gray film on one side; interference colors on the other	Thin film with interference colors on all surfaces; some stain retained
TJ-1	F		*b*	5.7642	5.6316		19.5				20.0								3380	54,100	Uniform gray scale except around holes	Thin film with interference colors on all surfaces
TJ-2	E		*b*	6.0024	5.9952		19.5				20.0								3255	52,100	Heavy rustlike scale on all surfaces	Thin film with interference colors on all surfaces; some spots of scale retained
Titanium C-130AM specimens																						
TE-3	C		5.2465	5.2628	5.2436	−2.9	19.5	0.01	0.1	0.1	20.0	0.01	0.1	0.1					4465	71,500	Heavy brown scale apparently thicker in center	Thin film with interference colors; some stain retained
TE-4	C		5.3506	5.3552	5.3469	−3.7	19.5	0.02	0.1	0.1	20.0	0.02	0.1	0.1					4775	76,500	Gray film over all surfaces, thin around holes	Thin film with interference colors; some stain retained
TE-5	D		5.3475	5.3475	5.3465	−1.0	19.5	0.01	0.02	0.03	20.0	0.01	0.02	0.03					5040	80,600	Heavy rustlike scale over all surfaces	Thin film with interference colors; some stain retained
TE-6	D		5.3647	5.3647	5.3639	−0.8	19.5	0.004	0.02	0.03	20.0	0.004	0.02	0.03					5050	80,800	Heavy rustlike scale over all surfaces	Thin film with interference colors; some stain retained
TE-1	H		5.3692	5.6514	5.3420	−27.2	19.5	0.12	0.5	0.7	20.0	0.12	0.5	0.7					5490	87,800	Heavy rustlike scale over all surfaces	Light-gray film with overlying interference colors; some spots; scale retained
TE-2	G		5.5978	5.6007	5.5970	−0.8	19.5	0.004	0.02	0.03	20.0	0.04	0.02	0.03					4940	79,000	Thin gray film with interference colors on all surfaces	Light-gray film with overlying interference colors; some spots; scale retained
Stainless steel, type 347 holders																						
SS-23	B		10.4985	10.5379	10.4861	−12.4	10.0	0.06	0.3	0.4	10.0	0.06	0.3	0.3					5365	85,800	Heavy dark rustlike scale over all surfaces	Apparently clean surfaces with machine marks visible; some scattered spots of stain
SS-24	A		10.6260	10.6303	10.6213	−4.7	10.0	0.02	0.1	0.1	10.0	0.02	0.1	0.1					5420	86,700	Heavy dark rustlike scale over all surfaces	Apparently clean surfaces with machine marks visible; some scattered spots of stain
SS-21	F		10.5334	10.6022	10.4431	−90.3	10.0	0.44	1.9	2.7	10.0	0.44	1.9	2.7					2550	73,900	Heavy dark rustlike scale over all surfaces	Scattered spots of scale with machine marks; the threads were stripped in disassembly
SS-22	E		10.4101	10.4319	10.4065	−3.6	10.0	0.02	0.9	0.1	10.0	0.02	0.1	0.1					2700	78,300	Heavy dark rustlike scale over all surfaces	Apparently clean surfaces with machine marks visible; some stain
Zircaloy-2 holders																						
Z-17	B		8.5386	(screw broke in holder)			10.0				10.0								4875	78,000	Heavy dark scale over all surfaces	
Z-18	A		8.6846	8.6856	8.6827	−1.9	10.0	0.01	0.1	0.1	10.0	0.01	0.1	0.1					5385	86,200	Heavy dark scale over all surfaces	Thin black film retained on all surfaces
Z-23	F		9.1654	9.2248	9.1854	+20.0	10.0				10.0								3380	54,100	Heavy dark scale over all surfaces	Thin film on one side and heavy rustlike scale retained on the other
Z-24	E		8.9567	8.9831	8.9817	+25.0	10.0				10.0								3255	52,100	Heavy dark scale over all surfaces	Rustlike scale retained on all surfaces
Titanium RC-70 holders																						
Ti-20	C		5.4843	5.4882	5.4826	−1.7	10.0	0.02	0.1	0.1	10.0	0.02	0.1	0.1					4465	71,500	Heavy dark scale over all surfaces	Thin film retained on all surfaces; machine marks visible
Ti-41	C		6.1564	6.1601	6.1566	+0.2	10.0				10.0								4775	76,500	Heavy dark scale over all surfaces	Thin film retained on all surfaces; machine marks visible; some spots of scale
Ti-21	D		5.6535	5.6594	5.6510	−2.5	10.0	0.02	0.1	0.1	10.0	0.02	0.1	0.1					5040	80,600	Heavy dark scale over all surfaces	Thin film retained on all surfaces; machine marks visible; some spots of scale
Ti-22	D		5.8157	5.8526	5.8068	−8.9	10.0	0.08	0.4	0.5	10.0	0.08	0.3	0.5					5050	80,800	Heavy dark scale over all surfaces	Thin film retained on all surfaces; machine marks visible; some spots of scale
Ti-24	H		6.3991	6.5589	6.3943	−4.8	10.0	0.04	0.2	0.3	10.0	0.04	0.2	0.3					5490	87,800	Heavy rustlike scale except around screw hole	Machine marks visible; some film retained on all surfaces

Table 40 (continued)

Sample Number	Position	Average Fluid Velocity Across Specimen (fps)	Weight Data: Initial (g)	Weight Data: As Removed (g)	Weight Data: Defilmed (g)	Weight Data: Change (mg)	Exposed Sample Area (cm^2)	Corrosion Penetration (mils)	Corrosion Rate[a] (Exposed Area) (mpy): 2020 hr	Corrosion Rate[a] (Exposed Area) (mpy): 1459 hr	Total Area (cm^2)	Corrosion Penetration (mils)	Corrosion Rate[a] (Total Area) (mpy): 2020 hr	Corrosion Rate[a] (Total Area) (mpy): 1459 hr	Distance from Front of First Core Coupon to Center of Specimen (in.)	Neutron Flux at Specimen Locations at 3 Mw (neutrons cm^{-2} sec^{-1})	Power Density at Specimen Locations at 3 Mw (w/ml)	Corrected[b] Corrosion Rate (mpy)	Strain (μ in./in.)	Stress (psi)	Remarks on Surface Appearance: As-Removed Surface	Remarks on Surface Appearance: Defilmed Surface
Titanium RC-70 holders																						
Ti-25	H		6.1777	6.2554	6.1755	−2.2	10.0	0.02	0.1	0.1	10.0	0.02	0.1	0.1					2750	79,700	Heavy rustlike scale except around screw hole	Machine marks visible; some film retained on all surfaces
Ti-26	G		6.2023	6.2538	6.2039	+1.6	10.0				10.0								4940	79,000	Heavy rustlike scale on all surfaces	Machine marks visible; some film retained with scattered flakes of scale
Ti-28	G		6.0020	6.0977	6.0029	+0.9	10.0				10.0								2750	79,700	Heavy rustlike scale on all surfaces	Machine marks visible; some film retained on all surfaces
4 Special in-line impact specimens																						
Zircaloy-2																						
798	F		18.7339	18.7697		+35.8	24.9				16.8										Heavy rustlike scale over all surfaces	
799	E		19.0725	19.1098		+37.3	24.9				16.8										Heavy rustlike scale over all surfaces	
Titanium RC-A-40																						
808	B		12.9388	12.9658		+27.0	24.9				26.7										Heavy rustlike scale over all surfaces	
809	C		13.1518	13.1751		+23.3	24.9				26.7										Heavy rustlike scale over all surfaces	
Titanium-55A, core coupon holders																						
A[i] No. 1			54.0545	54.0486	54.0002	−54.3	~160	0.06	0.3	0.4	~160	0.06	0.3	0.4							Uniform brass-colored scale with overlying dark scale at low flange end	Damaged in defilming
B[i]			54.7791	54.7595	54.2500	−529.1															Uniform brass-colored scale with overlying dark scale at low flange end	Damaged in defilming
Titanium-55A, in-line coupon holders																						
A[j] No. 9			65.9951	66.0710	65.9520	−43.1	~160	0.05	0.2	0.3	~160	0.05	0.2	0.3							Heavy rustlike scale over all surfaces except on clamping shoulder near outlet end	Thin gray film retained on all surfaces; clamping shoulder shows very little damage
B[j]			65.4294																			

[a]Two corrosion rates are presented: one based on the total operation time of 2020 hr and the other based on the total radiation time of 1459 hr (3 Mwhr of reactor time equivalent to 1 hr of total radiation time).
[b]Zircaloy-2 corrosion rates based on exposed area and radiation time corrected for reactor power level.
[c]Fluxes are log mean values for length of specimen. Impact specimen has 4.25 in. exposed length and stress specimen 3.5 in. length. Stress specimen holders have 0.875 in. exposed length.
[d]Believed to be Inconel.
[e]Adjacent to loose coupons.
[f]Coupons loose in holder.
[g]Positions G, E, C, and A are located in the vapor space of the pressurizer. Positions H, F, D, and B are located in the liquid space of the pressurizer.
[h]Initial weights for these specimens have been lost.
[i]There is evidence that this holder was damaged during the defilming process.
[j]Damaged in dismantling.

Table 41. Data for Corrosion Specimens for Loop L-4-13

Sample Number	Position	Average Flow Velocity Across Specimen (fps)	Weight Data: Initial (g)	Weight Data: As Removed (g)	Weight Data: Defilmed (g)	Weight Data: Change (mg)	Exposed Sample Area (cm^2)	Corrosion Penetration (mils)	Corrosion Rate[a] (Exposed Area) (mpy): 1042 hr	Corrosion Rate[a] (Exposed Area) (mpy): 787 hr	Total Area (cm^2)	Corrosion Penetration (mils)	Corrosion Rate[a] (Total Area) (mpy): 1042 hr	Corrosion Rate[a] (Total Area) (mpy): 787 hr	Distance from Front of First CC Specimen to Center of Specimen (in.)	Neutron Flux at Specimen Locations (neutrons cm^{-2} sec^{-1})	Power Density at Specimen Locations (w/ml)	Remarks on Surface Appearance: As-Removed Surface	Remarks on Surface Appearance: Defilmed Surface
24 Core coupon corrosion samples																			
Stainless steel, type 347																$\times 10^{12}$			
1021A	4	12.1	0.9517	0.9343	0.9333	−18.4	1.40	0.65	5.5	7.2	2.1	0.43	3.6	4.8	0.88	3.36	4.84	Soft dark scale uniform over all surfaces	Very shallow pits scattered over all surfaces; machine marks visible
1022A	5	13.4	0.9458	0.9401	0.9390	−6.8	1.40	0.24	2.0	2.7	2.1	0.16	1.3	1.8	1.13	3.08	4.44	Soft dark scale uniform over all surfaces	Very shallow pits scattered over all surfaces; machine marks visible
1023A	7	16.9	0.9416	0.9416	0.9404	−1.2	1.40	0.04	0.3	0.4	2.1	0.03	0.3	0.3	1.63	2.60	3.75	Heavy black scale uniform over all surfaces	Very shallow pits scattered over all surfaces; machine marks visible
1024A	10	29.4	0.9534	0.9540	0.9522	−1.2	1.40	0.04	0.3	0.4	2.1	0.03	0.3	0.3	2.38	1.99	2.87	Heavy black scale uniform over all surfaces	Some very thin film retained; machine marks visible
1025A	13	40.1	0.9530	0.9539	0.9519	−1.1	1.40	0.04	0.3	0.4	2.1	0.03	0.3	0.3	3.13	1.51	2.14	Heavy black scale uniform over all surfaces	Some very thin film retained; machine marks visible
1026A	18	20.3	0.9473	0.9486	0.9471	−0.2	1.40	0.01	0.1	0.1	2.1	0.01	0.1	0.1	4.38	1.10	1.59	Flakes of black scale scattered over all surfaces	Clean; machine marks visible
1027A	21	13.3	0.9580	0.9596	0.9568	−1.2	1.40	0.04	0.3	0.4	2.1	0.03	0.3	0.3	5.13	0.93	1.34	Heavy black scale uniform over all surfaces	Some staining; machine marks visible
1028A	24	9.9	0.9402	0.9424	0.9400	−0.2	1.57	0.01	0.1	0.1	2.1	0.01	0.1	0.1	5.88	0.78	1.13	Heavy black scale uniform over all surfaces	Some staining; machine marks visible
Stainless steel, type 309SCb																			
C-50	1	9.4	0.9531	0.5318	0.5307	−422.4	1.57	13.21	110.7	146.6	2.1	8.80	73.8	97.7	0.13	4.37	6.30	Heavily etched surface covered with a gray-brown film	All surfaces very rough; some very thin film retained
C-51	6	14.9	0.9564	0.9511	0.9495	−6.9	1.40	0.24	2.0	2.7	2.1	0.16	1.3	1.8	1.38	2.83	4.08	Heavy black scale uniform over all surfaces	Very shallow pits scattered over all surfaces; machine marks visible
C-52	9	23.4	0.9358	0.9364	0.9340	−1.8	1.40	0.06	0.5	0.7	2.1	0.04	0.3	0.4	2.13	2.19	3.16	Flakes of black scale over a dark-gray film on all surfaces	Very sballow pits scattered over all surfaces; machine marks visible
C-53	12	37.0	0.9608	0.9612	0.9595	−1.3	1.40	0.05	0.4	0.6	2.1	0.03	0.3	0.3	2.88	1.68	2.42	Heavy black scale uniform over all surfaces	Some very thin film retained; machine marks visible
C-54	16	30.0	0.9376	0.9391	0.9367	−0.9	1.40	0.03	0.3	0.3	2.1	0.02	0.2	0.2	3.88	1.22	1.76	Flakes of black scale scattered over all surfaces	Some very thin film retained; machine marks visible
C-55	17	24.1	0.9175	0.9192	0.9172	−0.3	1.40	0.01	0.1	0.1	2.1	0.01	0.1	0.1	4.13	1.15	1.66	Flakes of black scale scattered over all surfaces	Some very thin film retained; machine marks visible
C-56	19	17.2	0.9357	0.9376	0.9326	−3.1	1.40	0.11	0.9	1.2	2.1	0.07	0.6	0.8	4.63	1.03	1.49	Flakes of black scale scattered over all surfaces	Clean; machine marks visible
C-57	22	11.9	0.9642	0.9652	0.9624	−1.8	1.40	0.06	0.5	0.7	2.1	0.04	0.3	0.4	5.38	0.88	1.27	Heavy black scale uniform over all surfaces	Clean; machine marks visible
Crystal-bar zirconium																			
Z-100	2	10.1	0.7995	0.7918	0.7914	−8.1	1.40	0.35	2.9	3.9	2.1	0.23	1.9	2.6	0.38	4.00	5.77	Thin gray film witb overlying interference colors	Some very thin film retained; machine marks visible
Z-101	3	11.0	0.7819	0.7745	0.7745	−7.4	1.40	0.32	2.7	3.6	2.1	0.21	1.8	2.3	0.63	3.68	5.31	Thin gray film with overlying interference colors	Some very thin film retained; machine marks visible
Z-102	8	19.8	0.7930	0.7868	0.7871	−5.9	1.40	0.26	2.2	2.9	2.1	0.17	1.4	1.9	1.88	2.38	3.43	Thin gray film with overlying interference colors	Some very thin film retained; machine marks visible
Z-103	11	34.5	0.7858	0.7806	0.7808	−5.0	1.40	0.22	1.8	2.4	2.1	0.15	1.3	1.7	2.63	1.82	2.63	Thin gray film with overlying interference colors	Some very thin film retained; machine marks visible
Z-104	14	44.4	0.7777	0.7734	0.7729	−4.8	1.40	0.21	1.8	2.3	2.1	0.14	1.2	1.6	3.38	1.40	2.02	Thin gray film with overlying interference colors	Some very thin film retained; machine marks visible
Z-105	15	40.2	0.7846	0.7800	0.7800	−4.6	1.40	0.20	1.7	2.2	2.1	0.13	1.1	1.4	3.63	1.30	1.88	Thin gray film with overlying interference colors	Some very thin film retained; machine marks visible
Z-106	20	15.0	0.7910	0.7867	0.7868	−4.2	1.40	0.18	1.5	2.0	2.1	0.12	1.0	1.3	4.88	0.98	1.41	Thin gray film with overlying interference colors	Some very thin film retained; machine marks visible
Z-107	23	10.8	0.7715	0.7669	0.7666	−4.9	1.40	0.21	1.8	2.3	2.1	0.14	1.2	1.6	5.63	0.83	1.20	Thin gray film with overlying interference colors	Some very thin film retained; machine marks visible
6 Core impact specimens																			
Zircaloy-3a																			
873	D		18.7817	18.6980		−83.7	24.9	0.20	1.71	2.26	26.7	0.19	1.59	2.11	2.69	1.99[b]	2.87	Thin gray film witb overlying interference colors	
874	E		18.7936	18.7066		−87.0	24.9	0.21	1.80	2.37	26.7	0.20	1.67	2.22	2.69	1.99[b]	2.87	Thin gray film with overlying interference colors	
875	F		18.8398	18.7584		−81.4	24.9	0.20	1.71	2.26	26.7	0.19	1.59	2.11	2.69	1.99[b]	2.87	Thin gray film with overlying interference colors	
Zirconium–20% Nb (melt No. 9)																			
864	A		19.8535	19.8160		−37.5	24.9	0.09	0.72	0.95	26.7	0.08	0.67	0.89	2.69	1.99[b]	2.87	Hard black scale uniform over all surfaces	
Zirconium–20% Nb (melt No. 10)																			
867	B		17.7345	17.7064		−28.1	24.9	0.07	0.54	0.72	26.7	0.06	0.50	0.68	2.69	1.99[b]	2.87	Hard black scale uniform over all surfaces	
Zirconium–20% Nb (melt No. 11)																			
870	C		19.8300	19.7919		−38.1	24.9	0.09	0.72	0.95	26.7	0.08	0.67	0.89	2.69	1.99[b]	2.87	Hard black scale uniform over all surfaces	
2 Core tensile specimens																			
Zircaloy-3a																			
772-773	G		15.5661	15.4934		−72.7	19.0	0.23	1.95	2.57	20.5	0.22	1.80	2.39	2.69	1.99[b]	2.87	Thin gray film over all surfaces	
Titanium A-40																			
487A-487B	H		11.5648	11.5594		−5.4	18.1	0.03	0.22	0.29	21.2	0.02	0.19	0.25	2.69	1.99[b]	2.87	Thin brass-colored film over all surfaces	

Table 41 (continued)

Sample Number	Position	Average Flow Velocity Across Specimen (fps)	Weight Data: Initial (g)	Weight Data: As Removed (g)	Weight Data: Defilmed (g)	Weight Data: Change (mg)	Exposed Sample Area (cm^2)	Corrosion Penetration (mils)	Corrosion Rate[a] (Exposed Area) (mpy): 1042 hr	Corrosion Rate[a] (Exposed Area) (mpy): 787 hr	Total Area (cm^2)	Corrosion Penetration (mils)	Corrosion Rate[a] (Total Area) (mpy): 1042 hr	Corrosion Rate[a] (Total Area) (mpy): 787 hr	Distance from Front of First CC Specimen to Center of Specimen (in.)	Neutron Flux at Specimen Locations (neutrons cm^{-2} sec^{-1})	Power Density at Specimen Locations (w/ml)	Remarks on Surface Appearance: As-Removed Surface	Remarks on Surface Appearance: Defilmed Surface
24 In-line coupon corrosion samples																$\times 10^{12}$			
Stainless steel, type 347																			
1029A	4	12.1	0.9535	0.9565	0.9522	−1.3	1.40	0.05	0.42	0.56	2.1	0.03	0.25	0.33	0.875			Dark-brown uniform scale over all surfaces	Some very thin film retained; machine marks visible
1031A	5	13.4	0.9352	0.9389	0.9346	−0.6	1.40	0.02	0.17	0.22	2.1	0.01	0.08	0.11	1.125			Dark-brown uniform scale over all surfaces	Some spots of scale retained; machine marks visible
1032A	7	16.9	0.9543	0.9570	0.9534	−0.9	1.40	0.03	0.25	0.33	2.1	0.02	0.17	0.22	1.625			Dark-brown uniform scale over all surfaces	Some spots of scale retained; machine marks visible
1033A	10	29.4	0.9562	0.9587	0.9554	−0.8	1.40	0.03	0.25	0.33	2.1	0.02	0.17	0.22	2.375			Dark-brown uniform scale over all surfaces	Some spots of scale retained; machine marks visible
1034A	13	40.1	0.9216	0.9246	0.9213	−0.4	1.40	0.01	0.08	0.11	2.1	0.01	0.08	0.11	3.125			Dark-brown uniform scale over all surfaces	Some spots of scale retained; machine marks visible
1035A	18	20.3	0.9444	0.9468	0.9439	−0.5	1.40	0.02	0.17	0.22	2.1	0.01	0.08	0.11	4.375			Dark-brown uniform scale over all surfaces	Some very thin film retained; machine marks visible
1037A	21	13.3	0.9367	0.9392	0.9359	−0.8	1.40	0.03	0.25	0.33	2.1	0.02	0.17	0.22	5.125			Dark-brown uniform scale over all surfaces	Some very thin film retained; machine marks visible
1038A	24	9.9	0.9453	0.9474	0.9442	−1.1	1.57	0.03	0.25	0.33	2.1	0.02	0.17	0.22	5.875			Dark-brown uniform scale over all surfaces	Some spots of scale retained; machine marks visible
Stainless steel, type 309SCb																			
C-58	1	9.4	0.9431	0.9453	0.9424	−0.7	1.57	0.02	0.2	0.2	2.1	0.01	0.1	0.1	0.125			Dark-brown uniform scale over all surfaces	Some very thin film retained; machine marks visible
C-59	6	14.9	0.9534	0.9561	0.9517	−1.7	1.40	0.06	0.5	0.7	2.1	0.04	0.3	0.4	1.375			Dark-brown uniform scale over all surfaces	Some very thin film retained; machine marks visible
C-60	9	23.4	0.9563	0.9589	0.9551	−1.2	1.40	0.04	0.3	0.4	2.1	0.03	0.3	0.3	2.125			Dark-brown uniform scale over all surfaces	Some spots of scale retained; machine marks visible
C-61	12	37.0	0.9361	0.9387	0.9355	−0.6	1.40	0.02	0.2	0.2	2.1	0.02	0.2	0.2	2.875			Dark-brown uniform scale over all surfaces	Some very thin film retained; machine marks visible
C-62	16	30.0	0.9242	0.9280	0.9243	+0.1	1.40				2.1				3.875			Dark-brown uniform scale over all surfaces	Some very thin film retained; machine marks visible
C-63	17	24.1	0.9682	0.9709	0.9676	−0.6	1.40	0.02	0.2	0.2	2.1	0.02	0.2	0.2	4.125			Dark-brown uniform scale over all surfaces	Some very thin film retained; machine marks visible
C-64	19	17.2	0.9353	0.9374	0.9345	−0.8	1.40	0.03	0.3	0.3	2.1	0.02	0.2	0.2	4.625			Dark-brown uniform scale over all surfaces	Some very thin film retained; machine marks visible
C-65	22	11.9	0.9477	0.9488	0.9453	−2.4	1.40	0.08	0.7	0.9	2.1	0.06	0.5	0.7	5.375			Dark-brown uniform scale over all surfaces	Some very thin film retained; machine marks visible
Crysral-bar zirconium																			
Z-108	2	10.1	0.7822	0.7853	0.7836	+1.4	1.40				2.1				0.375			Dark-brown uniform scale over all surfaces	Scale flaked in spots; machine marks visible
Z-109	3	11.0	0.7776	0.7810	0.7806	+3.0	1.40				2.1				0.625			Dark-brown uniform scale over all surfaces	Scale flaked in spots; machine marks visible
Z-110	8	19.8	0.7640	0.7674	0.7669	+2.9	1.40				2.1				1.875			Dark-brown uniform scale over all surfaces	Scale flaked in spots; machine marks visible
Z-111	11	34.5	0.7862	0.7887	0.7883	+2.1	1.40				2.1				2.625			Dark-brown uniform scale over all surfaces	Scale flaked in spots; machine marks visible
Z-112	14	44.4	0.7800	0.7834	0.7824	+2.4	1.40				2.1				3.375			Dark-brown uniform scale over all surfaces	Scale flaked in spots; machine marks visible
Z-113	15	40.2	0.7756	0.7782	0.7780	+2.4	1.40				2.1				3.625			Dark-brown uniform scale over all surfaces	Scale flaked in spots; machine marks visible
Z-114	20	15.0	0.7936	0.7959	0.7953	+1.7	1.40				2.1				4.875			Dark-brown uniform scale over all surfaces	Scale flaked in spots; machine marks visible
Z-115	23	10.8	0.7509	0.7382	0.7377	−3.2	1.40	0.14	1.2	1.6	2.1	0.09	0.8	1.0	5.625			Dark-brown uniform scale over all surfaces	Scale flaked in spots; machine marks visible
6 In-line impact specimens																			
Zircaloy-3a																			
878	A		18.7416	18.7882		+46.6	24.9				26.7							Dark-brown uniform scale over all surfaces	
876	E		18.8400	18.8844		+44.4	24.9				26.7							Dark-brown uniform scale over all surfaces	
877	E		18.8848	18.9510		+66.2	24.9				26.7							Dark-brown uniform scale over all surfaces	
Zirconium–20% Nb (melt No. 9)																			
865	B		20.1579	20.2039		+46.0	24.9				26.7							Dark-brown uniform scale over all surfaces	
Zirconium–20% Nb (melt No. 10)																			
868	C		20.1521	20.1898		+37.7	24.9				26.7							Dark-brown uniform scale over all surfaces	
Zirconium–20% Nb (melt No. 11)																			
871	D		20.0386	20.0782		+39.6	24.9				26.7							Dark-brown uniform scale over all surfaces	
Core coupon holder No. 11																			
Stainless steel, type 347																			
			96.5732	(Damaged)			~160.0				~160.0							Soft black scale at inlet ranging to a rust red at the outlet	Very thin dark film retained on all surfaces
			96.5422	93.5544															
In-line coupon holder No. 12																			
Stainless steel, type 347																			
			113.5833	113.7564			~160.0				~160.0							Dark-brown uniform scale over all surfaces	Very thin black film with some spots of scale retained
			110.8743	(Damaged)															

[a]Two corrosion rates are presented: one based on the total operation time of 1042 hr and the other based on the total radiation time of 787 hr (3 Mwhr of reactor time equivalent to 1 hr of total radiation time).
[b]Log mean value for exposed length of specimen.

Table 42. Data for Corrosion Specimens for Loop L-4-18

Sample Number	Position	Average Solution Velocity Across Specimen (fps)	Weight Data: Initial (g)	Weight Data: As Removed (g)	Weight Data: Defilmed (g)	Weight Data: Change (mg)	Exposed Sample Area (cm^2)	Corrosion Penetration (mils)	Corrosion Rate[a] (Exposed Area) (mpy): 860 hr	Corrosion Rate[a] (Exposed Area) (mpy): 642 hr	Total Area (cm^2)	Corrosion Penetration (mils)	Corrosion Rate[a] (Total Area) (mpy): 860 hr	Corrosion Rate[a] (Total Area) (mpy): 642 hr	Distance from Front of First Specimen to Center of Specimen (in.)	Neutron Flux at Specimen Locations (neutrons cm^{-2} sec^{-1})	Power Density at Specimen Locations (w/ml)	Strain (μ in./in.)	Stress at 80°F (psi)	Stress at 600°F (psi)	Remarks on Surface Appearance: As-Removed Surface	Remarks on Surface Appearance: Defilmed Surface
																$\times 10^{12}$						
24 Core-channel coupons																						
Stainless steel, type 347																						
SA-1562	4	11.7	0.9046	0.9044	0.9035	−1.1	1.4	0.04	0.39	0.53	2.2	0.03	0.25	0.34	0.88	2.98	4.26				Dark-brown scale scattered over all surfaces	Metallic gray surfaces with some interference film retained; machine marks visible
SA-1563	5	12.9	0.8879	0.8888	0.8878	−0.1	1.4	0.003	0.04	0.05	2.2	0.002	0.02	0.03	1.13	2.80	4.00				Dark-brown scale scattered over all surfaces	Metallic gray surfaces with some interference film retained; machine marks visible
SA-1564	7	16.4	0.9143	0.9148	0.9134	−0.9	1.4	0.03	0.32	0.43	2.2	0.02	0.20	0.27	1.63	2.43	3.47				Dark-brown scale scattered over all surfaces	Metallic gray surfaces with some interference film retained; machine marks visible
SA-1565	10	28.1	0.9565	0.9583	0.9562	−0.3	1.4	0.01	0.11	0.14	2.2	0.01	0.07	0.09	2.38	2.00	2.86				Very dark-brown scale scattered over all surfaces	Metallic gray surfaces with some stains; machine marks visible
SA-1566	13	38.7	0.9090	0.9098	0.9078	−1.2	1.4	0.04	0.49	0.66	2.2	0.03	0.27	0.36	3.13	1.64	2.34				Very dark-brown almost black scale over all surfaces	Metallic gray surfaces with some stains; machine marks visible
SA-1567	18	19.4	0.9394	0.9412	0.9393	−0.1	1.4	0.003	0.04	0.05	2.2	0.002	0.02	0.03	4.38	1.19	1.70				Very dark-brown almost black scale over all surfaces	Metallic gray surfaces with some stains; machine marks visible
SA-1568	21	12.8	0.9650	0.9665	0.9647	−0.3	1.4	0.01	0.11	0.14	2.2	0.01	0.07	0.09	5.13	0.97	1.39				Very dark-brown almost black scale over all surfaces	Metallic gray surfaces with some stains; machine marks visible
SA-1569	24	9.6	0.9570	0.9582	0.9547	−2.3	1.57	0.07	0.73	0.98	2.2	0.05	0.52	0.70	5.88	0.80	1.14				Very dark-brown almost black scale with damaged ends	Metallic gray surfaces clamped ends damaged; machine marks visible
Zircaloy-2																						
ZB-130	2	9.8	0.7932	0.7899	0.7899	−3.3	1.4	0.14	1.45	1.94	2.2	0.09	0.92	1.24	0.38	3.40	4.86				Dark-gray film with interference colors	Some film retained; machine marks visible
ZB-131	3	10.6	0.7940	0.7909	0.7909	−3.1	1.4	0.13	1.36	1.83	2.2	0.09	0.87	1.16	0.63	3.19	4.56				Dark-gray film with interference colors with some scattered light-brown scale	Some film retained; machine marks visible
ZB-138	8	19.0	0.7949	0.7924	0.7922	−2.7	1.4	0.12	1.19	1.59	2.2	0.07	0.76	1.01	1.88	2.30	3.29				Dark-gray film with interference colors	Some film retained; machine marks visible
ZB-139	11	33.2	0.8031	0.8006	0.8006	−2.5	1.4	0.11	1.10	1.47	2.2	0.07	0.70	0.94	2.63	1.88	2.69				Dark-gray film with interference colors	Some film retained; machine marks visible
ZB-140	14	42.8	0.8193	0.8170	0.8169	−2.4	1.4	0.10	1.05	1.41	2.2	0.07	0.67	0.90	3.38	1.54	2.20				Dark-gray film with interference colors	Some film retained; machine marks visible
ZB-141	15	38.8	0.7821	0.7808	0.7806	−1.5	1.4	0.07	0.66	0.88	2.2	0.04	0.42	0.56	3.63	1.44	2.06				Dark-gray film with interference colors	Some film retained; machine marks visible
ZB-142	20	14.3	0.7982	0.7976	0.7973	−0.9	1.4	0.04	0.40	0.52	2.2	0.03	0.25	0.34	4.88	1.04	1.49				Dark-gray film with interference colors and some brown scale	Some film retained; machine marks visible
ZB-143	23	10.4	0.7910	0.7901	0.7898	−1.2	1.4	0.05	0.53	0.71	2.2	0.03	0.34	0.45	5.63	0.85	1.21				Dark-gray film with interference colors with scattered brown scale	Some film retained; machine marks visible
Stainless steel, type 430L																						
SL-15	1	9.6	0.9294	0.9183	0.9175	−11.9	1.57	0.39	3.94	5.27	2.2	0.28	2.81	3.76	0.13	3.61	5.16				Gray film with scattered dark-brown scale over all surfaces	Metallic gray with some interference films retained; machine marks visible
SL-16	6	14.3	0.9201	0.9192	0.9180	−2.1	1.4	0.08	0.78	1.04	2.2	0.05	0.50	0.66	1.38	2.60	3.71				Dark-brown scale over all surfaces	Metallic gray surfaces with some stains; machine marks visible
SL-17	9	22.4	0.9496	0.9499	0.9483	−1.3	1.4	0.05	0.48	0.65	2.2	0.03	0.31	0.41	2.13	2.14	3.06				Dark-brown scale over all surfaces	Metallic gray surfaces with some stains; machine marks visible
SL-18	12	35.7	0.9355	0.9356	0.9339	−1.6	1.4	0.06	0.59	0.79	2.2	0.04	0.38	0.51	2.88	1.75	2.50				Very dark-brown scale over all surfaces	Metallic gray surfaces with some stains; machine marks visible
SL-19	16	28.9	0.9170	0.9172	0.9152	−1.8	1.4	0.07	0.67	0.89	2.2	0.04	0.42	0.57	3.88	1.35	1.93				Very dark-brown almost black scale over all surfaces	Metallic gray surfaces with some stains; machine marks visible
SL-20	17	23.3	0.9349	0.9360	0.9334	−1.5	1.4	0.05	0.56	0.75	2.2	0.04	0.35	0.47	4.13	1.27	1.81				Very dark-brown almost black scale over all surfaces	Metallic gray surfaces with some stains; machine marks visible
SL-21	19	16.5	0.9334	0.9345	0.9319	−1.5	1.4	0.05	0.56	0.75	2.2	0.04	0.35	0.47	4.63	1.11	1.59				Very dark-brown almost black scale over all surfaces	Metallic gray surfaces with some stains; machine marks visible
SL-22	22	11.5	0.9331	0.9335	0.9312	−1.9	1.4	0.07	0.71	0.94	2.2	0.04	0.44	0.60	5.38	0.91	1.30				Very dark-brown almost black scale over all surfaces	Metallic gray surfaces with some stains; machine marks visible
Core ladder coupons																						
Stainless steel, type 347 (array SA12)																						
SA-1590	2		0.9391	0.9366	0.9350	−4.1	1.4	0.14	1.46	1.96	2.2	0.09	0.92	1.25	0.78	3.04	4.34				Dark gray-brown scale over all surfaces	Shiny metallic surfaces with some stains; pin point pitting; machine marks visible
SA-1591	4		0.9816	0.9827	0.9813	−0.3	1.4	0.01	0.11	0.14	2.2	0.007	0.07	0.09	1.03	2.85	4.07				Dark gray-brown scale over all surfaces	Shiny metallic surfaces with some stains; pin point pitting; machine marks visible
SA-1592	5		0.9611	0.9617	0.9604	−0.7	1.4	0.03	0.25	0.33	2.2	0.02	0.16	0.21	1.16	2.75	3.93				Dark gray-brown scale over all surfaces	Shiny metallic surfaces with some stains; pin point pitting; machine marks visible
SA-1593	8		0.9742	0.9753	0.9742		1.4				2.2				1.53	2.50	3.57				Dark-brown scale with scattered flakes over all surfaces	Shiny gray metallic surfaces with some stains; pin point pitting; machine marks visible
SA-1594	10		0.9485	0.9496	0.9485		1.4				2.2				1.78	2.33	3.33				Dark-brown scale over all surfaces darker along the edges	Metallic gray film with interference colors; machine marks visible
SA-1595	13		0.9454	0.9469	0.9450	−0.4	1.4	0.01	0.14	0.19	2.2	0.009	0.09	0.12	2.16	2.11	3.01				Dark-brown scale with scattered flakes over all surfaces	Metallic gray film with interference colors; machine marks visible
SA-1596	14		0.9760	0.9780	0.9760		1.4				2.2				2.28	2.05	2.93				Dark-brown scale with scattered flakes over all surfaces	Metallic gray film with interference colors; machine marks visible
Stainless steel, type 430L (array SA12)																						
SL-31	1		0.9203	0.9165	0.9145	−5.8	1.4	0.21	2.15	2.88	2.2	0.14	1.37	1.84	0.66	3.15	4.50				Dark-brown scale over all surfaces	Metallic gray surfaces with some stains; machine marks visible
SL-32	3		0.9099	0.9083	0.9072	−2.7	1.4	0.10	1.00	1.36	2.2	0.06	0.64	0.86	0.91	2.95	4.21				Dark-brown scale over all surfaces	Metallic gray surfaces with some stains; machine marks visible

Table 42 (continued)

Sample Number	Position	Average Solution Velocity Across Specimen (fps)	Weight Data: Initial (g)	Weight Data: As Removed (g)	Weight Data: Defilmed (g)	Weight Data: Change (mg)	Exposed Sample Area (cm^2)	Corrosion Penetration (mils)	Corrosion Rate[a] (Exposed Area) (mpy): 860 hr	Corrosion Rate[a] (Exposed Area) (mpy): 642 hr	Total Area (cm^2)	Corrosion Penetration (mils)	Corrosion Rate[a] (Total Area) (mpy): 860 hr	Corrosion Rate[a] (Total Area) (mpy): 642 hr	Distance from Front of First Specimen to Center of Specimen (in.)	Neutron Flux at Specimen Locations (neutrons cm^{-2} sec^{-1})	Power Density at Specimen Locations (w/ml)	Strain (μ in./in.)	Stress at 80°F (psi)	Stress at 600°F (psi)	Remarks on Surface Appearance: As-Removed Surface	Remarks on Surface Appearance: Defilmed Surface
																$\times 10^{12}$						
Stainless steel, type 430L (array SA12)																						
SL-33	6		0.9503	0.9506	0.9491	−1.2	1.4	0.04	0.45	0.60	2.2	0.03	0.28	0.38	1.28	2.68	3.83				Dark-brown scale with scattered flakes over all surfaces	Metallic gray surfaces with some stains; machine marks visible
SL-34	7		0.9217	0.9214	0.9201	−1.6	1.4	0.06	0.59	0.78	2.2	0.04	0.38	0.51	1.41	2.59	3.70				Dark-brown scale with scattered flakes over all surfaces	Metallic gray surfaces with some stains; machine marks visible
SL-35	9		0.9226	0.9224	0.9208	−1.8	1.4	0.07	0.67	0.90	2.2	0.05	0.42	0.56	1.66	2.41	3.44				Dark-brown scale with scattered flakes over all surfaces	Metallic gray film with interference colors; machine marks visible
SL-36	11		0.9208	0.9209	0.9191	−1.7	1.4	0.06	0.63	0.84	2.2	0.04	0.40	0.54	1.91	2.28	3.26				Dark-brown scale with scattered flakes over all surfaces	Metallic gray film with interference colors; machine marks visible
SL-37	12		0.9329	0.9333	0.9313	−1.6	1.4	0.06	0.59	0.79	2.2	0.04	0.38	0.51	2.03	2.20	3.14				Dark-brown scale with scattered flakes over all surfaces	Metallic gray film with interference colors; machine marks visible
SL-38	15		0.9537	0.9547	0.9522	−1.5	1.4	0.05	0.56	0.75	2.2	0.03	0.35	0.47	2.41	1.99	2.84				Dark-brown scale with scattered flakes over all surfaces	Metallic gray film with interference colors; machine marks visible
Zircaloy-2 (array TB4)																						
ZB-156	1		0.7823	0.7793	0.7790	−3.3	1.4	0.14	1.45	1.94	2.2	0.09	0.92	1.23	0.66	3.15	4.50				Dark-gray film with light-brown scale over all surfaces	Film retained with some staining; machine marks visible
ZB-157	5		0.7685	0.7658	0.7658	−2.7	1.4	0.12	1.19	1.59	2.2	0.07	0.75	1.00	1.16	2.75	3.93				Dark-brown scale over all surfaces	Dark-gray film retained with some staining; machine marks visible
ZB-158	9		0.7854	0.7835	0.7832	−2.2	1.4	0.08	0.86	1.09	2.2	0.05	0.52	0.70	1.66	2.41	3.44				Dark-gray film with spots of brown scale	Dark-gray film retained with grain pattern in gray brown and black colors
ZB-159	13		0.7812	0.7799	0.7795	−1.7	1.4	0.06	0.63	0.84	2.2	0.04	0.40	0.54	2.16	2.11	3.01				Dark-gray film with some interference colors	Dark-gray film retained with some staining; machine marks visible
Zr[b]–15% Nb (array TB4)																						
ZX-1	2		0.8170	0.8156	0.8151	−1.9	1.4	0.08	0.80	1.07	2.2	0.05	0.51	0.68	0.78	3.04	4.34				Thick scale with dark-gray and brown colors in grain patterns	Some film retained with the grain pattern appearing as more glossy colors
ZX-2	6		0.7963	0.7957	0.7957	−0.6	1.4	0.02	0.25	0.34	2.2	0.02	0.16	0.21	1.28	2.68	3.83				Thick scale with dark-gray and brown colors in grain patterns	Some film retained with interference colors; machine marks visible
ZX-3	10		0.8097	0.8084	0.8086	−1.1	1.4	0.05	0.46	0.62	2.2	0.03	0.29	0.39	1.78	2.33	3.33				Thick scale with dark-gray and brown colors in grain patterns	Some film retained with the grain pattern appearing as interference colors
ZX-4	14		0.7927	0.7927	0.7923	−0.4	1.4	0.02	0.17	0.22	2.2	0.01	0.11	0.14	2.28	2.05	2.93				Thick scale with dark-gray and brown colors in grain patterns	Some film retained with the grain pattern appearing as dark interference colors
Ti–3% Al (array TB4)																						
TJ-11	4		0.5482	0.5484	0.5476	−0.6	1.4	0.04	0.38	0.51	2.2	0.02	0.24	0.32	1.03	2.85	4.07				Rough bronze film on all surfaces	Bronze film retained; surface appears to be uniformly roughened
TJ-12	8		0.5321	0.5323	0.5315	−0.6	1.4	0.04	0.38	0.51	2.2	0.02	0.24	0.32	1.53	2.50	3.57				Rough bronze film on all surfaces	Some film retained; surface appears to be uniformly roughened
TJ-13	12		0.5282	0.5282	0.5275	−0.7	1.4	0.04	0.44	0.60	2.2	0.03	0.28	0.38	2.03	2.20	3.14				Rough bronze film on all surfaces	Some film retained; surface appears to be uniformly roughened
TJ-14	15		0.4920	0.4931	0.4922	+0.2	1.4				2.2				2.41	1.99	2.84				Rough bronze film on all surfaces	Some film retained; surface appears to be uniformly roughened
Ti–A55 (array TB4)																						
TI-70	3		0.5344	0.5344	0.5341	−0.3	1.4	0.02	0.19	0.25	2.2	0.01	0.12	0.16	0.91	2.95	4.21				Metallic bronze scale with some staining	Some film retained; machine marks visible
TI-71	7		0.5315	0.5316	0.5313	−0.2	1.4	0.02	0.13	0.17	2.2	0.01	0.08	0.11	1.41	2.59	3.70				Metallic bronze scale on all surfaces	Bronze film retained; machine marks visible
TI-72	11		0.5389	0.5393	0.5386	−0.3	1.4	0.02	0.19	0.25	2.2	0.01	0.12	0.16	1.91	2.28	3.26				Metallic bronze scale with some dark-brown scale on all surfaces	Bronze film retained; machine marks visible
Zircaloy-2, core annulus stress specimens																						
ZB-2			8.4955	8.4729	8.4701	−25.4	15.9	0.10	0.98	1.3	19.7	0.08	0.79	1.1	2.47	1.81	2.59	1300	17,500	10,400	Dark-gray film with scattered flakes of brown scale	Dark-gray film retained with interference colors; machine marks visible
ZB-5			8.8664	8.8471	8.8416	−24.8	15.9	0.09	0.96	1.3	19.7	0.08	0.77	1.0	2.47	1.81	2.59	1510	20,400	12,100	Dark-gray film with scattered flakes of brown scale	Dark-gray film retained with interference colors; machine marks visible
Stress specimen holders, Zircaloy-2																						
ZB-35			9.3218	9.3179	9.3066	−15.2					10.7	0.09	0.87	1.2	4.16	1.25	1.79				Rough dark-gray scale over all surfaces	Shiny metallic gray film retained; machine marks visible
ZB-36			9.3055	9.2917	9.2879	−17.6					10.7	0.10	1.0	1.4	0.78	3.04	4.34				Dark-gray film with dark rustlike scale scattered over all surfaces	Shiny metallic gray film retained; machine marks visible
24 In-line–channel specimen																						
Stainless steel, type 347																						
SA-1570	4	11.7	0.9167	0.9181	0.9161	−0.6	1.4	0.02	0.21	0.28	2.2	0.01	0.13	0.18							Dull dark-brown rustlike scale with some flaking over all surfaces	Metallic gray surfaces with stains; machine marks visible
SA-1571	5	12.9	0.9784	0.9807	0.9790	+0.6	1.4				2.2										Dull dark-brown rustlike scale with some flaking over all surfaces	Metallic gray surfaces with stains; machine marks visible
SA-1572	7	16.4	0.8970	0.8992	0.8974	+0.4	1.4				2.2										Dull dark-brown rustlike scale with some flaking over all surfaces	Metallic gray surfaces with stains; machine marks visible
SA-1573	10	28.1	0.9579	0.9597	0.9580	+0.1					2.2										Dull dark-brown rustlike scale with some flaking over all surfaces	Metallic gray surfaces with stains; machine marks visible

Table 42 (continued)

Sample Number	Position	Average Solution Velocity Across Specimen (fps)	Weight Data: Initial (g)	Weight Data: As Removed (g)	Weight Data: Defilmed (g)	Weight Data: Change (mg)	Exposed Sample Area (cm^2)	Corrosion Penetration (mils)	Corrosion Rate[a] (Exposed Area) (mpy): 860 hr	Corrosion Rate[a] (Exposed Area) (mpy): 642 hr	Total Area (cm^2)	Corrosion Penetration (mils)	Corrosion Rate[a] (Total Area) (mpy): 860 hr	Corrosion Rate[a] (Total Area) (mpy): 642 hr	Distance from Front of First Specimen to Center of Specimen (in.)	Neutron Flux at Specimen Locations (neutrons cm^{-2} sec^{-1})	Power Density at Specimen Locations (w/ml)	Strain (μ in./in.)	Stress at 80°F (psi)	Stress at 600°F (psi)	Remarks on Surface Appearance: As-Removed Surface	Remarks on Surface Appearance: Defilmed Surface
Stainless steel, type 347																						
SA-1574	13	38.7	0.9327	0.9343	0.9325	−0.2	1.4	0.01	0.07	0.10	2.2	0.01	0.05	0.06							Dull dark-brown rustlike scale with some flaking over all surfaces	Metallic gray surfaces with stains; machine marks visible
SA-1575	18	19.4	0.9123	0.9138	0.9122	−0.1	1.4	0.004	0.04	0.05	2.2	0.002	0.02	0.03							Dull dark-brown rustlike scale with some flaking over all surfaces	Metallic gray surfaces with stains and interference colors; machine marks visible
SA-1576	21	12.8	0.9293	0.9306	0.9291	−0.2	1.4	0.01	0.07	0.10	2.2	0.01	0.05	0.06							Dull dark-brown rustlike scale with some flaking over all surfaces	Metallic gray surfaces with stains and interference colors; machine marks visible
SA-1577	24	9.6	0.9566	0.9559	0.9538	−2.8	1.57	0.09	0.89	1.19	2.2	0.06	0.57	0.76							Dull dark-brown rustlike scale with some flaking over all surfaces	Metallic gray surfaces with some scale in clamping areas; machine marks visible
Stainless steel, type 430L																						
SL-23	1	9.6	0.9420	0.9438	0.9404	−1.6	1.57	0.05	0.53	0.71	2.2	0.03	0.34	0.45							Dull dark-brown rustlike scale with some flaking over all surfaces	Metallic gray surfaces with stains; machine marks visible
SL-24	6	14.3	0.9237	0.9240	0.9215	−2.2	1.4	0.08	0.82	1.09	2.2	0.05	0.52	0.70							Dull dark-brown rustlike scale with some flaking over all surfaces	Metallic gray surfaces with stains; machine marks visible
SL-25	9	22.4	0.9191	0.9193	0.9170	−2.1	1.4	0.08	0.78	1.04	2.2	0.05	0.50	0.66							Dull dark-brown rustlike scale with some flaking over all surfaces	Metallic gray surfaces with stains; machine marks visible
SL-26	12	35.7	0.9482	0.9492	0.9460	−2.2	1.4	0.08	0.82	1.09	2.2	0.05	0.52	0.70							Dull dark-brown rustlike scale with some flaking over all surfaces	Metallic gray surfaces with stains and interference colors; machine marks visible
SL-27	16	28.9	0.9250	0.9256	0.9231	−1.9	1.4	0.07	0.70	0.94	2.2	0.04	0.45	0.60							Dull dark-brown rustlike scale with some flaking over all surfaces	Metallic gray surfaces with stains; machine marks visible
SL-28	17	23.3	0.9378	0.9389	0.9362	−1.6	1.4	0.06	0.59	0.79	2.2	0.04	0.38	0.51							Dull dark-brown rustlike scale with some flaking over all surfaces	Metallic gray surfaces with stains; machine marks visible
SL-29	19	16.5	0.9392	0.9402	0.9376	−1.6	1.4	0.06	0.59	0.79	2.2	0.04	0.38	0.51							Dull dark-brown rustlike scale with some flaking over all surfaces	Metallic gray surfaces with stains; machine marks visible
SL-30	22	11.5	0.8983	0.8995	0.8960	−2.3	1.4	0.08	0.85	1.14	2.2	0.05	0.54	0.73							Dull dark-brown rustlike scale with some flaking over all surfaces	Interference films with stains and scattered spots; thin brown scale; machine marks visible
Zircaloy-2																						
ZB-144	2	9.8	0.7942	0.7964	0.7960	+1.8	1.4				2.2										Dull dark-brown rustlike scale with some flaking over all surfaces	Dark-gray film with scattered flakes of scale; machine marks apparent
ZB-145	3	10.6	0.8108	0.8124	0.8120	+1.2	1.4				2.2										Dull dark-brown rustlike scale with some flaking over all surfaces	Dark-gray film with scattered flakes of scale; machine marks apparent
ZB-146	8	19.0	0.7935	0.7961	0.7960	+2.5	1.4				2.2										Dull dark-brown rustlike scale with some flaking over all surfaces	Dark-gray film with scattered flakes of scale; machine marks apparent
ZB-147	11	33.2	0.8010	0.8026	0.8026	+1.6	1.4				2.2										Dull dark-brown rustlike scale with some flaking over all surfaces	Dark-gray film with scattered flakes of scale; rough on one edge; machine marks visible
ZB-148	14	42.8	0.7865	0.7892	0.7890	+2.5	1.4				2.2										Dull dark-brown rustlike scale with some flaking over all surfaces	Dark-gray film with scattered flakes of scale; machine marks visible
ZB-149	15	38.8	0.7870	0.7896	0.7895	+2.5	1.4				2.2										Dull dark-brown rustlike scale with some flaking over all surfaces	Dark-gray film with scattered flakes of scale; machine marks visible
ZB-150	20	14.3	0.7787	0.7809	0.7807	+2.0	1.4				2.2										Dull dark-brown rustlike scale with some flaking over all surfaces	Dark-gray film with scattered flakes of scale; machine marks visible
ZB-151	23	10.4	0.7926	0.7946	0.7940	+1.4	1.4				2.2										Dull dark-brown rustlike scale with some flaking over all surfaces	Dark-gray film with scattered flakes of scale; machine marks visible
In-line ladder coupons																						
Stainless steel, type 347 (array SA13)																						
SA-1597	2		0.9740	0.9760	0.9744	+0.4	1.4				2.2										Dull dark-brown scale heavier on the edges	Metallic gray surfaces with stains; machine marks visible
SA-1598	4		0.9489	0.9500	0.9488	−0.1	1.4	0.004	0.04	0.05	2.2	0.002	0.02	0.03							Dull dark-brown scale heavier on the edges	Metallic gray surfaces with stains; machine marks visible
SA-1599	5		0.9157	0.9164	0.9154	−0.3	1.4	0.01	0.11	0.14	2.2	0.01	0.07	0.09							Dull dark-brown scale heavier in spots	Metallic gray surfaces with stains; machine marks visible
SA-1600	8		0.9306	0.9316	0.9303	−0.3	1.4	0.01	0.11	0.14	2.2	0.01	0.07	0.09							Dull dark-brown scale with a rough surface	Metallic gray surfaces with stains; machine marks visible
SA-1601	10		0.9820	0.9837	0.9825	+0.5	1.4				2.2										Dull dark-brown scale heavier on the edges	Metallic gray surfaces with stains; machine marks visible
SA-1602	13		0.9704	0.9719	0.9707	+0.3	1.4				2.2										Dull dark-brown scale heavier on the edges	Metallic gray surfaces with stains; machine marks visible
SA-1603	14		0.9724	0.9741	0.9727	+0.3	1.4				2.2										Dull dark-brown scale heavier in spots	Metallic gray surfaces with stains; machine marks visible
Stainless steel, type 430L (array SA13)																						
SL-39	1		0.9360	0.9364	0.9339	−2.1	1.4	0.08	0.78	1.04	2.2	0.05	0.50	0.66							Dull dark-brown scale heavier on the edges	Metallic gray surfaces with stains; machine marks visible
SL-40	3		0.9289	0.9289	0.9251	−3.8	1.4	0.14	1.41	1.89	2.2	0.09	0.90	1.20							Dull dark-brown scale heavier on the edges	Metallic gray surfaces with stains; machine marks visible
SL-41	6		0.9106	0.9104	0.9089	−1.7	1.4	0.06	0.63	0.84	2.2	0.04	0.40	0.54							Dark-gray film with scattered areas of dark-brown scale	Metallic gray surfaces with stains; machine marks visible

Table 42 (continued)

Sample Number	Position	Average Solution Velocity Across Specimen (fps)	Weight Data: Initial (g)	Weight Data: As Removed (g)	Weight Data: Defilmed (g)	Weight Data: Change (mg)	Exposed Sample Area (cm^2)	Corrosion Penetration (mils)	Corrosion Rate[a] (Exposed Area) (mpy): 860 hr	Corrosion Rate[a] (Exposed Area) (mpy): 642 hr	Total Area (cm^2)	Corrosion Penetration (mils)	Corrosion Rate[a] (Total Area) (mpy): 860 hr	Corrosion Rate[a] (Total Area) (mpy): 642 hr	Distance from Front of First Specimen to Center of Specimen (in.)	Neutron Flux at Specimen Locations (neutrons cm^{-2} sec^{-1})	Power Density at Specimen Locations (w/ml)	Strain (μ in./in.)	Stress at 80°F (psi)	Stress at 600°F (psi)	Remarks on Surface Appearance: As-Removed Surface	Remarks on Surface Appearance: Defilmed Surface
																$\times 10^{12}$						
Stainless steel, type 430L (array SA13)																						
SL-42	7		0.9134	0.9134	0.9116	−1.8	1.4	0.07	0.67	0.89	2.2	0.04	0.43	0.57							Dark-gray film with scattered areas of dark-brown scale	Metallic gray surfaces with stains; machine marks visible
SL-43	9		0.9374	0.9374	0.9354	−2.0	1.4	0.07	0.74	0.99	2.2	0.05	0.47	0.63							Uniform dark-gray scale on all surfaces	Metallic gray surfaces with stains; machine marks visible
SL-44	11		0.9160	0.9156	0.9139	−2.1	1.4	0.08	0.78	1.04	2.2	0.05	0.50	0.66							Dull dark-brown scale heavier on the edges	Metallic gray surfaces with stains; machine marks visible
SL-45	12		0.9315	0.9317	0.9269	−4.6	1.4	0.17	1.71	2.28	2.2	0.11	1.09	1.45							Dull dark-brown scale heavier on the edges	Metallic gray surfaces with stains; machine marks visible
SL-46	15		0.9287	0.9289	0.9270	−1.7	1.4	0.06	0.63	0.84	2.2	0.04	0.40	0.54							Dull dark-brown scale heavier in spots	Metallic gray surfaces with stains; machine marks visible
Zircaloy-2 (array TB2)																						
ZB-160	1		0.7924	0.7964	0.7942	+1.8	1.4				2.2										Heavy dark shiny scale with rough surfaces	Dark-gray film with scattered flakes of brown scale; machine marks visible
ZB-161	5		0.7823	0.7861	0.7840	+1.7	1.4				2.2										Heavy dark shiny scale with rough surfaces	Dark-gray film with scattered flakes of brown scale; machine marks visible
ZB-162	9		0.7649	0.7688	0.7665	+1.6	1.4				2.2										Heavy dark shiny scale with rough surfaces	Dark-gray film with scattered flakes of brown scale; machine
ZB-163	13		0.7689	0.7714	0.7704	+1.5	1.4				2.2										Heavy dark shiny scale with rough surfaces	Dark-gray film with scattered flakes of brown scale; machine marks visible
Zr[b]–15% Nb (array TB2)																						
ZX-5	2		0.8096	0.8126	0.8103	+0.7	1.4				2.2										Heavy dark shiny scale with rough surfaces	Dark-gray film with spots of brown scale in grain pattern; machine marks visible
ZX-6	6		0.8136	0.8155	0.8143	+0.7	1.4				2.2										Heavy dark shiny scale with rough surfaces	Dark-gray film with spots of brown scale in grain pattern; machine marks visible
ZX-7	10		0.8045	0.8064	0.8053	+0.8	1.4				2.2										Dark scale with a granular pattern	Dark-gray film with spots of brown scale in grain pattern; machine marks visible
ZX-8	14		0.7882	0.7899	0.7894	+1.2	1.4				2.2										Dark scale with a granular pattern	Dark-gray film with spots of brown scale in grain pattern; machine marks visible
Ti–3% Al (array TB2)																						
TJ-15	4		0.5475	0.5499	0.5476	+0.1	1.4				2.2										Heavy bronze scale with spots of shiny dark rough surfaces	Shiny bronze surfaces with rough surfaces and interference colors
TJ-16	8		0.5352	0.5375	0.5352	0.0	1.4	0.0	0.0	0.0	2.2	0.0	0.0	0.0							Heavy bronze scale with spots of shiny dark rough surfaces	Shiny bronze surfaces with rough surfaces and interference colors
TJ-17	12		0.5603	0.5625	0.5606	+0.3	1.4														Heavy bronze scale with spots of shiny dark rough surfaces	Shiny bronze surfaces with rough surfaces and interference colors
TJ-18	15		0.5423	0.5428	0.5422	−0.1	1.4	0.01	0.01	0.01	2.2	0.01	0.01	0.01							Heavy bronze scale with spots of shiny dark rough surfaces	Shiny bronze surfaces with rough surfaces and interference colors
Ti–A55 (array TB2)																						
T-173	3		0.5333	0.5378	0.5335	+0.2	1.4				2.2										Heavy dark shiny scale with rough surfaces	Metallic gray surfaces with interference colors; machine marks visible
T-174	7		0.5373	0.5387	0.5374	+0.1	1.4				2.2										Heavy bronze-colored scale	Metallic gray surfaces with interference colors; machine marks visible
T-175	11		0.5428	0.5444	0.5430	+0.2					2.2										Heavy bronze-colored scale	Metallic gray surfaces with interference colors; machine marks visible
Stress specimen (in-line)																						
Zircaloy-2, stress specimen																						
ZB-6			8.4771	8.4867	8.4833	+6.2	15.9				19.7							1300	17,500	10,400	Uniform dark-brown scale over all surfaces	Dull gray under flakes of retained brown scale; machine marks visible
ZB-9			8.4198	8.4286	8.4262	+6.4	15.9				19.7							1305	17,500	10,400	Uniform dark-brown scale over all surfaces	Dull gray under flakes of retained brown scale; machine marks visible
Stress specimen holders, Zircaloy-2																						
ZB-37			9.2006	9.2040	9.2016	+1.0					10.7										Very dark rustlike scale scattered over all surfaces	Dull gray under flakes of retained brown scale; machine marks visible
ZB-38			9.3038	9.3131	9.3100	+6.2					10.7										Very dark rustlike scale scattered over all surfaces	Dull gray under flakes of retained brown scale; machine marks visible
Stainless steel, type 347, core-channel coupon holder																						
A			94.5817	94.4873	94.4176	164.1	~160	0.10	1.0	1.4	~160	0.10	1.0	1.4		3.0	1.9	2.7			Metallic gray to dark gray; scale on one end; pitting on other	Metallic gray scale with a darker gray where bands clamped holder
B			95.4924													3.0	1.9	2.7				
Stainless steel, type 347, in-line–channel coupon holder																						
A			113.5866	113.5790	113.5326	54.0	~160	0.03	0.3	0.5	~160	0.03	0.3	0.5							Dark-brown scale ranging to a rust-colored scale	Patches of dark-brown to rust-red scale; scattered gray underlay
B			113.3152																			

[a]Two corrosion rates are presented: one based on the total operation time of 860 hr and the other based on the total radiation time of 642 hr (3 Mwhr of reactor time equivalent to 1 hr of total radiation time).

[b]Zr–15% Nb, material No. 84; annealed for 2 hr at 1000°C, water-quenched, rolled to 0.090 in.; annealed 2 hr at 900°C, water-quenched, sand blasted to remove oxide, pickled to mirror finish, sawed to size, surface ground to 0.065 in., and chemically polished to 0.060 in.

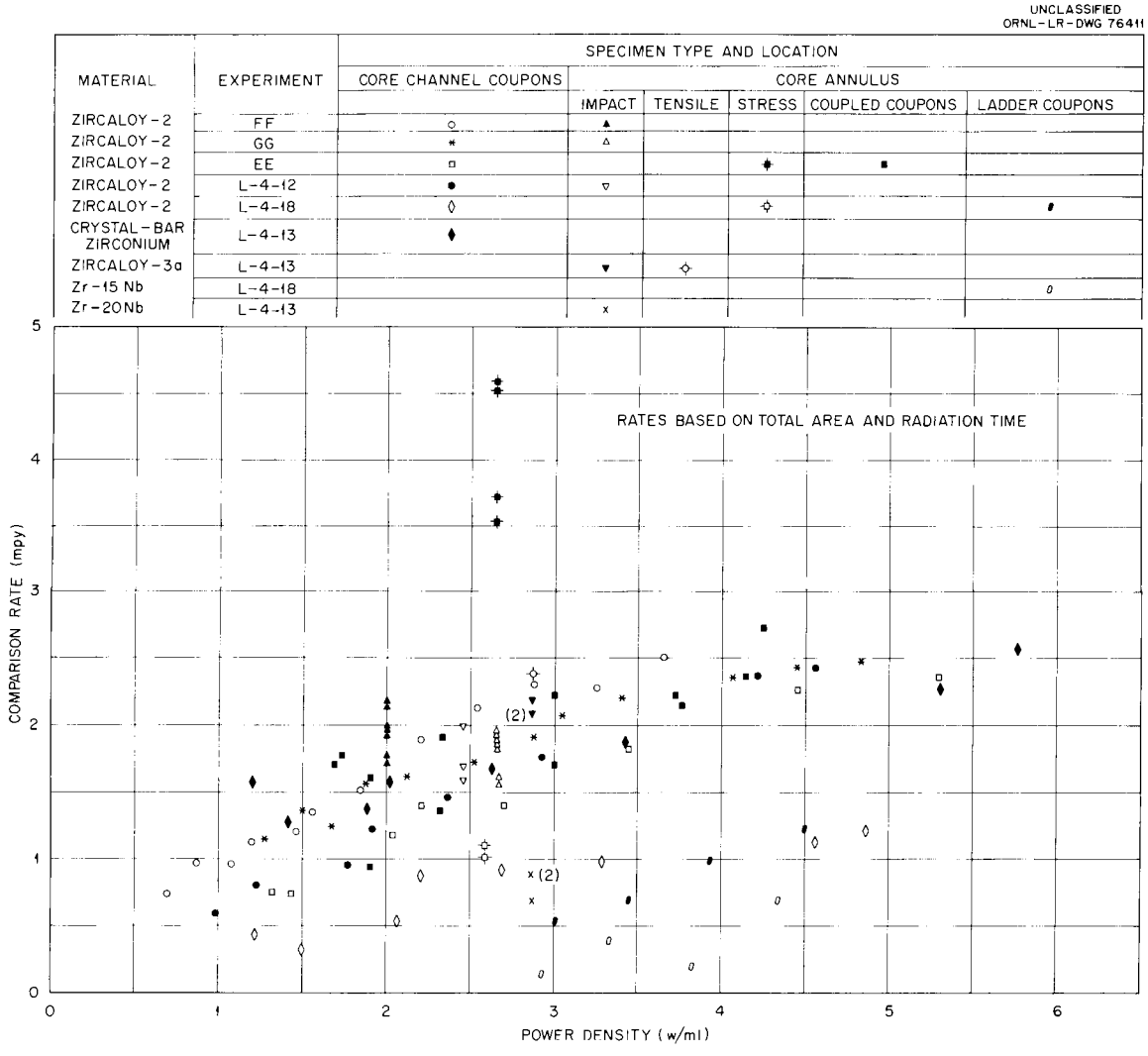

Fig. 75. Crystal-Bar Zirconium and Zirconium-Alloy Corrosion Data.

5.1.1 Charged Solutions – Nonradioactive Samples

These solutions were regularly analyzed for U, Cu, SO_4, Ni, and pH. In two experiments, free-acid analyses were also made. Considerations of the cation-anion balances and the pH results for loops DD through L-4-12 show some inconsistencies which, in general, can be explained either by an error of –0.05 in the pH measurements or by errors in the ion analyses, with the maximum error for any one analysis as follows: uranium, –2.5%; sulfate, +2.5%; or copper, –20%. In experiment FF, the discrepancies were greater, and the errors in the ion analyses or pH required to explain the results were about three points greater than those mentioned above. In experiments L-4-13 and L-4-18, the cation-anion balances and the

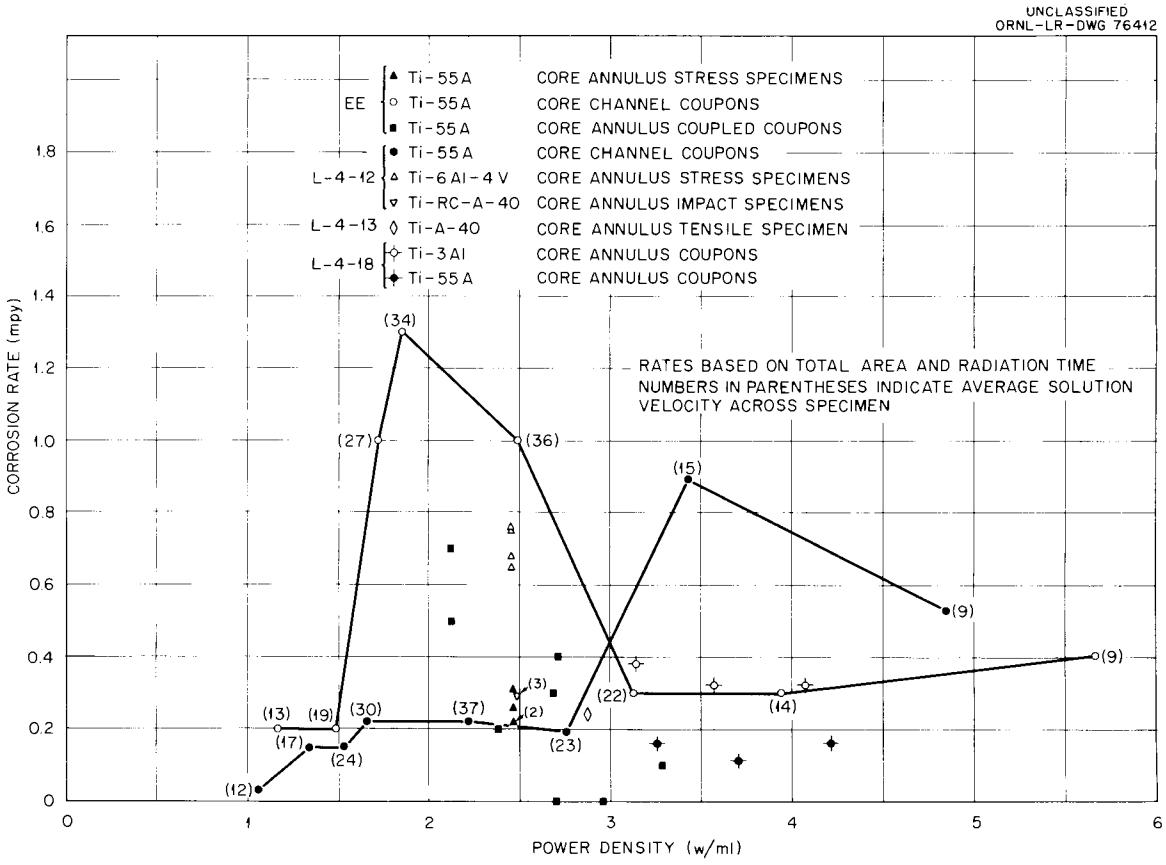

Fig. 76. Titanium Corrosion Data.

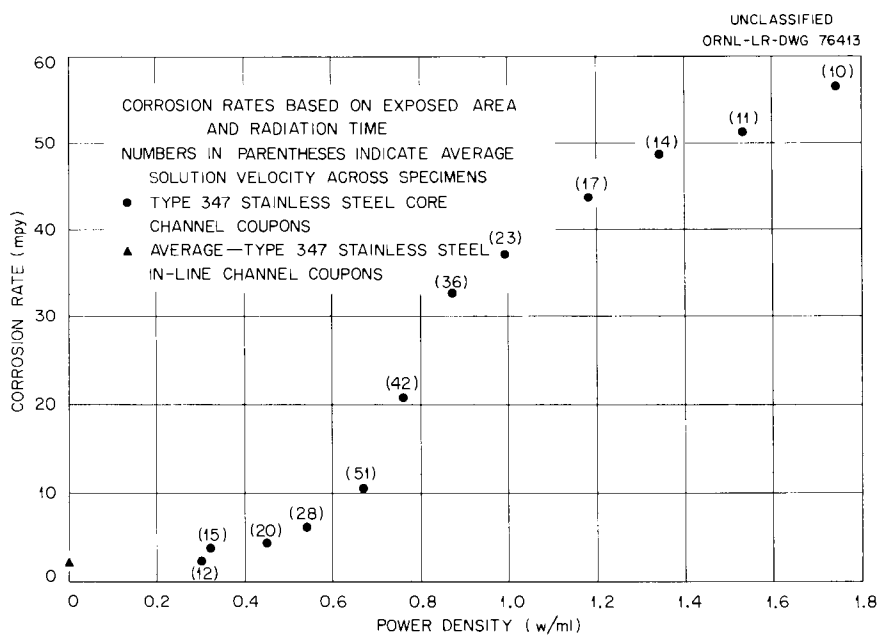

Fig. 77. Stainless Steel Corrosion Data, Loop DD.

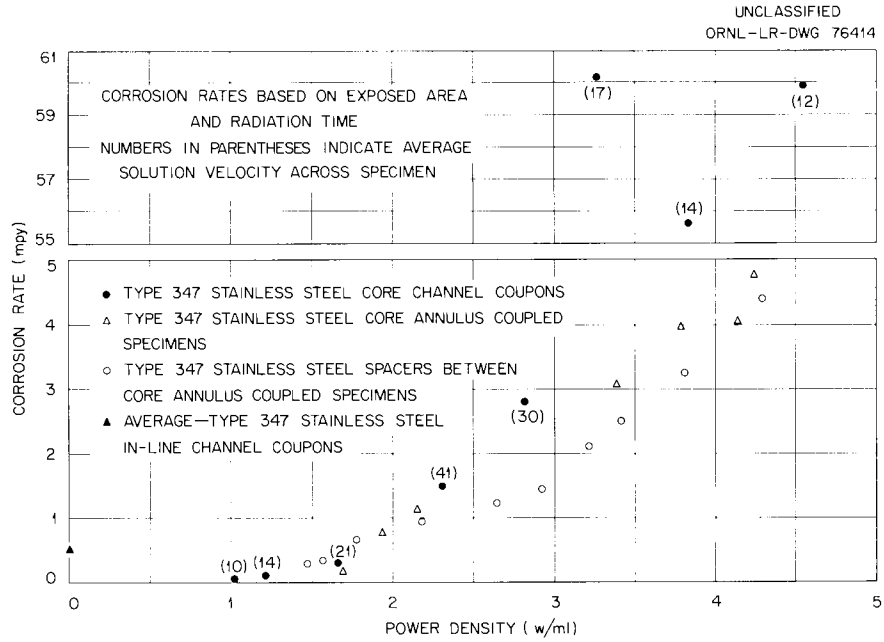

Fig. 78. Stainless Steel Corrosion Data, Loop EE.

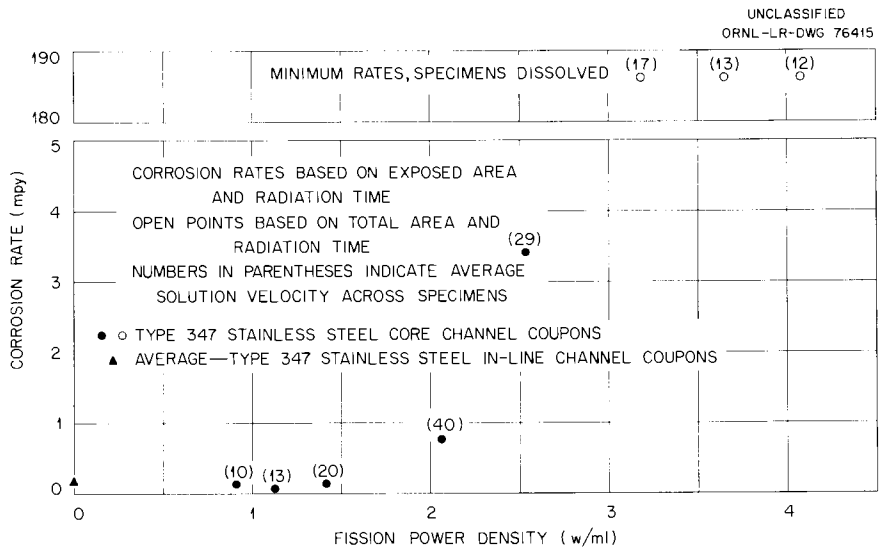

Fig. 79. Stainless Steel Corrosion Data, Loop L-4-12.

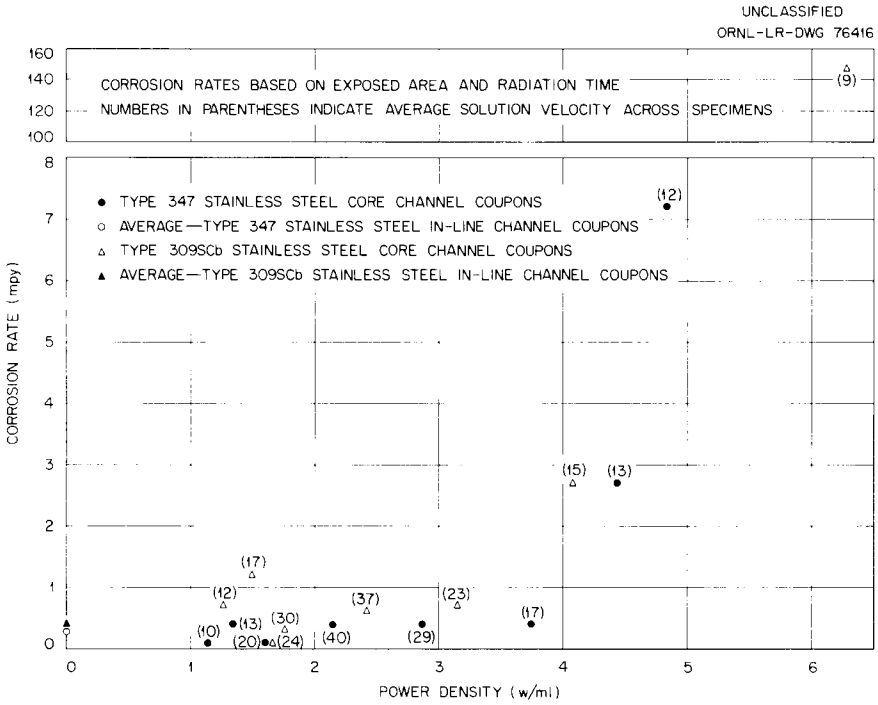

Fig. 80. Stainless Steel Corrosion Data, Loop L-4-13.

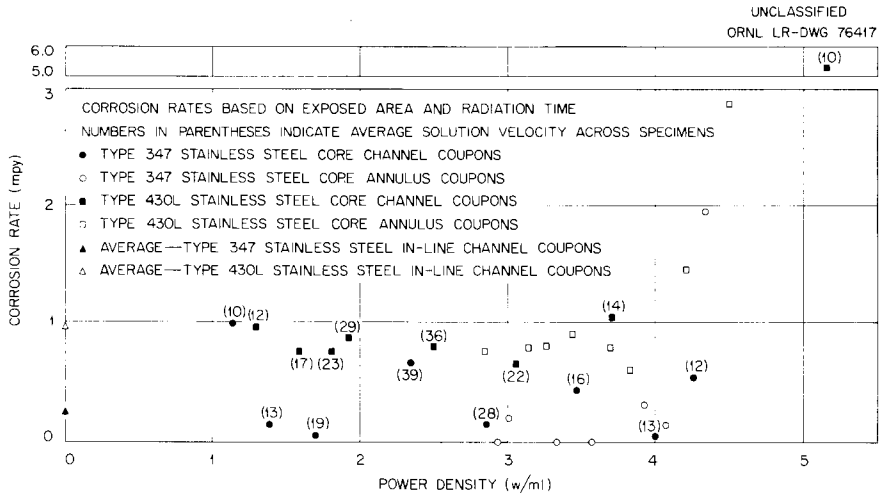

Fig. 81. Stainless Steel Corrosion Data, Loop L-4-18.

free-acid analyses are in near agreement. The relationship between free-acid and glass-electrode pH readings on these D_2O solutions was not established independently, and the pH readings were not employed in evaluating the results.

Considering that highly developed, accurate methods for uranium analyses and for pH measurements were available from the start of these experiments and that very large errors in the copper analyses are required to explain the discrepancies, it is believed that errors in sulfate analyses were largely responsible for the observed discrepancies.

5.1.2 Uranium, Copper, and Sulfate in Loop Solutions During Irradiations

Experiments Employing Li_2SO_4 Tracer to Establish Sample Dilutions – Loops GG, EE, L-4-12, L-4-13, and L-4-18. – From reference to the plots of the analytical data for these experiments (Figs. 9, 11–14), it can be seen that appreciable scatter occurred both in the analytical values reported for the samples and in those values obtained by correcting reported values by the lithium dilution factors. In general, however, the corrected values fall nearest the calculated values, that is, to the values calculated from inventory balance, assuming no loss of solutes from solution. Within the scatter of the data, there are no apparent trends to lower or higher concentrations for uranium, copper, or sulfate during in-pile exposure of these experiments, and consideration of these analytical data in terms of the average values appears valid.

In Table 43, average values are set forth for (1) analytical values for uranium, sulfate, and copper corrected for dilution, using the lithium dilution factor in one case and the uranium dilution factor in another case, and (2) calculated values for the same species. The uranium dilution factor was taken as the ratio of the calculated to reported uranium. Considering first those values corrected by the lithium dilution factor, the corrected uranium values are near the calculated but are slightly higher in each case (from 0.5% for L-4-12 to 6.2% for L-4-18). The corrected values in most cases are also higher than the calculated, while the corrected copper values are lower in most cases. The sulfate values calculated with the uranium dilution factor fall within 2% of the calculated values for L-4-12, L-4-13, and L-4-18. The sulfate value for GG is about 5% greater than the calculated value, while the corrected value for EE is about 4% below the calculated. The corrected copper values fall below the calculated by amounts varying from 1 to 11%.

A further evaluation of the data for the major consituents, uranium and sulfate, can be made from comparisons between free-acid values for solution samples from (1) cation-anion balance, (2) inventory balance, assuming that acid was consumed only in the dissolution of nickel and manganese in the amounts found in the samples, and (3) pH measurements. The acid values determined from cation-anion balance are generally greater than those estimated by the other methods, as illustrated in Fig. 82 for those samples from experiment GG for which Li_2SO_4 tracer was employed. For these samples the acid values from cation-anion balance were consistently greater than those estimated by the other methods, and the average amount of the difference was 0.035 *m*. These discrepancies cannot readily be explained by assuming that the corrected uranium values were lower than the true values, since the corrected values were near or above the calculated ones in all cases. Also, they are not readily explained by the assumption of errors

Table 43. Average of Values for Concentrations of Uranium, Sulfate, and Copper in the Experiments

Experiments	Average of Values (mg/ml)							
	Uranium		Sulfate			Copper		
	Corrected[a] (Li_2SO_4)	Calculated[b]	Corrected[a] (Li_2SO_4)	Corrected[c] (U)	Calculated[b]	Corrected[a] (Li_2SO_4)	Corrected[c] (U)	Calculated[b]
With Li_2SO_4 tracer								
GG	40.0	39.5	25.8	24.9	23.4	1.68	1.66	1.73
EE	39.5	38.4	20.3	20.3	21.2	1.72	1.67	1.76
L-4-12 (1st solution)	40.0	39.8	25.2	25.1	24.5	2.00	1.99	2.01
L-4-13	42.5	41.0	23.1	22.5	22.2	1.98	1.93	2.14
L-4-18	42.3	39.8	27.1	25.4	24.9	4.37	4.11	4.35
Without Li_2SO_4 tracer								
DD		35.0		19.7	18.1		1.71	1.71
FF		39.3		25.8	24.8		1.97	1.76
GG		39.8		25.0	23.4		1.85	1.75

[a]Reported results corrected by lithium dilution factor.
[b]Obtained from inventory balance of charged and removed solutions.
[c]Reported results corrected by uranium dilution factor.

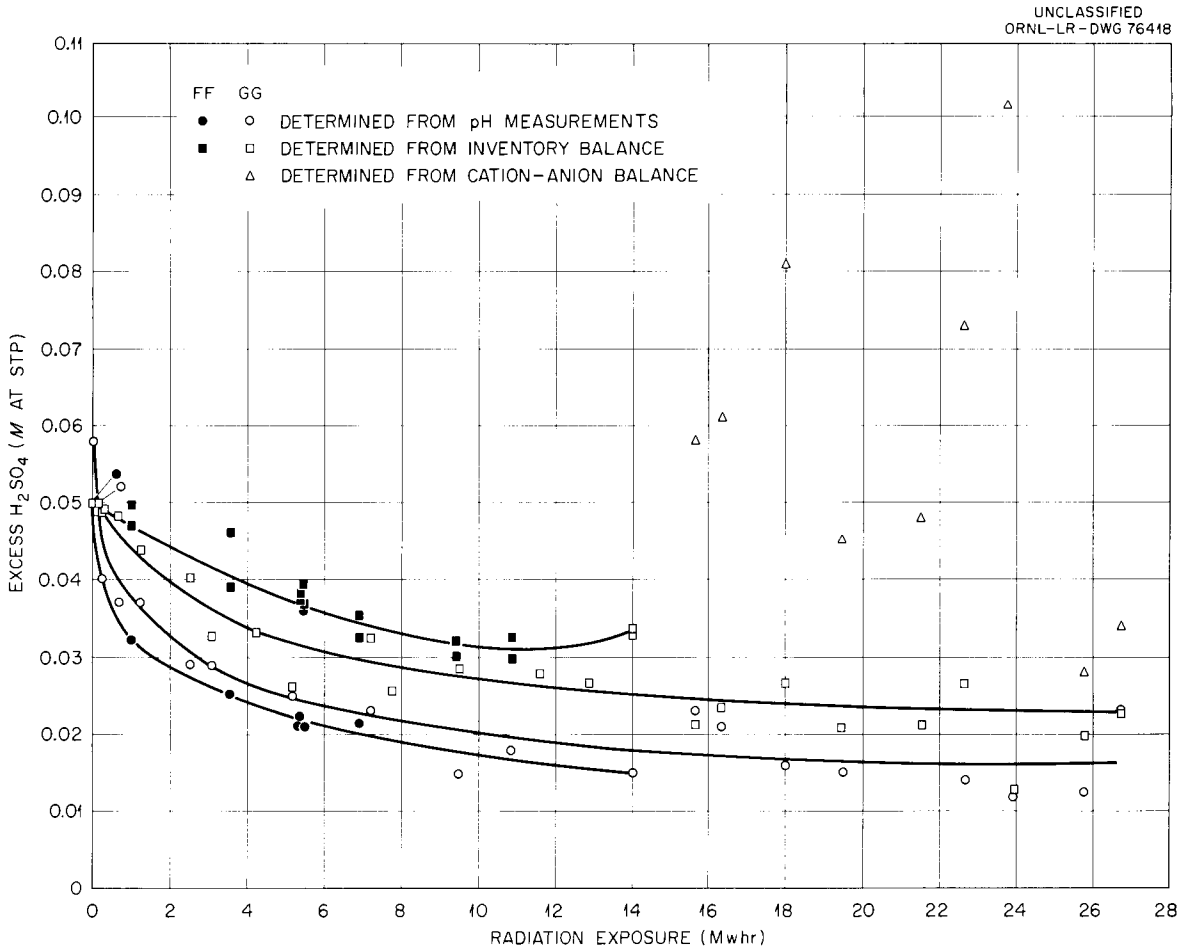

Fig. 82. Excess H_2SO_4 Concentration in Loops FF and GG.

in the analytical results for other cations such as nickel, since such errors would have to amount to factors of 2 or more in most cases. The discrepancies can be explained by assuming that the reported and corrected values for sulfate were generally in error on the high side, and this is believed to be the correct explanation.

On the basis of such considerations, the interpretations of the analytical results believed to be most reasonable and likely are the following:

1. On the average, there was no significant loss of uranium or sulfate from any of the solutions under consideration.

2. The average value for the dilution factor deduced from lithium was somewhat high in most experiments (in the range 0 to 5% for experiments L-4-12 and L-4-18 respectively).

3. Significant amounts of copper were lost from most of the solutions. The percentage losses ranged from 1% in L-4-12 to 11% in L-4-13.

Experiments Which Did Not Employ Li_2SO_4 Tracer – DD, FF, and GG. – Since it is considered likely that no uranium was lost from experiments employing Li_2SO_4 tracer, it is also likely that no uranium was lost from those other experiments which employed comparable solutions but no tracer. The averages of reported analytical values for sulfate and copper, corrected for dilution by using the uranium factors, are listed in Table 43. These sulfate results are comparable to those for the previously mentioned experiments. However, no loss of copper was indicated for these experiments.

5.1.3 Free Acid in Solutions During Irradiation

The free-acid values considered most reliable are those determined from direct analytical measurements, where such measurements were made, or from pH readings in other experiments. The results of free-acid measurements and estimates have been illustrated previously (Fig. 82).

The data in Fig. 83 show that the free acid in some of the experiments decreased rapidly following the initiation of irradiation and then tended to level off. In other experiments for which the initial excess acid concentrations were lower, the initial decrease was less marked. In some experiments no decreases occurred, but instead the acidities increased slightly. These changes in acid concentration and the difference between the several experiments are qualitatively explained by several factors: (1) much of the decrease in acidity resulted from stainless steel corrosion and the concomitant neutralization of acid by the dissolution of nickel and manganese, (2) the rate of corrosion of steel under irradiation was dependent upon the excess acid concentration, increasing with increasing acidity, and (3) acid was added to the loops with makeup solutions during irradiation, and in cases where the corrosion rates were low, the additions counter-balanced or outweighed the loss resulting from corrosion. The effect of acid on steel corrosion will be discussed in detail in later paragraphs.

In general, the acidity values determined from inventory balance, considering acid addition and withdrawals and neutralization of acid by nickel and manganese in solution, and from pH measurements were in rather poor agreement, as illustrated in Figs. 82 and 84 for the data from FF, GG, and L-4-12. The sources of the discrepancies between the values determined by the different methods are unknown. Sources which are considered possible include (1) errors in nickel and manganese analyses, (2) loss of acid by sorption on corrosion product oxides, and (3) loss of nickel by sorption as nickel sulfate, as mentioned in the following section. Some uncertainty exists also in the acid values from pH measurements, but pH measurements comprise direct determinations of acidities which are considered more reliable than those determined from inventory balance.

5.1.4 Nickel in Irradiated Solutions

The analytical data for nickel in solution can be used to calculate the total amount of steel oxidized at a given time if it is assumed that no selective oxidation of any steel component occurred and that all oxidized nickel was in solution. The steel corrosion calculated in this way was shown graphically and compared with the oxygen consumption data in Figs. 15–21. However, the oxygen data shown there were

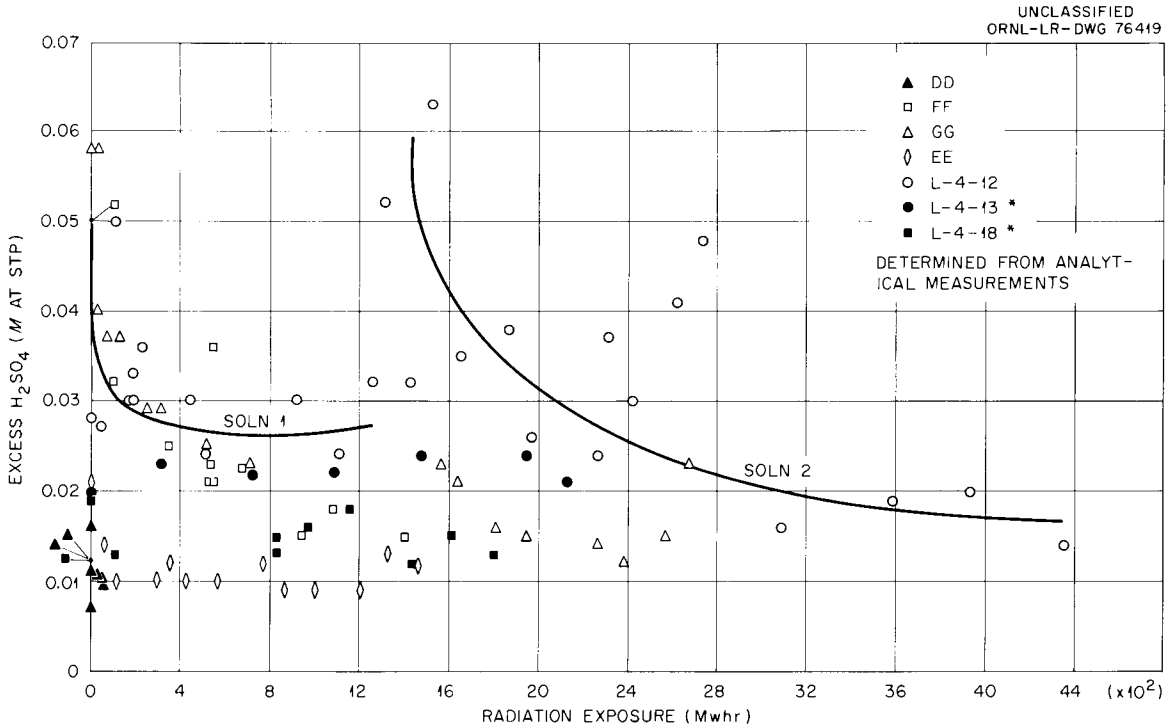

Fig. 83. Excess H_2SO_4 Concentration in Several Loop Experiments Determined from pH or Analytical Measurements.

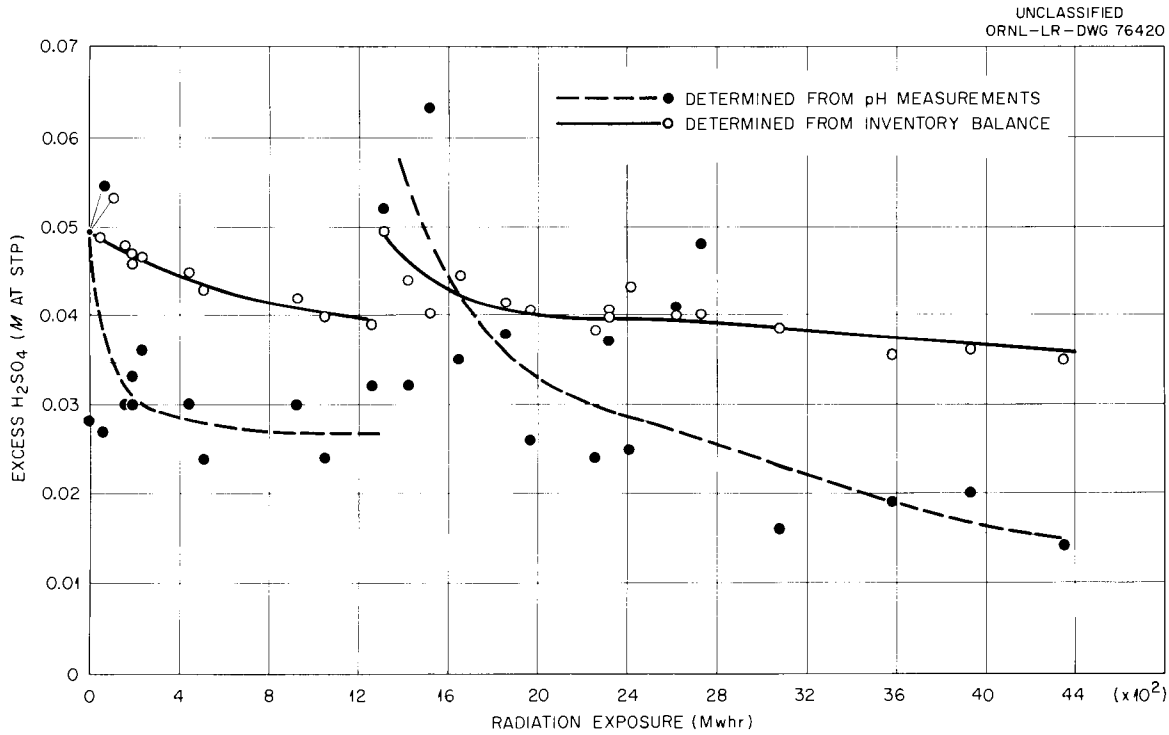

Fig. 84. Excess H_2SO_4 Concentration in Loop L-4-12.

uncorrected for consumption by zirconium and titanium alloys. The best values for total oxygen consumption by steel determined from oxygen and nickel data are compared in Table 44. The nickel values were determined from those shown in Figs. 15–21. The oxygen values, corrected for consumption by zirconium and titanium alloys, were taken from the plots shown in Fig. 30. The time selected for comparison was near the end of the in-pile exposure in each case.

Table 44. Comparison of Total Amounts of Steel Corrosion Determined from Oxygen Uptake and Dissolved Nickel Data

Experiment	Time (Mwhr)	Calculated Oxygen Consumption by Steel		Ratio of Consumption from Oxygen Data to That from Nickel Data
		Oxygen Consumption Data[a] (cc at STP)	Nickel Data[b] (cc at STP)	
DD	840	1730	1200	1.44
FF	1400	4760	2440	1.95
GG	2550	4470	3760	1.18
EE	1460	2100	1750	1.20
L-4-13	2300	3220	1760	1.83
L-4-18	1920	760	510	1.49

[a]From graphs shown in Fig. 30.

[b]Calculated from data in Tables 6–12, assuming (1) no selective oxidation of any steel component, (2) all oxidized nickel in solution, and (3) that the type 347 steel contained 12.5% nickel.

As listed in the final column of Table 44, the total steel corrosion indicated by the oxygen was appreciably greater than that indicated by nickel – nearly a factor of 2 in one case, and an average difference of a factor of 1.5 for the six experiments. These results indicate (1) that the nickel analyses were in error or (2) that part of the nickel formed in corrosion either did not dissolve or, if dissolved, left solution by sorption or precipitation. The latter indication is supported by the significant amounts of nickel found in the heavy scales in the in-line positions. (Scale from the in-line Zircaloy-2 holder in experiment GG contained 2% nickel by weight. Bulk scale from experiment L-4-18 contained 2 to 7% nickel.) It is also supported by results obtained in subsequent experiments at higher temperatures which have shown appreciable amounts of nickel in the heavy scales.[34,35] In one of the high-temperature experiments, the total amount of nickel found in scales and solution indicated that nickel was selectively oxidized from the type 347 stainless steel.[35]

[34]G. H. Jenks and J. E. Baker, *HRP Radiation Corrosion Studies: In-Pile Loops L-2-15 and L-4-16*, ORNL-3099 (in preparation).

[35]G. H. Jenks and J. E. Baker, *HRP Radiation Corrosion Studies: In-Pile Loop L-2-17*, ORNL-2974 (in preparation).

As shown in Fig. 16, the amounts of manganese in solution were sometimes in rough agreement with those estimated from the nickel data, assuming (1) about 1% manganese in the type 347 steel, (2) no selective oxidation of any of the steel constituents, and (3) complete solubility of the nickel and manganese. Usually, however, the amounts of manganese found in solution were much less than the proportionate amount estimated from the nickel in solution (Figs. 19 and 20). This shows that the oxidized manganese was usually not completely dissolved or, if dissolved, was deposited and retained on loop surfaces.

It may be pointed out here that a possible explanation for the observed discrepancies between free-acid concentrations calculated from pH and from inventory balance, assuming acid neutralization by nickel and manganese in solution (Figs. 82 and 84), is that nickel was sorbed from solution as nickel sulfate, so that the amounts of acid neutralized were greater than those calculated from the amounts of nickel in solution.

5.1.5 Other Constituents of Loop Solutions

Zirconium in amounts ranging up to 50 ppm and more (greater than 100 ppm in some cases) was found in all solutions during in-pile operations. These findings indicate an appreciable solubility for this material or its compounds. (It is considered possible that the material in solution was in a colloidal form.) The appreciable solubility is consistent with the findings made in subsequent loop experiments[34] that most of the zirconium oxide formed in loop cores is transported to and deposited on surfaces outside the high-flux regions of the core.

Significant amounts of chromium were found in many of the loop samples (usually less than 100 ppm). The valence state for this chromium is unknown. Considerations by Banter *et al.*[36] of the possible oxidizing effects of radicals produced during irradiation and of the reducing environment provided by hydrogen and copper in solution suggest that both valence states may be present during irradiation.

Iron was also found in most of the loop samples, again at concentrations usually less than 100 ppm. The identity of the soluble species is unknown.

Cobalt was sought in several of the early experiments which employed stellite pump-journals in order to follow the corrosion of the stellite. The cobalt found in solution was small in all cases and was less than 25 ppm in experiments FF and EE. In the first experiment DD, the cobalt reached a concentration of about 160 ppm.

Chlorine was detected at a concentration level of a few parts per million in most of the experiments. It is believed that these low concentrations had negligible effects on the steel corrosion. No stress cracking has been observed in any out-of-pile tests with solutions containing <5 ppm of chloride ion.[37]

---

[36] J. C. Banter, J. E. Baker, and R. J. Davis, *Analysis of the Status of Chromium in Solution Under In-Pile Conditions*, ORNL CF-58-7-63 (July 1958).

[37] E. G. Bohlmann, "Integrity of Metals in Homogeneous Reactor Media," p 283 in *Fluid Fuel Reactors* (ed. by J. A. Lane *et al.*), Pt. 1, Addison-Wesley, Reading, Mass., 1958.

5.2 Corrosion of Type 347 Stainless Steel During In-Pile Exposure

5.2.1 General

The principal material of construction in these loops was type 347 stainless steel. The overall corrosion of this material was followed by oxygen consumption and nickel accumulation measurements. Corrosion in specific locations was followed in some of the loops through corrosion specimens. Metallographic and visual examinations were made of loop components and of specimens when available.

Steel specimens exposed in the loop cores showed increases in corrosive attack over that expected out-of-radiation, as illustrated in Figs. 77–81. As shown, the average rates of corrosion increased with power density in adjacent solution, but below certain power densities the average rate was not noticeably different from that occurring on in-line specimens. The corrosion occurring on in-line and low-power-density specimens was not significantly different from that expected during out-of-pile exposures (weight losses of 1 mg/cm^2 or less on pretreated specimens[38]). These specimen results thus indicate that the effects of in-pile exposure on steel corrosion were confined to the core.

The results of metallographic and visual examinations of specimens and components also indicated that, for surfaces located outside the core and at low-power densities within the core, the corrosion was not signficantly different from that expected out-of-pile, with the possible exception of the deep corrosion pit which formed at the site of the pinhole weld in loop FF (see Sec 4.6.2).

A like indication was given also by the oxygen consumption results for the titanium-core experiment, L-4-12, in comparison with those of other steel-core experiments which employed solutions of about the same composition. As shown in Fig. 19, the rate of oxygen consumption on steel in L-4-12 at the initiation of irradiation with the first solution charge did not differ significantly from that prevailing prior to irradiation. With the second solution charge, the maximum at the initiation of irradiation was 4.6 cc/3 Mwhr or less. In comparison, the initial consumption rates in experiments GG and FF were about 25 and 16 cc/3 Mwhr respectively. The lower initial rates in L-4-12 can be explained by assuming that the major effects of irradiation on steel corrosion occurred only on surfaces exposed to fissioning solution in the core, and that the rate of oxygen consumption by steel in experiment L-4-12 was much lower than those in experiments GG or FF because of the lower area of steel in the core of L-4-12 (37 cm^2 vs 445 cm^2 in GG or FF).

Based on the above observations it has been concluded that the irradiation effect on steel corrosion was confined to the surfaces within the core.

The power-density value at which the radiation effects became noticeable varied from 0.3 w/ml in DD to 3.8 w/ml in L-4-13 for the 250°C experiments. In the 235°C experiment, L-4-18, the value was 4.2 w/ml. The corrosion of those core specimens of type 347 stainless steel which were most severely attacked appeared to proceed through formation of pits, about 1 mil in depth, which then spread laterally to result in a fairly uniform attack of a surface. It should be noted that although the core specimen results are presented in terms of average rate values, the actual rates probably changed considerably during

---

[38] J. C. Griess and R. E. Wacker, *HRP Quart. Progr. Rept. Jan. 31, 1954*, ORNL-1678, pp 60–63.

the course of an experiment as indicated by the changes in rate of oxygen consumption (at the extremes, a factor of about 40 from the maximum to minimum in experiment GG, and a factor of 2 in experiment EE, Figs. 16 and 18).

There was no effect of stress on core and in-line steel corrosion in the one experiment, EE, in which this factor was investigated. Also there was no effect of galvanic coupling with other materials tested in the same experiment. In general, the amount of scale removed from core specimens by defilming was small and much less than that from in-line specimens. This indicates that much of the steel corrosion product oxides found in the core were transferred to and deposited on in-line surfaces. Zirconium-alloy corrosion products behave similarly.[34]

Type 309SCb stainless steel specimens tested in one experiment, L-4-13, exhibited about the same general relationship between power density and rate as type 347 stainless steel, but the type 309 rates at a given power density were somewhat greater than those for type 347. A similar difference between the radiation effect on the two steels has been observed in subsequent loop experiments at higher temperatures.[34]

Type 430L stainless steel specimens in experiment L-4-18 were affected by exposure to fissioning solution to about the same extent as type 347 steel. It may be noted, however, that in a subsequent experiment at 300°C (ref 31) type 430 steel performed better than type 347.

5.2.2 Effects of Solution Velocity on Core Specimen Corrosion

Most of the core specimens of stainless steel were mounted in the main core channel holders, where they were exposed to solution velocities ranging from about 10 fps for the forward and rear specimens to about 40 fps for the central specimens. For experiment DD the shape of the rate–power-density curve (Fig. 77) suggests an effect of solution velocity on the corrosion. An analyses of these data by the Mathematics Division produced the following relationship between these variables:

$$\log \text{penetration } (100 \times \text{mils}) = 0.791 - 0.21V + 0.603P - 0.0885P^2 + 0.0237PV,$$

where P = power density (w/ml), V = solution velocity (fps). This analysis indicates that the net effect of increasing velocity within the range 10 to 40 fps was to reduce the power-density effect on corrosion. The channel data from the other experiments have not been analyzed in a similar fashion. However, in another 250°C experiment reported elsewhere,[39] there was an obvious adverse effect of high solution velocities on the corrosion of the CC specimens. In experiment EE, specimens exposed in the low-velocity (~1 fps) annulus regions exhibited penetrations which were lower than those for the channel specimens, but in L-4-18 the annulus rates were about the same or only a little less than those in the channel.

In summary, some of the data obtained in these and subsequent experiments[35] indicate an adverse effect of increasing solution velocity on steel corrosion under exposure to fissioning uranyl sulfate solutions, while others indicate beneficial effects. It may be speculated that either effect may occur, depending upon the experimental conditions. A beneficial effect might be expected to occur by the mechanism

---

[39] J. E. Baker and G. H. Jenks, *HRP Radiation Corrosion Studies: In-Pile Loop L-4-8*, ORNL-2042 (Aug. 8, 1956).

prevailing in Zircaloy-2 corrosion in which the amounts of uranium sorbed near a surface and, thus, the effective power density at the surface decreased with increasing solution velocity. An adverse effect of velocity occurs out-of-radiation on unpretreated specimens, and a similar effect may occur in-pile after the protective film has been damaged during irradiation. The experimental conditions under which one or the other effects predominates are unknown.

5.2.3 Comparison Between Total Amounts of Steel Corrosion Determined from Oxygen Consumption and from Nickel Accumulation

A comparison between the amounts of steel corrosion determined by the two methods was presented in Table 44 and discussed in Sec 5.1.4. The oxygen data indicate the greater amount of steel corrosion and are considered the most accurate measure of the total steel corrosion.

5.2.4 Correlations Between Solution Composition and Rate of Oxygen Consumption by Steel

As shown in Figs. 15–21, the rates of oxygen consumption by steel during irradiation varied from one experiment to another. Also, the rate in a given experiment changed to generally lower values as the exposure progressed. Variations in the total consumption of oxygen by steel also occurred. As shown in Fig. 30, plots of total consumption vs exposure time exhibited a characteristic pattern (except L-4-12) in which the rate of consumption remained essentially constant for a long period following the initiation of irradiation and then changed to a second, lower rate which, in general, prevailed for the remainder of the exposure. However, the initial rates as well as the total consumption prior to the break were different for the different experiments.

A cursory examination of the conditions and results for the 250°C experiments reported here, together with those for the previously reported experiment L-4-11,[40] shows that the differences in steel corrosion were related to differences in the concentrations of excess acid and, probably, nickel in the test solutions. For example, total oxygen consumption prior to the break (Fig. 30) was greater for experiments GG and FF, which were charged with solution containing about 0.05 *m* excess acid, than for the experiments employing initial acidities of 0.015 to 0.02 *m* (DD, EE, L-4-13). Also, in experiment L-4-11, for which the initial solution contained about 0.01 *m* $NiSO_4$ but was otherwise comparable to that employed with GG and FF, the total consumption prior to the break was less than in either FF or GG. The initial rates under irradiation were also greatest for those solutions with the highest acidities.

The results of efforts to obtain quantitative correlations between steel corrosion rates and solution compositions are shown in Figs. 85 and 86 and in Table 45. In Fig. 85, values for the rate of oxygen consumption per unit area of exposed steel surface in the core and per unit fission power in the core during irradiation at 3 Mw LITR power are plotted vs excess H_2SO_4 concentration for all the present 250°C experiments which employed steel cores except DD and for the previously reported experiment L-4-11. In Fig.

---

[40] J. R. McWherter and J. E. Baker, *HRP Radiation Corrosion Studies: In-Pile Loop L-4-11*, ORNL-2152 (June 11, 1958).

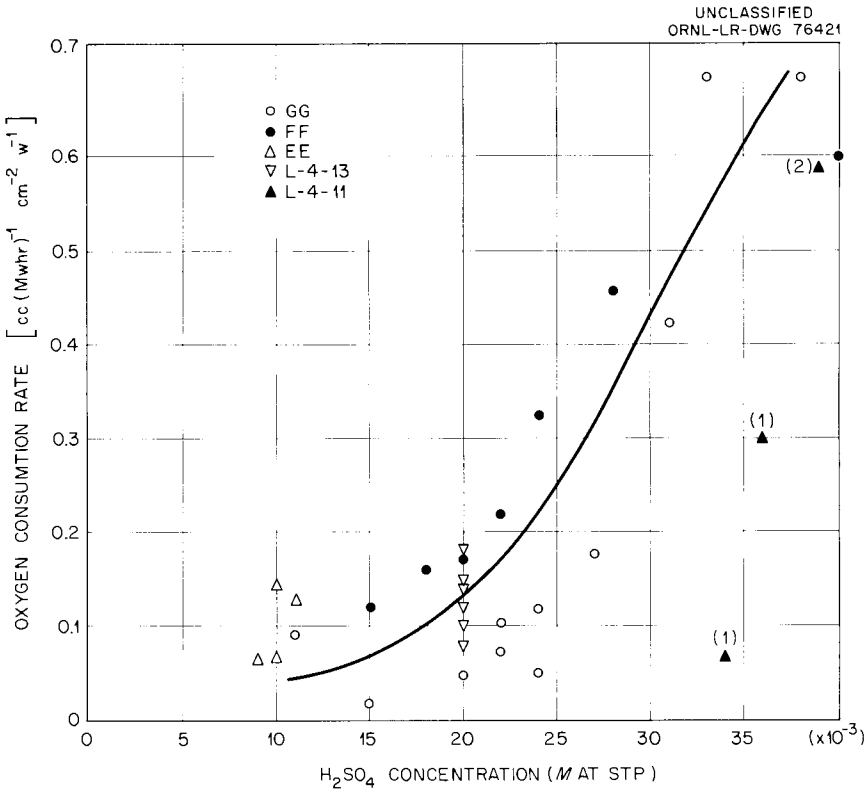

Fig. 85. Rate of O_2 Consumption per Unit Area of Exposed Steel in Core and per Unit Fission Power in Core at 3-Mw LITR Power vs Excess H_2SO_4 Concentration.

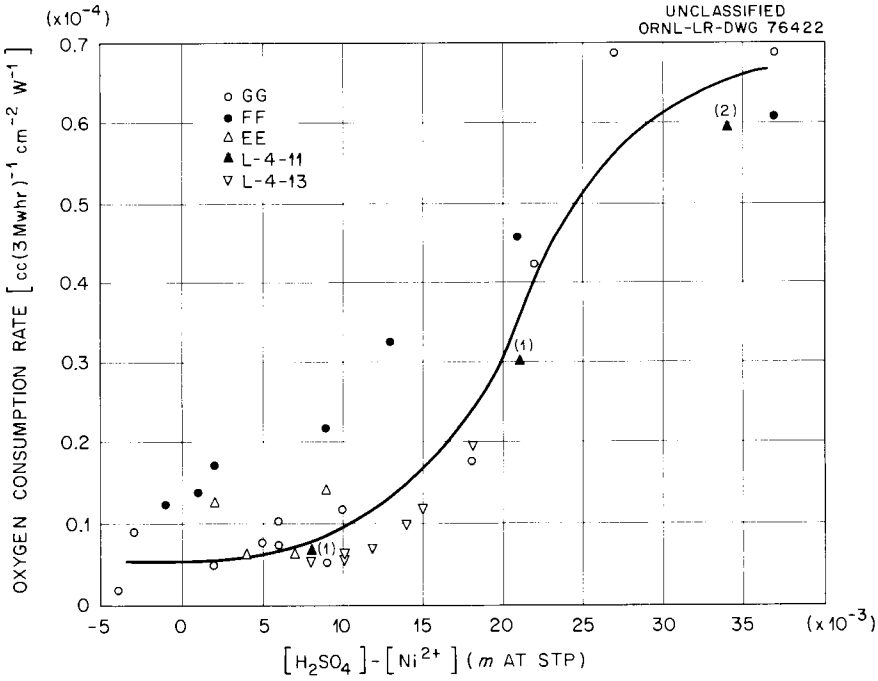

Fig. 86. Rate of O_2 Consumption per Unit Area of Exposed Steel in Core and per Unit Fission Power in Core at 3-Mw LITR Power vs H_2SO_4 Concentration Less $NiSO_4$ Concentration.

86, the rate values are plotted vs the concentrations of excess H_2SO_4 less the concentration of $NiSO_4$. Set forth in Table 45 are values for the concentrations of excess H_2SO_4 and $NiSO_4$ and for the difference between these values at the time of the break in rate of total oxygen consumption. Two values for each quantity are given for experiments FF and L-4-11. The break in the consumption rates in these experiments occurred during long periods of operation with the reactor down, and appreciable changes in acid and nickel concentrations occurred during these periods. The two values in each case are those for the concentrations at the beginning and the end of the reactor-down period.

Steel areas and fission-power values used in the average rate calculations are listed in Table 46. The acidity values are those obtained from pH measurements of loop solution samples. The data from loop DD

Table 45. Correlations Between Solution Composition and Occurrence of Break in Oxygen Consumption Rate

Experiment	Radiation Exposure at Time of Break (Mwhr)	Concentration of Excess H_2SO_4 (*M* at STP)	$[Ni^{2+}]$ (*M* at STP)	Excess H_2SO_4 Less $[Ni^{2+}]$ (*M* at STP)
FF	540	0.023[a]	0.010	0.013
		0.021[a]	0.012	0.009
GG	330	0.019[a]	0.010	0.009
EE	300	0.010[a]	0.002	0.008
L-4-13[b]	590	0.020[c]	0.006	0.014
L-4-11	200	0.034[a]	0.015	0.019
(1st solution)		0.030[a]	0.020	0.010

[a]Determined from pH measurements.
[b]Solvent D_2O. All other experiments employed H_2O solvent.
[c]From analytical determinations of free acid.

Table 46. Steel Areas and Fission Powers for Loop Experiments

Experiment	Steel Surface Areas in Core			Fission Power at 3-Mwhr LITR Power (w)
	Core Body (cm^2)	Exposed Specimen Surface (cm^2)	Total Area (cm^2)	
FF	445	0	445	606
GG	445	0	445	830
EE	445	201	646	528
L-4-13	318	195	513	690
L-4-11	445	255	700	810

were excluded from this comparison because the loop solution was diluted with water during the exposure. Each of the other solutions was about 0.17 *m* UO_2SO_4 and 0.03 *m* $CuSO_4$ throughout the exposure. The rate values for experiments FF, GG, EE, and L-4-13 were calculated from the values shown in Fig. 85, and all data points are plotted. For experiment L-4-11 the data points labeled (1) were obtained shortly after the initiation of irradiation with the first solution, which contained the $NiSO_4$ additive. The point labeled (2) was obtained near the start of irradiation with the second solution, which contained no $NiSO_4$.

The average corrosion rate per unit area of exposed steel surface in the core was selected for comparisons in Figs. 85 and 86, because, as discussed in previous paragraphs, most of the accelerated steel corrosion under irradiation occurred in the core, and it appears reasonable to assume that the average rate of oxygen consumption in the core was roughly proportional to the total steel area. The true relationship between power density and the average steel corrosion rate is unknown. However, the average rate on specimens increased with increasing power density, and, for the small differences in power density involved (530 to 830 w total with core volumes about equal), it appears reasonable to assume a linear increase in average rate with increasing power density for all steel surfaces in the cores.

Most of the data plotted in Fig. 85 group together and tend to support the concept of a direct correlation between average rate and acidity. Some of the spread of the values probably resulted from differences between background rates for different experiments. For example, the corrosion of the pinhole weld in the core of loop FF probably increased the total oxygen consumption substantially throughout the exposure. However, the two data points for the L-4-11 solution with added $NiSO_4$ are obviously out of line and, in comparison with the other data, show that the $NiSO_4$ addition effected a reduction of the steel corrosion rate under irradiation.

The rate as plotted in Fig. 86 indicates that for the data from experiments GG, EE, L-4-13, and L-4-11, a somewhat better correlation exists between the rate and the difference between the concentrations of excess H_2SO_4 and $NiSO_4$ than between the rate and excess H_2SO_4. The FF values are separated from the others to a greater extent than in Fig. 85. However, as mentioned previously, it is possible that localized attack tended to produce relatively higher rates in FF.

The data set forth in Table 45 show that the concentrations of excess acid ranged from about 0.01 to 0.03 *m* at the occurrence of the break in rate of total oxygen consumption for the several experiments, and no direct correlation between the two factors is apparent. However, the values for the difference between the concentrations of excess acid and $NiSO_4$ at the breaks are apparently in better agreement. Assuming that the minimum values for FF and L-4-11 represent the concentrations at the occurrence of the breaks, the values for the differences are between 0.008 and 0.010 for the H_2O experiments FF, GG, EE, and L-4-11, while the value for the D_2O experiment, L-4-13, is 0.014.

On the basis of the above considerations, it is concluded that the average rate of steel corrosion in the in-pile loop cores in the several 250°C experiments was dependent upon the concentrations of excess H_2SO_4 and of $NiSO_4$, with the rate decreasing with decreasing acid and with increasing $NiSO_4$. The explanation for these effects which is considered most likely is that the corrosion was influenced by the hydrogen ion concentration at the exposure temperature, and that the $NiSO_4$ in solution tended to reduce

this concentration through the formation of HSO_4^-. The latter ion is known to be very stable at 250°C.[41] The true extent to which $NiSO_4$ influenced the hydrogen ion concentration is unknown. However, for purposes of estimating corrosion in solutions of these particular concentrations of UO_2SO_4 and $CuSO_4$ at 250°C, it can be assumed that the excess acid is consumed mole for mole by the $NiSO_4$. More data at other solution concentrations and temperatures will be required to evaluate the effects of H_2SO_4 and $NiSO_4$ at other conditions. (Such data are available but have not yet been analyzed for the effects.)

It may be noted that on the basis of the above interpretation of the effects of $NiSO_4$, other corrosion products would be expected to exercise similar effects if they were dissociated at the exposure temperature. However, other corrosion products which entered solution and which might be in this category, for example, manganese and iron, were present at low concentrations and could be neglected. Changes in $CuSO_4$ concentrations during exposure or differences in concentration between experiments, if sufficiently large, might also affect the relative acidities and corrosion rates. However, these differences were small and can be neglected to a first approximation.

All the discussion of the effect of acid on corrosion has been related to the average corrosion rate of steel in the loop cores within which the fission-power densities varied by factors of 4 to 5 from the front to the rear. The data are not sufficient to determine either the rate prevailing for a surface at a given power density and solution composition or the effects of changes in these variables on the rates.

Although the steel data presented here have been reported and discussed elsewhere, it should be noted that the correlations between solution acidity, nickel accumulation in solution, and solution velocity and steel corrosion were not yet formulated. Consequently, some of the previously reported data from these and subsequent loop experiments may require reconsideration.

5.3 Corrosion of Zircaloy-2 and Crystal-Bar Zirconium

Data for the corrosion of these materials have been previously reviewed[42] and correlated with other data from loop and autoclave experiments, and they are not discussed further in this report.

5.4 Corrosion of Titanium Alloys

Fewer corrosion data are available for these alloys than for stainless steels and zirconium alloys. The available data have been reviewed previously[43,44] and are not discussed further in this report.

---

[41] M. H. Lietzke, R. W. Stoughton, and T. F. Young, "The Bisulfate Acid Constant from 25° to 225°C, as Computed from Solubility Data," to be published in the *Journal of Physical Chemistry.*

[42] G. H. Jenks, *Review and Correlation of In-Pile Zircaloy-2 Corrosion Data and a Model for the Effect of Irradiation,* ORNL-3039 (July 1961).

[43] G. H. Jenks and J. E. Baker, *HRP Radiation Corrosion Studies: In-Pile Loop L-2-17,* ORNL-2974 (in preparation).

[44] G. H. Jenks and J. E. Baker, *In-Pile Loop Investigation of Corrosion of Zircaloy-2 and Other Reactor Materials in 0.04 m UO_2SO_4 at 280°C,* ORNL-2962, in press.

ORNL-3131
UC-25 – Metals, Ceramics, and Materials
TID-4500 (20th ed., Rev.)

INTERNAL DISTRIBUTION

1. G. M. Adamson
2. A. L. Bacarella
3. J. E. Baker
4. J. M. Baker
5. S. E. Beall
6. E. G. Bohlmann
7. S. E. Bolt
8. G. E. Boyd
9. R. B. Briggs
10. W. D. Burch
11. T. A. Butler
12. W. E. Clark
13. E. L. Compere
14. F. L. Culler
15. R. J. Davis
16. V. A. DeCarlo
17. J. L. English
18. D. E. Ferguson
19. J. H Frye, Jr.
20. W. R. Gall
21. J. C. Griess
22. W. R. Grimes
23. P. N. Haubenreich
24. J. W. Hill, Jr.
25. G. H. Jenks
26. M. T. Kelley
27. M. J. Kelly
28. R. B. Korsmeyer
29. J. A. Lane
30. C. E. Larson
31. C. G. Lawson
32. R. A. Lorenz
33. R. N. Lyon
34. W. L. Marshall
35. J. P. McBride
36. R. E. McDonald
37. H. F. McDuffie
38. J. R. McWherter
39. A. R. Olsen
40. J. R. Parrott
41. M. L. Picklesimer
42. H. C. Savage
43. M. J. Skinner
44. I. Spiewak
45. J. A. Swartout
46. A. Taboada
47. E. H. Taylor
48. G. M. Watson
49. A. M. Weinberg
50. F. Daniels (consultant)
51. F. T. Gucker (consultant)
52. F. T. Miles (consultant)

53-54. Central Research Library
55. Reactor Division Library
56-75. Laboratory Records Department
76. Laboratory Records, ORNL RC
77-78. ORNL–Y-12 Technical Library, Document Reference Section

EXTERNAL DISTRIBUTION

79. Research and Development Division, AEC, ORO

80-658. Given distribution as shown in TID-4500 (20th ed., Rev.) under Metals, Ceramics, and Materials Category (75 copies – OTS)